

MODELLING THE INFRARED ASSISTED HOT AIR DRYING OF BEEF FOR BILTONG PRODUCTION

FC Muga

Submitted in fulfilment of the requirements

for the degree of PhD

School of Engineering

University of KwaZulu-Natal

Pietermaritzburg

May 2021

PREFACE

The research contained in this thesis was completed by the candidate while based in the Discipline of Bioresources Engineering, School of Engineering, College of Agriculture, Engineering and Science, University of KwaZulu-Natal, Pietermaritzburg, South Africa. The research was financially supported by the University of KwaZulu-Natal through the research cost centre of Professor Tilahun Seyoum Workneh.

ABSTRACT

This study investigated the drying kinetics of hot air drying (HAD) and infrared assisted hot air drying (IRHAD) of beef being processed into biltong. Subsequently, the study modelled the heat and mass transfer, as well as the energy and exergy variations during the IRHAD of beef into biltong. Marinated slabs of beef of dimensions 150 x 50 x 15 mm were dried under HAD and IRHAD. The HAD drying experiments were conducted in a cabinet dryer at drying air temperature of 30, 35, and 40 °C; and drying air velocity of 1.5 and 2.5 m.s⁻¹. The cabinet dryer was retrofitted with infrared (IR) emitter for the IRHAD experiments. The IRHAD experiments were conducted at IR emitter power level of 500, 750, and 1000 W, drying air temperature of 30, 35, and 40 °C; and drying air velocity of 1.5 and 2.5 m.s⁻¹. The results indicate that the HAD drying process occurred in the falling rate period. The temperature of the drying air significantly ($p \leq 0.05$) influenced drying time, drying rate, and the effective moisture diffusivity. The velocity of the drying air only had a significant ($p \leq 0.05$) effect on the drying rate during the first falling rate period. The predominant mode of moisture transport during the HAD of marinated beef to produce biltong is diffusion. The effective moisture diffusivity of marinated beef being processed into biltong ranged between $1.60 \times 10^{-10} \text{ m}^2.\text{s}^{-1}$ and $2.28 \times 10^{-10} \text{ m}^2.\text{s}^{-1}$, while the activation energy was 28.2126 and 17.7068 kJ.mol⁻¹ at drying air velocity of 1.5 and 2.5 m.s⁻¹, respectively. The HAD kinetics of marinated beef is best described by the Two-Term thin layer drying model. Results from the IRHAD experiments indicate that increasing the power level of the IR emitter and the drying air temperature increased the temperature of the IR emitter, the core temperature of the marinated beef sample, and the drying rate. The air velocity had an inverse relationship with the IR emitter temperature, core temperature of the marinated beef sample, and the drying rate. The IRHAD process was characterised by a rising rate period in the first half hour, followed by a falling rate period which implies that moisture transport occurred partly by surface evaporation and predominantly by diffusion. The effective moisture diffusivity ranged between 4.560×10^{-10} and $13.7 \times 10^{-10} \text{ m}^2.\text{s}^{-1}$, whereas the activation energy was in the 40.97 and 59.16 kJ.mol⁻¹ range. The IRHAD of marinated beef during its processing to biltong is also best described by the Two-Term thin layer drying model. From these findings, the IRHAD is a possible alternative to the conventional HAD of biltong. The application of IRHAD in biltong processing would require a better understanding of the mechanisms of heat and mass transfer

during the drying process. This study developed a coupled heat and mass transfer model to predict the temperature and moisture content of beef during biltong processing using IRHAD. The developed model was implemented and solved using Ansys Fluent CFD software. The IRHAD experiments were used to determine the moisture diffusivity, and the heat and mass transfer coefficients used in the model. The developed model was validated using a different set of experimental data and its suitability was assessed using the R^2 and RMSE. The value of R^2 was 0.9790 and 0.9579 for the temperature and MR, respectively. The value of RMSE was 1.99 and 0.0698 for the temperature and MR, respectively. In addition, a thermodynamic model was formulated to evaluate the energy and exergy efficiency, drying efficiency, energy utilisation, and specific energy consumption (SEC) during HAD and IRHAD. Data collected during HAD and IRHAD experiments were used to verify the developed thermodynamic model and to illustrate its applicability in assessing the energy and exergy use during drying of a beef slab. The results indicated that increasing the drying air temperature increased the energy and exergy efficiency while decreasing the specific energy consumption during HAD. However, increasing the air velocity decreased the energy and exergy efficiency and increased the SEC. The power level of the IR emitter significantly ($p \leq 0.05$) affected the efficiencies of the IRHAD. Increasing the level of power of the IR emitter increased both the energy and exergy efficiency, whereas increasing the drying air temperature and velocity decreased the energy and exergy efficiency during IRHAD. The IRHAD had significantly higher energy and exergy efficiency compared to HAD. The mathematical models presented in this study are useful in optimising drying of marinated beef during biltong processing. The models provide a scientifically sound basis for applying IRHAD in the processing of biltong.

Keywords: Ansys Fluent, Biltong, Computerised Fluid Dynamics, Energy, Heat and mass transfer, Modelling

DECLARATION ON PLAGIARISM

I, Francis Collins Muga, declare that:

- (i) The research reported in this thesis, except where otherwise indicated, is my original work.
- (ii) This thesis has not been submitted for any degree or examination at any other university.
- (iii) This thesis does not contain other persons' data, pictures, graphs or other information unless specifically acknowledged as being sourced from other persons.
- (iv) This thesis does not contain other persons' writing unless specifically acknowledged as being sourced from other persons. Where other written sources have been cited, then;
 - (a) Their words have been re-written, but the general information attributed to them has been referenced.
 - (b) Where their exact words have been used, their writing has been placed inside quotation marks and referenced.
- (v) Where I have reproduced a publication of which I am an author, co-author or editor, I have indicated in detail which part of the publication was written by myself alone and have fully referenced such publications.
- (vi) This thesis does not contain text, graphics or tables copied and pasted from the Internet, unless specifically acknowledged, and the source being detailed in this thesis and the references section.

Signed: _____ Date// 2021

FC Muga

Supervisor: _____ Date// 2021

Prof TS Workneh

Co-supervisor: _____ Date// 2021

Dr MO Marenya

DECLARATION OF PUBLICATIONS

All the research papers, manuscripts, and presentations in this thesis were conceptualised by FC Muga (student) together with TS Workneh and MO Marenya (supervisors). FC Muga conducted the research, analysed the data, and prepared the manuscripts. The supervisors, TS Workneh and MO Marenya reviewed the manuscripts.

Published papers

Muga, F. C., Workneh, T. S., and Marenya, M. O. 2020. Modelling the thin layer drying of beef biltong processed using hot air drying. *Journal of Biosystems Engineering*, 45(4): 362-373. DOI: <https://doi.org/10.1007/s42853-020-00076-5>.

Muga, F. C., Marenya, M. O., and Workneh, T. S. 2021. Modelling the thin layer drying kinetics of marinated beef during infrared-assisted hot air processing of biltong. *International Journal of Food Science*, 2021(2021): 1-14. DOI: <https://doi.org/10.1155/2021/8819780>.

Muga, F. C., Marenya, M. O., and Workneh, T. S. 2021. A heat and mass transfer model for predicting the drying of beef during biltong processing using infrared assisted hot air drying. *Journal of Biosystems Engineering*, (online). DOI: <https://doi.org/10.1007/s42853-021-00105-x>.

Manuscripts under peer review

Muga, F. C., Workneh, T. S., and Marenya, M. O. A review of the state of art in biltong processing. *Meat Science*. Manuscript ID MEATSCI-D-20-00359.

Muga, F. C., Workneh, T. S., and Marenya, M. O. Thermodynamic modelling of the hot air drying and infrared assisted hot air drying of beef biltong. *Journal of Food and Bioprocess Technology*. Manuscript ID FABT-D-21-00404.

Paper presented at conference (Webinar)

Muga, F. C., Marenya, M. O., and Workneh, T. S. 2020. Modelling the thin-layer drying kinetics of marinated beef during infrared-assisted hot air processing of biltong. Postgraduate Research and Innovation Symposium (PRIS) – UKZN. Online, South Africa. 10th – 11th December 2020.

ACKNOWLEDGEMENTS

I wish to express my sincere appreciation to my supervisors, Prof TS Workneh and Dr MO Marenya, for their guidance and critique throughout my research study and in the preparation of this thesis. Additionally, I am grateful to Prof TS Workneh for availing the research and subsistence funds for this study. The financial support was critical for the smooth running and completion of this research.

I would like to gratefully acknowledge the following persons for their assistance during this study.

- i. Ms Natasha Moneyvalu, the Administrator in the Department of Bioresources Engineering, University of KwaZulu-Natal.
- ii. Messrs Alan Hill and Thabo Hlatshwayo, formerly the Technical Manager and the Technical Assistant, respectively, in the Agricultural Engineering Workshop, University of KwaZulu-Natal. They played an important role in the setup and instrumentation of the research equipment.
- iii. Ms Elsie Correia, Chief Technologist in the Department of Dietetics and Human Nutrition, University of KwaZulu-Natal. Her guidance in developing the biltong marinade and sample preparation procedures was instrumental in this work.
- iv. Dr Winnie Martins and the entire staff at the Centre for Community Justice and Development (CCJD) for providing a conducive accommodation and social support during my studies.
- v. Dr Mubanga Chisenga for his invaluable friendship, guidance, and social support.
- vi. My fellow postgraduate students, Tinashe Dirwai, Luwam Ziena, Reiner Omondi, and Tageldeen Ibrahim.

Finally, I am entirely grateful to my family, relatives, and friends for their endless prayers, emotional support, and encouragements during my studies.

SUPERVISORS' APPROVAL

Subject to the regulations of the School of Engineering, we the supervisors of the candidate, consent to the submission of this thesis for examination.

Supervisor: _____ Date// 2021
Prof TS Workneh

Co-supervisor: _____ Date// 2021
Dr MO Marenya

In memory of my father

SAMWEL ONYANDO SUDHE

TABLE OF CONTENTS

	Page
PREFACE	ii
ABSTRACT	iii
DECLARATION ON PLAGIARISM.....	v
DECLARATION OF PUBLICATIONS	vi
ACKNOWLEDGEMENTS.....	vii
SUPERVISORS' APPROVAL	viii
TABLE OF CONTENTS	x
LIST OF FIGURES	xiv
LIST OF TABLES.....	xvii
LIST OF ABBREVIATIONS AND SYMBOLS	xix
1.INTRODUCTION	1
1.1 Aim and Objectives.....	3
1.2 Outline of The Thesis.....	4
1.3 References	5
2.REVIEW ON THE PROCESSING AND MODELLING OF THE DRYING OF BILTONG.....	10
2.1 Introduction.....	11
2.2 Quality of Biltong	11
2.2.1 Physical quality of biltong.....	11
2.2.2 Microbial quality of biltong.....	12
2.3 Biltong Processing	13
2.3.1 Selection and preparation of meat	13
2.3.2 Marination of meat	15
2.3.3 Drying of meat.....	17
2.4 Infrared Drying.....	19
2.4.1 Effect of IR on food quality.....	19
2.4.2 Effect of IR on food safety	20
2.4.3 IR drying kinetics	22
2.5 Modelling The Drying Process	23
2.5.1 Thin layer drying models.....	25

2.5.2	Modelling the heat and mass transfer during drying	28
2.5.3	Computational methods	32
2.6	Discussion	33
2.7	Conclusion.....	35
2.8	References	35
3.	MODELLING THE THIN-LAYER DRYING OF BEEF BILTONG PROCESSED USING HOT AIR DRYING.....	50
3.1	Introduction	51
3.2	Materials and Methods	53
3.2.1	Sample preparation	53
3.2.2	The drying unit	53
3.2.3	Drying procedure	55
3.2.4	Evaluation of the drying characteristics and thin layer modelling of the drying curves	55
3.3	Results and Discussion.....	59
3.3.1	Drying characteristics	59
3.3.2	Thin layer modelling of the drying curves	64
3.3.3	Effective moisture diffusivity	69
3.3.4	Activation energy.....	70
3.4	Conclusion.....	71
3.5	References	72
4.	MODELLING THE THIN-LAYER DRYING KINETICS OF MARINATED BEEF DURING INFRARED ASSISTED HOT AIR PROCESSING OF BILTONG.....	78
4.1	Introduction	79
4.2	Materials and Methods	80
4.2.1	Sample preparation	80
4.2.2	The drying unit	80
4.2.3	Drying experiments	81
4.2.4	Evaluation of the drying characteristics	82
4.2.5	Selection of the best thin layer drying model	82
4.3	Results and Discussion.....	83

4.3.1	IR emitter temperature	83
4.3.2	Core temperature of the beef sample during drying	84
4.3.3	Drying time	88
4.3.4	Drying rate	91
4.3.5	Effective moisture diffusivity	94
4.3.6	Activation energy	95
4.3.7	Selection of the best thin layer drying model	96
4.4	Conclusion	98
4.5	References	99
5.A HEAT AND MASS TRANSFER MODEL FOR PREDICTING THE DRYING OF BEEF DURING BILTONG PROCESSING USING INFRARED ASSISTED HOT AIR DRYING.....		
		105
5.1	Introduction	107
5.2	Development of The Coupled Heat and Mass Transfer Model for IRHAD of Beef Biltong	109
5.2.1	Momentum equation	111
5.2.2	Heat transfer	111
5.2.3	Mass transfer	114
5.2.4	Boundary and initial conditions	115
5.2.5	Heat and mass transfer coefficients	116
5.2.6	Thermophysical properties of beef	117
5.2.7	Model Inputs	118
5.3	Implementation and Solution of The Heat and Mass Transfer Model	119
5.3.1	Geometry and mesh generation	120
5.3.2	Implementation of the CFD model	121
5.4	Materials and Methods	122
5.4.1	Sample preparation	122
5.4.2	The drying unit	122
5.4.3	Drying experiments	123
5.4.4	Validation of the heat and mass transfer model	123
5.5	Results and Discussion	123
5.5.1	Air flow characteristics	123

5.5.2	Temperature distribution	125
5.5.3	Mean moisture content and temperature curves	127
5.5.4	Model validation	128
5.6	Conclusion.....	130
5.7	References	130
6.	THERMODYNAMIC MODELLING OF THE HOT AIR DRYING AND INFRARED ASSISTED HOT AIR DRYING OF BEEF BILTONG	136
6.1	Introduction.....	138
6.2	Development of The Thermodynamic Model for The HAD and IRHAD of Beef Biltong	139
6.2.1	Energy analysis.....	140
6.2.2	Exergy analysis.....	142
6.2.3	Determination of the thermophysical properties of air and meat	145
6.2.4	Model Inputs	145
6.3	Materials and Methods.....	146
6.3.1	Sample preparation	146
6.3.2	The drying unit	146
6.3.3	Drying experiments	147
6.3.4	Thermodynamic model verification and data analysis	147
6.4	Results and Discussion.....	147
6.4.1	Energy Analysis.....	147
6.4.2	Exergy Analysis.....	157
6.5	Conclusion.....	159
6.6	References	160
7.	conclusion and recommendation	165
7.1	Conclusion.....	165
7.2	Recommendations	169
8.	Appendix	170
8.1	Appendix A.....	170
8.2	Appendix B	174
8.3	Appendix C	176
8.4	Appendix D.....	181

LIST OF FIGURES

	Page
Figure 2.1 Beef cuts (Beef + Lamb, 2019)	14
Figure 2.2 Piece of beef silverside cut along the meat fibres	15
Figure 2.3 Effect of pH on water holding capacity of meat (Miller (2014)).	16
Figure 3.1 A schematic representation of the drying unit; 1 - weighing balance, 2 - digital control panel, 3 - power knob, 4 - drying platform, 5 - beef sample, 6 - K-type thermocouple, 7 - anemometer, 8 - temperature datalogger, and 9 - computer monitor	54
Figure 3.2 Average sample temperature curves versus time at drying air temperatures of 30, 35, and 40 °C; and drying air velocities of 1.5 (V1) and 2.5 m.s-1 (V2).....	60
Figure 3.3 Curves of moisture ratio versus drying time of marinated beef at drying air temperatures of 30, 35, and 40 °C; and air velocities of 1.5 (V1) and 2.5 m.s-1 (V2).....	61
Figure 3.4 Curves of the drying rate versus time (a) and the rate of change in sample temperature vs time (b)	62
Figure 3.5 Experimental and predicted MR curves of the best three models at: (a) 30 °C and 1.5 m.s-1 (b) 35 °C and 1.5 m.s-1 (c) 35 °C and 2.5 m.s-1 (c) 40 °C and 2.5 m.s-1	68
Figure 3.6 Arrhenius relationship between Deff and temperature at drying air velocity	71
Figure 4.1 Schematic of the drying cabinet; 1 - Weighing balance, 2 - Digital control panel,	81
Figure 4.2 Variation in core temperature of the beef sample during drying at selected IR emitter power temperature and air velocity of the drying air (V1 = 1.5 m.s-1 and V2 = 2.5 m.s-1)	87
Figure 4.3 Variation in the MR of marinated beef during IRHAD.....	90
Figure 4.4 Variation in the drying rate and the rate of change in the core temperature of the beef sample during drying.....	93

Figure 4.5	Activation Energy of marinated beef under different IRHAD experimental conditions.....	95
Figure 4.6	Comparison between the MR predicted by the Two-Term model and the experimental MR for all the drying conditions	98
Figure 5.1	A schematic representation of the coupled heat and mass transfer during IRHAD process; 1 - IR radiation, 2 - convective heat transfer, 3 - evaporation, 4 - incoming drying air, 5 - outgoing moist drying air, 6 - volumetric heating due to absorbed IR radiation, 7 - internal heat transfer, 8 - internal moisture transfer	110
Figure 5.2	Flowchart of the procedure for the implementation of the heat and mass transfer model and simulation of temperature and moisture content during IRHAD	119
Figure 5.3	The 2D geometry of the beef sample and the surrounding drying air; 1 – beef sample, 2 – incoming drying air, 3 – outgoing moist drying air	120
Figure 5.4	The final mesh generated from Ansys Fluent for use in the simulation of the heat and mass transfer	121
Figure 5.5	Velocity contour around the beef sample; 1 – recirculation zone, 2 – beef sample,	124
Figure 5.6	Turbulence intensity of the drying air around the beef sample	124
Figure 5.7	Temperature distribution in meat at different times during drying. The temperature scale is in Kelvin (K).....	126
Figure 5.8	Experimental and predicted moisture content at an IR power level of 750 W, drying air temperature of 30 °C and drying air velocity of 2.5 m.s-1	127
Figure 5.9	Experimental and simulated core temperature of the beef sample at an IR power level of 750 W, drying air temperature of 30 °C and drying air velocity of 2.5 m.s-1	128
Figure 5.10	Comparison between the predicted and actual MR at an IR power level of 1000 W, drying air temperature of 40 °C and velocity of 1.5 m.s-1	129
Figure 5.11	Comparison between the predicted and experimental core sample temperature at IR power level of 1000 W, drying air temperature of 40 °C and velocity of 1.5 m.s-1	129

Figure 6.1	The exchange of energy and mass during IRHAD process; 1 – IR radiation, 2 – convective heat transfer from hot air to product, 3 - evaporation, 4 - incoming drying air, 5 - outgoing moist drying air, 6 – IR energy absorbed by the product.....	139
Figure 6.2	Energy efficiency and specific energy consumption at the selected HAD conditions ($V_1 = 1.5 \text{ m.s}^{-1}$ and $V_2 = 2.5 \text{ m.s}^{-1}$). Means with the same letter are not significantly different according to Fisher's unprotected least significant difference test ($p < 0.05$)	148
Figure 6.3	Variations in the energy efficiency of IRHAD with IR emitter power level and drying air temperature at (a) 1.5 m.s^{-1} and (b) 2.5 m.s^{-1} . Means with the same letter are not significantly different according to Fisher's unprotected LSD test ($p < 0.05$)	151
Figure 6.4	Variations in energy utilisation and energy efficiency over time during IRHAD at 500 W (a, d), 750 W (b, e), and 1000 W (c, f).....	155
Figure 6.5	Variation in exergy efficiency with the drying air temperature and velocity during HAD ($V_1 = 1.5 \text{ m.s}^{-1}$ and $V_2 = 2.5 \text{ m.s}^{-1}$). Means with the same letter are not significantly different according to Fisher's unprotected LSD test ($p < 0.05$)	158
Figure 6.6	Variations in the exergy efficiency of IRHAD with IR emitter power level and drying air temperature at (a) 1.5 m.s^{-1} and (b) 2.5 m.s^{-1} . Means with the same letter are not significantly different according to Fisher's unprotected LSD test ($p < 0.05$)	159
Figure 8.1	Layout of the laboratory drying unit	170
Figure 8.2	Top view of the laboratory drying unit	171
Figure 8.3	Front view of the laboratory drying unit	172
Figure 8.4	Left view of the laboratory drying unit	173
Figure 8.5	Standard k- ϵ model parameters	176
Figure 8.6	Solution setup in Ansys Fluent.....	177
Figure 8.7	Residual monitors for convergence	178
Figure 8.8	Solution initialization methods.....	179
Figure 8.9	Run calculation setup	180

LIST OF TABLES

	Page
Table 2.1 Growth conditions for microorganisms identified in biltong	13
Table 2.2 Biltong drying equipment and process parameters (after Jones et al. (2017))	17
Table 2.3 Quality attributes of food subjected to IR treatment	20
Table 2.4 Summary of thin layer drying models used in IR drying	27
Table 3.1 Thin layer drying models.....	58
Table 3.2 Average drying rate (Dr) in the first 10 hrs and the entire drying period	64
Table 3.3 Model coefficients and statistical parameters for Two term, Approximation of diffusion and Midilli models	65
Table 3.4 Model coefficients and Statistical parameters for Page, Logarithmic and Simplified diffusion models	66
Table 3.5 Effective moisture diffusivity of marinated beef during hot air drying	69
Table 4.1 Selected thin layer drying models used in the study (Muga et al., 2020)	82
Table 4.2 Temperature of the IR emitter	83
Table 4.3 Average core temperature of the beef sample	85
Table 4.4 Summary of the drying time for marinated beef at the selected drying conditions	88
Table 4.5 Effective moisture diffusivity of marinated beef during IRHAD	94
Table 4.6 The average R ² and RMSE for the thin layer models at different IR power levels.....	96
Table 4.7 Model coefficient and statistical parameters for the Two-Term thin-layer drying model.....	97
Table 5.1 Model input parameters	118
Table 6.1 Model input parameters	146
Table 6.2 Heat and mass transfer coefficient and energy content of drying air at selected drying conditions during HAD.....	149

Table 6.3	Temperature of the IR emitter, IR intensity and the IR energy absorbed by the marinated meat sample during IRHAD at selected drying conditions	150
Table 6.4	Specific energy consumption at the selected IRHAD conditions	152
Table 6.5	Improvement in energy efficiency during IRHAD over energy efficiency during HAD.....	156
Table 6.6	Comparison between the energy and drying efficiency at selected IRHAD conditions.....	157
Table 8.1	ANOVA results for the IR emitter temperature	174
Table 8.2	ANOVA results for the core temperature of the beef sample	174
Table 8.3	ANOVA results for the drying time	175
Table 8.4	ANOVA results for the SEC	175

LIST OF ABBREVIATIONS AND SYMBOLS

A	Surface area, m^2	T	Temperature, K
c_p	Specific heat, $J.kg^{-1}.K^{-1}$	u	Velocity, $m.s^{-1}$
C	Moisture concentration, $mol.m^{-3}$	V	Volume, m^3
D	Moisture diffusivity of beef, $m^2.s^{-1}$	W	Width of IR emitter, m
D_a	Mass diffusivity of air-vapour, $m^2.s^{-1}$	y	Mass fraction
ex	Specific exergy, $J.kg^{-1}$	Z	Distance between the emitter and the surface of the sample, m
\dot{E}	Energy flow rate, W		
\dot{E}_x	Exergy rate, W		
EU	Energy utilisation rate, W		
F	Shape view factor		
h	Heat transfer coefficient, $W.m^{-2}.K^{-1}$		
h_m	Mass transfer coefficient, $m.s^{-1}$		
h_{lv}	Latent heat of evaporation, $J.kg^{-1}$		
HAD	Hot air drying		
IR	Infrared		
IRD	Infrared drying		
IRHAD	Infrared assisted hot air drying		
K	Thermal conductivity of beef, $W.m^{-1}.K^{-1}$		
L	Length of IR emitter, m		
Le	Lewis number		
m	Molecular mass, $kg.mol^{-1}$		
\dot{m}	Mass flow rate, $kg.s^{-1}$		
M	Moisture content wet basis, $kg.kg^{-1}$		
P	Pressure, Pa		
P_0	Rate of radiation heat transfer, W		
QIR	volumetric IR heat source, $W.m^{-3}$		
R_t	Total thermal resistivity, m^{-2}		
SEC	Specific energy consumption, $J.kg^{-1}$		
t	Time, s		

Subscripts

<i>a</i>	Air
<i>abs</i>	Absorbed energy
<i>b</i>	Beef
<i>c</i>	Carbohydrates
<i>des</i>	Destruction
<i>D</i>	Drying
<i>eff</i>	Effective
<i>eq</i>	Equilibrium
<i>ev</i>	Evaporation
<i>ex</i>	Exergy
<i>E</i>	Energy
<i>f</i>	Fats
<i>HAD</i>	Hot air drying
<i>in</i>	Inlet
<i>IR</i>	Infrared emitter
<i>IRHAD</i>	Infrared assisted hot air drying
<i>out</i>	Outlet
<i>p</i>	Protein
<i>t</i>	Instantaneous
<i>w</i>	Water
<i>0</i>	Initial

Greek letters

α	IR absorption coefficient
α_a	Thermal diffusivity of air, $\text{W.m}^{-1}.\text{K}^{-1}$
β	Quality factor
P	Density, kg.m^{-3}
δ	IR penetration depth, m
ε	Emissivity
μ	Viscosity of air, Pa.s^{-1}
η	Efficiency
σ	Stefan-Boltzmann constant, $\text{W.m}^{-2}.\text{K}^{-4}$

1. INTRODUCTION

Biltong is a dried meat product that is predominantly consumed in South Africa. The market for biltong has expanded both locally and internationally (Attwell, 2003), prompting its increased production. The market value of biltong in South Africa was estimated at US\$ 170 million in 2015 (Jones *et al.*, 2017). However, the expansion and acquisition of new markets for biltong is hampered by its food safety concerns and inconsistent quality characteristics (Attwell, 2003; Burfoot *et al.*, 2010).

Biltong is widely made from beef and game meat (kudu, springbok and gemsbok), chicken, or ostrich (Dzimba *et al.*, 2007; Naidoo and Lindsay, 2010a; Strydom and Zondagh, 2014; Jones *et al.*, 2017). The meat is cut into thin slices and marinated with a mixture of salt, vinegar, and dry spices (Muga *et al.*, 2020). Traditionally biltong is sun dried (Strydom and Zondagh, 2014). However, the rising popularity of biltong has spurred the development of a variety of biltong dryers. The available dryers range from simple domestic types to high capacity commercial hot air dryers.

The variety in driers and recipes used by biltong producers result in a wide range of physico-chemical properties *viz.* moisture content, salt content, water activity, and pH (Van der Riet, 1976; Osterhoff and Leistner, 1984; Attwell, 2003; Nortjé *et al.*, 2005; Petit *et al.*, 2014; Strydom and Zondagh, 2014). In addition, biltong production methods are not entirely inhibitory to microbial contamination (Wolter *et al.*, 2000; Burfoot *et al.*, 2010; Mhlambi *et al.*, 2010; Naidoo and Lindsay, 2010a; Naidoo and Lindsay, 2010c; Allotey *et al.*, 2014). The conventional hot air drying (HAD) method used in commercial production of biltong, does not achieve the recommended microbial levels in the resultant biltong (Nortjé *et al.*, 2005). Furthermore, HAD is a slow and energy intensive drying method that significantly degrades the physical quality of dried biltong (Ratti, 2001; Sharma and Prasad, 2001; Kowalski and Mierzwa, 2009). Case hardening (Bellagha *et al.*, 2007) and shrinkage (Duan *et al.*, 2011), are of particular concern to biltong producers. These concerns underscore the need for alternative drying methods that would preserve the quality and ensure the microbial safety of biltong in a cost-effective way.

Novel heating technologies like microwave, inductive heating, radio frequency, and infrared (IR) provide volumetric heating that positively impacts on the energetic, exergetic, and heating efficiency (Rastogi, 2012). Li *et al.* (2018) reported that IR radiation improved the dehydration efficiency of beef jerky (a dried meat product popular in the Americas). Similarly, Cheronno *et al.* (2016) reported that the drying rates of beef improved during IR drying (IRD) of biltong. Moreover, the IR dried biltong exhibited lower microbial loads than the hot air dried biltong. However, moisture condensation observed on the surface of biltong during IRD highlights the inability of natural convection to cope with the increased drying rates during IRD (Cheronno, 2014; Cheronno *et al.*, 2016). A combined infrared and hot air drying (IRHAD) could accelerate the removal of moisture from the meat surface to sustain the high drying rates. Drying agricultural products using IRHAD requires less energy and produces dried products of higher quality compared to using IRD or HAD independently (Afzal *et al.*, 1999; Hebbar *et al.*, 2004).

Understanding the dehydration process is key to the development of new efficient drying methods (Defraeye, 2014). According to Jones *et al.* (2017), the drying kinetics of meat during biltong processing have not been sufficiently characterised. Recent studies (Cheronno, 2014; Jones, 2017) have provided some insight into the HAD kinetics of meat during biltong production. Cheronno (2014) reported the drying kinetics during IRD of beef biltong and selected the approximation of diffusion model as the most suitable thin layer drying model. Other studies have identified suitable models for the IRD and IRHAD of agricultural products such as; Page model for IRD of rice (Abe and Afzal, 1997; Das *et al.*, 2004), Midilli model for IRHAD of apple, murta berries, wine grape pomace, and tomato slices (Toğrul, 2005; Puente-Díaz *et al.*, 2013; Sui *et al.*, 2014), and Logarithmic model for IRD of sweet potatoes (Doymaz, 2012). Nevertheless, there is no documented study on the drying kinetics or the drying models suitable for the IRHAD of beef for biltong production.

Modelling and simulation tools are useful in decoding the mechanism of the drying processes and predicting the drying behaviour of products (Feyissa *et al.*, 2009; Onwude *et al.*, 2018). Drying of food materials causes changes such as evaporation of water, shrinkage, pore formation, case-hardening, and colour changes (Yang *et al.*, 2001; Talla *et al.*, 2004; Tornberg, 2005; Jefferson *et al.*, 2006; Adler-Nissen, 2007; Datta, 2007; Purlis, 2010). Such changes may directly influence the heat and mass transfer processes or influence the heat and mass transfer properties

during drying (Feyissa *et al.*, 2009). The mechanistic modelling of the transfer of heat and mass during the IRHAD of meat is critical in the design, application, and optimisation of IRHAD as an alternative methods of processing biltong.

Mechanistic models of heat and mass transfer are complex and require computerised numerical methods to solve. Computational fluid dynamics (CFD) based software such as COMSOL Multiphysics and Ansys Fluent have been used to solve the partial differential equations that constitute the heat and mass transfer models (Solomon *et al.*, 2021). Several researchers (Erriguible *et al.*, 2007; Wang *et al.*, 2008; Feyissa *et al.*, 2009; Feyissa *et al.*, 2013; Darabi *et al.*, 2015; Onwude *et al.*, 2018; Khan *et al.*, 2020; Pham *et al.*, 2020; Solomon *et al.*, 2021) have used these software to implement the heat and mass transfer models and predict the temporal and spatial variations in temperature and moisture content during the drying of food materials.

Drying is an energy intensive process, thus improving the energy use efficiency is critical in reducing the costs associated with the drying of food materials (Aghbashlo, 2016). Evaluating the energy and exergy available at different points in the system informs the selection of optimal operating conditions and parameters that aid in the design, analysis, and optimisation of the drying systems (Aghbashlo *et al.*, 2008; Liu *et al.*, 2019; Golpour *et al.*, 2020). A number of studies (Midilli and Kucuk, 2003; Akbulut and Durmuş, 2010; Nazghelichi *et al.*, 2010; Reyes *et al.*, 2013; Şevik *et al.*, 2013; Liu *et al.*, 2019; Golpour *et al.*, 2020; Lingayat *et al.*, 2020) have analysed the energy and exergy during the drying of food materials. However, there is no literature on the analysis of the energy and exergy usage during the drying of beef to produce biltong at different drying conditions. Evaluating the energy and exergy usage during the drying of beef for biltong production using HAD and IRHAD would highlight the suitability of IRHAD as an alternative to HAD in biltong production.

1.1 Aim and Objectives

The aim of this study was to model the infrared assisted hot air drying of beef being processed into biltong. The specific objectives of the study were to:

- i. evaluate the drying kinetics during HAD and IRHAD of beef being processed into biltong,

- ii. evaluate the suitability of selected thin layer drying models for simulating the HAD and IRHAD of beef being processed into biltong,
- iii. formulate the governing equations and boundary conditions for the coupled heat and mass transfer process during the IRHAD of beef biltong,
- iv. identify the numerical solution for the coupled heat and mass transfer model using CFD and validate the model using experimental data,
- v. formulate and verify a thermodynamic model for evaluating the energy and exergy use during HAD and IRHAD of beef being processed into biltong.

1.2 Outline of The Thesis

The thesis comprises of seven chapters:

- | | |
|-----------|--|
| Chapter 1 | Introduction |
| Chapter 2 | Provides a detailed review on the processing of biltong with a major focus on the drying methods. The chapter identifies IR as a potential heat source during the processing of biltong. A detailed review of the IR drying kinetics and the strategies for modelling the heat and mass transfer is also provided. |
| Chapter 3 | Focuses on the drying kinetics of beef during processing of biltong using HAD. The chapter also details the selection of a suitable thin layer drying model for predicting the moisture ratio during HAD of beef being processed into biltong. |
| Chapter 4 | Focuses on the drying kinetics of beef during processing of biltong using IRHAD. The chapter also details the selection of a suitable thin layer drying model for predicting the moisture ratio during IRHAD of beef being processed into biltong. |
| Chapter 5 | Provides a detailed formulation of the coupled heat and mass transfer model for the IRHAD of beef biltong. The chapter outlines the implementation of the heat and mass transfer model in Ansys Fluent CFD software and the simulation of the temperature and moisture content of beef undergoing IRHAD. |
| Chapter 6 | Outlined the formulation of the thermodynamic model for the HAD and IRHAD of beef being processed into biltong. The chapter provides a detailed analysis of the variations in energy and exergy use during HAD and IRHAD of beef biltong. |

Chapter 7 Provides the overall conclusion and recommendation. It highlights the major findings of the study and makes recommendations for future work.

1.3 References

- Abe, T and Afzal, T. 1997. Thin-layer infrared radiation drying of rough rice. *Journal of Agricultural Engineering Research* 67 (4): 289-297.
- Adler-Nissen, J. 2007. Continuous wok-frying of vegetables: Process parameters influencing scale up and product quality. *Journal of food engineering* 83 (1): 54-60.
- Afzal, T, Abe, T and Hikida, Y. 1999. Energy and quality aspects during combined FIR-convection drying of barley. *Journal of food engineering* 42 (4): 177-182.
- Aghbashlo, M. 2016. Exergetic simulation of a combined infrared-convective drying process. *Heat and Mass Transfer* 52 (4): 829-844.
- Aghbashlo, M, Kianmehr, MH and Arabhosseini, A. 2008. Energy and exergy analyses of thin-layer drying of potato slices in a semi-industrial continuous band dryer. *Drying Technology* 26 (12): 1501-1508.
- Akbulut, A and Durmuş, A. 2010. Energy and exergy analyses of thin layer drying of mulberry in a forced solar dryer. *Energy* 35 (4): 1754-1763.
- Allotey, J, Gashe, BA, Coetzee, SH, Mpuchane, S, Khonga, EB, Matsheka, MI and Murindamombe, G. 2014. Microbial quality assessment and predominant microorganism of biltong produced in butcheries in Gaborone, Botswana. *Food and Nutrition sciences* 2014 (2014): 1 - 12.
- Attwell, E. 2003. Biltong wakes up. *Food Reviews* 30 (2): 11-13.
- Bellagha, S, Sahli, A, Farhat, A, Kechaou, N and Glenza, A. 2007. Studies on salting and drying of sardine (*Sardinella aurita*): Experimental kinetics and modeling. *Journal of Food Engineering* 78 (3): 947-952.
- Cherono, K. 2014. Infrared Drying of Biltong. Unpublished MSc thesis, Bioresources Engineering, University of KwaZulu-Natal, Pietermaritzburg, South Africa.

- Cherono, K, Mwithiga, G and Schmidt, S. 2016. Infrared drying as a potential alternative to convective drying for biltong production. *Italian journal of food safety* 5 (3): 140-145.
- Darabi, H, Zomorodian, A, Akbari, M and Lorestani, A. 2015. Design a cabinet dryer with two geometric configurations using CFD. *Journal of Food Science and Technology* 52 (1): 359-366.
- Das, I, Das, S and Bal, S. 2004. Drying performance of a batch type vibration aided infrared dryer. *Journal of Food Engineering* 64 (1): 129-133.
- Datta, A. 2007. Porous media approaches to studying simultaneous heat and mass transfer in food processes. II: Property data and representative results. *Journal of food engineering* 80 (1): 96-110.
- Defraeye, T. 2014. Advanced computational modelling for drying processes—A review. *Applied Energy* 131(1): 323-344.
- Doymaz, İ. 2012. Infrared drying of sweet potato (*Ipomoea batatas* L.) slices. *Journal of food science and technology* 49 (6): 760-766.
- Duan, Z-h, Jiang, L-n, Wang, J-l, Yu, X-y and Wang, T. 2011. Drying and quality characteristics of tilapia fish fillets dried with hot air-microwave heating. *Food and Bioproducts processing* 89 (4): 472-476.
- Dzimba, FEJ, Faria, J and Walter, EHM. 2007. Testing the sensory acceptability of biltong formulated with different spices. *African Journal of Agricultural Research* 2 (11): 547-577.
- Erriguible, A, Bernada, P, Couture, F and Roques, M-A. 2007. Simulation of vacuum drying by coupling models. *Chemical Engineering and Processing: Process Intensification* 46 (12): 1274-1285.
- Feyissa, AH, Adler-Nissen, J and Gernaey, K.2009. Model of Heat and Mass Transfer with Moving Boundary during Roasting of Meat in Convection-Oven. *Excerpt from the Proceedings of the COMSOL Conference, Milan, Italy,*
- Feyissa, AH, Gernaey, KV and Adler-Nissen, J. 2013. 3D modelling of coupled mass and heat transfer of a convection-oven roasting process. *Meat science* 93 (4): 810-820.
- Golpour, I, Kaveh, M, Chayjan, RA and Guiné, RP. 2020. Energetic and exergetic analysis of a convective drier: A case study of potato drying process. *Open Agriculture* 5 (1): 563-572.
- Hebbar, HU, Vishwanathan, K and Ramesh, M. 2004. Development of combined infrared and hot air dryer for vegetables. *Journal of food engineering* 65 (4): 557-563.

- Jefferson, D, Lacey, A and Sadd, P. 2006. Understanding crust formation during baking. *Journal of Food Engineering* 75 (4): 515-521.
- Jones, M. 2017. Profiling of traditional South African biltong in terms of processing, physicochemical properties and microbial stability during storage. Unpublished PhD thesis, Food Science, Stellenbosch University, Stellenbosch, South Africa.
- Jones, M, Arnaud, E, Gouws, P and Hoffman, LC. 2017. Processing of South African biltong—A review. *South African Journal of Animal Science* 47 (6): 743-757.
- Khan, MIH, Welsh, Z, Gu, Y, Karim, M and Bhandari, B. 2020. Modelling of simultaneous heat and mass transfer considering the spatial distribution of air velocity during intermittent microwave convective drying. *International Journal of Heat and Mass Transfer* 153(3): 119-126.
- Kowalski, SJ and Mierzwa, D. 2009. Convective drying in combination with microwave and IR drying for biological materials. *Drying Technology* 27 (12): 1292-1301.
- Li, X, Xie, X, Zhang, C-h, Zhen, S and Jia, W. 2018. Role of mid-and far-infrared for improving dehydration efficiency in beef jerky drying. *Drying Technology* 36 (3): 283-293.
- Lingayat, A, Chandramohan, V and Raju, V. 2020. Energy and exergy analysis on drying of banana using indirect type natural convection solar dryer. *Heat Transfer Engineering* 41 (6-7): 551-561.
- Liu, Z-L, Bai, J-W, Wang, S-X, Meng, J-S, Wang, H, Yu, X-L, Gao, Z-J and Xiao, H-W. 2019. Prediction of energy and exergy of mushroom slices drying in hot air impingement dryer by artificial neural network. *Drying Technology* 45 (5): 1-12.
- Mhlambi, S, Naidoo, K and Lindsay, D. 2010. Enterotoxin-producing *Staphylococcus* strains associated with South African biltong at point of sale. *Journal of food safety* 30 (2): 307-317.
- Midilli, A and Kucuk, H. 2003. Energy and exergy analyses of solar drying process of pistachio. *Energy* 28 (6): 539-556.
- Muga, F, Workneh, T and Marennya, M. 2020. Modelling the Thin-Layer Drying of Beef Biltong Processed Using Hot Air Drying. *Journal of Biosystems Engineering* 45 (4) 1-12.
- Naidoo, K and Lindsay, D. 2010a. Pathogens associated with biltong product and their in vitro survival of hurdles used during production. *Food Protection Trends* 30 (9): 532-538.

- Naidoo, K and Lindsay, D. 2010b. Survival of *Listeria monocytogenes*, and enterotoxin-producing *Staphylococcus aureus* and *Staphylococcus pasteurii*, during two types of biltong-manufacturing processes. *Food Control* 21 (7): 1042-1050.
- Nazghelichi, T, Kianmehr, MH and Aghbashlo, M. 2010. Thermodynamic analysis of fluidized bed drying of carrot cubes. *Energy* 35 (12): 4679-4684.
- Nortjé, K, Buys, E and Minnaar, A. 2005. Effect of γ -irradiation on the sensory quality of moist beef biltong. *Meat science* 71 (4): 603-611.
- Onwude, DI, Hashim, N, Abdan, K, Janius, R, Chen, G and Kumar, C. 2018. Modelling of coupled heat and mass transfer for combined infrared and hot-air drying of sweet potato. *Journal of Food Engineering* 13 (2): 228 12-24.
- Osterhoff, D and Leistner, L. 1984. South African biltong--another close look. *Journal of the South African Veterinary Association* 55 (4): 201-202.
- Petit, T, Caro, Y, Petit, A-S, Santchurn, SJ and Collignan, A. 2014. Physicochemical and microbiological characteristics of biltong, a traditional salted dried meat of South Africa. *Meat science* 96 (3): 1313-1317.
- Pham, ND, Khan, M and Karim, M. 2020. A mathematical model for predicting the transport process and quality changes during intermittent microwave convective drying. *Food chemistry* 325 (4): 12-32.
- Puente-Díaz, L, Ah-Hen, K, Vega-Gálvez, A, Lemus-Mondaca, R and Scala, KD. 2013. Combined infrared-convective drying of murta (*Ugni molinae* Turcz) berries: kinetic modeling and quality assessment. *Drying Technology* 31 (3): 329-338.
- Purlis, E. 2010. Browning development in bakery products--A review. *Journal of Food Engineering* 99 (3): 239-249.
- Rastogi, NK. 2012. Recent trends and developments in infrared heating in food processing. *Critical reviews in food science and nutrition* 52 (9): 737-760.
- Ratti, C. 2001. Hot air and freeze-drying of high-value foods: a review. *Journal of food engineering* 49 (4): 311-319.
- Reyes, A, Mahn, A, Cubillos, F and Huenulaf, P. 2013. Mushroom dehydration in a hybrid-solar dryer. *Energy conversion and management* 70 (3): 31-39.
- Şevik, S, Aktaş, M, Doğan, H and Koçak, S. 2013. Mushroom drying with solar assisted heat pump system. *Energy Conversion and Management* 72 (2): 171-178.

- Sharma, G and Prasad, S. 2001. Drying of garlic (*Allium sativum*) cloves by microwave–hot air combination. *Journal of food engineering* 50 (2): 99-105.
- Solomon, AB, Fanta, SW, Delele, MA and Vanierschot, M. 2021. Modeling and simulation of heat and mass transfer in an Ethiopian fresh injera drying process. *Heliyon* 7 (2): e06201.
- Strydom, P and Zondagh, B. 2014. Biltong: A major South African ethnic meat product. In: eds. Dikeman, M and Devine, C, *Encyclopaedia of meat sciences*. Academic Press, London, UK.
- Sui, Y, Yang, J, Ye, Q, Li, H and Wang, H. 2014. Infrared, convective, and sequential infrared and convective drying of wine grape pomace. *Drying Technology* 32 (6): 686-694.
- Talla, A, Puiggali, J-R, Jomaa, W and Jannot, Y. 2004. Shrinkage and density evolution during drying of tropical fruits: application to banana. *Journal of Food Engineering* 64 (1): 103-109.
- Toğrul, H. 2005. Simple modeling of infrared drying of fresh apple slices. *Journal of Food Engineering* 71 (3): 311-323.
- Tornberg, E. 2005. Effects of heat on meat proteins–Implications on structure and quality of meat products. *Meat science* 70 (3): 493-508.
- Van der Riet, W. 1976. Studies on the mycoflora of biltong. *S Afr Food Rev* 3 (1): 105-113.
- Wang, H, Yang, W, Senior, P, Raghavan, R and Duncan, S. 2008. Investigation of batch fluidized-bed drying by mathematical modeling, CFD simulation and ECT measurement. *AIChE Journal* 54 (2): 427-444.
- Wolter, H, Laing, E and Viljoen, BC. 2000. Isolation and identification of yeasts associated with intermediate moisture meats. *Food Technology and Biotechnology* 38 (1): 69-76.
- Yang, H, Sakai, N and Watanabe, M. 2001. Drying model with non-isotropic shrinkage deformation undergoing simultaneous heat and mass transfer. *Drying Technology* 19 (7): 1441-1460.

2. REVIEW ON THE PROCESSING AND MODELLING OF THE DRYING OF BILTONG

Sections of this chapter are based on the following manuscript.

Muga, F. C., Workneh, T. S., and Marenya, M. O. A review of the state of art in biltong processing. *Meat Science*. Manuscript number, MEATSCI-D-20-00359.

Abstract

The popularity of biltong as a ready-to-eat meat-based snack, continues to expand within South Africa and globally. Consumer demands for consistency in quality and safety, especially for European markets, is a major hindrance to the full exploitation of the increasing market opportunities. Previous research on biltong indicate that the current methods of processing meat into biltong are incapable of ensuring its microbial safety. Hence, the need to explore other technologies that are more efficient and can maintain the nutritive quality of biltong and ensure its microbiological safety. Infrared heating is an alternative drying method that produces dried products of better quality, significantly reduces the risk of pathogenic bacteria and toxigenic fungi, and impacts positively on the energetic, exergetic, and heating efficiency. A combined infrared heating and hot air drying offers significant advantages and could be a viable alternative to hot air drying for processing meat into biltong. The application of new technologies to dry agricultural products, require a scientific understanding of the drying process. Modelling the drying process is key to decoding the mechanisms of heat and water transport. This chapter gives an overview of the thin layer drying models and the mechanistic modelling approaches that can be applied in the drying of meat into biltong. The mechanistic models are complex in their formulation and solution. The chapter highlights some of the computerised tools that are useful for implementing the mechanistic heat and mass transfer models. Computerised fluid dynamics softwares such as Ansys Fluent and COMSOL Multiphysics have been highlighted as the most popular software for solving the heat and mass transfer models. Information presented in this chapter is helpful in improving the processing of biltong and other related meat products

Keywords: Biltong, Drying, Heat and mass transfer, Hot air drying, Infrared, Modelling.

2.1 Introduction

Biltong is a dried, spiced meat-based ready-to-eat snack that is widely consumed in South Africa (Cherono *et al.*, 2016). It can be compared to other dried meat products across the world such as; carne seca (Mexico), charqui (South America), jerky (USA), kilshi (Sahel), and rou gan (China) (Dzimba *et al.*, 2007; Mhlambi *et al.*, 2010; Petit *et al.*, 2014). Salt is the main curing agent. The salt, together with other spices contained in the marinating mixture, give biltong its distinctive flavour. Traditionally, biltong is dried under ambient conditions whereas commercial producers use convective hot air dryers (Naidoo and Lindsay, 2010c). Currently, both small and large scale biltong producers use a variety of recipes and processes to accommodate consumer demands (Strydom and Zondagh, 2014).

The market for biltong is expanding both locally and internationally. However, there is no official estimation of the annual biltong production in South Africa (Strydom and Zondagh, 2014; Jones *et al.*, 2017). Biltong has gained popularity in regional and international markets such as Namibia, Australia, New Zealand, USA, Canada, the United Kingdom, Denmark, Netherlands, and Switzerland (Attwell, 2003). Nonetheless, it is difficult to fully exploit these export opportunities. A majority of the biltong processing factories in South Africa do not have an EU and hazard analysis and critical control points (HACCP) certification which are crucial to exporting biltong to EU countries (Attwell, 2003; Jones *et al.*, 2017). Consumer demand for consistent quality is also a problem for local and regional market, as well as the international markets.

2.2 Quality of Biltong

There is a wide range in the physical and microbial quality attributes of biltong.

2.2.1 Physical quality of biltong

Biltong is produced using several recipes and drying methods which results in a wide array of characteristics reported in literature (Van der Riet, 1976; Osterhoff and Leistner, 1984; Nortjé *et al.*, 2005; Petit *et al.*, 2014; Strydom and Zondagh, 2014; Jones *et al.*, 2017). Meat being processed to biltong is dried to a weight loss of 50 % or more to accommodate consumer preferences (Strydom and Zondagh, 2014). A number of studies have reported a wide range of

moisture content (10 – 50 %) and water activity (0.54 – 0.93) (Van der Riet, 1976; Osterhoff and Leistner, 1984; Nortjé *et al.*, 2005; Petit *et al.*, 2014; Jones *et al.*, 2017). The salt content and the pH of biltong ranges between 2 – 11 % and 4.8 – 5.9, respectively (Petit *et al.*, 2014; Strydom and Zondagh, 2014).

Petit *et al.* (2014) classified biltong as either dry or moist, based on their moisture content. Biltong with moisture content ranging between 21 and 25 % were classified as dry while those with moisture content ranging between 35 and 42 % classified as moist. Attwell (2003) and Nortjé *et al.* (2005) reported an increase in consumer preference towards biltong of higher moisture content. The high level of moisture content increases the risk of microbial attack which shortens the potential shelf-life of the biltong.

2.2.2 Microbial quality of biltong

Although biltong is considered a safe product, some studies have raised concern over its microbial profile (Wolter *et al.*, 2000; Mhlambi *et al.*, 2010; Naidoo and Lindsay, 2010a; Naidoo and Lindsay, 2010c). These studies reported high levels of potential spoilage organisms as well as occasional presence of pathogens in biltong. The occurrence of pathogenic bacteria and toxigenic fungi such as *B. cereus* and *A. niger*, indicate the latent risk associated with biltong consumption (Allotey *et al.*, 2014).

Biltong can serve as a vector for foodborne pathogens such as *Listeria*, *Salmonella*, enterotoxigenic *Staphylococci spp* and *E. coli* O157:H7 (Abong'o and Momba, 2009; Naidoo and Lindsay, 2010a; Naidoo and Lindsay, 2010c). Outbreaks of foodborne illnesses associated with the consumption of biltong have previously been reported (Allotey *et al.*, 2014). One fatality and at least two cases of severe gastroenteritis outbreaks attributed to *Salmonella* have been documented in South Africa while 17 individuals died in Botswana as a result of consuming contaminated biltong (Allotey *et al.*, 2014).

Microbial growth studies have demonstrated that salt, presence of organic acids, and spices are not in themselves inhibitory to microbial contamination in biltong (Burfoot *et al.*, 2010). The pH, water activity (a_w), and temperature used during the processing of biltong, fall within the tolerable

limits for growth of some of the pathogenic microorganisms commonly found in biltong (Table 2.1). Therefore, it is important to critically examine the processes of making biltong with a view to improving its food safety while maintaining the nutritional properties and improving the energy efficiency of the process.

Table 2.1 Growth conditions for microorganisms identified in biltong

Microorganism	Growth conditions	Reference
<i>Bacillus Cereus</i>	Temperature range = 12-37 °C pH = 4.9-10.0 a_w = 0.93-0.99	ICMSF (1996)
<i>Staphylococci Aureus</i>	Temperature range = 37-45 °C pH = 4.0-10.0 a_w = 0.83-0.99	Stewart (2003) Montville and Matthews (2008)
<i>Listeria monocytogenes</i>	Temperature range= 30-37 °C pH = 4.0-9.6 a_w = 0.90-0.97 a_w = 0.81-0.97	Lado and Yousef (2007) Lado and Yousef (2007) Johnson <i>et al.</i> (1988)
<i>Salmonella</i>	Temperature range = 35-43 °C pH = 3.8-9.5 a_w = 0.93-0.99	Podolak <i>et al.</i> (2010)
<i>Escherichia Coli O157:H7</i>	Temperature range 30-40 °C pH = 4.4-9.0 a_w = 0.950-0.995	Desmarchelier and Grau (1997)

2.3 Biltong Processing

Biltong is processed in a series of steps beginning with the selection and preparation of meat, followed by marination, and finally drying of the meat.

2.3.1 Selection and preparation of meat

Meat from young carcasses is preferred since old animals produce tough, sinewy biltong. Muscles low in connective tissue from the round (buttock) and sometimes from the loin and tenderloin are used (Strydom and Zondagh, 2014). Topside (semimembranosus) and silverside

(biceps femoris) are the most preferred muscles for making biltong. Other popular muscles include; eye of round (semitendinosus), thick flank (rectus abdominus), and fillet (psoas) (Jones *et al.*, 2017). The different cuts available from a whole beef carcass are shown in Figure 2.1

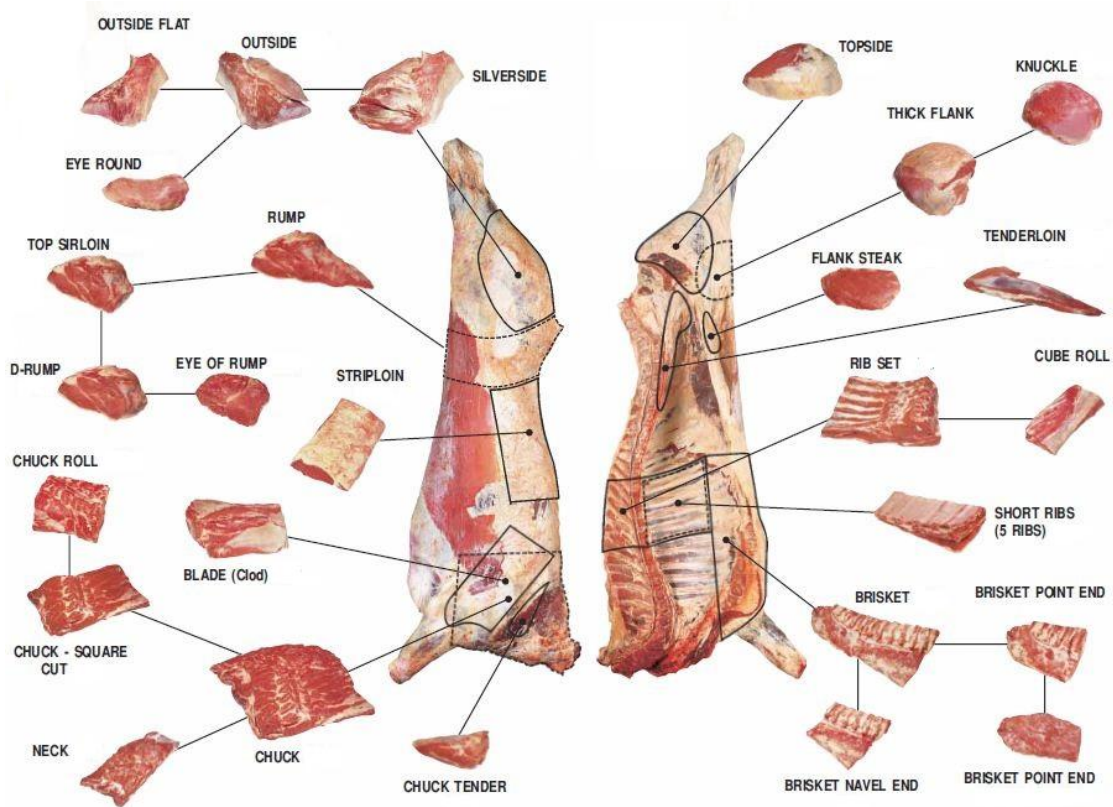


Figure 2.1 Beef cuts (Beef + Lamb, 2019)

The meat is generally cut along the meat fibres, into thin long strips (Van der Riet, 1982) as shown in Figure 2.2. The average dimensions of biltong strips range between 1 – 5 cm thick, 4 – 15 cm wide and 30 – 60 cm long (Van der Riet, 1982; Prior, 1984; Nortjé *et al.*, 2005; Naidoo and Lindsay, 2010c; Strydom and Zondagh, 2014). According to Jones *et al.* (2017), cutting the meat parallel to the meat fibres enhances the salt and spice absorption during marination of the meat, and improves the texture of the biltong. Eating quality and appearance of biltong could also be enhanced by cutting the meat diagonally across the grain (Jones *et al.*, 2017).



Figure 2.2 Piece of beef silverside cut along the meat fibres

While ostrich and game meat produce lean biltong, beef biltong can sometimes be fatty. Fatty biltong is gaining popularity with consumers (Strydom and Zondagh, 2014). However, excess fat should be trimmed off to avoid rancidity and low salt absorption by the meat (Strydom and Zondagh, 2014). According to Palumbo *et al.* (1977), fat can also decrease the water diffusivity of meat, consequently, increasing the drying time of meat during biltong production.

2.3.2 Marination of meat

Marination is the process of soaking meat in a liquid before drying. Salt and vinegar are the basic ingredients of a biltong marinade (Strydom and Zondagh, 2014). A vast array of seasonings such as; coriander, black paper, and brown sugar are included in the marinating mixture to provide biltong consumers with flavours (Burfoot *et al.*, 2010).

Salt acts as a curing agent during marination. The salt lowers the moisture content of meat through osmotic dehydration (Guizani *et al.*, 2008; Hui, 2012). Moreover, the salt reduces the water activity of the meat by immobilising the water molecules, making them unavailable for chemical, enzymatic, or microbial activity. Adding a 2 % salt solution to meat can potentially reduce the water activity of meat to between 0.97-0.93 (Toldrá, 2010). Salt solution of between

2.5 – 4.0 % is normally used for biltong (Van der Riet, 1976; Van der Riet, 1982). This range of salt concentration can reduce the water activity of meat to ≤ 0.93 , thus, inhibiting the growth of bacteria responsible for meat spoilage (Lawrie, 2017).

Similar to salt, vinegar is added to influence the flavour, inhibit microbial growth and influence water holding capacity of biltong (Naidoo and Lindsay, 2010c; Strydom and Zondagh, 2014). Brown spirit vinegar and apple cider vinegar are commonly used in biltong production (Jones *et al.*, 2017). The level of vinegar added to biltong ranges between 3 and 6 % (Naidoo and Lindsay, 2010c). The dilute acetic acid contained in vinegar reduces the ionic strength of meat by lowering the pH of the meat proteins from 6.0 to around 5.0 which is the isoelectric point of meat proteins (Cheng and Sun, 2008; Hui, 2012; Brewer, 2014). The minimum water holding capacity of meat occurs at the isoelectric point (Brewer, 2014). The meat losses water through drip as the pH moves closer to the isoelectric point (Miller, 2014). The variations in the water holding capacity of meat with changing pH is shown in Figure 2.3.

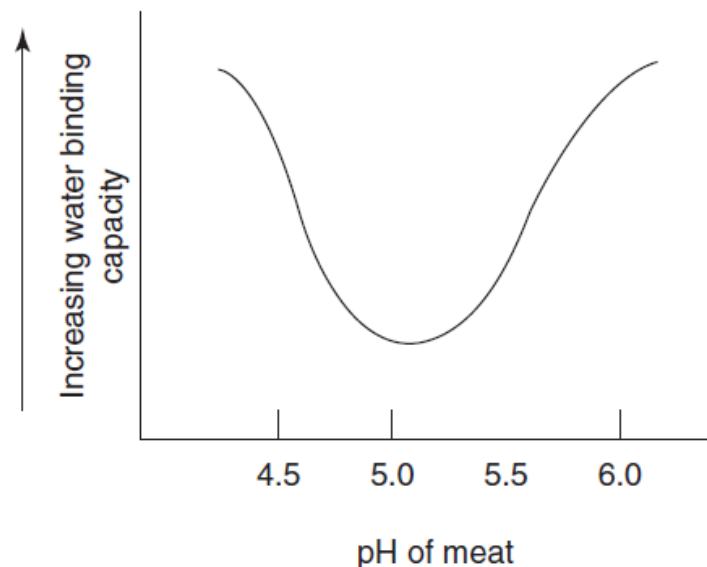


Figure 2.3 Effect of pH on water holding capacity of meat (Miller (2014)).

Biltong marinade also includes an array of seasonings such as black pepper, brown sugar, and coriander. The marinade is applied in several ways depending on the scale of production. For domestic biltong production;

- i. the meat can be dipped in dry spices (Van der Riet, 1976), or
- ii. dipped in dry spices then dipped in vinegar (Leistner, 1987), or
- iii. dipped in vinegar, drained, then dipped in dry spices (Naidoo and Lindsay, 2010c).

In the case of commercial biltong production, the meat pieces are dipped in a marinade made of a mix of vinegar and spice. Tumbling is done immediately after to ensure the meat is fully coated with marinade (Naidoo and Lindsay, 2010c). The meat is refrigerated at 4 °C for 18 – 20 hours prior to drying (Burfoot *et al.*, 2010). The refrigerated storage period allows for osmotic dehydration, water loss through drip, and ensures uniform distribution of the moisture content in meat, prior to drying.

2.3.3 Drying of meat

Traditionally biltong is produced by hanging marinated pieces of meat to dry under ambient conditions. Currently, biltong drying units range from simple domestic dryers to high capacity commercial dryers (Burfoot *et al.*, 2010; Naidoo and Lindsay, 2010c). Commercial dryers are predominantly temperature controlled with only a few having both temperature and humidity control (Jones *et al.*, 2017). A summary of various drying equipment and their process parameters is given in Table 2.2.

Table 2.2 Biltong drying equipment and process parameters (after Jones *et al.* (2017))

Equipment	Temperature (°C)	RH (%)	Air Velocity (m/s)	Time (days)	Reference
Homemade dryer with a bulb	25	-	-	4	Naidoo and Lindsay (2010c)
Environmental chamber	20-22	38-64	-	17-26	Burnham <i>et al.</i> (2008)
Drying cabinet	35	-	-	-	Dzimba <i>et al.</i> (2007)
Drying cabinet	28-32	70	-	2	Nortjé <i>et al.</i> (2005)
Drying cabinet	35	30	3	6	Taylor (1976)

Commercial biltong dryers use hot air to dry the meat to the desired moisture content. Hence, the hot air parameters *viz.* temperature, relative humidity, and velocity must be well chosen to obtain the desired product. Generally, the drying air temperature used when processing biltong ranges from 25 to 35 °C (Jones *et al.*, 2017). There is little scientific literature on the levels of drying air relative humidity and velocity that is appropriated for processing biltong (Table 2.2). It is necessary to characterise the hot air drying parameters (Temperature, relative humidity, and velocity) since they have a huge implication on the drying kinetics of meat during biltong processing, the quality of biltong produced, and the energy consumption (Chabbouh *et al.*, 2011; Hii *et al.*, 2014; Ahmat *et al.*, 2015; Kucerova *et al.*, 2015; Petrova *et al.*, 2015).

HAD is an energy intensive drying method. Drying products using HAD is slow and degrades the quality of the dried product (Ratti, 2001; Sharma and Prasad, 2001). HAD has been associated with deleterious physical and nutritional quality effects such as loss of colour, loss of heat sensitive nutrients, and deformation or even internal structure damage (Kowalski and Mierzwa, 2009).

HAD imposed changes such as case hardening (Bellagha *et al.*, 2007) and shrinkage (Duan *et al.*, 2011) may be of concern during biltong production. Case hardening is caused by rapid drying due to high drying temperatures coupled with low relative humidity and high air velocity. The high surface evaporation rates dry out the surface quickly and prevents the moisture inside the meat from moving out (Serra *et al.*, 2005).

During HAD of meat products, the loss of water and mobility of the solid matrix makes the meat to shrink which causes stress in the cellular structure of the meat (Mayor and Sereno, 2004). Shrinkage can also be caused by the drying of collagen, transforming it into soluble gelatin. Prolonged heating and drying causes gelatin to bind the muscle fibres, forming an intact structure, which causes the meat to bend, and become tough (Huang and Nip, 2001). This phenomenon may result in undesirable biltong that is difficult to eat.

HAD is extensively used in the drying of meat products such as pork and beef (Poligné *et al.*, 2001; Banout *et al.*, 2012; Strydom and Zondagh, 2014). However, the low thermal conductivity and case hardening of the material decelerate the moisture migration during HAD of meats. This

results in longer drying time and increases energy consumption (Soydan Karabacak *et al.*, 2014). The need to heat up the drying air coupled with low thermal conductivity of the food material, further amplifies the energy demands (Łechtańska *et al.*, 2015). The thermal energy necessary for drying can, alternatively, be supplied through electromagnetic waves such as IR and microwaves. IR heating transfers energy directly to the product without heating the surrounding air, thus, improving the energy efficiency and reducing the drying time (Riadh *et al.*, 2015).

2.4 Infrared Drying

IR radiation can replace, or supplement HAD to enhance the overall efficiency of the drying process. IR radiation transfers thermal energy in the form of electromagnetic waves which are converted into heat when they impinge on the surface of a product (Krishnamurthy *et al.*, 2008b). IR radiation generates heat directly inside the product providing volumetric heating (Khir *et al.*, 2011; Riadh *et al.*, 2015). This positively impacts the energetic, exergetic, and heating efficiency (Onwude *et al.*, 2016). Infrared heating results in uniform product heating, reduced processing time, lower energy consumption, and better nutritional value of the processed product (Pan *et al.*, 2014; El-Mesery and Mwithiga, 2015). Consequently, IR heating has been applied widely in recent years in different thermal processing operations in the food industry such as pasteurization, drying, and frying (Riadh *et al.*, 2015).

2.4.1 Effect of IR on food quality

The suitability of IR for drying a given food product depends on the quality (sensory, nutritional and functional) attributes of the final product. Some quality loss may be observed in heat sensitive products such as fruits and vegetable during IR drying (Pan and Atungulu, 2010a). Nonetheless, IR drying generally results in minimal quality losses in the final product (Riadh *et al.*, 2015). A study by Cheroni *et al.* (2016) highlighted the improved colour, texture and microbial quality of biltong dried using IR. A summary of some of the quality attributes of different food materials subjected to IR drying or heating is shown in Table 2.3.

Table 2.3 Quality attributes of food subjected to IR treatment

Method	Food	Food quality	Reference
IR drying	Beef jerky	Improved dehydration efficiency	Li <i>et al.</i> (2018)
IR drying	Biltong	Improved colour, texture, microbial quality	Cherono <i>et al.</i> (2016)
IR drying	Beef	Similar taste and colour to HAD	Burgheimer and Nelson (1971)
IRHAD IR and heat pump	Longan fruit	less shrinkage and less hardness	Nathakaranakule <i>et al.</i> (2010)
IRHAD	Onion	Better rehydration capacity	Kumar <i>et al.</i> (2005)
IR freeze drying	Yam	High rehydration ratio	Lin <i>et al.</i> (2007)
IR drying	Lentils	Better rehydration capacity Dark colour	Arntfield <i>et al.</i> (2001)
IR drying	Onion	Dark colour	Gabel <i>et al.</i> (2006)
IR heating	Deli turkey	Roasted appearance and brown colour	Muriana <i>et al.</i> (2004)
IR drying	Noodles	Reduced cooking loss Reduced loss in total organic matter	Basman and Yalcin (2011)

2.4.2 Effect of IR on food safety

Food safety is a key concern to consumers and processors alike. Food safety can be compromised by enzymes or microorganisms that degrade the food. IR heating can be used for enzyme inactivation to limit food spoilage (Krishnamurthy *et al.*, 2008b). The enzymatic reactions involving lipases and α amylases are affected by IR radiation at a bulk temperature of 30 to 40 °C (Kohashi *et al.*, 1993; Rosenthal *et al.*, 1996; Sawai *et al.*, 2003). Kouzeh-Kanani *et al.* (1982) reported a 95.5 % inactivation of lipoxygenase (an enzyme responsible for deterioration in soybeans) within 60 s of IR treatment. The findings by Van Zuilichem *et al.* (1986) showed that

far IR successfully inactivated enzymes responsible for the development of off-flavours in peas, while Sawai *et al.* (2003) reported that IR treatment inactivated several enzymes and bacteria.

Nonchemical decontamination of pathogenic microorganisms is possible through proper application of IR heating (Pan *et al.*, 2014). The efficacy of using IR heating for food safety enhancement has been studied for various applications such as pathogen inactivation (Krishnamurthy *et al.*, 2010), milk sterilization (Krishnamurthy *et al.*, 2008a; Krishnamurthy *et al.*, 2008b), fruit surface decontamination (Tanaka *et al.*, 2007; Tanaka and Uchino, 2010), almond pasteurization (Bari *et al.*, 2009; Yang *et al.*, 2010), rice disinfestation (Pan *et al.*, 2008), and improving the microbial quality of biltong (Cherono *et al.*, 2016).

IR heating can inactivate bacteria, spores, yeast, and mold in both liquid and solid foods (Rastogi, 2012). Sawai *et al.* (2006) indicated that the death rate constant of *E. coli* is higher for far-IR heating than conductive heating. Jun and Irudayaraj (2003) showed that selective far-IR heating (5.88 to 6.66 μm) resulted in 40 % increase in inactivation of *A. niger* and *F. proliferatum* in cornmeal as compared to normal IR heating. The absorption of energy by the fungal spores increased during selective heating, leading to a higher lethality rate (Jun and Irudayaraj, 2003). Conversely, Hamanaka *et al.* (2006) reported that pathogen inactivation was higher at IR radiations of shorter wavelengths than longer wavelength (0.95 > 1.1 > 1.15 μm). The foregoing studies demonstrate that inactivation efficiency using IR is dependent on the radiation spectrum.

IR radiation has a poor penetration capacity which makes it mostly suited for surface decontamination (Riadh *et al.*, 2015). The effect of IR radiation on the microbial inactivation diminishes as the sample thickness increases (Sawai *et al.*, 1997). Decreasing the sample thickness accelerates the inactivation of spores, *E. coli*, and *S. aureus* (Hashimoto *et al.*, 1992; Sawai *et al.*, 1997; Sawai *et al.*, 2006). Rosenthal *et al.* (1996) indicated that IR heating at 70 °C for 5 min effectively reduced the growth of yeasts and fungi on the surface of cheese without affecting the quality of the product. In related studies, James *et al.* (2002) demonstrated the potential use of IR treatments to pasteurize the surface of eggs without significantly raising the interior temperature that would otherwise cause coagulation of egg contents.

Huang (2004) indicated the suitability of IR for the surface pasteurization of turkey frankfurters. IR heating to 80, 75, and 70 °C reduced the counts of *L. monocytogenes* by 4.5, 4.3, and 3.5 log units, respectively. IR pasteurization can also be used to effectively inactivate *L. monocytogenes* and *E. coli* on ready-to-eat meats such as hotdogs (Huang and Sites, 2008) and biltong (Cherono *et al.*, 2016), respectively.

IR drying is a promising method that is best suited for thin, flat products (Riadh *et al.*, 2015). It is not easily applicable to food products with irregular shape and sizes as this would result in uneven heating (Krishnamurthy *et al.*, 2008b). Furthermore, prolonged exposure to IR heat can adversely affect the physical, mechanical, chemical, and functional properties of biological material (Fasina *et al.*, 1996; Fasina *et al.*, 1997). These limitations can be overcome by combining IR heating with other drying methods (Riadh *et al.*, 2015). Some typical applications of IR heating combined with other drying methods include; vacuum IR drying of carrots (Nimmol *et al.*, 2005), IR microwave drying of beetroot (Kowalski and Mierzwa, 2009), and combined IR and HAD (IRHAD) of sweet potatoes (Onwude *et al.*, 2018).

Application of combined electromagnetic radiation and convective heating is more efficient over the independent use of radiation or convective heating (Krishnamurthy *et al.*, 2008b). According to Afzal *et al.* (1999), IRHAD has a more synergistic effect which results in improved physical and nutritional quality as well as energy conservation, compared to the independent use of either IR or HAD. Findings by Hebbar *et al.* (2004) confirmed that the synergistic effect of IR and hot air promotes rapid heating that results in a higher rate of mass transfer during IRHAD of vegetables. Hebbar *et al.* (2004) observed a 48 % reduction in drying time and improved energy utilisation efficiency in IRHAD of potato and carrot.

2.4.3 IR drying kinetics

The drying kinetics of agricultural materials depend on the process conditions and their properties (Arsoy, 2008). The IR energy is transferred from the IR emitter to the material surface without heating the surrounding air. Hence, most of the energy coming from the IR emitter is delivered to the material being dried (Wang and Sheng, 2004). Consequently, the power density in IR drying is 6 – 10 times greater than in HAD (Abukhalifeh *et al.*, 2005).

Applying a high power density to a material can significantly reduce the drying time. Bualuang *et al.* (2013) observed that increased IR intensity shortened drying time due to higher heat and mass transfer coefficient and increased rate of diffusion. Similar findings were made by Chen *et al.* (2012) and Ponkham *et al.* (2012). According to Doymaz (2012) the IR density directly relates to the effective diffusivity and inversely affects the drying time. Findings by Nasiroglu and Kocabiyik (2009) showed that the increase in the infrared power and the decrease in the air velocity caused a reduction in the drying time of red pepper.

The drying behavior of food subjected to IR radiation is also dependent on the distance between the IR emitter and the sample being dried (Ježek *et al.*, 2008; Kocabiyik and Tezer, 2009). Increasing the distance between the IR emitter and the sample increases drying time due to reduction of energy transfer to the product (Sadin *et al.*, 2014). According to Nathakaranakule *et al.* (2010), varying the distance between the IR emitter and the sample being dried significantly affected the IR intensity and subsequently the drying rate of longan fruit during IRHAD. A critical assessment of the drying parameters of interest is necessary to improve the efficiency of the drying processes and quality of the dried products. Mathematical modelling provides an effective way of assessing and manipulating the process parameters to determine the optimal drying conditions.

2.5 Modelling The Drying Process

The HAD and IRHAD are thermal food processing techniques. Modelling these drying processes is essential in evaluating their performance and safety of the dried products (Riadh *et al.*, 2015). Mathematical models and simulations represent a powerful alternative to the traditional, time-consuming temperature/moisture measurements, and microbiological and food quality analyses (Feyissa *et al.*, 2009). Moreover, the models can be used to predict the influence of the process variables on the drying kinetics and quality parameters of dried products (Pawar and Pratape, 2017). Drying processes can be modelled using distributed models or lumped parameter models (Erbay and Icier, 2010).

The simultaneous heat and mass transfer are satisfactorily predicted using distributed models. The distributed models predict the temperature and moisture gradient in a product by considering

both the external and internal heat and mass transfer (Erbay and Icier, 2010). These models depend on the Luikov equations (Equation 2.1 – 2.3) which are derived from Fick's second law of diffusion (Luikov, 1975).

$$\frac{\delta M}{\delta t} = \nabla^2 K_{11}M + \nabla^2 K_{12}T + \nabla^2 K_{13}P \quad (2.1)$$

$$\frac{\delta T}{\delta t} = \nabla^2 K_{21}M + \nabla^2 K_{22}T + \nabla^2 K_{23}P \quad (2.2)$$

$$\frac{\delta P}{\delta t} = \nabla^2 K_{31}M + \nabla^2 K_{32}T + \nabla^2 K_{33}P \quad (2.3)$$

Where:

t = drying time (s),

M = moisture content of the product (kg of water/kg of sample),

T = temperature of the product (K),

P = pressure (Pa),

K₁₁, K₂₂, K₃₃ = phenomenological coefficients, and

K₁₂, K₁₃, K₂₁, K₂₃, K₃₁, K₃₂ = coupling coefficients.

According to Brooker *et al.* (1992), the effect of pressure can be neglected, giving rise to the modified Luikov equations (Equations 2.4 and 2.5).

$$\frac{\delta M}{\delta t} = \nabla^2 K_{11}M + \nabla^2 K_{12}T \quad (2.4)$$

$$\frac{\delta T}{\delta t} = \nabla^2 K_{21}M + \nabla^2 K_{22}T \quad (2.5)$$

The modified Luikov equations cannot be solved analytically. Their numerical solution is obtained using the finite element method (Özilgen and Özdemir, 2001). Further modification of the Luikov equations can enable their analytical solution through the lumped parameter models. The lumped parameter models assume a uniform product temperature distribution, that is equal

to the drying air temperature (Erbay and Icier, 2010). The Luikov equations, as used in the lumped parameter models, is as expressed in Equations 2.6 and 2.7.

$$\frac{\delta M}{\delta t} = K_{11} \nabla^2 M \quad (2.6)$$

$$\frac{\delta T}{\delta t} = K_{22} \nabla^2 T \quad (2.7)$$

The phenomenological coefficients, K_{11} and K_{22} become the effective moisture diffusivity (D_{eff}) and thermal diffusivity (α), respectively. For a constant D_{eff} and α , Equations 2.6 and 2.7 can be rewritten as shown in Equation 2.8 and 2.9 (Ekechukwu, 1999).

$$\frac{\delta M}{\delta t} = D_{eff} \left[\frac{\delta^2 M}{\delta x^2} + \frac{a_1}{x} \frac{\delta M}{\delta x} \right] \quad (2.8)$$

$$\frac{\delta T}{\delta t} = \alpha \left[\frac{\delta^2 T}{\delta x^2} + \frac{a_1}{x} \frac{\delta T}{\delta x} \right] \quad (2.9)$$

Where:

$a_1 = 0, 1, \text{ or } 2$ for planar, cylindrical, and spherical geometry, respectively, and

$D_{eff} = \text{effective moisture diffusivity (m}^2 \cdot \text{s}^{-1}\text{)}.$

The assumption of uniform temperature distribution that is equivalent to the ambient temperature causes errors which can be minimised by reducing the thickness of the product (Erbay and Icier, 2010). Hence the thin layer drying models.

2.5.1 Thin layer drying models

Thin layer drying models assumes isothermal conditions during the drying process; thus, they only describe the mass transfer. The fundamental assumptions (Erbay and Icier, 2010) made during the development of thin layer drying models enable the analytical solution of Equation 2.8, as shown in Equation 2.10 (Crank, 1979).

$$MR = \frac{8}{\pi^2} \sum_{n=0}^{\infty} \frac{1}{(2n+1)^2} \times \exp \left[-(2n+1)^2 \frac{\pi^2 D_{\text{eff}} t}{b^2} \right] \quad (2.10)$$

Where:

MR = moisture ratio, and

b = half thickness of the sample in case of a slab (m).

The MR is calculated using Equation 2.11 (Ertekin and Firat, 2017).

$$MR = \frac{M(t)}{M_0} \quad (2.11)$$

Where:

M_0 = initial moisture content of the sample (kg of water/kg of dry solid), and

$M(t)$ = moisture content of the sample at time t (kg of water/kg of dry solid).

The thin layer drying models describe the variation of MR with drying time. Several thin layer drying models have been developed and used to describe the drying of different food materials (Ertekin and Firat, 2017). The appropriateness of a given model is determined through regression analysis of the experimental data and the selected models (Kucuk *et al.*, 2014). The best models are chosen based on high coefficient of determination (R^2) and modeling efficiency, and low values for mean bias error (MBE), root mean square error (RMSE), chi square (χ^2), and the sum of residuals (Workneh and Muga, 2018). Some of the thin layer drying models used to describe the IR drying of food materials are listed in Table 2.4.

Table 2.4 Summary of thin layer drying models used in IR drying

	Drying method	Food material	Model	Model Equation	Reference
1	IRHAD	Onion slices	Modified page	$MR = K \exp(-t/d^2)^n$	Kumar <i>et al.</i> (2006)
2	IR	Sweet potato slices	Logarithmic model	$MR = a \exp(-kt)$	Doymaz (2012)
3	IRHAD	Murta berries	Midili <i>et al.</i>	$MR = a \exp(-kt^n) + bt$	Puente-Díaz <i>et al.</i> (2013)
4	IRHAD	Wine grape pomace	Midili <i>et al.</i>	$MR = a \exp(-kt^n) + bt$	Sui <i>et al.</i> (2014)
5	IR	Peach slices	Midili <i>et al.</i>	$MR = a \exp(-kt^n) + bt$	Doymaz (2014)
6	IR	Biltong	Diffusion approximation model	$MR = a \exp(-kt) + (1 - a) \exp(-kbt)$	Cherono (2014)
7	IR	Mint leaves	Modiffied Henderson and Pabis-II	$MR = a \exp(-kt^n) + b \exp(-gt) + C \exp(-ht)$	Ertekin and Heybeli (2014)
8	IRHAD	Shredded squids	Page model	$MR = \exp(-kt^n)$	Wang <i>et al.</i> (2014)
9	IR	Jujube	Two term model	$MR = a \exp(-k_0t) + b \exp(-k_1t)$	Chen <i>et al.</i> (2015)
10	IRHAD	Green peas	Three term model	$MR = a \exp(-k_0t) + b \exp(-k_1t) + C \exp(-k_2t) + d$	Eshtiagh and Zare (2015)
11	IRHAD	Tomato slices	Midili <i>et al.</i>	$MR = a \exp(-kt^n) + bt$	Sadin <i>et al.</i> (2017)

The thin layer drying models are practical and give acceptable results. These models are less demanding computationally, hence easily are adopted for automated control of drying processes (Ertekin and Firat, 2017). However, their use is limited to the prediction of average moisture content and drying time for the drying conditions at which they were developed (Erbay and Icier, 2010). The mechanistic modelling of the heat and mass transfer during the drying process using distributed models provides a better understanding of the drying process and gives more accurate results compared to the thin layer drying models (Özilgen and Özdemir, 2001).

2.5.2 Modelling the heat and mass transfer during drying

The heat and mass transfer play an important role in drying of products (Srikiatden and Roberts, 2007). The temperature and water content inside a solid food product vary in space and time during heat treatment (Feyissa *et al.*, 2009). Their entire history and spatial distribution influence the quality and the safety of the processed foods. A solid food system undergoes several changes during drying. The food system undergoes phase changes during evaporation of water (Adler-Nissen, 2007; Datta, 2007), shrinkage and pore formation (Yang *et al.*, 2001; Talla *et al.*, 2004; Tornberg, 2005), crust formation (Jefferson *et al.*, 2006), and colour change (Purlis, 2010) during drying processes. These changes may influence the heat and mass transfer mechanisms directly (e.g., phase change, formation of porous media) or influence the heat and mass transfer properties such as thermal conductivity, diffusivity and permeability (Feyissa *et al.*, 2009).

The heating of solid foods involve external and internal heat transfer processes (Therdthai and Zhou, 2003). External heat transfer takes place between the heating medium (fluid or solid) and the solid food, whereas internal heat transfer takes place within the solid food itself. The external heat transfer is often considered as the boundary condition governing heat transfer (Bird *et al.*, 2001). A solid food and a heating medium exchange heat at their boundaries by conduction, convection or radiation, or a combination of these mechanisms (Gupta, 2001; Therdthai and Zhou, 2003).

The governing equations for the heat transfer inside a solid food is based on the principle of conservation of energy (Bird *et al.* 2001). The convective heat flux at the boundary of the food is characterised by the surface heat transfer coefficient (Incropera and Dewitt, 1981). The surface

heat transfer coefficient is a critical parameter in the model of heat transfer and it can be determined using the time-temperature matching method, heat flux method, dimensionless correlation, and the lumped parameter method (Feyissa *et al.*, 2009). The lumped parameter method assumes a spatially uniform temperature in the calculation of the surface heat transfer coefficient. Feyissa *et al.* (2013) and (Onwude *et al.*, 2018) used the lumped parameter method to determine the heat transfer coefficient of meat and sweet potatoes during hot air roasting and IRHAD respectively.

The IR heat flux is dependent on the surface temperature and radiation properties of the food material (Krishnamurthy *et al.*, 2008a; Pan and Atungulu, 2011). The IR energy absorption and extinction in food materials is described by the Lambert's law of electromagnetic extinction (Prakash, 2011; Tanaka and Uchino, 2011). IR power absorption by food can be considered as an exponential decay function penetrating from the surface to the interior of food materials (Datta and Ni, 2002; Tanaka and Uchino, 2011). Consequently, the IR power absorption is modelled as a volumetric heat source term in the energy balance equation (Onwude *et al.*, 2018). Alternatively, all the IR energy can be absorbed at the food surface without penetration into the food. Therefore, the heat flux of IR radiation is incorporated in the boundary condition at the modeled food surface (Li, 2012). At shallow (<1 mm) IR penetration depths, no significant difference has been found in the accuracy of temperature prediction when the IR radiation is modelled as a volumetric heat source term or as a boundary layer condition (Prakash, 2011; Tanaka and Uchino, 2011).

Drying of food materials is also characterized by mass loss mainly in the form of water (Mondal and Datta, 2008; Sumnu and Sahin, 2008). The transport of water is driven by the gradients in the water concentration. Water migrates during the heating of solid foods by different mechanisms: molecular diffusion, pressure driven flow, capillary diffusion, and thermo-diffusions (Srikiatden and Roberts, 2007). The governing equation for mass transfer in solid foods is based on the principle of conservation of mass (Bird *et al.*, 2001; Celma *et al.*, 2008; Ponkham *et al.*, 2012).

A number of water transport models are based on the Fick's equation of diffusion (Feyissa *et al.*, 2009). The ensuing transient diffusion equation for water transport is solved using experimentally

determined effective diffusivity (Shilton *et al.*, 2002; Wang and Singh, 2004; Kondjoyan *et al.*, 2006). However, not all water transport during heating of solid foods can be attributed to diffusion. Other phenomena such as pressure-driven flow is critical during intensive heating such as roasting of meat. According to Srikiatden and Roberts (2007) better predictions of moisture distribution for drying of porous materials could be obtained if Fick's diffusion equation is expressed in terms of vapor pressure gradient as the driving force for diffusion rather than moisture concentration gradient.

The mechanisms of water transport during the drying of food and bio-based materials is determined by the composition and structural makeup of the material (Feyissa *et al.*, 2009). A major portion of whole meat is water (75 %), with the remaining portion made up of proteins (20 %), fat (3 %), and non-soluble protein (2 %) (Tornberg, 2005). Water in the meat muscle is held within the cell structures as bound, immobilised, and free water (McDonnell *et al.*, 2013). Free water is easily lost through drip, whereas immobilised water can be removed through heating. Bound water has low mobility and is resistant to conventional heating (Huff-Lonergan and Lonergan, 2005).

The movement of bound water can be induced through electromagnetic drying such as IR, microwave, and UV heating methods. The heat denatures the myofibrillar protein and causes other physicochemical changes that are reflected in the microstructure of the meat muscle (Aguilera, 2005; Tornberg, 2005). The induced structural changes generate compressive stresses that expels more water from the meat structure causing shrinkage of the meat. Tornberg (2005) reported multidirectional shrinkage in meat during cooking that resulted into large irregularities in the shape of the final product. The extent of shrinkage increases with increase in temperature, subsequently accelerating the water loss from the meat.

Incorporating shrinkage in the model for water transport is key to accurate prediction of water movement in meat during drying. Some studies (Van der Sman, 2007; Feyissa *et al.*, 2009; Feyissa *et al.*, 2013) have catered for shrinkage by incorporating the pressure driven flow in the model for water transport. Van der Sman (2007) quantitatively described the pressure that drives water transport in meat using the Flory-Rehner theory. Feyissa *et al.* (2009) and Feyissa *et al.* (2013) used the Darcy's Law of porous media to model the water flow inside meat as a function

of the pressure gradient. Studies by Kumar *et al.* (2015), Kumar *et al.* (2016) and Onwude *et al.* (2018) incorporated shrinkage in their water transport models by using shrinkage dependent moisture diffusivity values that were determined based on the thickness ratio of the product during drying.

The transfer of heat and mass transfer in a food material occurs simultaneously. A number of coupled heat and mass transfer models have been developed to simulate the drying of food material. Liu *et al.* (2014) developed a mathematical model of heat and mass transfer based on energy and diffusion equations, to simulate vacuum far-IR drying of potato slices. Ranjan *et al.* (2002) used the control volume formulation to develop a three-dimensional model for IR heating based on moisture transfer, heat, and pressure equations. A combined heat and mass transfer model was developed by Rudobashta *et al.* (2014) to analyze the dynamics of oscillating IR heating of a layer of seeds. Islam *et al.* (2007) presented results of a simple diffusion-based model to predict the drying performance of a pilot-scale twin-drum dryer.

A multiphase model developed by Datta and Ni (2002) for energy and moisture determination could also simulate the temperature and moisture profiles of food during drying. Dagerskog (1979) successfully predicted the temperature distribution of slices of beef undergoing IRHAD. Salagnac *et al.* (2004) developed a one-dimensional model based on temperature and moisture content of a porous material. The Salagnac *et al.* (2004) model successfully described the heat and mass transfer during IRHAD of a rectangular-shaped porous material. However, none of these models considered key drying factors such as evaporation, shrinkage dependent moisture distribution, and variable material properties.

Kumar *et al.* (2015) used both evaporation and shrinkage dependent diffusivity to successfully develop a coupled heat and mass transfer model for HAD of banana. In a related study, Kumar *et al.* (2016) developed a coupled multiphase heat and mass transfer model for apple undergoing intermittent combined microwave and HAD. The model considered evaporation, shrinkage dependent effective moisture diffusivity and microwave heat source based on Lambert's law. It acceptably explained the drying process and mechanism of intermittent microwave and HAD of an apple. Similarly, Onwude *et al.* (2018) developed a coupled heat and mass transfer model to

describe the mechanism of the IRHAD of sweet potato by considering evaporation, shrinkage dependent moisture distribution and IR heating source based on Lambert's law.

The heat and mass transfer models consist of a number of partial differential equations that cannot be solved analytically (Özilgen and Özdemir, 2001). The solutions to these equation are obtained using computerized numerical techniques that are based on the finite difference, finite element, or finite/control volume methods (Srikiatden and Roberts, 2007).

2.5.3 Computational methods

COMSOL Multiphysics, Ansys Fluent, and MATLAB are the most popular computerised mathematical tools for solving the coupled heat and mass transfer equations (Solomon *et al.*, 2021). COMSOL Multiphysics and Ansys Fluent are computational fluid dynamics (CFD) based computer software. Several studies (Feyissa *et al.*, 2009; Feyissa *et al.*, 2013; Onwude *et al.*, 2018; Khan *et al.*, 2020; Pham *et al.*, 2020) have used COMSOL Multiphysics to implement and simulate different drying models. Similarly, Ansys Fluent has been used to predict the heat and moisture transfer during drying of food products (Erriguible *et al.*, 2007; Wang *et al.*, 2008; Darabi *et al.*, 2015).

Multidimensional models have been increasingly investigated in order to gain more insight into IR heating characteristics (Tanaka *et al.*, 2007; Dhall *et al.*, 2009; Prakash, 2011). Tanaka *et al.* (2007) used a three-dimensional geometry of a real strawberry to simulate IR radiation for the surface decontamination. The complex view factors caused by the irregular shape of the strawberry, were quantified using the Monte Carlo ray tracing approach integrated in ANSYS software (Tanaka *et al.*, 2007). Howell *et al.* (2015) outlines the different mathematical routines developed for computing the radiation view factors of complex geometric configurations for multidimensional models. IR irradiance flux calculated from the view factors on strawberry surface was incorporated into a Neumann boundary condition to solve the heat transfer problem in strawberry (Tanaka *et al.*, 2007). The multidimensional models are complex in their formulation and solution. However, they provide a detailed account of heat and mass transfer mechanisms and give better prediction of the drying process.

A three-dimensional geometric model developed by Li *et al.* (2011) accurately described the variability in shape and size of tomatoes. Using the model, the temperature distribution on the surface and within a tomato undergoing a double-sided IR heating for a dry-peeling process was satisfactorily predicted. IR irradiance of the tomato surface was calculated based on differential view factors using the hemicube method implemented in COMSOL Multiphysics . Onwude *et al.* (2018) also used COSMOL Multiphysics to solve a coupled heat and mass transfer model for IRHAD of sweet potatoes.

2.6 Discussion

The increased demand of biltong both locally and internationally makes it an economically important product in the South African meat industry. Quality-conscience export markets in Europe and the USA highlight the need to standardise the production methods of biltong. It is evident from the literature reviewed that there is limited control in production of biltong. Consequently, there is a wide spectrum of biltong characteristics. Moreover, existing literature highlight food safety concerns of consuming biltong owing to the lack of control of its production process. The food safety concerns, and inconsistent quality characteristic hamper the expansion of existing markets and acquisition of new markets for biltong.

The microbial and fungal contamination in biltong is mainly prevented using vinegar and by reducing the water activity through salting and drying of the meat. The addition of vinegar and other ingredients in the marinating mixture lowers the pH from 6.0 in raw meat to a value ranging between 4.8 and 5.9 in biltong. This range of pH (4.8 – 5.9) falls within the tolerable limits of most microorganisms found in biltong (Table 2.1, §2.2.3). Thus, the addition of vinegar is not enough to inhibit the growth of spoilage and potentially toxic microorganism in biltong.

Reducing the water activity effectively limits microbial and fungal activity in biltong. The addition of salt at the recommended levels in the range of 2.5 - 4.0 % in the biltong marinade can reduce the water activity of meat to < 0.93 . This reduction in water activity inhibits the growth of the bacteria found in biltong. Further reduction in water activity through drying is necessary to inhibit fungal growth. Drying of meat to a weight loss of 50 % reduces the water activity to ≤ 0.65 which inhibits all microbial and fungal growth in the resulting biltong. Changing consumer

preference towards high moisture biltong increases the risk of microbial and fungal attack. The possibility of rehydration due to improper storage or packaging may also provide suitable environment to revive microbial and fungal activity in biltong.

Alternative drying methods such as IR have shown potential in decontamination of food products without compromising their quality. IR energy is absorbed by the bacterial and fungal spores, leading to a high lethality rate. This contrasts with hot air drying which inactivates the microorganisms by reducing the water activity in the meat.

A combined Infrared and hot air drying could be a possible alternative drying method for biltong production. The synergistic effect between the IR and hot air improves the energy efficiency and reduces the drying time. The literature reviewed indicate that IRHAD results in dried products with better physical and nutritional quality. Nonetheless, there is need for sufficient information regarding the drying process variables (temperature, relative humidity and air velocity) and the corresponding associated drying kinetics to ascertain the suitability of IRHAD for biltong production.

Mathematical models provide great insight into the interaction between the process variables, their influence on the drying kinetics and quality of the dried products. Thin layer drying models have been used to model the drying of many agricultural products. Thin layer drying models are practical and provide acceptable results for predicting the drying kinetics of many agricultural products. However, these models are empirical models, and the validity of their prediction is limited to the drying condition for which they were tested. Moreover, the thin layer models can only predict the variations in moisture ratio with drying time. A better understanding of the drying process is achieved by the mechanistic modelling of the transfer of heat and mass during the drying of agricultural products. The transfer of heat and mass occurs simultaneously during drying. Therefore, mechanistic drying models couple the heat and mass transfer processes to give better prediction of the distribution of temperature and moisture within the product being dried.

Many previous researchers have reported the coupled heat and mass transfer models for meat under HAD but no studies have been done on modelling the coupled heat and mass transfer of IRHAD of meat being processed into biltong. It is necessary to investigate and model the

mechanisms of heat and mass transfer in meat during the processing of biltong. Realistic representation of the food material and the drying process can guarantee precision when simulating industrial food process operations. CFD based software like ANSYS Fluent and COMSOL Multiphysics enable the implementation and solution of the complex multidimensional heat and mass transfer models. The implementation of coupled heat and mass transfer models provides a comprehensive spatial and temporal distribution of the temperature and moisture content within the food material.

2.7 Conclusion

The literature reviewed indicates the need to improve the biltong processing procedures to assure product quality and energy efficiency of the process. IRHAD is a possible alternative to the HAD of biltong. Modelling the coupled heat and mass transfer in beef as well as the energy use during IRHAD will ascertain the suitability of the application of IRHAD in the drying of beef to produce biltong.

2.8 References

- Abong'o, BO and Momba, MN. 2009. Prevalence and characterization of Escherichia coli O157: H7 isolates from meat and meat products sold in Amathole District, Eastern Cape Province of South Africa. *Food microbiology* 26 (2): 173-176.
- Abukhalifeh, H, Dhib, R and Fayed, M. 2005. Model predictive control of an infrared-convective dryer. *Drying technology* 23 (3): 497-511.
- Adler-Nissen, J. 2007. Continuous wok-frying of vegetables: Process parameters influencing scale up and product quality. *Journal of food engineering* 83 (1): 54-60.
- Afzal, T, Abe, T and Hikida, Y. 1999. Energy and quality aspects during combined FIR-convection drying of barley. *Journal of food engineering* 42 (4): 177-182.
- Aguilera, JM. 2005. Why food microstructure? *Journal of food engineering* 67 (1-2): 3-11.
- Ahmat, T, Barka, M, Aregba, AW and Bruneau, D. 2015. Convective drying kinetics of fresh beef: An experimental and modeling approach. *Journal of food processing and preservation* 39 (6): 2581-2595.

- Allotey, J, Gashe, BA, Coetzee, SH, Mpuchane, S, Khonga, EB, Matsheka, MI and Murindamombe, G. 2014. Microbial quality assessment and predominant microorganism of biltong produced in butcheries in Gaborone, Botswana. *Food and Nutrition sciences* 2014 (2014): 1 - 12.
- Arntfield, S, Scanlon, M, Malcolmson, L, Watts, B, Cenkowski, S, Ryland, D and Savoie, V. 2001. Reduction in lentil cooking time using micronization: comparison of 2 micronization temperatures. *Journal of Food Science* 66 (3): 500-505.
- Arsoy, S. 2008. Temperature-controlled infrared drying characteristics of soils. *Drying Technology* 26 (12): 1477-1483.
- Attwell, E. 2003. Biltong wakes up. *Food Reviews* 30 (2): 11-13.
- Banout, J, Kucerova, I and Marek, S. 2012. Using a double-pass solar drier for jerky drying. *Energy Procedia* 30 (4): 738-744.
- Bari, ML, Nei, D, Sotome, I, Nishina, I, Isobe, S and Kawamoto, S. 2009. Effectiveness of sanitizers, dry heat, hot water, and gas catalytic infrared heat treatments to inactivate Salmonella on almonds. *Foodborne pathogens and disease* 6 (8): 953-958.
- Basman, A and Yalcin, S. 2011. Quick-boiling noodle production by using infrared drying. *Journal of Food Engineering* 106 (3): 245-252.
- Bellagha, S, Sahli, A, Farhat, A, Kechaou, N and Glenza, A. 2007. Studies on salting and drying of sardine (*Sardinella aurita*): Experimental kinetics and modeling. *Journal of Food Engineering* 78 (3): 947-952.
- Bird, R, Sterwart, W and Lightfoot, E. 2001. *Transport phenomena*. John Wiley and Sons Inc., New York.
- Brewer, M. 2014. Chemical and physical characteristics of meat| Water-holding capacity. In: eds. Dikeman, M and Devine, C, *Encyclopedia of meat sciences*. Oxford: Academic Press, London.
- Brooker, DB, Bakker-Arkema, FW and Hall, CW. 1992. *Drying and storage of grains and oilseeds*. Springer Science & Business Media,
- Bualuang, O, Tirawanichakul, Y and Tirawanichakul, S. 2013. Comparative study between hot air and infrared drying of parboiled rice: Kinetics and qualities aspects. *Journal of Food Processing and Preservation* 37 (6): 1119-1132.
- Burgheimer, FSM and Nelson, AI. 1971. Effect of near infrared energy on rate of freeze drying of beef spectral distribution. . *Journal of Food Science* 36 (1): 273–276.

- Burnham, GM, Hanson, DJ, Koshick, CM and Ingham, SC. 2008. Death of Salmonella serovars, Escherichia coli O157: H7, Staphylococcus aureus and Listeria monocytogenes during the drying of meat: a case study using biltong and droëwors. *Journal of food safety* 28 (2): 198-209.
- Celma, AR, Rojas, S and Lopez-Rodriguez, F. 2008. Mathematical modelling of thin-layer infrared drying of wet olive husk. *Chemical Engineering and Processing: Process Intensification* 47 (9-10): 1810-1818.
- Chabbouh, M, Hajji, W, Hadj Ahmed, SB, Farhat, A, Bellagha, S and Sahli, A. 2011. Combined effects of osmotic dehydration and convective air drying on kaddid meats: Kinetics and quality. *Drying Technology* 29 (13): 1571-1579.
- Chen, D, Li, K and Zhu, X. 2012. Determination of effective moisture diffusivity and activation energy for drying of powdered peanut shell under isothermal conditions. *BioResources* 7 (3): 3670-3678.
- Chen, Q, Bi, J, Wu, X, Yi, J, Zhou, L and Zhou, Y. 2015. Drying kinetics and quality attributes of jujube (*Zizyphus jujuba* Miller) slices dried by hot-air and short-and medium-wave infrared radiation. *LWT-Food Science and Technology* 64 (2): 759-766.
- Cheng, Q and Sun, D-W. 2008. Factors affecting the water holding capacity of red meat products: a review of recent research advances. *Critical reviews in food science and nutrition* 48 (2): 137-159.
- Cherono, K. 2014. Infrared Drying of Biltong. Unpublished MSc thesis, Bioresources Engineering, University of KwaZulu-Natal, Pietermaritzburg, South Africa.
- Cherono, K, Mwithiga, G and Schmidt, S. 2016. Infrared drying as a potential alternative to convective drying for biltong production. *Italian journal of food safety* 5 (3): 140-145.
- Crank, J. 1979. *The mathematics of diffusion*. Oxford university press,
- Dagerskog, M. 1979. Infrared radiation for food processing II. Calculation of heat penetration during infrared frying of meat products. *Lebensmittel Wissenschaft und Technologie* 12 (4): 252-257.
- Darabi, H, Zomorodian, A, Akbari, M and Lorestani, A. 2015. Design a cabinet dryer with two geometric configurations using CFD. *Journal of Food Science and Technology* 52 (1): 359-366.

- Datta, A. 2007. Porous media approaches to studying simultaneous heat and mass transfer in food processes. II: Property data and representative results. *Journal of food engineering* 80 (1): 96-110.
- Datta, A and Ni, H. 2002. Infrared and hot-air-assisted microwave heating of foods for control of surface moisture. *Journal of Food Engineering* 51 (4): 355-364.
- Desmarchelier, P and Grau, F. 1997. Escherichia coli. In: eds. Hocking, A, Arnold, G, Jenson, I, Newton, K and Sutherland, P, *Foodborne microorganisms of public health importance*. AIFST (NSW Branch), Sydney, Australia.
- Dhall, A, Datta, AK, Torrance, KE and Almeida, MF. 2009. Radiative heat exchange modeling inside an oven. *AIChE journal* 55 (9): 2448-2460.
- Doymaz, I. 2014. Suitability of thin-layer drying models for infrared drying of peach slices. *Journal of food processing and preservation* 38 (6): 2232-2239.
- Doymaz, İ. 2012. Infrared drying of sweet potato (*Ipomoea batatas* L.) slices. *Journal of food science and technology* 49 (6): 760-766.
- Duan, Z-h, Jiang, L-n, Wang, J-l, Yu, X-y and Wang, T. 2011. Drying and quality characteristics of tilapia fish fillets dried with hot air-microwave heating. *Food and Bioproducts processing* 89 (4): 472-476.
- Dzimba, FEJ, Faria, J and Walter, EHM. 2007. Testing the sensory acceptability of biltong formulated with different spices. *African Journal of Agricultural Research* 2 (11): 547-577.
- Ekechukwu, O. 1999. Review of solar-energy drying systems I: an overview of drying principles and theory. *Energy conversion and management* 40 (6): 593-613.
- El-Mesery, HS and Mwithiga, G. 2015. Performance of a convective, infrared and combined infrared-convective heated conveyor-belt dryer. *Journal of food science and technology* 52 (5): 2721-2730.
- Erbay, Z and Icier, F. 2010. A review of thin layer drying of foods: theory, modeling, and experimental results. *Critical reviews in food science and nutrition* 50 (5): 441-464.
- Erriguible, A, Bernada, P, Couture, F and Roques, M-A. 2007. Simulation of vacuum drying by coupling models. *Chemical Engineering and Processing: Process Intensification* 46 (12): 1274-1285.
- Ertekin, C and Firat, MZ. 2017. A comprehensive review of thin-layer drying models used in agricultural products. *Critical reviews in food science and nutrition* 57 (4): 701-717.

- Ertekin, C and Heybeli, N. 2014. Thin-layer infrared drying of mint leaves. *Journal of food processing and preservation* 38 (4): 1480-1490.
- Eshtiagh, A and Zare, D. 2015. Modeling of thin layer hot air-infrared drying of green peas. *Agric Eng Int: CIGR Journal* 23 (4): 246-258.
- Fasina, O, Tyler, B and Pickard, M. 1997. Infrared heating of legume seeds effect on physical and mechanical properties. *Amer. Soc. Agric. Eng. Annual Meeting*,
- Fasina, O, Tyler, R and Pickard, M. 1996. Effect of infrared heat treatment on the chemical composition and functionality of cereal grains-comparison of hullless and pearled barley. *Progress Report, Dept. of Applied Microbiology and Food Science, Univ. of Saskatchewan, Saskatoon*
- Feyissa, AH, Adler-Nissen, J and Gernaey, K. 2009. Model of Heat and Mass Transfer with Moving Boundary during Roasting of Meat in Convection-Oven. *Excerpt from the Proceedings of the COMSOL Conference, Milan, Italy*,
- Feyissa, AH, Gernaey, KV and Adler-Nissen, J. 2013. 3D modelling of coupled mass and heat transfer of a convection-oven roasting process. *Meat science* 93 (4): 810-820.
- Gabel, MM, Pan, Z, Amaratunga, K, Harris, LJ and Thompson, JF. 2006. Catalytic infrared dehydration of onions. *Journal of Food Science* 71 (9): E351-E357.
- Guizani, N, Al-Shoukri, AO, Mothershaw, A and Rahman, MS. 2008. Effects of salting and drying on shark (*Carcharhinus sorrah*) meat quality characteristics. *Drying technology* 26 (6): 705-713.
- Gupta, T. 2001. Individual heat transfer modes during contact baking of Indian unleavened flat bread (chapati) in a continuous oven. *Journal of Food Engineering* 47 (4): 313-319.
- Hamanaka, D, Uchino, T, Furuse, N, Han, W and Tanaka, S-i. 2006. Effect of the wavelength of infrared heaters on the inactivation of bacterial spores at various water activities. *International journal of food microbiology* 108 (2): 281-285.
- Harmathy, T. 1969. Simultaneous moisture and heat transfer in porous systems with particular reference to drying. *Industrial & Engineering Chemistry Fundamentals* 8 (1): 92-103.
- Hashimoto, A, Sawai, J, Igarashi, H and Shimizu, M. 1992. Effect of far-infrared irradiation on pasteurization of bacteria suspended in liquid medium below lethal temperature. *Journal of chemical engineering of Japan* 25 (3): 275-281.
- Hebbar, HU, Vishwanathan, K and Ramesh, M. 2004. Development of combined infrared and hot air dryer for vegetables. *Journal of food engineering* 65 (4): 557-563.

- Hii, C, Itam, C and Ong, S. 2014. Convective air drying of raw and cooked chicken meats. *Drying technology* 32 (11): 1304-1309.
- Howell, JR, Menguc, MP and Siegel, R. 2015. *Thermal radiation heat transfer*. CRC press,
- Huang, H, Lin, P and Zhou, W. 2007. Moisture transport and diffusive instability during bread baking. *SIAM Journal on Applied Mathematics* 68 (1): 222-238.
- Huang, L. 2004. Infrared surface pasteurization of turkey frankfurters. *Innovative Food Science & Emerging Technologies* 5 (3): 345-351.
- Huang, L and Sites, J. 2008. Elimination of *Listeria monocytogenes* on hotdogs by infrared surface treatment. *Journal of Food Science* 73 (3): 27-31.
- Huang, T and Nip, W. 2001. Intermediate-moisture meat and dehydrated meat. *Meat science and applications* 25 (4): 403-442.
- Huff-Lonergan, E and Lonergan, SM. 2005. Mechanisms of water-holding capacity of meat: The role of postmortem biochemical and structural changes. *Meat science* 71 (1): 194-204.
- Hui, YH. 2012. *Handbook of meat and meat processing*. CRC press,
- ICMSF. 1996. *Bacillus cereus*. In: ed. ICMSF, *Microorganisms in food 5: Microbiological specifications of food pathogens*. Blackie Academic and Professional London.
- Incropera, FP and Dewitt, DP. 1981. *Solutions Manual to Accompany Fundamentals of Heat Transfer*. Wiley,
- Islam, MR, Thaker, KS and Mujumdar, A. 2007. A diffusion model for a drum dryer subjected to conduction, convection, and radiant heat input. *Drying Technology* 25 (6): 1033-1043.
- James, C, Lechevalier, V and Ketteringham, L. 2002. Surface pasteurisation of shell eggs. *Journal of Food Engineering* 53 (2): 193-197.
- Jefferson, D, Lacey, A and Sadd, P. 2006. Understanding crust formation during baking. *Journal of Food Engineering* 75 (4): 515-521.
- Ježek, D, Tripalo, B, Brnčić, M, Karlović, D, Rimac Brnčić, S, Vikić-Topić, D and Karlović, S. 2008. Dehydration of celery by infrared drying. *Croatica Chemica Acta* 81 (2): 325-331.
- Johnson, J, Doyle, M, Cassens, R and Schoeni, J. 1988. Fate of *Listeria monocytogenes* in tissues of experimentally infected cattle and in hard salami. *Applied Environmental Microbiology* 54 (2): 497-501.
- Jones, M, Arnaud, E, Gouws, P and Hoffman, LC. 2017. Processing of South African biltong—A review. *South African Journal of Animal Science* 47 (6): 743-757.

- Jun, S and Irudayaraj, J. 2003. A dynamic fungal inactivation approach using selective infrared heating. *Transactions of the ASAE* 46 (5): 1407.
- Khan, MIH, Welsh, Z, Gu, Y, Karim, M and Bhandari, B. 2020. Modelling of simultaneous heat and mass transfer considering the spatial distribution of air velocity during intermittent microwave convective drying. *International Journal of Heat and Mass Transfer* 153 (2): 119 -128.
- Khair, R, Pan, Z, Salim, A, Hartsough, BR and Mohamed, S. 2011. Moisture diffusivity of rough rice under infrared radiation drying. *LWT-Food Science and Technology* 44 (4): 1126-1132.
- Kocabiyik, H and Tezer, D. 2009. Drying of carrot slices using infrared radiation. *International journal of food science & technology* 44 (5): 953-959.
- Kohashi, M, Akao, K-i and Watanabe, T. 1993. Non-thermal effects of a ceramics heater radiation on xanthine oxidase activity. *Bioscience, biotechnology, and biochemistry* 57 (12): 1999-2004.
- Kondjoyan, A, Rouaud, O, McCann, M, Havet, M, Foster, A, Swain, M and Daudin, J. 2006. Modelling coupled heat–water transfers during a decontamination treatment of the surface of solid food products by a jet of hot air. I. Sensitivity analysis of the model and first validations of product surface temperature under constant air temperature conditions. *Journal of Food Engineering* 76 (1): 53-62.
- Kouzeh-Kanani, M, Van Zuilichem, D, Roozen, J and Pilnik, W. 1982. A modified procedure for low temperature infrared radiation of soybeans. II. Inactivation of lipoxygenase and keeping quality of full-fat-flour. *Food Science and Technology= Lebensmittel-Wissenschaft und Technologie* 15 (1): 139-142.
- Kowalski, SJ and Mierzwa, D. 2009. Convective drying in combination with microwave and IR drying for biological materials. *Drying Technology* 27 (12): 1292-1301.
- Krishnamurthy, K, Jun, S, Irudayaraj, J and Demirci, A. 2008a. Efficacy of infrared heat treatment for inactivation of staphylococcus aureus in milk. *Journal of food process engineering* 31 (6): 798-816.
- Krishnamurthy, K, Khurana, HK, Soojin, J, Irudayaraj, J and Demirci, A. 2008b. Infrared heating in food processing: an overview. *Comprehensive reviews in food science and food safety* 7 (1): 2-13.

- Krishnamurthy, K, Tewari, JC, Irudayaraj, J and Demirci, A. 2010. Microscopic and spectroscopic evaluation of inactivation of *Staphylococcus aureus* by pulsed UV light and infrared heating. *Food and Bioprocess Technology* 3 (1): 93 - 100.
- Kucerova, I, Hubackova, A, Rohlik, B-A and Banout, J. 2015. Mathematical modeling of thin-layer solar drying of Eland (*Taurotragus oryx*) Jerky. *International journal of food engineering* 11 (2): 229-242.
- Kucuk, H, Midilli, A, Kilic, A and Dincer, I. 2014. A review on thin-layer drying-curve equations. *Drying Technology* 32 (7): 757-773.
- Kumar, C, Joardder, M, Farrell, TW and Karim, M. 2016. Multiphase porous media model for intermittent microwave convective drying (IMCD) of food. *International Journal of Thermal Sciences* 104 (2): 304-314.
- Kumar, C, Millar, GJ and Karim, M. 2015. Effective diffusivity and evaporative cooling in convective drying of food material. *Drying Technology* 33 (2): 227-237.
- Kumar, DP, Hebbar, HU and Ramesh, M. 2006. Suitability of thin layer models for infrared-hot air-drying of onion slices. *LWT-Food Science and Technology* 39 (6): 700-705.
- Kumar, PD, Umesh Hebbar, H, Sukumar, D and Ramesh, M. 2005. Infrared and hot-air drying of onions. *Journal of Food Processing and Preservation* 29 (2): 132-150.
- Lado, B and Yousef, A. 2007. Characteristics of *Listeria monocytogenes* important to food processors. In: eds. Ryser, ET and Marth, EH, *Listeria, Listeriosis, and Food Safety, Third Edition*. CRC Press, Boca Raton.
- Lawrie, R. 2017. The conversion of muscle to meat. In: ed. Toldra, F, *Lawrie's Meat Science*. Woodhead Publishing Ltd, Cambridge, UK.
- Łechtańska, J, Szadzińska, J and Kowalski, S. 2015. Microwave-and infrared-assisted convective drying of green pepper: Quality and energy considerations. *Chemical Engineering and Processing: Process Intensification* 98 (2015): 155-164.
- Leistner, L. 1987. Shelf-stable products and intermediate moisture foods based on meat. *Water activity: Theory and applications to food* 8 (2): 295-327.
- Li, X. 2012. A study of infrared heating technology for tomato peeling: Process characterization and modeling. Unpublished thesis, University of California, Davis, California.
- Li, X, Pan, Z, Upadhyaya, S, Atungulu, G and Delwiche, M. 2011. Three-dimensional geometric modeling of processing tomatoes. *Transactions of the ASABE* 54 (6): 2287-2296.

- Li, X, Xie, X, Zhang, C-h, Zhen, S and Jia, W. 2018. Role of mid-and far-infrared for improving dehydration efficiency in beef jerky drying. *Drying Technology* 36 (3): 283-293.
- Lin, Y-P, Lee, T-Y, Tsen, J-H and King, VA-E. 2007. Dehydration of yam slices using FIR-assisted freeze drying. *Journal of Food Engineering* 79 (4): 1295-1301.
- Liu, Y, Zhu, W, Luo, L, Li, X and Yu, H. 2014. A mathematical model for vacuum far-infrared drying of potato slices. *Drying technology* 32 (2): 180-189.
- Luikov, AV. 1975. Systems of differential equations of heat and mass transfer in capillary-porous bodies. *International Journal of Heat and mass transfer* 18 (1): 1-14.
- Mayor, L and Sereno, A. 2004. Modelling shrinkage during convective drying of food materials: a review. *Journal of Food Engineering* 61 (3): 373-386.
- McDonnell, CK, Allen, P, Duggan, E, Arimi, JM, Casey, E, Duane, G and Lyng, JG. 2013. The effect of salt and fibre direction on water dynamics, distribution and mobility in pork muscle: A low field NMR study. *Meat science* 95 (1): 51-58.
- Mhlambi, S, Naidoo, K and Lindsay, D. 2010. Enterotoxin-producing Staphylococcus strains associated with South African biltong at point of sale. *Journal of food safety* 30 (2): 307-317.
- Miller, R. 2014. Chemical and physical characteristics of meat| Palatability. In: eds. Dikeman, M and Devine, C, *Encyclopedia of meat sciences*. Oxford: Academic Press, London.
- Mondal, A and Datta, A. 2008. Bread baking—a review. *Journal of Food Engineering* 86 (4): 465-474.
- Muriana, P, Gande, N, Robertson, W, Jordan, B and Mitra, S. 2004. Effect of prepackage and postpackage pasteurization on postprocess elimination of *Listeria monocytogenes* on deli turkey products. *Journal of food protection* 67 (11): 2472-2479.
- Naidoo, K and Lindsay, D. 2010a. Pathogens associated with biltong product and their in vitro survival of hurdles used during production. *Food Protection Trends* 30 (9): 532-538.
- Naidoo, K and Lindsay, D. 2010b. Survival of *Listeria monocytogenes*, and enterotoxin-producing *Staphylococcus aureus* and *Staphylococcus pasteurii*, during two types of biltong-manufacturing processes. *Food Control* 21 (7): 1042-1050.
- Nasiroglu, S and Kocabiyik, H. 2009. Thin-layer infrared radiation drying of red pepper slices. *Journal of Food Process Engineering* 32 (1): 1-16.
- Nathakaranakule, A, Jaiboon, P and Soponronnarit, S. 2010. Far-infrared radiation assisted drying of longan fruit. *Journal of Food Engineering* 100 (4): 662-668.

- Nimmol, C, Devahastin, S, Swasdisevi, T and Soponronnarit, S. 2005. Drying kinetics and quality of carrot dried by far-infrared radiation under vacuum condition. *International Agricultural Engineering Conference*,
- Nortjé, K, Buys, E and Minnaar, A. 2005. Effect of γ -irradiation on the sensory quality of moist beef biltong. *Meat science* 71 (4): 603-611.
- Onwude, DI, Hashim, N, Abdan, K, Janius, R, Chen, G and Kumar, C. 2018. Modelling of coupled heat and mass transfer for combined infrared and hot-air drying of sweet potato. *Journal of Food Engineering* 228 (1): 12-24.
- Onwude, DI, Hashim, N and Chen, G. 2016. Recent advances of novel thermal combined hot air drying of agricultural crops. *Trends in Food Science & Technology* 57 (3): 132-145.
- Osterhoff, D and Leistner, L. 1984. South African biltong--another close look. *Journal of the South African Veterinary Association* 55 (4): 201-202.
- Özilgen, M and Özdemir, M. 2001. A review on grain and nut deterioration and design of the dryers for safe storage with special reference to Turkish hazelnuts. *Critical reviews in food science and nutrition* 41 (2): 95-132.
- Palumbo, S, Komanowsky, M, Metzger, V and Smith, J. 1977. Kinetics of pepperoni drying. *Journal of Food Science* 42 (4): 1029-1033.
- Pan, Z, Atungulu, G and Li, X. 2014. Infrared heating. In: ed. Sun, D-W, *Emerging technologies for food processing*. Elsevier.
- Pan, Z and Atungulu, GG. 2010. Commercialization of food processing using infrared. In: eds. Doona, CJ, Kustin, K and Feehery, FE, *Case studies in novel food processing technologies: innovations in processing, packaging, and predictive modelling*. Woodhead Publishing Limited.
- Pan, Z and Atungulu, GG. 2011. Combined infrared heating and freeze-drying. In: eds. Pan, Z and Atungulu, GG, *Infrared heating for food and agricultural processing*. CRC Press, Nwey York.
- Pan, Z, Khir, R, Godfrey, LD, Lewis, R, Thompson, JF and Salim, A. 2008. Feasibility of simultaneous rough rice drying and disinfestations by infrared radiation heating and rice milling quality. *Journal of food engineering* 84 (3): 469-479.
- Pawar, SB and Pratape, V. 2017. Fundamentals of infrared heating and its application in drying of food materials: a review. *Journal of food process engineering* 40 (1): e12308.

- Petit, T, Caro, Y, Petit, A-S, Santchurn, SJ and Collignan, A. 2014. Physicochemical and microbiological characteristics of biltong, a traditional salted dried meat of South Africa. *Meat science* 96 (3): 1313-1317.
- Petrova, I, Bantle, M and Eikevik, TM. 2015. Manufacture of dry-cured ham: A review. Part 2. Drying kinetics, modeling and equipment. *European Food Research and Technology* 241 (4): 447-458.
- Pham, ND, Khan, M and Karim, M. 2020. A mathematical model for predicting the transport process and quality changes during intermittent microwave convective drying. *Food chemistry* 325 (4): 12-32.
- Podolak, R, Enache, E, Stone, W, Black, DG and Elliott, PH. 2010. Sources and risk factors for contamination, survival, persistence, and heat resistance of Salmonella in low-moisture foods. *Journal of food protection* 73 (10): 1919-1936.
- Poligné, I, Collignan, A and Trystram, G. 2001. Characterization of traditional processing of pork meat into boucané. *Meat Science* 59 (4): 377-389.
- Ponkham, K, Meeso, N, Soponronnarit, S and Siriamornpun, S. 2012. Modeling of combined far-infrared radiation and air drying of a ring shaped-pineapple with/without shrinkage. *Food and Bioproducts Processing* 90 (2): 155-164.
- Prakash, B. 2011. Mathematical modeling of moisture movement within a rice kernel during convective and infrared drying. Unpublished thesis, University of California, Davis,
- Prior, B. 1984. Role of micro-organisms in biltong flavour development. *Journal of Applied Bacteriology* 56 (1): 41-45.
- Puente-Díaz, L, Ah-Hen, K, Vega-Gálvez, A, Lemus-Mondaca, R and Scala, KD. 2013. Combined infrared-convective drying of murta (*Ugni molinae* Turcz) berries: kinetic modeling and quality assessment. *Drying Technology* 31 (3): 329-338.
- Purlis, E. 2010. Browning development in bakery products—A review. *Journal of Food Engineering* 99 (3): 239-249.
- Ranjan, R, Irudayaraj, J and Jun, S. 2002. Simulation of infrared drying process. *Drying Technology* 20 (2): 363-379.
- Rastogi, NK. 2012. Recent trends and developments in infrared heating in food processing. *Critical reviews in food science and nutrition* 52 (9): 737-760.
- Ratti, C. 2001. Hot air and freeze-drying of high-value foods: a review. *Journal of food engineering* 49 (4): 311-319.

- Riadh, MH, Ahmad, SAB, Marhaban, MH and Soh, AC. 2015. Infrared heating in food drying: An overview. *Drying Technology* 33 (3): 322-335.
- Rosenthal, I, Rosen, B and Bernstein, S. 1996. Surface pasteurization of cottage cheese. *Milchwissenschaft (Germany)*
- Rudobashta, S, Zueva, G and Zuev, N. 2014. Mathematical modeling and numerical simulation of seeds drying under oscillating infrared irradiation. *Drying Technology* 32 (11): 1352-1359.
- Sadin, R, Chegini, G-R and Khodadadi, M. 2014. Development and performance evaluation of a combined infrared and hot air dryer. *Journal of Biological and Environmental Sciences* 8 (22): 11-18.
- Sadin, R, Chegini, G and Khodadadi, M. 2017. Drying characteristics and modeling of tomato thin layer drying in combined infrared-hot air dryer. *Agricultural Engineering International: CIGR Journal* 19 (1): 150-157.
- Salagnac, P, Glouannec, P and Lecharpentier, D. 2004. Numerical modeling of heat and mass transfer in porous medium during combined hot air, infrared and microwaves drying. *International Journal of heat and mass transfer* 47 (19-20): 4479-4489.
- Sawai, J, Fujisawa, M, Kokugan, T, Shimizu, M, Igarashi, H, Hashimoto, A and Kojima, H. 1997. Pasteurization of bacterial spores in liquid medium by far-infrared irradiation. *Journal of chemical engineering of Japan* 30 (1): 170-172.
- Sawai, J, Isomura, Y, Honma, T and Kenmochi, H. 2006. Characteristics of the Inactivation of *Escherichia coli* by Infrared Irradiative Heating. *Biocontrol science* 11 (2): 85-90.
- Sawai, J, Sagara, K, Hashimoto, A, Igarashi, H and Shimizu, M. 2003. Inactivation characteristics shown by enzymes and bacteria treated with far-infrared radiative heating. *International journal of food science & technology* 38 (6): 661-667.
- Serra, X, Ruiz-Ramírez, J, Arnau, J and Gou, P. 2005. Texture parameters of dry-cured ham m. biceps femoris samples dried at different levels as a function of water activity and water content. *Meat Science* 69 (2): 249-254.
- Sharma, G and Prasad, S. 2001. Drying of garlic (*Allium sativum*) cloves by microwave-hot air combination. *Journal of food engineering* 50 (2): 99-105.
- Shilton, N, Mallikarjunan, P and Sheridan, P. 2002. Modeling of heat transfer and evaporative mass losses during the cooking of beef patties using far-infrared radiation. *Journal of Food Engineering* 55 (3): 217-222.

- Solomon, AB, Fanta, SW, Delele, MA and Vanierschot, M. 2021. Modeling and simulation of heat and mass transfer in an Ethiopian fresh injera drying process. *Heliyon* 7 (2): e06201.
- Soydan Karabacak, M, Esin, A and Cekmecelioglu, D. 2014. Drying behavior of meat samples at various fiber directions and air conditions. *Drying technology* 32 (6): 695-707.
- Srikiatden, J and Roberts, JS. 2007. Moisture transfer in solid food materials: A review of mechanisms, models, and measurements. *International Journal of Food Properties* 10 (4): 739-777.
- Stewart, C. 2003. Staphylococcus aureus and staphylococcal enterotoxins. In: ed. Hocking, A, *Foodborne microorganisms of public health significance*. Australian Institute of Food Science and Technology (NSW Branch), Sydney.
- Strydom, P and Zondagh, B. 2014. Biltong: A major South African ethnic meat product. In: eds. Dikeman, M and Devine, C, *Encyclopaedia of meat sciences*. Academic Press, London, UK.
- Sui, Y, Yang, J, Ye, Q, Li, H and Wang, H. 2014. Infrared, convective, and sequential infrared and convective drying of wine grape pomace. *Drying Technology* 32 (6): 686-694.
- Sumnu, SG and Sahin, S. 2008. *Food engineering aspects of baking sweet goods*. CRC Press,
- Talla, A, Puiggali, J-R, Jomaa, W and Jannot, Y. 2004. Shrinkage and density evolution during drying of tropical fruits: application to banana. *Journal of Food Engineering* 64 (1): 103-109.
- Tanaka, F and Uchino, T. 2010. Heat and Mass Transfer Modeling of Infrared Radiation for Heating. In: eds. Pan, Z and Atungulu, G, *Infrared Heating for Food and Agricultural Processing*, CRC Press.
- Tanaka, F and Uchino, T. 2011. Heat and Mass Transfer Modeling of Infrared Radiation for Heating. In: eds. Pan, Z and Atungulu, G, *Infrared Heating for Food and Agricultural Processing*. CRC Press, New York.
- Tanaka, F, Verboven, P, Scheerlinck, N, Morita, K, Iwasaki, K and Nicolai, B. 2007. Investigation of far infrared radiation heating as an alternative technique for surface decontamination of strawberry. *Journal of food engineering* 79 (2): 445-452.
- Taylor, M. 1976. Changes in microbial flora during biltong production. *South African Food Review* 3 (2): 120-123.

- Therdthai, N and Zhou, W. 2003. Recent advances in the studies of bread baking process and their impacts on the bread baking technology. *Food Science and Technology Research* 9 (3): 219-226.
- Toldrá, F. 2010. *Handbook of meat processing*. John Wiley & Sons,
- Tornberg, E. 2005. Effects of heat on meat proteins—Implications on structure and quality of meat products. *Meat science* 70 (3): 493-508.
- Van der Riet, W. 1976. Studies on the mycoflora of biltong. *S Afr Food Rev* 3 (1): 105-113.
- Van der Riet, W. 1982. Biltong-A south-african dried meat product. *Fleischwirtschaft* 62 (8): 970-983.
- Van der Sman, R. 2007. Soft condensed matter perspective on moisture transport in cooking meat. *AIChE Journal* 53 (11): 2986-2995.
- Van Zuilichem, D, Van't Reit, K and Stolp, W. 1986. An overview of new infrared radiation processes for various agricultural products. *Food Engineering Process and Application* 1 5 (1): 595-610.
- Wang, H, Yang, W, Senior, P, Raghavan, R and Duncan, S. 2008. Investigation of batch fluidized-bed drying by mathematical modeling, CFD simulation and ECT measurement. *AIChE Journal* 54 (2): 427-444.
- Wang, J and Sheng, K. 2004. Modeling of multi-layer far-infrared dryer. *Drying technology* 22 (4): 809-820.
- Wang, L and Singh, R. 2004. Finite element modeling and sensitivity analysis of double-sided contact-heating of initially frozen hamburger patty. *Transactions of the ASAE* 47 (1): 147.
- Wang, Y, Zhang, M, Mujumdar, AS and Chen, H. 2014. Drying and quality characteristics of shredded squid in an infrared-assisted convective dryer. *Drying technology* 32 (15): 1828-1839.
- Wolter, H, Laing, E and Viljoen, BC. 2000. Isolation and identification of yeasts associated with intermediate moisture meats. *Food Technology and Biotechnology* 38 (1): 69-76.
- Workneh, T and Muga, F. 2018. Microwave-assisted forced hot air circulation drying of thin-layer teff (*Eragrostis tef*). *Journal of Food, Agriculture & Environment* 16 (2): 34-42.
- Yang, H, Sakai, N and Watanabe, M. 2001. Drying model with non-isotropic shrinkage deformation undergoing simultaneous heat and mass transfer. *Drying Technology* 19 (7): 1441-1460.

Yang, J, Bingol, G, Pan, Z, Brandl, MT, McHugh, TH and Wang, H. 2010. Infrared heating for dry-roasting and pasteurization of almonds. *Journal of Food Engineering* 101 (3): 273-280.

3. MODELLING THE THIN-LAYER DRYING OF BEEF BILTONG PROCESSED USING HOT AIR DRYING

This chapter is based on the following publication.

Muga, F. C., Workneh, T. S., and Marenya, M. O. 2020. Modelling the thin layer drying of beef biltong processed using hot air drying. *Journal of Biosystems Engineering*, 45(4): 362-373. DOI: <https://doi.org/10.1007/s42853-020-00076-5>.

Abstract

This chapter explored the drying characteristics of marinated beef under hot air drying (HAD). The drying experiments were conducted in a cabinet dryer at drying air temperature of 30, 35, and 40 °C; and drying air velocity of 1.5 and 2.5 m.s⁻¹. The results indicate that the drying process occurred in the falling rate period. The temperature of the drying air significantly ($p \leq 0.05$) influenced the drying characteristics such as drying time, drying rate, and the effective moisture diffusivity. The velocity of the drying air only had a significant ($p \leq 0.05$) effect on the drying rate during the first falling rate period. Diffusion is the predominant mode of moisture transport during the drying of marinated beef used to produce biltong. The drying kinetics of marinated beef during the processing of biltong is best described by the Two term model. The effective moisture diffusivity of marinated beef being processed into biltong ranges between 1.60×10^{-10} m².s⁻¹ and 2.28×10^{-10} m².s⁻¹, while, the activation energy is 28.2126 and 17.7068 kJ.mol⁻¹ at a drying air velocity of 1.5 and 2.5 m.s⁻¹, respectively. The drying characteristics and the thin layer model recommended in this study cover the range of temperature and air velocity commonly used in biltong processing, hence, they can be used to optimise the drying process of marinated beef during biltong production.

Keywords: Activation energy, Biltong, Drying kinetics, Effective moisture diffusivity, Hot air drying, Thin layer modelling.

3.1 Introduction

Biltong is a dried, spiced meat-based ready-to-eat snack that is widely consumed in South Africa (Cherono *et al.* 2016). It can be compared to other dried meat products across the world such as; carne seca (Mexico), charqui (South America), jerky (USA), kaddid (Tunisia), kilshi (Sahel), and rou gan (China) (Dzimba *et al.* 2007; Mhlambi *et al.* 2010; Petit *et al.* 2014). Biltong is made by air drying marinated meat strips at moderate temperatures ranging between 20 and 40 °C (Burnham *et al.* 2008; Dzimba *et al.* 2007; Nortjé *et al.* 2005). Salt is the main curing agent in the making of biltong. The salt, together with vinegar and other spices give biltong its distinctive flavor (Strydom and Zondagh 2014).

Both small and large scale biltong producers use a variety of recipes and processes to accommodate consumer preferences. Meat from the topside (semimembranosus) and silverside (biceps femoris) of young carcasses are the most preferred muscles for making biltong (Jones 2017). The meat is cut along the muscle fibers into thin slices of dimension; 20 – 50 mm thick, 40 – 150 mm wide, and 300 – 600 mm long (Strydom and Zondagh 2014). Traditionally, the slices of meat are dipped in vinegar after which salt and dry spices (black, pepper, coriander, and brown sugar) are sprinkled on all sides of the meat (Burfoot *et al.* 2010). Modern methods combine the vinegar, salt, and spices into a marinade that is applied onto the slices of meat (Naidoo and Lindsay 2010a). The meat slices are normally dried to a weight loss $\geq 50\%$ (Strydom and Zondagh 2014). The resulting biltong has a wide range of physicochemical properties. The moisture content and water activity range between 10 – 50 % and 0.54 – 0.93, respectively (Jones *et al.* 2017; Nortjé *et al.* 2005; Osterhoff and Leistner 1984; Petit *et al.* 2014; Van der Riet 1976). The salt content and the pH of biltong range between 2 – 11 % and 4.8 – 5.9, respectively (Petit *et al.* 2014; Strydom and Zondagh 2014).

Traditionally, biltong is produced during the winter season by hanging marinated pieces of meat to dry under ambient conditions (low temperature < 20 °C and low relative humidity < 40 %) (Strydom and Zondagh 2014). Modern biltong drying units range from simple domestic dryers to high capacity commercial dryers (Burfoot *et al.* 2010; Naidoo and Lindsay 2010b). Commercial dryers are predominantly temperature controlled hot air dryers. The temperature of the drying air used in commercial biltong processing ranges from 25 to 40 °C (Dzimba *et al.*

2007; Naidoo and Lindsay 2010b; Nortjé *et al.* 2005). Apart from the study by Taylor (1976) and Jones (2017) that used a drying air velocity of 3 and 2 m.s⁻¹, respectively, no other reviewed literature specified the air velocity used.

Despite, the improvement in dryers, microbial safety is still a major concern for biltong. According to Jones (2017) increasing the amount of vinegar and salt may help delay the growth of total microbial count. However, increasing the amount of vinegar may alter the penetration and diffusion of salt into the meat and its subsequent drying. It is necessary to characterise the influence of hot air drying parameters *viz.* temperature and velocity, on the drying kinetics of meat during biltong productions, so as to form a baseline from which the effect of varying the relative proportions of vinegar and salt content may be assessed.

The drying kinetics obtained by Hii *et al.* (2014) and Ahmat *et al.* (2015) for the drying of meat samples less than 10 mm thick, may not sufficiently characterise the drying of the thicker meat slices (20 – 50 mm thick) used to make biltong. A closer insight into the drying kinetics of meat for biltong production is provided by Cherono (2014) and Jones (2017). However, the studies by Cherono (2014) and Jones (2017) used a single level of drying air temperature of 25 °C. Cherono (2014) did not specify the air velocity, whereas Jones (2017) used a drying air velocity of 2 m.s⁻¹. The results obtained from these studies cannot adequately represent the wide variations in drying temperature and air velocity used during biltong processing.

A good understanding of the drying kinetics is essential in modelling the drying process. Thin layer drying models have been used to model the drying curves of several meat products such as; fish (Guan *et al.* 2013; Mujaffar and Sankat 2015), eland jerky (Kucerova *et al.* 2015), poultry (Ismail 2017; Javeed and Omre 2017), and beef (Mewa *et al.* 2018). Cherono (2014), recommended the approximation of diffusion model as the best model to describe the drying kinetics of beef during the processing of biltong. According to Erbay and Icier (2010) and Ertekin and Firat (2017), semi-theoretical models like the approximation of diffusion model are only valid within the process conditions for which they were developed. Cherono (2014) used a temperature of 25 °C and one level of drying air velocity, hence, the recommended model cannot confidently describe the drying kinetics of beef for the wide range of temperatures and drying air velocities used by commercial biltong processors.

The aim of this study was to establish the drying kinetics, select the best thin layer drying model, determine the effective moisture diffusivity, and the activation energy of beef being processed into biltong at hot air temperatures ranging between 30 and 40 °C and drying air velocity of 1.5 and 2.5 m s⁻¹.

3.2 Materials and Methods

3.2.1 Sample preparation

Portions of beef carcass were procured from a local butchery (Pick n Pay, Pietermaritzburg, South Africa). The portions were cut from the loin region of the carcass. The cuts were made 20 mm below the carcass surface to ensure uniform moisture content in the samples (Trujillo *et al.* 2003). The samples were sliced along the muscle fibres to dimensions of 150 x 50 x 15 mm (Dzimba *et al.* 2007). The initial moisture content of each sample was determined using the oven (AX 60, Carbolite Gero Ltd, Hope Valley, UK) drying method at 105 °C for 24 hours (AOAC 2012). Thereafter, the samples were put in sealed polythene bags and stored in a refrigerator (Defy C250, Defy Appliances (Pty) Ltd, Durban, South Africa) set at 4 °C, awaiting marination.

The biltong marinade was made using sodium chloride and vinegar in the ratio of 1:2, respectively. The beef samples were retrieved from the refrigerator and placed in sterilised containers. The marinade was then added to the beef samples in proportions of 0.075 kg of marinade per kg of beef (Jones 2017; Strydom and Zondagh 2014). The marinade was spread manually to ensure that all sides of the beef samples were uniformly coated with the marinade. The marinated samples were placed in a refrigerator set at 4 °C, for 24 hours. The samples were turned every six hours during the refrigerated storage period to ensure uniform distribution of marinade (von Gersdorff *et al.* 2018). The whole process of sample preparation, from slicing, marination to finally storing in a refrigerator took approximately 10 minutes.

3.2.2 The drying unit

A schematic of the drying unit is shown in Figure 3.1 and detailed drawings provided in Appendix A. The drying unit is a cabinet dryer made of stainless steel. The drying chamber has

a 100 mm thick, polyurethane insulation. A suspended drying platform (200 × 100 mm) made of stainless-steel mesh is hung on a weighing balance (Shimadzu UW6200H, Shimadzu Corporation, Kyoto, Japan) that is placed on top of the drying cabinet. The weighing balance is connected to a computer via an RS-232C connector to continuously log the mass of the sample being dried. The dryer is equipped with heating elements to heat the drying air. The temperature of the drying air is measured using T-type thermocouples (Pt100, Pentronic AB, Gunnebo, Sweden). A set of three centrifugal fans (intake, recirculation and discharge) facilitate the movement of air in the drying chamber. The velocity of the drying air is measured using an omnidirectional hot wire anemometer probe attached to an active air speed transmitter (HD 103T.0, Delta Ohm, Podova, Italy). The temperature and velocity of the drying air is set from the digital control panel and monitored using a supervisory control and data acquisition (SCADA) system installed in the dryer. The temperature of the sample placed on the drying platform is measured using a K-type thermocouple (Temperature Controls (Pty), Pinetown, South Africa) inserted in the centre of the sample. The K-type thermocouple is connected to a data logger (OM-DAQ-USB-2401, Omega, UK) linked to a computer to continuously record the temperature data.

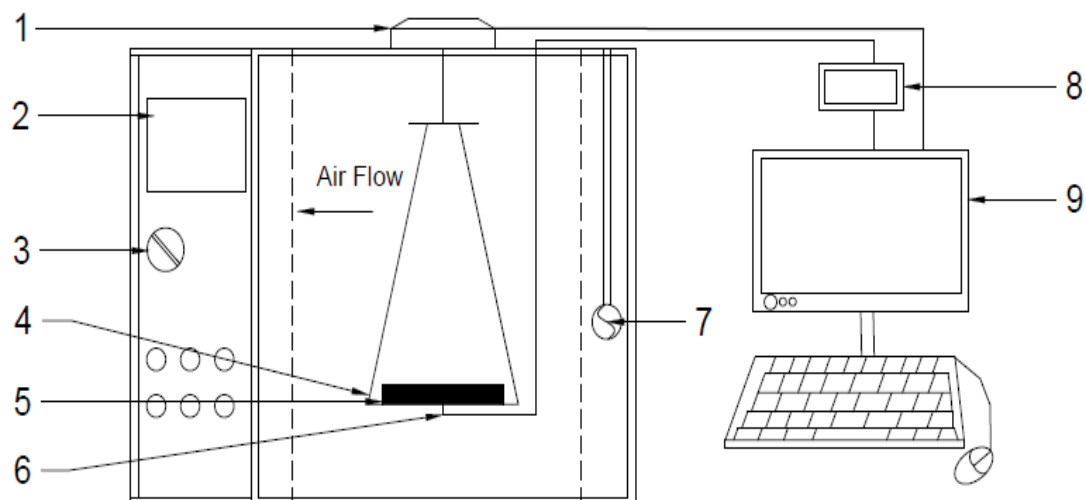


Figure 3.1 A schematic representation of the drying unit; 1 - weighing balance, 2 - digital control panel, 3 - power knob, 4 - drying platform, 5 - beef sample, 6 - K-type thermocouple, 7 - anemometer, 8 - temperature datalogger, and 9 - computer monitor

3.2.3 Drying procedure

A marinated beef sample was retrieved from the refrigerator and its moisture content determined using the oven drying method at 105 °C for 24 hours (AOAC 2012). The sample was allowed to equilibrate to room temperature (20 ± 1.5 °C) for at least 60 minutes to ensure all samples had relatively similar temperature, prior to drying. The dryer was preheated for at least 60 minutes to achieve uniform distribution of the set temperature and drying air velocity before commencement of the drying experiments. A K-type thermocouple was inserted into the centre of the beef sample and the sample placed on the drying platform (Figure 3.1). The mass and temperature of the sample were continuously measured by the weighing balance and the thermocouple, respectively; and logged on the computer. The beef sample was dried until 50 % of its mass was lost (Jones 2017).

The drying experiments employed a full factorial design. The experimental factors comprised of the drying air temperature (30, 35, and 40 °C) and the drying air velocity (1.5 and 2.5 m.s⁻¹). Each treatment had three replications resulting in a total of eighteen drying runs. The temperature of the drying air was selected from the range of temperature used in biltong processing (25 – 40 °C), while the choice of drying air velocity was guided by the two studies that specified the range of the air velocity used (2 and 3 m.s⁻²) (Jones 2017; Taylor 1976).

The data obtained from the experiments was subjected to the analysis of variance (ANOVA) at 5 % level of significance. Where significant ANOVA results of the treatment were found, a mean comparison was done using Fisher's Unprotected LSD method. All data analysis was done using GenStat® 18th Edition (VSN International Ltd, Hemel Hempstead, United Kingdom).

3.2.4 Evaluation of the drying characteristics and thin layer modelling of the drying curves

The instantaneous moisture content was calculated from the moisture loss data, obtained from the drying experiments using Equations 3.1 – 3.4.

$$Y_{w0} = \frac{m_{w0}}{m_0} \quad (3.1)$$

$$m_w = m - (1 - Y_{w0})m_0 \quad (3.2)$$

$$m_d = (1 - Y_{w0})m_0 \quad (3.3)$$

$$X = \frac{m_w}{m_d} = \frac{m_t}{(1 - Y_{w0})m_0} - 1 \quad (3.4)$$

Where:

Y_{w0} = initial moisture content of the sample (kg of water/kg of sample),

m_{w0} = initial mass of water in the sample (kg),

m_0 = initial mass of the sample (kg),

m_t = instantaneous mass of sample (kg),

m_w = mass of water (kg),

m_d = mass of solid (kg), and

X = moisture content of the sample expressed in dry basis (kg of water/kg of dry matter).

The instantaneous moisture content data was used to calculate the moisture ratio (MR) as shown in Equation 3.5. Thereafter, the drying rate (D_R) was obtained as a derivative of the MR with respect to drying time (Equation 3.6).

$$MR = \frac{X_t}{X_0} \quad (3.5)$$

$$D_R = \frac{dMR}{dt} \quad (3.6)$$

Where:

T = drying time (s),

X_t = instantaneous moisture content (kg of water/kg of dry matter), and

X_0 = initial moisture content (kg of water/kg of dry matter).

Fickian diffusion is the predominant mode of moisture transport in meat (Trujillo *et al.* 2007).

The page model and five thin layer models derived from Fick's Second Law of Diffusion (Table 3.1) were fitted to the experimental data using the non-linear least square analysis in MATLAB (MATLAB R18.2b, MathWorks, Inc., Natick, MA, USA). The Page model was chosen based on its excellent performance in describing the drying kinetics of different food products (Ertekin and Firat 2017), whereas the other five models were selected based on previous research on biltong (Cherono 2014) and kaddid (Chabbouh *et al.* 2013). The suitability of the models was assessed based on the coefficient of determination (R^2) and the root mean square error (RMSE) (Equations 3.7 and 3.8, respectively). The best model was chosen based on a high R^2 and a low RMSE.

$$R^2 = \frac{\sum_{i=1}^n (MR_{model} - MR_{exp})^2}{\sum_{i=1}^n (MR_{model} - \overline{MR})^2} \quad (3.7)$$

$$RMSE = \sqrt{\frac{\sum_{i=1}^n (MR_{model} - MR_{exp})^2}{n}} \quad (3.8)$$

Where:

- MR_{model} = predicted MR,
- MR_{exp} = MR obtained from experiment data,
- \overline{MR} = mean of the experimental data, and
- N = number of observations.

The effective moisture diffusivity (D_{eff}) was obtained using Fick's Second Law of Diffusion. The solution to Fick's equation, for an infinite slab, assuming negligible shrinkage, negligible external resistance, uniform initial moisture distribution, and a constant diffusivity; is shown in Equation 3.9 (Ertekin and Firat 2017).

$$MR = \frac{8}{\pi^2} \sum_{n=0}^{\infty} \frac{1}{(2n+1)^2} \times \exp \left[-(2n+1)^2 \frac{\pi^2 D_{eff} t}{4L^2} \right] \quad (3.9)$$

Where:

- L = half thickness of the slab (m), and
- N = number of observations

Table 3.1 Thin layer drying models

S/N	Name	Equation	Reference
1	Page model	$MR = \exp(-kt^n)$	Hii <i>et al.</i> (2008)
2	Approximation of diffusion model	$MR = a \exp(-kt) + (1 - a)\exp(-kbt)$	Botelho <i>et al.</i> (2011)
3	Simplified Fick's diffusion model	$MR = \exp(-k(t/L^n))$	Mahdhaoui <i>et al.</i> (2013)
4	Midilli model	$MR = \exp(-k(t^n)) + b \times t$	Midilli <i>et al.</i> (2002)
5	Logarithmic model	$MR = a \exp(-kt) + c$	Wang <i>et al.</i> (2007)
6	Two-term model	$MR = a \exp(-kt) + b \exp(-k_2t)$	Erbay and Icier (2010)

Equation 3.9 can be linearised as shown in Equation 3.10 and the D_{eff} determined from the slope of the graph of $\ln(MR)$ against drying time (Equation 3.11).

$$\ln MR = \ln \frac{8}{\pi^2} - \left(\frac{\pi}{2L}\right)^2 D_{\text{eff}} t \quad (3.10)$$

$$\text{Slope} = \frac{\pi^2 D_{\text{eff}}}{4L^2} \quad (3.11)$$

The drying temperature has an Arrhenius type relationship with the D_{eff} (Equation 3.12) (Zhu and Shen 2014).

$$D_{\text{eff}} = D_0 \exp\left(-\frac{E_a}{RT}\right) \quad (3.12)$$

Where:

D_0 = pre-exponential factor of Arrhenius equation equivalent to diffusivity at the maximum temperature ($\text{m}^2 \text{s}^{-1}$),

E_a = activation energy (kJ mol^{-1}),
 R = universal gas constant ($\text{kJ mol}^{-1} \text{K}^{-1}$), and
 T = the temperature (K).

The activation energy (E_a) was obtained from the linear form of Equation 3.12 (Equation 3.13) by determining the slope of the graph of $\ln(D_{\text{eff}})$ against $\left(-\frac{1}{RT}\right)$.

$$\ln D_{\text{eff}} = \left(-\frac{1}{RT}\right) E_a + \ln D_o \quad (3.13)$$

3.3 Results and Discussion

3.3.1 Drying characteristics

The initial moisture content of the beef samples was 74.38 ± 0.27 %. The moisture content of the marinated beef samples reduced to 71.60 ± 0.27 % after 24 hours of storage at 4 °C. The reduction in moisture is attributed to the action of the salt and vinegar contained in the biltong marinade. These results are consistent with the findings of Medyński *et al.* (2000) and Goli *et al.* (2014) who reported increased drip in minced pork and beef; and turkey breast meat that were pre-treated with salt and acid. Salt acts as a curing agent and lowers the moisture content of the beef samples through osmotic dehydration (Guizani *et al.* 2008; Hui 2012). Simultaneously, the acetic acid in the vinegar lowers the pH of meat proteins, thus reducing its water holding capacity. Consequently, the meat losses water through dripping (Brewer 2014; Cheng and Sun 2008; Miller 2014). The dried samples had an average moisture content of 42.49 ± 0.81 %. This is within the range of 35 – 50 % reported for high moisture biltong reported by previous researchers (Jones 2017; Nortjé *et al.* 2005; Petit *et al.* 2014).

The temperature profile of the marinated beef samples at different drying air temperature and velocity is shown in Figure 3.2. The temperature of the beef samples increased with increasing drying time. The highest temperature recorded in all the samples was between $0.5 - 1.8$ °C below the respective drying air temperatures. The reduced temperature is because of heat lost as the moisture evaporates from the sample surface being dried (Srikiatden and Roberts 2007).

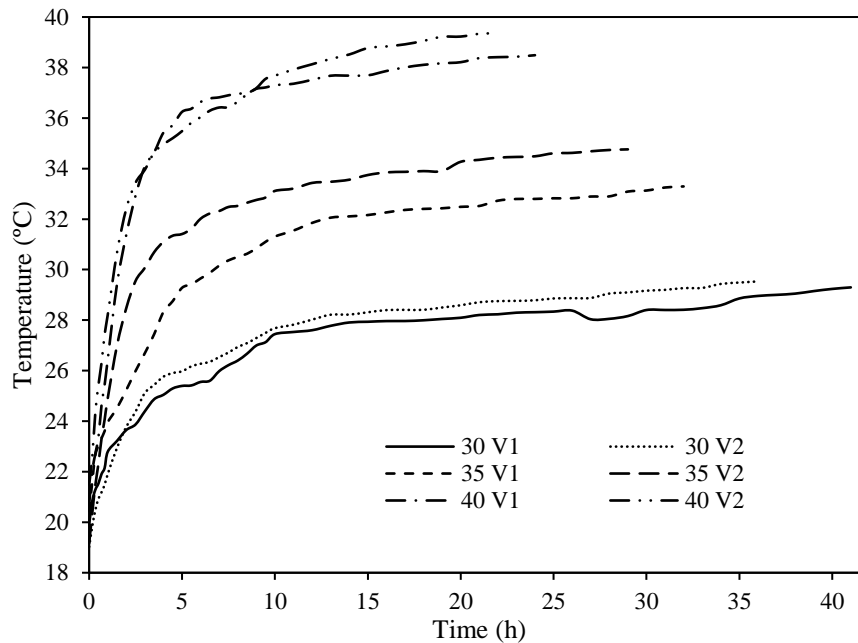


Figure 3.2 Average sample temperature curves versus time at drying air temperatures of 30, 35, and 40 °C; and drying air velocities of 1.5 (V1) and 2.5 m.s⁻¹ (V2)

The average sample temperature was significantly ($p \leq 0.05$) affected by the drying air temperature. The drying air temperature of 40 °C had the highest average sample temperature of 34.26 ± 5.38 °C at the drying air velocity of 1.5 m.s⁻¹, and 34.57 ± 5.40 °C at the drying air velocity of 2.5 m.s⁻¹. A drying air temperature of 30 °C had the lowest average sample temperature of 26.57 ± 2.45 and 26.68 ± 2.84 °C at the drying air velocity of 1.5 and 2.5 m.s⁻¹, respectively. Higher drying air temperature results in higher average sample temperature because of the increased heat flux into the sample. Increasing the drying air temperature increases the temperature gradient between the drying air and the sample surface and subsequently the heat flux into the sample.

A change in the drying air velocity from 1.5 to 2.5 m.s⁻¹, resulted in slightly higher average sample temperature. A higher air velocity increases the mass flow rate of air and consequently its total heat content. The increased heat content promotes an increase in heat transferred into the sample which results in a higher sample temperature at a higher drying air velocity. Similar findings were made by Soydan Karabacak *et al.* (2014) who reported a significant increase in the average sample temperature with increasing drying air velocity. The increase in sample

temperature with increase in air velocity in the current study was, however, not significant ($p \geq 0.05$). The lack of significant effect on the sample temperature due to the drying air velocity in the current study can be attributed to the low temperature range of 30 – 40 °C used in the study, compared to the high temperature range of 48 – 70 °C used by Soydan Karabacak *et al.* (2014).

The change in moisture content (expressed as MR) with drying time is shown in Figure 3.3. The MR curves follow an exponential decay reported in many previous research on drying of agricultural products (Mewa *et al.* 2018; Nguyen *et al.* 2019; Onwude *et al.* 2019). The temperature of the drying air significantly ($p \leq 0.05$) influenced the drying time. The longest drying times of 41 and 36 hours were observed at 30 °C and drying air velocities of 1.5 and 2.5 m.s^{-1} , respectively. The drying air temperature of 40 °C resulted in the shortest drying times of 24 and 22 hours at drying air velocities of 1.5 and 2.5 m.s^{-1} , respectively. At a drying air temperature of 35 °C, the recorded drying times were 32 and 29 hours at drying air velocities of 1.5 and 2.5 m.s^{-1} , respectively. The difference in drying time is due to the increase in heat flux into the sample at higher temperatures. The increased heat flux accelerates the vaporisation of water in the sample (Srikiatden and Roberts 2007). Consequently, the vapour pressure of the sample increases, expediting moisture transport out of the sample (Mewa *et al.* 2018).

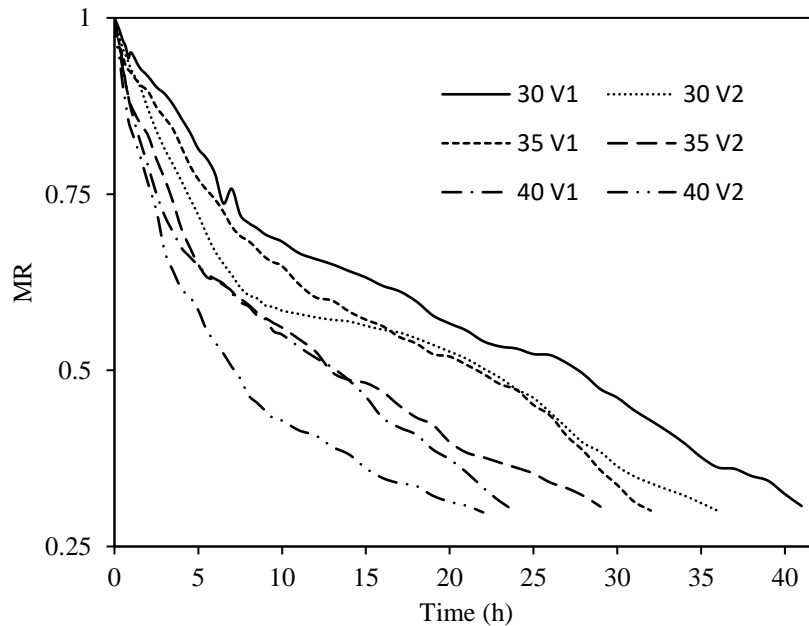


Figure 3.3 Curves of moisture ratio versus drying time of marinated beef at drying air temperatures of 30, 35, and 40 °C; and air velocities of 1.5 (V1) and 2.5 m.s^{-1} (V2)

The results presented in Figure 3.3 indicate that the drying time decreased when the velocity of the drying air changed from 1.5 to 2.5 m.s⁻¹. However, the velocity of the drying air had no statistically significant ($p \geq 0.05$) influence on the drying times obtained in this study. According to Jason (1958), as reported by Srikiatden and Roberts (2007), external resistance to moisture transfer becomes negligible when the drying air velocity is ≥ 1 m.s⁻¹. The drying of the sample is thus, an internally controlled process and varying the air velocity between 1.5 and 2.5 m.s⁻¹ has no significant effect on the drying time.

The variation in drying rate with drying time during the drying process is presented in Figure 3.4 (a). The drying process can be divided into a falling rate and a constant rate drying. The falling rate drying period occurred within the first 10 hours of drying and is characterised by a rapid decrease in the drying rate. The drying rate decreases primarily due to the reduction in heat flux into the sample as the sample temperature approaches the drying air temperature (Rizvi 2005). The reduction in heat flux is caused by the decrease in the temperature gradient between the sample and the drying air as the sample temperature approaches the temperature of the drying air. The reduction in heat flux is exemplified by the rapid decrease in the rate of change in sample temperature as shown in Figure 3.4 (b).

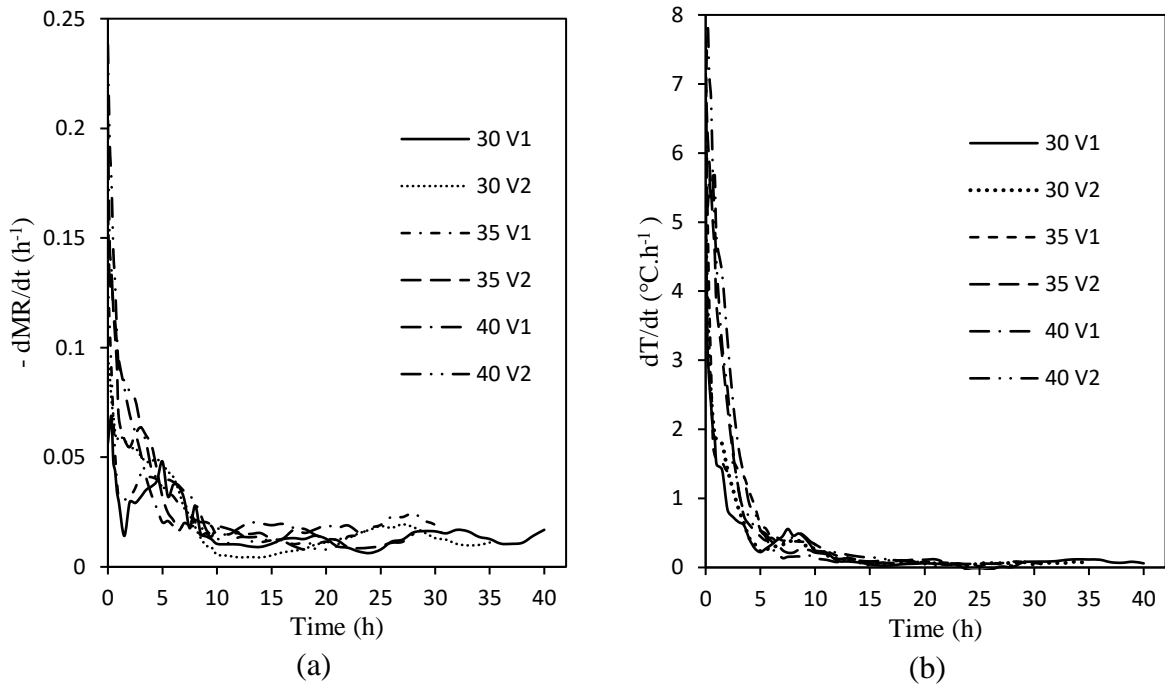


Figure 3.4 Curves of the drying rate versus time (a) and the rate of change in sample temperature vs time (b)

The constant rate drying period occurs after the first 10 hours of drying and is characterised by extremely low drying rate (Figure 3.4 (a)). The constant rate drying period corresponds with a constant rate of change in sample temperature (Figure 3.4 (b)). During this period, the sample temperature has reached its maximum and remains fairly constant which indicates low heat flux into the sample. According to Feyissa *et al.* (2013), heat transfer is the key driver of moisture transfer in meat, consequently, low heat flux into the sample results in low drying rates. Additionally, the low drying rate can also be attributed to the additional internal resistance to moisture transfer as the sample moisture content decreases (Karel and Lund 2003).

The velocity of the drying air had no significant ($p \geq 0.05$) effect on the average drying rate over the entire drying process which corroborates the aforementioned lack of significant effect on the drying time. This is exemplified by the small deviation between the average drying rate at 1.5 and 2.5 m.s⁻¹ over the entire drying period (Table 3.2). Comparatively, a greater deviation was observed between the average drying rate at 1.5 and 2.5 m.s⁻¹ within the first 10 hours of drying. This indicates that the drying air velocity significantly ($p \leq 0.05$) influenced the drying rate during the falling rate period ($t \leq 10$ hours). Babalis and Belessiotis (2004) reported similar findings during the thin layer drying of figs. The strong influence of drying air velocity at the onset of drying suggests that the initial drying phase is dominated by surface evaporation which is influenced by the velocity of the drying air. As the drying progresses, the evaporation front recedes into the sample, making diffusion the most important driver of moisture transport, thus overriding the influence of the velocity of the drying air.

Table 3.2 Average drying rate (Dr) in the first 10 hrs and the entire drying period

Temp (°C)	Dr in the first 10 hours		Standard deviation
	1.5 m.s ⁻¹	2.5 m.s ⁻¹	
30	0.0337	0.0456	0.0060
35	0.0423	0.0566	0.0072
40	0.0595	0.0736	0.0070
Dr for the entire drying period			
30	0.0219	0.0264	0.0022
35	0.0299	0.0354	0.0027
40	0.0453	0.0514	0.0300

3.3.2 Thin layer modelling of the drying curves

The results of the non-linear least square analysis of the six thin layer drying models compared to the experimental data are in Tables 3.3 and 3.4. All the models had an $R^2 > 0.9284$ and $RMSE < 0.08613$, hence, could suitably predict the changes in MR over time (Nguyen *et al.* 2019). The two term model was the most suitable model with an average R^2 and RMSE values of 0.99297 and 0.0161, respectively. The approximation of diffusion model was the second ($R^2 = 0.99268$, $RMSE = 0.01647$) and Midilli model the third ($R^2 = 0.99083$ and $RMSE = 0.01845$). The simplified Fick's diffusion model was the least suitable model across all drying conditions ($R^2 = 0.95475$ and $RMSE = 0.04989$). These results are in agreement with previous research that have reported the suitability of the Two term model, Midilli model, and Page model in describing the hot air drying kinetics of meat products (Guan *et al.* 2013; Javeed and Omre 2017; Kucerova *et al.* 2015; Mewa *et al.* 2018; Mujaffar and Sankat 2015).

Table 3.3 Model coefficients and statistical parameters for Two term, Approximation of diffusion and Midilli models

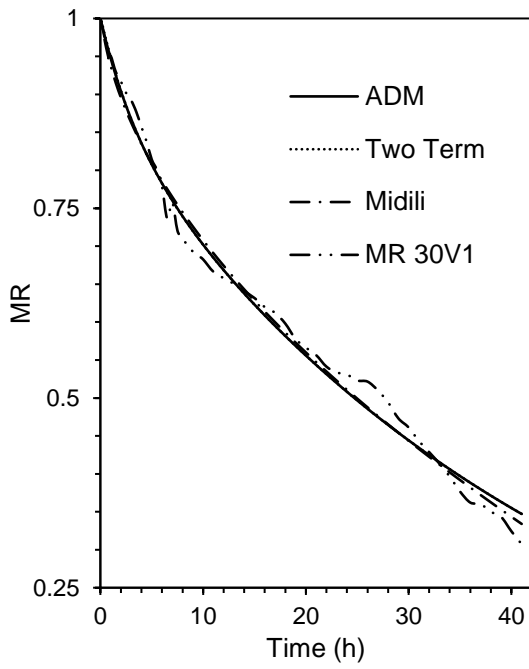
T (°C)	Air vel (m.s ⁻¹)	Model	Model Coefficient					R ²	RMSE
			K	K2	a	b	n		
30	1.5	Two term	0.2980	0.0224	0.1340	0.8693		0.9911	0.0198
30	2.5		0.0222	0.3574	0.7526	0.2619		0.9828	0.0272
35	1.5		0.0280	0.3284	0.8617	0.1253		0.9906	0.0199
35	2.5		0.0295	0.3877	0.7331	0.2592		0.9976	0.0103
40	1.5		0.0374	0.7335	0.7893	0.2153		0.9973	0.0106
40	2.5		0.2867	0.0264	0.4487	0.5302		0.9984	0.0089
Average								0.9930	0.0161
30	1.5	Approximation of Diffusion Model (ADM)	0.2918		0.1306	0.0767		0.9911	0.0196
30	2.5		0.3318		0.2499	0.0664		0.9825	0.0273
35	1.5		0.3846		0.1344	0.0733		0.9902	0.0200
35	2.5		0.4132		0.2624	0.0720		0.9975	0.0104
40	1.5		0.7091		0.2116	0.0526		0.9973	0.0105
40	2.5		0.3439		0.4281	0.0884		0.9975	0.0110
Average								0.9927	0.0165
30	1.5	Midilli	0.0844		1.0250	-0.0045	0.5636	0.9909	0.0200
30	2.5		0.1511		1.0470	-0.0018	0.5160	0.9750	0.0328
35	1.5		0.0920		1.0120	-0.0056	0.5727	0.9911	0.0193
35	2.5		0.1530		1.0200	0.0004	0.6112	0.9959	0.0135
40	1.5		0.1739		1.0270	-0.0043	0.5118	0.9936	0.0164
40	2.5		0.1867		1.0070	0.0068	0.7390	0.9985	0.0087
Average								0.9908	0.0185

Table 3.4 Model coefficients and Statistical parameters for Page, Logarithmic and Simplified diffusion models

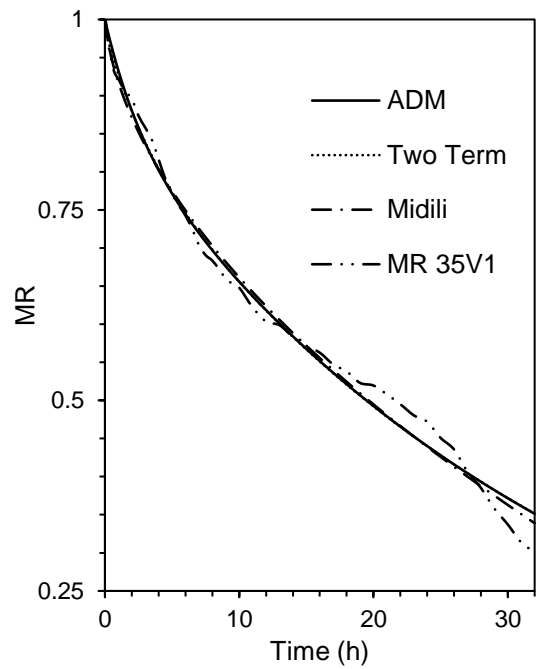
T (°C)	Air vel (m.s ⁻¹)	Model	Model Coefficient					R ²	RMSE	
			K	a	b	c	n			
30	1.5	Page	0.0590					0.7723	0.9885	0.0221
30	2.5		0.1119					0.6316	0.9727	0.0336
35	1.5		0.0745					0.7561	0.9888	0.0212
35	2.5		0.1388					0.6293	0.9952	0.0142
40	1.5		0.1457					0.6344	0.9918	0.0180
40	2.5		0.1960					0.6151	0.9917	0.0198
Average								0.9881	0.0215	
30	1.5	Logarithmic model	0.0413	0.7468		0.2197		0.9825	0.0275	
30	2.5		0.0841	0.6175		0.3438		0.9570	0.0426	
35	1.5		0.0525	0.7347		0.2245		0.9840	0.0257	
35	2.5		0.1057	0.6360		0.3172		0.9872	0.0236	
40	1.5		0.1032	0.6434		0.2957		0.9767	0.0308	
40	2.5		0.1771	0.6544		0.3086		0.9961	0.0138	
Average								0.9806	0.0273	
30	1.5	Simplified Fick's Diffusion Model (SFDM)	186.60	0.9458			-4.6790	0.9783	0.0307	
30	2.5		0.0260	0.9000			0.09672	0.9284	0.0550	
35	1.5		2.3680	0.9389			-2.2560	0.9793	0.0292	
35	2.5		68.140	0.8929			-3.8930	0.9515	0.0861	
40	1.5		11.150	0.8972			-2.8720	0.9572	0.0417	
40	2.5		0.4263	0.8842			-0.9828	0.9338	0.0567	
Average								0.9548	0.0499	

A graph of the experimental and predicted moisture ratio values against drying time, indicates that the accuracy of the thin layer models increased with increasing drying air temperature and velocity. At a low drying air velocity of 1.5 m.s⁻¹, the predicted MR showed more deviation from the experimental MR for both drying temperatures of 30 and 35 °C, especially towards the end of the drying period (Figure 3.5 (a) and (b)). The predicted MR values were closer to the

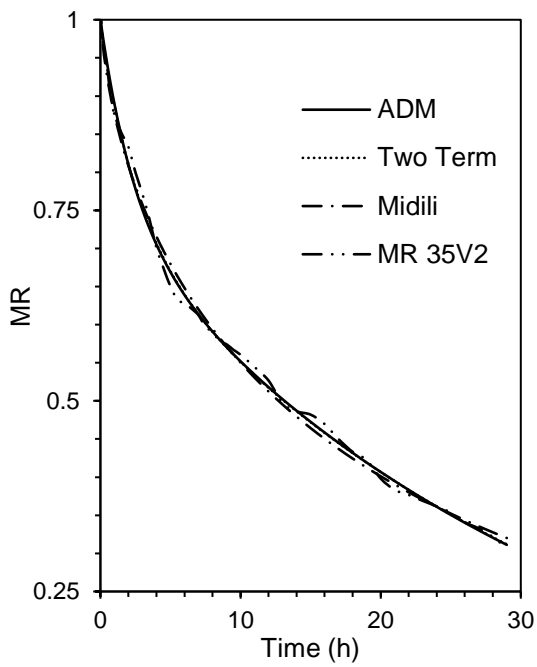
experimental ones at the drying air velocity of 2.5 m.s^{-1} and drying temperatures of 35 and 40 °C (Figure 3.5 (c) and (d)). Mewa *et al.* (2018) report similar improvement in the accuracy of model prediction with increase in the drying air temperature. At higher temperature and velocity, the surface moisture dries off quickly, thus, moisture movement out of the meat is predominantly controlled by internal diffusion (Trujillo *et al.* 2007). Consequently, the thin layer model assumption of negligible external resistance to moisture diffusion is more applicable at these drying conditions which results in the improved accuracy of the model predictions.



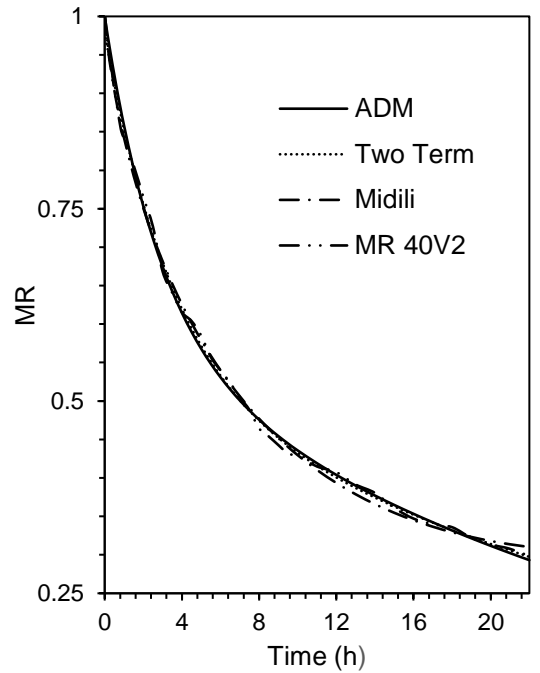
(a)



(b)



(c)



(d)

Figure 3.5 Experimental and predicted MR curves of the best three models at: (a) 30 °C and 1.5 m.s⁻¹ (b) 35 °C and 1.5 m.s⁻¹ (c) 35 °C and 2.5 m.s⁻¹ (d) 40 °C and 2.5 m.s⁻¹

3.3.3 Effective moisture diffusivity

The values of the D_{eff} during hot air drying of marinated beef ranged between $1.60 \times 10^{-10} \text{ m}^2 \cdot \text{s}^{-1}$ and $2.28 \times 10^{-10} \text{ m}^2 \cdot \text{s}^{-1}$ (Table 3.5). The D_{eff} values obtained in this study fall within the range of values obtained by previous studies on kaddid (Chabbouh *et al.* 2013), eland jerky (Kucerova *et al.* 2015), chicken breast meat (Ismail 2017), and beef (Mewa *et al.* 2018).

Table 3.5 Effective moisture diffusivity of marinated beef during hot air drying

Temperature (°C)	Air velocity (m.s ⁻¹)	D_{eff} (m ² .s ⁻¹)
30	1.5	$1.60 \times 10^{-10} \text{ m}^2 \cdot \text{s}^{-1}$
	2.5	$1.83 \times 10^{-10} \text{ m}^2 \cdot \text{s}^{-1}$
35	1.5	$2.05 \times 10^{-10} \text{ m}^2 \cdot \text{s}^{-1}$
	2.5	$2.28 \times 10^{-10} \text{ m}^2 \cdot \text{s}^{-1}$
40	1.5	$2.28 \times 10^{-10} \text{ m}^2 \cdot \text{s}^{-1}$
	2.5	$2.28 \times 10^{-10} \text{ m}^2 \cdot \text{s}^{-1}$

The drying air temperature had a significant ($p \leq 0.05$) influence on the D_{eff} . The D_{eff} increased with an increase in the drying air temperature. Similar observations have been made in previous research on the drying of meat and meat products (Ismail 2017; Kucerova *et al.* 2015; Mewa *et al.* 2018). The increase in the D_{eff} with temperature is attributed to increased heat flux as the temperatures increases. According to Shi *et al.* (2008) high heat energy accelerates the movement of water molecules leading to a high moisture diffusivity.

A change in velocity of the drying air led to a marginal increase in the D_{eff} at drying air temperatures of 30 and 35 °C but not at 40 °C. Nevertheless, the velocity of the drying air had no significant ($p \geq 0.05$) influence on the D_{eff} . This concurs with the findings of Clemente *et al.* (2011) that reported a lack of significant change in D_{eff} when the velocity of the drying air is varied beyond 2 m.s⁻¹. According to Clemente *et al.* (2011) the D_{eff} is an intrinsic transport

property of the material, hence, not influenced by external conditions. On the contrary, research by Lopez *et al.* (2000) and Velić *et al.* (2004) on kitchen wastes and potatoes, respectively, reported an increase in D_{eff} with increase in drying air velocity. The lack of significant influence of the drying air velocity on the D_{eff} in this study can be attributed to the overriding influence of the drying air temperature, as observed by Akpınar *et al.* (2003) on potato slices.

3.3.4 Activation energy

The E_a was determined from the Arrhenius type relationship between the D_{eff} and the temperature of the drying air (Figure 3.6). The E_a derived from this relationship was 28.2126 and 17.7068 $\text{kJ}\cdot\text{mol}^{-1}$ at a drying air velocity of 1.5 and 2.5 $\text{m}\cdot\text{s}^{-1}$, respectively. This is within the range of 23.75 – 26.22 $\text{kJ}\cdot\text{mol}^{-1}$ reported for eland jerky (Kucerova *et al.* 2015) and 16.3 – 22.8 $\text{kJ}\cdot\text{mol}^{-1}$ reported for chicken meat (Hii *et al.* 2014; Ismail 2017). The value of activation energy dropped with increase in the drying air velocity. This observation is consistent with the findings of Mirzaee *et al.* (2009). According to Oliveira *et al.* (2016), higher drying temperatures result in lower entropy and enthalpy values of activation, subsequently lowering the activation energy. Higher drying air velocity resulted in slightly higher average sample temperatures, thus, lowering activation energy. The lower E_a value obtained at the drying air velocity of 2.5 $\text{m}\cdot\text{s}^{-1}$ indicates that the D_{eff} is less sensitive to temperature variations at a higher drying air velocity than at lower drying air velocity.

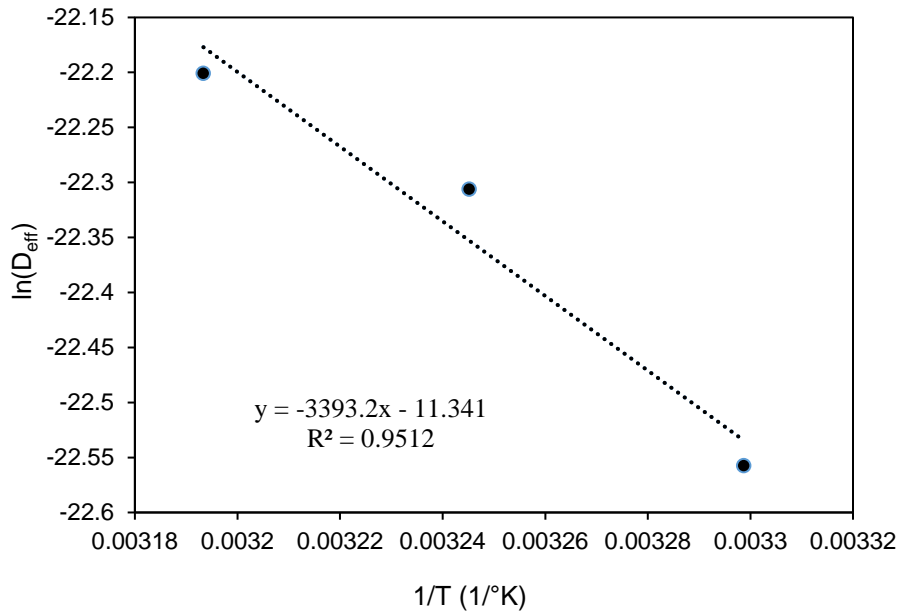


Figure 3.6 Arrhenius relationship between D_{eff} and temperature at drying air velocity of 1.5 m s^{-1}

3.4 Conclusion

This chapter determined the drying kinetics, effective moisture diffusivity, activation energy and suitable thin layer model for the drying of marinated beef at drying air temperature of between $30 - 40 \text{ }^\circ\text{C}$ and drying air velocity of 1.5 and 2.5 m.s^{-1} . The drying air temperature has a significant influence on the drying kinetics of the marinated beef, whereas the velocity of the drying air only influences the drying rate in the first falling rate period. The results indicate that processing biltong at HAD temperature of $40 \text{ }^\circ\text{C}$ increases the core sample temperatures and drying rate by 28% and 100% , respectively, and reduces the drying time by 40% compared to HAD at $30 \text{ }^\circ\text{C}$. The initial stages of drying occur under the falling rate drying period while the later stages occur under a constant rate drying period. The onset of the drying process is dominated by surface evaporation, hence the significant influence of air velocity on the drying rate during this phase. Across the entire drying period, diffusion is the predominant mode of moisture transport during the drying of marinated beef used to produce biltong. Drying kinetics of marinated beef during the processing of biltong is best described by the two-term model. Nonetheless, approximation of diffusion and Midilli models also give very good approximation of the MR over the drying period. The accuracy of the drying models increases with the increase

in temperature and drying air velocity which highlights the bias towards diffusion moisture transport with increase in temperature and air velocity. The D_{eff} of marinated meat being processed into biltong ranges from $1.60 \times 10^{-10} \text{ m}^2 \cdot \text{s}^{-1}$ and $2.28 \times 10^{-10} \text{ m}^2 \cdot \text{s}^{-1}$, while the E_a is 28.2126 and 17.7068 $\text{kJ} \cdot \text{mol}^{-1}$ at a drying air velocity of 1.5 and 2.5 $\text{m} \cdot \text{s}^{-1}$, respectively. The higher E_a at 1.5 $\text{m} \cdot \text{s}^{-1}$ indicates the high sensitivity of the D_{eff} to changes in drying air temperature at lower air velocity. The results from this study cover the range of temperatures (30 – 40 °C) predominantly used by biltong processors and also offer new information on the influence of two levels of air velocity on the drying kinetics of marinated beef, thus, can be used to optimise the processing of biltong. Moreover, the results provide a good basis on which to assess the influence of variation in the salt and vinegar content (which may be necessary to limit microbial growth) on the drying kinetics of meat during biltong processing.

3.5 References

- Ahmat, T., Barka, M., Aregba, A. W., & Bruneau, D. 2015. Convective drying kinetics of fresh beef: An experimental and modeling approach. *Journal of food processing and preservation* 39 (6): 2581-2595.
- Akpınar, E., Midilli, A., & Bicer, Y. 2003. Single layer drying behaviour of potato slices in a convective cyclone dryer and mathematical modeling. *Energy conversion and management* 44 (10): 1689-1705.
- AOAC. 2012. *Official Methods of Analysis of AOAC International*. Gaithersburg, USA: AOAC International.
- Babalıs, S. J., & Belessiotıs, V. G. 2004. Influence of the drying conditions on the drying constants and moisture diffusivity during the thin-layer drying of figs. *Journal of food engineering* 65 (3): 449-458.
- Botelho, F. M., Corrêa, P. C., Goneli, A., Martins, M. A., Magalhães, F. E., & Campos, S. C. 2011. Periods of constant and falling-rate for infrared drying of carrot slices. *Revista Brasileira de Engenharia Agrícola e Ambiental* 15 (8): 845-852.
- Brewer, M. 2014. Chemical and physical characteristics of meat| Water-holding capacity. In M. Dikeman, & C. Devine (Eds.), *Encyclopedia of meat sciences*. London: Oxford: Academic Press.

- Burfoot, D., Everis, L., Mulvey, L., Wood, A., & Campden, R. 2010. Literature review of microbiological hazards associated with biltong and similar dried meat products. Food Standard Agency, London. https://www.food.gov.uk/sites/default/files/media/document/574-1-1007_B13015_Final_Report.pdf. Accessed on 21 January 2020.
- Burnham, G. M., Hanson, D. J., Koshick, C. M., & Ingham, S. C. 2008. Death of Salmonella serovars, Escherichia coli O157: H7, Staphylococcus aureus and Listeria monocytogenes during the drying of meat: a case study using biltong and droëwors. *Journal of food safety* 28 (2): 198-209.
- Chabbouh, M., Hajji, W., Hadj Ahmed, S. B., Farhat, A., Bellagha, S., & Sahli, A. 2011. Combined effects of osmotic dehydration and convective air drying on kaddid meats: Kinetics and quality. *Drying Technology* 29(13): 1571-1579.
- Chabbouh, M., Sahli, A., & Bellagha, S. 2013. Does the spicing step affect the quality and drying behaviour of traditional kaddid, a Tunisian cured meat? *Journal of the Science of Food and Agriculture* 93 (14): 3634-3641.
- Cheng, Q., & Sun, D.-W. 2008. Factors affecting the water holding capacity of red meat products: a review of recent research advances. *Critical reviews in food science and nutrition* 48 (2): 137-159.
- Cherono, K. 2014. *Infrared Drying of Biltong*. MSc, University of KwaZulu-Natal, Pietermaritzburg, South Africa.
- Cherono, K., Mwithiga, G., & Schmidt, S. 2016. Infrared drying as a potential alternative to convective drying for biltong production. *Italian journal of food safety* 5 (3): 140-145.
- Clemente, G., Bon, J., Sanjuán, N., & Mulet, A. 2011. Drying modelling of defrosted pork meat under forced convection conditions. *Meat science* 88 (3): 374-378.
- Dzimba, F. E. J., Faria, J., & Walter, E. H. M. 2007. Testing the sensory acceptability of biltong formulated with different spices. *African Journal of Agricultural Research* 2 (11): 547-577.
- Erbay, Z., & Icier, F. 2010. A review of thin layer drying of foods: theory, modeling, and experimental results. *Critical reviews in food science and nutrition* 50 (5): 441-464.
- Ertekin, C., & Firat, M. Z. 2017. A comprehensive review of thin-layer drying models used in agricultural products. *Critical reviews in food science and nutrition* 57 (4): 701-717.
- Feyissa, AH, Gernaey, KV and Adler-Nissen, J. 2013. 3D modelling of coupled mass and heat transfer of a convection-oven roasting process. *Meat science* 93 (4): 810-820.

- Goli, T., Ricci, J., Bohuon, P., Marchesseau, S., & Collignan, A. 2014. Influence of sodium chloride and pH during acidic marination on water retention and mechanical properties of turkey breast meat. *Meat science* 96 (3): 1133-1140.
- Guan, Z., Wang, X., Li, M., & Jiang, X. 2013. Mathematical modeling on hot air drying of thin layer fresh tilapia fillets. *Polish journal of food and nutrition sciences* 63 (1): 25-33.
- Guizani, N., Al-Shoukri, A. O., Mothershaw, A., & Rahman, M. S. 2008. Effects of salting and drying on shark (*Carcharhinus sorrah*) meat quality characteristics. *Drying Technology* 26 (6): 705-713.
- Hii, C., Itam, C., & Ong, S. 2014. Convective air drying of raw and cooked chicken meats. *Drying Technology* 32 (11): 1304-1309.
- Hii, C., Law, C., & Cloke, M. 2008. Modeling of thin layer drying kinetics of cocoa beans during artificial and natural drying. *Journal of Engineering Science and Technology* 3 (1): 1-10.
- Hui, Y. H. 2012. *Handbook of meat and meat processing*: London. CRC press.
- Ismail, O. 2017. An experimental and modeling investigation on drying of chicken meat in convective dryer. *Studia Universitatis Babeş-Bolyai Chimia* 62 (4): 459-469.
- Jason, A. 1958. Fundamental aspects of the dehydration of foodstuffs. *Society of Chemical Industry, London* 10 (3): 103-135.
- Javeed, A., & Omre, P. 2017. Mathematical modeling evaluation for convective hot air drying of poultry meat. *International Journal of Agricultural Engineering* 10 (1): 168-178.
- Jones, M. 2017. *Profiling of traditional South African biltong in terms of processing, physicochemical properties and microbial stability during storage*. PhD, Stellenbosch University, Stellenbosch, South Africa.
- Jones, M., Arnaud, E., Gouws, P., & Hoffman, L. C. 2017. Processing of South African biltong—A review. *South African Journal of Animal Science* 47 (6): 743-757.
- Karel, M., & Lund, D. B. 2003. *Physical principles of food preservation* (2ed.). New York, United States: Marcel Dekker, Inc.
- Kucerova, I., Hubackova, A., Rohlik, B.-A., & Banout, J. 2015. Mathematical modeling of thin-layer solar drying of Eland (*Taurotragus oryx*) Jerky. *International journal of food engineering* 11 (2): 229-242.
- Lopez, A., Iguaz, A., Esnoz, A., & Virseda, P. 2000. Thin-layer drying behaviour of vegetable wastes from wholesale market. *Drying Technology* 18 (4-5): 995-1006.

- Mahdhaoui, B., Mechlouch, R. F., Mahjoubi, A., Zahafi, K., & Brahim, A. B. 2013. Mathematical model on thin layer drying of olive fruit (*Olea europaea* L.). *Journal of Agricultural Technology* 9 (5): 1097-1110.
- Medyński, A., Pospiech, E., & Kniat, R. 2000. Effect of various concentrations of lactic acid and sodium chloride on selected physico-chemical meat traits. *Meat science* 55 (3): 285-290.
- Mewa, E. A., Okoth, M. W., Kunyanga, C. N., & Rugiri, M. N. 2018. Drying modelling, moisture diffusivity and sensory quality of thin layer dried beef. *Current Research in Nutrition and Food Science Journal* 6 (2): 552-565.
- Mhlambi, S., Naidoo, K., & Lindsay, D. 2010. Enterotoxin-producing *Staphylococcus* strains associated with South African biltong at point of sale. *Journal of food safety* 30 (2): 307-317.
- Midilli, A., Kucuk, H., & Yapar, Z. 2002. A new model for single-layer drying. *Drying Technology* 20 (7): 1503-1513.
- Miller, R. 2014. Chemical and physical characteristics of meat| Palatability. In M. Dikeman, & C. Devine (Eds.), *Encyclopedia of meat sciences*. London: Oxford: Academic Press.
- Mirzaee, E., Rafiee, S., Keyhani, A., & Emam-Djomeh, Z. 2009. Determining of moisture diffusivity and activation energy in drying of apricots. *Research in Agricultural Engineering* 55 (3): 114-120.
- Mujaffar, S., & Sankat, C. 2015. Modeling the Drying Behavior of Unsalted and Salted Catfish (*Arius* sp.) Slabs. *Journal of food processing and preservation* 39 (6): 1385-1398.
- Naidoo, K., & Lindsay, D. 2010a. Potential cross-contamination of the ready-to-eat dried meat product, biltong. *British Food Journal* 112 (4): 350-363.
- Naidoo, K., & Lindsay, D. 2010b. Survival of *Listeria monocytogenes*, and enterotoxin-producing *Staphylococcus aureus* and *Staphylococcus pasteurii*, during two types of biltong-manufacturing processes. *Food Control* 21 (7): 1042-1050.
- Nguyen, T. V. L., Nguyen, M. D., Nguyen, D. C., Bach, L. G., & Lam, T. D. 2019. Model for Thin Layer Drying of Lemongrass (*Cymbopogon citratus*) by Hot Air. *Processes* 7 (1): 21-30.
- Nortjé, K., Buys, E., & Minnaar, A. 2005. Effect of γ -irradiation on the sensory quality of moist beef biltong. *Meat science* 71 (4): 603-611.

- Onwude, D. I., Hashim, N., Abdan, K., Janius, R., & Chen, G. 2019. The effectiveness of combined infrared and hot-air drying strategies for sweet potato. *Journal of food engineering* 241 (2019): 75-87.
- Osterhoff, D., & Leistner, L. 1984. South African biltong--another close look. *Journal of the South African Veterinary Association* 55 (4): 201-202.
- Oliveira, G. H. H., Costa, M. R., Botelho, F. M., Viana, J. L., & Garcia, T. R. B. 2016. Thermodynamic properties and kinetics of drying process of chia seeds (*Salvia hispanica* L.). *Research Journal of Seed Science* 9 (2): 36-41.
- Petit, T., Caro, Y., Petit, A.-S., Santchurn, S. J., & Collignan, A. 2014. Physicochemical and microbiological characteristics of biltong, a traditional salted dried meat of South Africa. *Meat science* 96 (3): 1313-1317.
- Petrova, I., Bantle, M., & Eikevik, T. M. 2015. Manufacture of dry-cured ham: A review. Part 2. Drying kinetics, modeling and equipment. *European Food Research and Technology* 241 (4): 447-458.
- Rizvi, S. 2005. Thermodynamic Properties of Foods in Dehydration. In M. Rao, S. Rizvi, & A. Datta (Eds.), *Engineering properties of foods* (3 ed.). New York, United States: Marcel Dekker, Inc.
- Shi, J., Pan, Z., McHugh, T. H., Wood, D., Hirschberg, E., & Olson, D. 2008. Drying and quality characteristics of fresh and sugar-infused blueberries dried with infrared radiation heating. *LWT-Food Science and Technology* 41 (10): 1962-1972.
- Soydan Karabacak, M., Esin, A., & Cekmecelioglu, D. 2014. Drying behavior of meat samples at various fiber directions and air conditions. *Drying Technology* 32 (6): 695-707.
- Srikiatden, J., & Roberts, J. S. 2007. Moisture transfer in solid food materials: A review of mechanisms, models, and measurements. *International Journal of Food Properties* 10 (4): 739-777.
- Strydom, P., & Zondagh, B. 2014. Biltong: A major South African ethnic meat product. In M. Dikeman, & C. Devine (Eds.), *Encyclopaedia of meat sciences*. London, UK: Academic Press.
- Taylor, M. 1976. Changes in microbial flora during biltong production. *South African Food Review* 3 (2): 120-123.
- Trujillo, F. J., Wiangkaew, C., & Pham, Q. T. 2007. Drying modeling and water diffusivity in beef meat. *Journal of food engineering* 78 (1): 74-85.

- Trujillo, F. J., Yeow, P. C., & Pham, Q. T. 2003. Moisture sorption isotherm of fresh lean beef and external beef fat. *Journal of food engineering* 60 (4): 357-366.
- Van der Riet, W. 1976. Studies on the mycoflora of biltong. *South African Food Reviews* 3 (1): 105-113.
- Velić, D., Planinić, M., Tomas, S., & Bilić, M. 2004. Influence of airflow velocity on kinetics of convection apple drying. *Journal of food engineering* 64 (1): 97-102.
- von Gersdorff, G. J., Porley, V. E., Retz, S. K., Hensel, O., Crichton, S., & Sturm, B. 2018. Drying behavior and quality parameters of dried beef (biltong) subjected to different pre-treatments and maturation stages. *Drying Technology* 36 (1): 21-32.
- Wang, Z., Sun, J., Liao, X., Chen, F., Zhao, G., Wu, J.. 2007. Mathematical modeling on hot air drying of thin layer apple pomace. *Food Research International* 40 (1): 39-46.
- Zhu, A., & Shen, X. 2014. The model and mass transfer characteristics of convection drying of peach slices. *International Journal of heat and mass transfer* 72 (4): 345-351.

4. MODELLING THE THIN-LAYER DRYING KINETICS OF MARINATED BEEF DURING INFRARED ASSISTED HOT AIR PROCESSING OF BILTONG

This chapter is based on the following publication.

Muga, F. C., Marenya, M. O., and Workneh, T. S. 2021. Modelling the thin layer drying kinetics of marinated beef during infrared-assisted hot air processing of biltong. *International Journal of Food Science*, 2021(2021): 1-14. DOI: <https://doi.org/10.1155/2021/8819780>.

Abstract

The aim of this chapter was to establish the effect of the infrared (IR) power, the temperature and velocity of the drying air on the drying kinetics of marinated beef and subsequently select the best thin layer drying model for IRHAD during biltong processing. Marinated beef samples were dried at IR power levels of 500, 750, and 1000 W; drying air temperatures of 30, 35, and 40 °C; and air velocity of 1.5 and 2.5 m.s⁻¹. Results indicate that increasing the IR power and the drying air temperature increased the IR emitter temperature and the core temperature of the marinated beef sample. Consequently, increasing the drying rate, thus reduced drying time. The air velocity had an inverse relationship with the IR emitter temperature, core temperature of the marinated beef sample, and the drying rate. The drying process was characterised by a rising rate period in the first half an hour, followed by a falling rate period which implies that moisture transport during occurred partly by surface evaporation and predominantly by diffusion. The effective moisture diffusivity ranged from 4.560×10^{-10} to 13.7×10^{-10} m².s⁻¹, while, the activation energy ranged between 40.97 and 59.16 kJ.mol⁻¹. The IRHAD of marinated beef during its processing to biltong was best described by the Two-Term model since it had the highest R² (0.9982-0.9993) and the lowest RMSE (0.0062-0.0099). The power level of the IR emitter of 1000 W combined with a drying air temperature and velocity of 40 °C and 1.5 m.s⁻¹, respectively, showed the highest improvement in the drying kinetics and the lowest drying time of 5.61±0.35 hours, hence, is recommended as a possible drying alternative for the processing of biltong.

Keywords: Activation energy, biltong, drying kinetics, effective moisture diffusivity, infrared, thin-layer modelling

4.1 Introduction

The conventional hot air drying (HAD) method used in commercial production of biltong is an energy intensive drying method (Xie *et al.*, 2013). The low thermal conductivity of agricultural products combined with the case hardening of these products during HAD decelerate the moisture migration which results in longer drying time and increased energy consumption (Soydan Karabacak *et al.*, 2014; Aboud *et al.*, 2019). HAD degrades the quality of agricultural products through the loss of colour, loss of heat sensitive nutrients, deformation, and internal structure damage (Bellagha *et al.*, 2007; Kowalski and Mierzwa, 2009; Duan *et al.*, 2011). Moreover, the temperature range of 20 – 40 °C used in conventional HAD of meat during biltong production is not sufficient to achieve the recommended microbial reduction in the resultant biltong (Nortjé *et al.*, 2005). These concerns underscore the need for alternative drying methods for biltong production.

Alternative heating technologies like microwave, inductive heating, radio frequency, and infrared (IR) provide volumetric heating that positively impacts on the energetic, exergetic, and heating efficiency (Rastogi, 2012). According to Li *et al.* (2018), IR radiation improves the dehydration efficiency of beef jerky by promoting protein denaturation which transforms immobilised water to free water, consequently, reducing the activation energy. Cherono *et al.* (2016) noted that IR drying of beef reduced the microbial count on the resulting biltong. However, moisture condensation observed on the surface of biltong during IR drying highlights the inability of natural convection to cope with the improved drying rates (Cherono, 2014). A combined infrared and hot air drying (IRHAD) could accelerate the removal of moisture from the meat surface to sustain the high drying rates. Drying agricultural products using IRHAD requires less energy and produces dried products of higher quality compared to using IR drying or HAD independently (Afzal *et al.*, 1999; Hebbar *et al.*, 2004).

The application of IRHAD as a possible alternative to HAD in the making of biltong requires a quantitative understanding of the heat and mass transfer in meat subjected to IRHAD. According to Trujillo *et al.* (2007), Fickian diffusion is the predominant mode of moisture transport in meat during drying. The Page model and thin layer models derived from the Fick's Second Law of

diffusion suitably describe the drying behaviour of agricultural products. Abe and Afzal (1997) and Das *et al.* (2004) identified the Page model as the best model for describing the thin-layer IR drying of rough rice. According to Toğrul (2005), Puente-Díaz *et al.* (2013), Sui *et al.* (2014), and Sadin *et al.* (2017), the Midilli model is the most suitable model for predicting the drying kinetics of apple, murta berries, wine grape pomace, and tomato slices, respectively, when subjected to IRHAD. The Logarithmic model was identified by Doymaz (2012) as the best model for the IR drying of sweet potatoes. The study by Cheron (2014) identified the Approximation of diffusion model as the best model for the IR drying of marinated beef. Nonetheless, the Two-Term model and the Midilli model also showed good accuracy in predicting the IR drying of marinated beef.

A complete characterisation of the drying kinetics is critical in modelling the drying process (Feyissa *et al.*, 2009). The aforementioned studies highlight the research done in modelling the drying of a number of agricultural products subjected to IR drying and IRHAD. However, there is no literature on the drying characteristics of marinated beef subjected to IRHAD. A good understanding of the drying kinetics of marinated beef subjected to IRHAD would guide the application of IRHAD as a possible alternative to HAD in the processing of biltong. Therefore, the aim of this study was to establish the effect of the IR power, the temperature and velocity of the drying air on the drying kinetics of marinated beef and subsequently select the best thin layer drying model.

4.2 Materials and Methods

4.2.1 Sample preparation

The samples were prepared as outlined in Muga *et al.* (2020).

4.2.2 The drying unit

The infrared assisted hot air dryer was made by retrofitting an existing hot air cabinet dryer with an IR emitter. A complete description of the hot air cabinet drier is provided in Muga *et al.* (2020). A schematic of the IRHAD experimental set-up is shown in Figure 4.1.

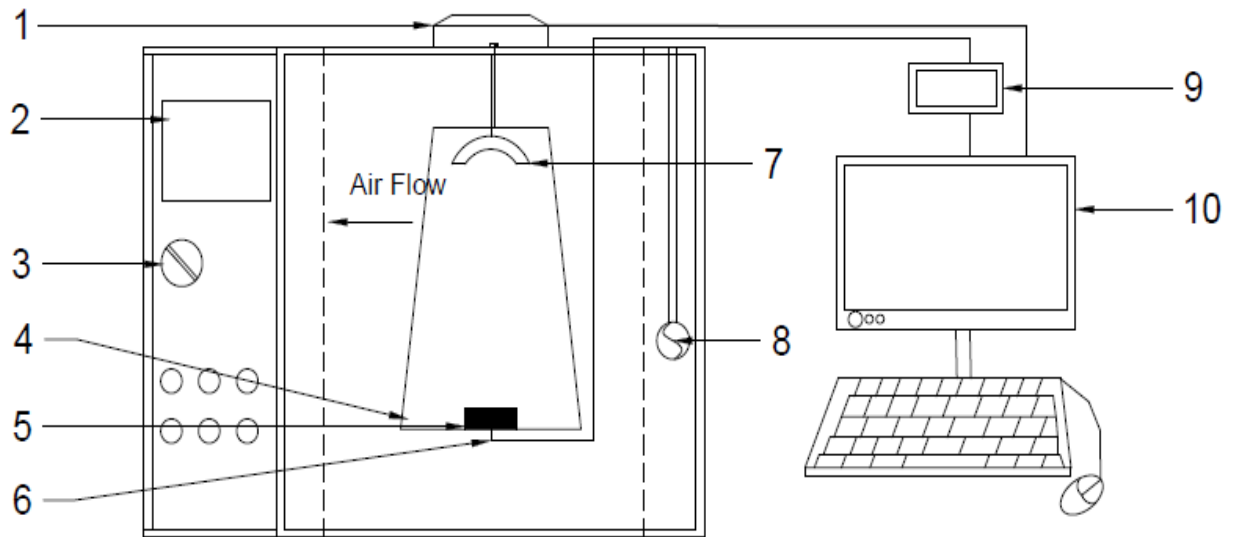


Figure 4.1 Schematic of the drying cabinet; 1 - Weighing balance, 2 - Digital control panel, 3 - Power knob, 4 - Drying platform, 5 - beef sample, 6 - K-type thermocouple, 7 - Infrared emitter, 8 - Anemometer, 9 - Temperature datalogger, 10 - Computer monitor

A ceramic IR emitter (T-FSR, Elstein-Werk M. Steinmetz GmbH & Co. KG, Northeim, Germany) is attached to the roof of the drying chamber, directly above the drying platform (Figure 5.1). The distance between the IR emitter and the drying platform is 280 mm. The IR emitter has a power rating of 1000 W and is of dimensions 250 by 62.5 mm. The wavelength of the IR radiation from the IR emitter ranges from 2 to 10 μm (Elstein, 2014). The power to the IR emitter was varied between 500 and 1000 W by regulating the current using a variable resistor. The IR emitter has an inbuilt K-type thermocouple that was connected to a data logger (OM-DAQ-USB-2401, Omega, UK) to record its temperature.

4.2.3 Drying experiments

The IRHAD experiments followed the same procedure described by Muga *et al.* (2020) with the inclusion of the IR emitter. The IR emitter was instantaneously switched on when the marinated beef sample was placed on the drying platform.

The drying experiment employed a three factor, full-factorial experimental design. The factors studied were the IR power (500, 750, and 1000 W), the temperature of the drying air (30, 35, and 40 °C), and the velocity of the drying air (1.5 and 2.5 m.s⁻¹).

The data obtained from the experiments was subjected to the analysis of variance (ANOVA) at 5 % level of significance. Where a significant ANOVA result was found, the mean comparison was done using Fisher’s Unprotected LSD method. All data analysis was done using GenStat® 18th Edition (VSN International Ltd, Hemel Hempstead, United Kingdom).

4.2.4 Evaluation of the drying characteristics

The moisture ratio (MR), drying rate (D_R), effective moisture diffusivity (D_{eff}), and the activation energy (E_a) were determined following the procedure outlined by Muga *et al.* (2020).

4.2.5 Selection of the best thin layer drying model

The thin layer drying models considered in this study are outlined in Table 4.1. The models were selected based on research by Muga *et al.* (2020).

Table 4.1 Selected thin layer drying models used in the study (Muga *et al.*, 2020)

S/N	Thin-layer model	Equation	References
1	Approximation of diffusion model (ADM)	$MR = a \exp(-kt) + (1 - a)\exp(-kbt)$	Cherono (2014)
2	Logarithmic model	$MR = a \exp(-kt) + c$	Wang <i>et al.</i> (2007)
3	Midilli model	$MR = \exp(-k(t^n)) + b \times t$	Midilli <i>et al.</i> (2002)
4	Page model	$MR = \exp(-kt^n)$	Ertekin and Firat (2017)
5	Two-Term model	$MR = a \exp(-k_1t) + b \exp(-k_2t)$	Erbay and Icier (2010)

The experimental data was fitted to the selected thin layer drying models using the non-linear least square analysis in MATLAB (MATLAB R18.2b, MathWorks, Inc., Natick, MA, USA). The best model was chosen based on a combination of the highest R^2 and the lowest RMSE (Muga *et al.*, 2020).

4.3 Results and Discussion

4.3.1 IR emitter temperature

The temperature of the IR emitter recorded for the tested drying conditions, is presented in Table 4.2. The temperature of the IR emitter was significantly ($p \leq 0.05$) affected by the power level of the IR emitter. The highest and lowest IR emitter temperatures of 566.51 ± 3.6 °C and 219.03 ± 2.62 °C, were observed at an IR power level of 1000 W and 500 W, respectively. Increasing the IR emitter power consumption increased the temperature of the IR emitter. The increase in the emitter temperatures is caused by the increase in ohmic losses as the power level of the IR emitter increases (Aboud *et al.*, 2019). These results are consistent with previous findings by Ali *et al.* (2015) and Ott *et al.* (2015).

Table 4.2 Temperature of the IR emitter

Drying air temperature (°C)	Drying air velocity (m.s ⁻¹)	IR emitter temperature (°C)		
		1000 W	750 W	500 W
30	1.5	543.30±8.73 ^k	396.16±5.39 ^g	233.10±2.61 ^c
35	1.5	548.21±7.36 ^k	407.60±5.23 ^h	232.19±3.1 ^{bc}
40	1.5	566.51±3.6 ^l	426.42±6.09 ⁱ	237.59±2.05 ^c
30	2.5	523.98±4.47 ^j	346.65±9.85 ^d	220.63±1.46 ^a
35	2.5	524.49±5.32 ^j	361.69±9.12 ^e	219.03±2.62 ^a
40	2.5	527.21±6.169 ^j	374.10±12.17 ^f	222.80±2.62 ^{ab}

Means within a column followed by the same letter are not significantly different according to Fisher's unprotected least significant difference test ($p < 0.05$). ANOVA table attached in appendix B.

A change in the velocity of the drying air resulted in significant ($p \leq 0.05$) variation in the temperature of the IR emitter. Higher IR emitter temperatures were observed at a low drying air

velocity of 1.5 m.s^{-1} , while the drying air velocity of 2.5 m.s^{-1} resulted in low IR emitter temperatures. The reduction in the temperature of the IR emitter at higher drying air velocity is attributed to the cooling effect induced by the drying air on the IR emitter due to convective heat losses. According to Pan and Atungulu (2010b) the radiation efficiency of mid to far IR emitters range between 40 – 60 % with some heat lost via convection. Increasing the drying air velocity increases the mass flow rate of air which increases the convective heat losses, thus reducing the IR emitter temperature.

The temperature of the drying air also had a significant ($p \leq 0.05$) effect on the temperature of the IR emitter. The temperature of the IR emitter increased with increase in the drying air temperature. An increase in the drying air temperature reduced the temperature gradient between the IR emitter and the drying air, thus reducing the convective heat losses and vice versa. Consequently, the IR emitter temperatures increased with increase in drying air temperature.

The power level of the IR emitter had a synergistic interaction with the temperature and velocity of the drying air, that significantly ($p \leq 0.05$) affected the temperature of the IR emitter. However, the two-way interaction between the drying air temperature and velocity, and the three-way interaction of all the experimental factors, had no significant effect on the IR emitter temperature.

4.3.2 Core temperature of the beef sample during drying

The average core temperature of the beef sample over the entire drying period ranged from 30.62 ± 0.08 to 51.16 ± 0.36 °C (Table 4.3). The core temperature of the beef sample was significantly ($p \leq 0.05$) affected by the power level of the IR emitter. Higher core temperatures of the sample were observed at higher power levels of IR emitter. The increase in the core temperature of the beef sample with increasing power level of the IR emitter is caused by the high temperatures of the IR emitter achieved at high power levels of the IR emitter.

Table 4.3 Average core temperature of the beef sample

Drying air temperature (°C)	Drying air velocity (m.s ⁻¹)	Core temperature (°C)		
		1000 W	750 W	500 W
30	1.5	47.23±0.26 ^l	35.57±0.20 ^e	31.74±0.07 ^b
35	1.5	47.91±0.22 ^m	43.29±0.15 ^j	34.04±0.05 ^d
40	1.5	51.16±0.36 ⁿ	44.97±0.19 ^k	36.80±0.18 ^g
30	2.5	42.59±0.26 ⁱ	31.73±0.26 ^b	30.62±0.08 ^a
35	2.5	42.90±0.30 ^{ij}	39.38±0.54 ^h	32.60±0.06 ^c
40	2.5	47.74±0.41 ^m	42.83±0.42 ⁱ	36.15±0.28 ^f

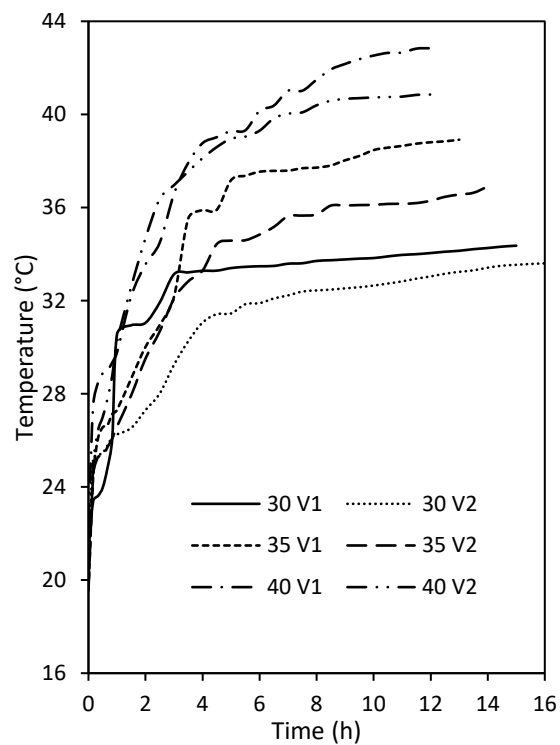
Means within a column followed by the same letter are not significantly different according to Fisher's unprotected least significant difference test ($p < 0.05$). ANOVA results contained in appendix B.

The temperature of the IR emitter determines the quality and intensity of IR radiation (Ratti and Mujumdar, 2007). According to Planck's law, higher temperatures of the IR emitter shift the peak IR energy wavelengths towards the shorter wavelength (Pan *et al.*, 2014). The short IR wavelengths are associated with higher IR energy flux and vice versa (Riadh *et al.*, 2015). The peak IR wavelengths calculated using the Wien's displacement law and the average temperatures of the IR emitter were, 5.39 ± 0.17 , 7.51 ± 0.48 , and 12.73 ± 0.43 μm , at 1000, 750, and 500 W, respectively. The shorter wavelength of 5.39 ± 0.17 μm observed at an IR power level of 1000 W indicates an increase in the IR energy flux into the beef sample. The increased IR energy flux into the beef sample increases the core temperature of the beef sample at the IR power level of 1000 W compared to the IR power level of 750 and 500 W. These results concur with previous research that reported an increase in the core temperature of the sample with increase in IR power (Cherono, 2014; Onwude *et al.*, 2019).

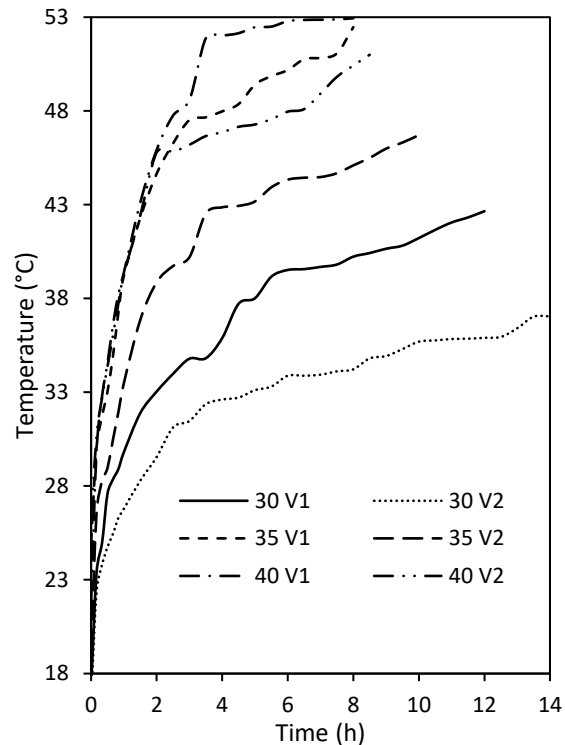
The velocity of the drying air caused significant ($p \leq 0.05$) variation in the average core temperature of the beef sample. Higher core temperature of the beef samples were observed at a drying air velocity of 1.5 m.s⁻¹, whereas, lower core temperatures were observed at a drying air velocity of 2.5 m.s⁻¹. An increase in the air velocity is associated with low IR emitter temperature which reduces the radiant energy flux into the sample, resulting in low core temperature of the samples. The inverse relationship between the drying air velocity and the core temperature of the

beef sample can also be attributed to the evaporative cooling due the increased mass flow rate of the drying air as observed by Kocabiyik and Tezer (2009) during the IR drying of carrots.

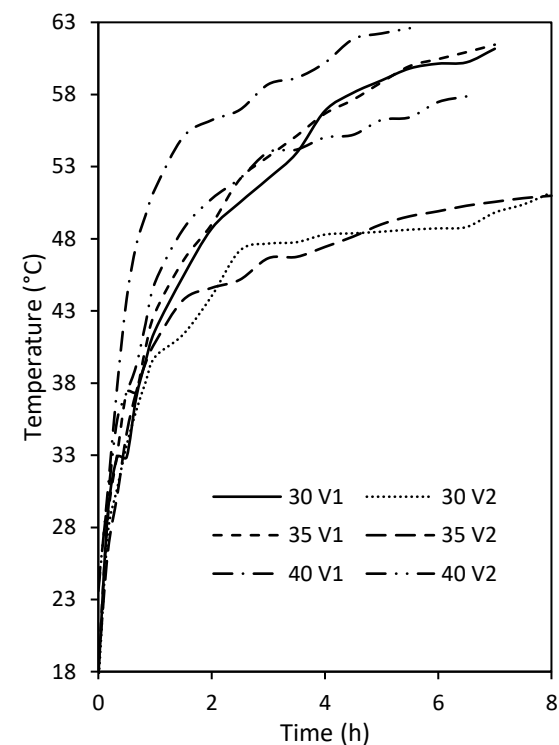
The core temperature of the beef sample also varied significant ($p \leq 0.05$) with the temperature of the drying air. Increasing the temperature of the drying air increased the core temperature of the sample. The variation in core temperature of the sample became pronounced over time as shown by the divergence of the sample temperature curves in the later stages of drying (Figure 4.2). This variation can be attributed to the synergistic transfer of energy from both the IR and the hot drying air to the beef sample from the onset of drying until the sample temperature reaches the drying air temperature (Hebbar *et al.*, 2004). Thereafter, there is simultaneous energy transfer into and out of the beef sample. The energy influx is primarily due to the radiant flux from the IR emitter while the energy outflux is driven by the temperature gradient between the sample and the drying air. The temperature gradient between the beef sample and the drying air increases with a decrease in the drying air temperature, thus promoting a high energy outflux which results in lower core temperature of the beef sample.



(a) 500 W



(b) 750 W



(c) 1000 W

Figure 4.2 Variation in core temperature of the beef sample during drying at selected IR emitter power temperature and air velocity of the drying air ($V1 = 1.5 \text{ m.s}^{-1}$ and $V2 = 2.5 \text{ m.s}^{-1}$)

4.3.3 Drying time

The drying time is the duration spent in drying the beef sample until 50 % of the original mass was lost. The drying time ranged from 5.61 ± 0.35 to 16.22 ± 0.25 hours (Table 4.4). This is significantly lower than the 24 – 230 hours required to dry biltong using the conventional hot air drying (Nortjé *et al.*, 2005; Naidoo and Lindsay, 2010c; Cherono, 2014; Jones *et al.*, 2017). The drying time achieved in this study is also lower than the range of drying time of 10.25 – 36 hours, achieved by Cherono (2014) that solely used IR drying to make biltong. Similar reduction in drying times have been reported by Sharma *et al.* (2005) and Li *et al.* (2018) on IRHAD of onions and beef jerky, respectively. According to Hebbar *et al.* (2004), the synergistic interaction between IR and hot air promotes rapid heating of the product being dried which accelerates the rate of mass transfer, thus improving the dehydration efficiency and subsequently lowering the drying time.

Table 4.4 Summary of the drying time for marinated beef at the selected drying conditions

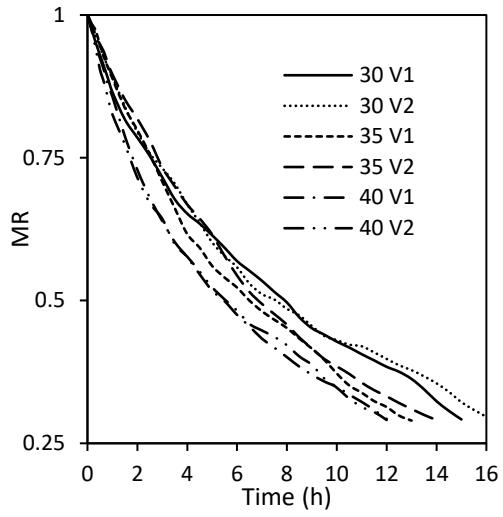
Drying air temperature (°C)	Drying air velocity (m.s ⁻¹)	Drying time (h)		
		1000 W	750 W	500 W
30	1.5	7.17±0.17 ^c	11.72±0.25 ^f	15.00±0.17 ⁱ
35	1.5	7.11±0.10 ^c	8.11±0.19 ^d	13.00±0.17 ^g
40	1.5	5.61±0.35 ^a	8.10±0.24 ^d	11.83±0.165 ^f
30	2.5	8.11±0.19 ^d	14.50±0.50 ⁱ	16.22±0.25 ^j
35	2.5	8.22±0.19 ^d	10.06±0.10 ^e	13.94±0.42 ^h
40	2.5	6.50±0.17 ^b	8.39±0.19 ^d	11.78±0.25 ^f

Means within a column followed by the same letter are not significantly different according to Fisher's unprotected least significant difference test ($p < 0.05$). ANOVA results contained in appendix B.

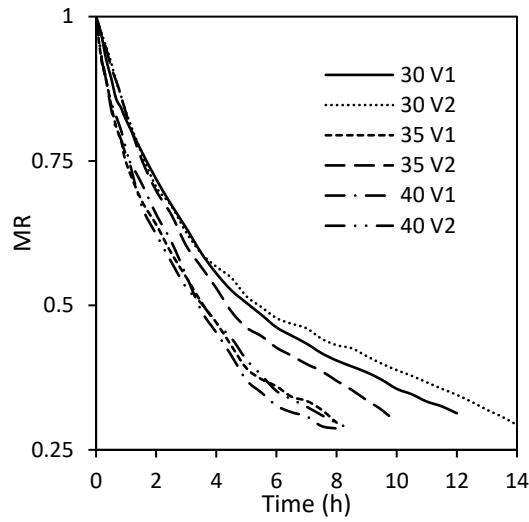
The variation in MR over the drying period is presented in Figure 4.3. The IR power significantly ($p \leq 0.05$) affected the drying time. Shorter drying times were observed at 1000 W while the longest drying time was observed at an IR power level of 500 W. Similarly, the drying time decreased significantly ($p \leq 0.05$) with increase in temperature of the drying air. These observations are in agreement with the findings of Sharma *et al.* (2005), Kumar *et al.* (2006), and

Nasiroglu and Kocabiyik (2009). An increase in both the IR power and the drying air temperature increases the core temperature of the beef sample. The increase in the core temperature of the beef sample indicates the increased heat influx which accelerates the vapourisation of water in the beef sample, thus increasing the vapour pressure and expediting the moisture transport out of the sample (Srikiatden and Roberts, 2007). According to Jaturonglumlert and Kiatsiroat (2010), increasing the power of the IR emitter and the temperature of the drying air increases the ratio of heat and mass transfer coefficient, thus leading to the shortening of the drying time.

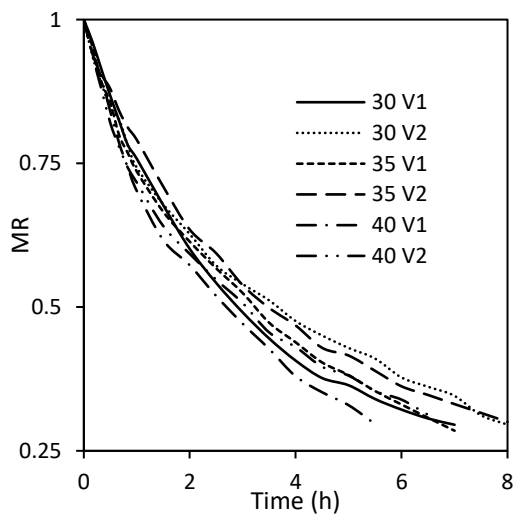
Contrary to the effect of the power level of the IR emitter and the temperature of the drying air, increasing the velocity of the drying air increased the drying time. Similar findings were reported by Afzal *et al.* (1999) and Kocabiyik and Tezer (2009). This observation can be attributed to the negative effect of the drying air velocity on the core temperature of the beef sample. Increasing the drying air velocity decreases the ratio of heat and mass transfer coefficient, thus, lengthening the drying time (Jaturonglumlert and Kiatsiroat, 2010).



(a) 500 W



(b) 750 W



(c) 1000 W

Figure 4.3 Variation in the MR of marinated beef during IRHAD

4.3.4 Drying rate

The drying rate refers to the rate of moisture removal from the beef sample. The variation in the drying rate during the drying process is shown in Figure 4.4. The drying rate curves at IR power level of 500 and 750 W indicated a short rising rate drying period followed by the first and second falling rate drying periods which is typical of drying rate curves obtained from IRHAD (Kocabiyik, 2010). The drying rate curve obtained at the IR power level of 1000 W showed a short constant rate drying period immediately after the rising rate period and just before the first falling rate period. This observation is consistent with the results obtained by Mongpraneet *et al.* (2002) when drying welsh onions under IR radiation.

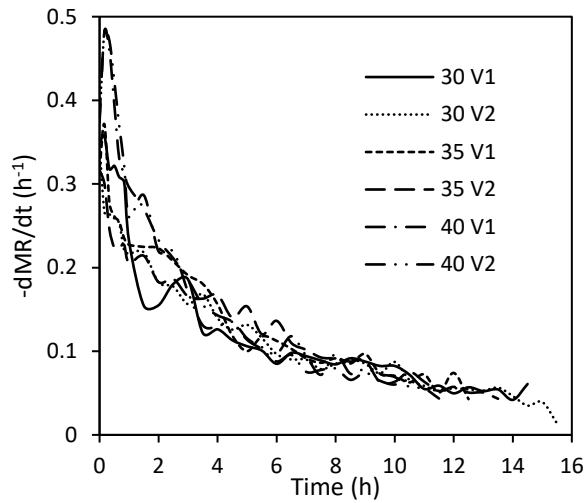
IR radiation has an efficient heat transfer mechanism that promotes a rapid increase in the core temperature of the beef sample at the onset of drying, thus increasing the drying rate (Pan *et al.*, 2014). The rising rate drying period occurred within the first 30 minutes of drying and coincided with an increase in the rate of change in the core temperature of the beef sample (Figure 4.4). The moisture transport during this period can be attributed to surface evaporation (Kocabiyik, 2010).

The rising rate drying period is superseded by the first falling rate drying period. The first falling rate drying period coincides with a decrease in the rate of change in the core temperature of the beef sample (Figure 4.4). This drying period occurred between 30 minutes – 6 hours of drying at IR power levels of 500 and 750 W, while the same occurred at between 30 minutes – 2 hours of drying at IR power level of 1000 W. According to Trujillo *et al.* (2007), diffusion is the predominant mode of moisture transport during the first falling rate drying period. The decrease in drying rate can be attributed to the reduced heat flux into the sample which lowers the vapour pressure gradient and subsequently reduces the moisture transport out of the sample.

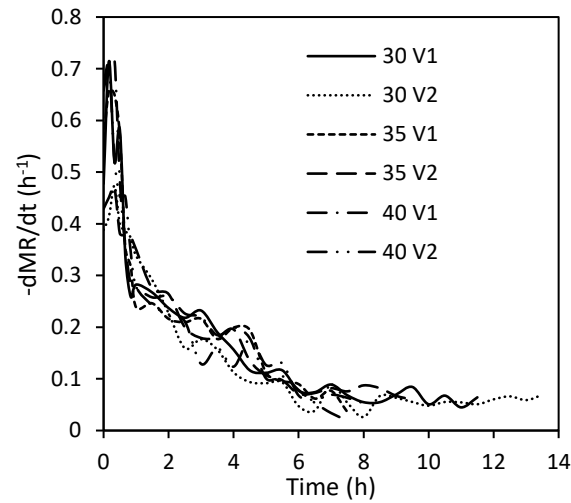
The second falling rate period occurred after the first 6 hours of drying at IR power levels of 500 and 750 W, while the same occurred after the first 2 hours of drying at IR power level of 1000 W. The second falling rate period is characterised by low and fluctuating drying rate. According Kocabiyik (2010), most of the free water is lost during the first falling rate period leaving the bound water to play an active role in the second falling rate period. Bound water requires more

energy to extract from the food matrix. However, there is minimal heat flux into the beef sample during this drying period as indicated by the relatively constant product temperature. The low drying rate may also be attributed to the additional internal resistance to moisture movement as the sample moisture content decreases (Karel and Lund, 2003).

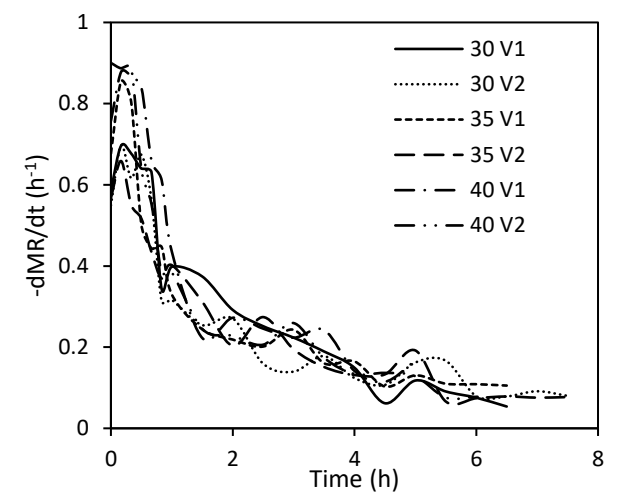
The drying rate was significantly ($p \leq 0.05$) affected by the power level of the IR emitter, the temperature and velocity of the drying air. This is attributed to the effect that these factors had on the core temperature of the beef sample, consequently affecting the amount of heat flux into the sample. Feyissa *et al.* (2013) reported that heat transfer is the key driver of mass transfer during the roasting of chicken meat. The coupled relationship between the core temperature of the beef sample and the moisture transport is illustrated by the synchrony between the drying rate curve and the curve depicting the rate of increase in sample temperature (Figure 4.4).



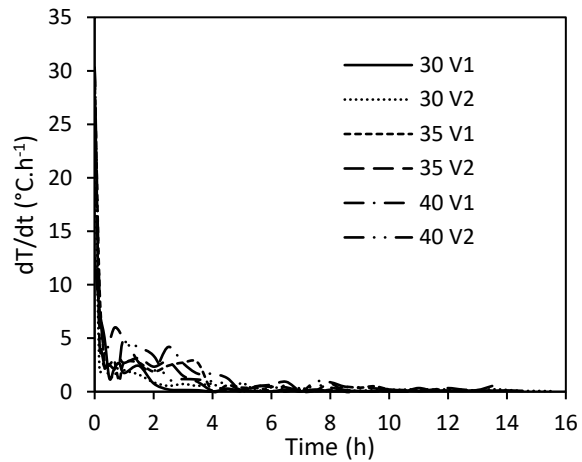
(a) Drying rate at 500 W



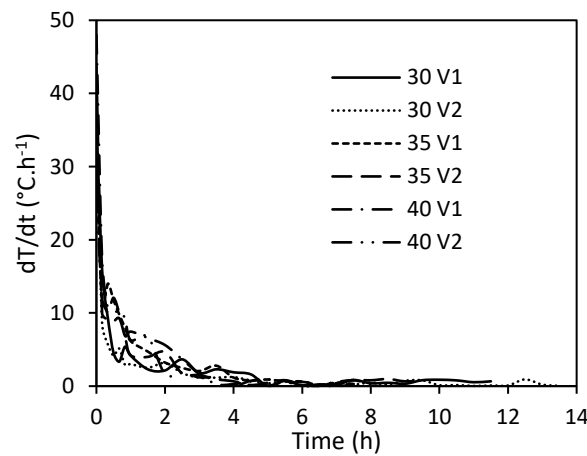
(b) Drying rate at 750 W



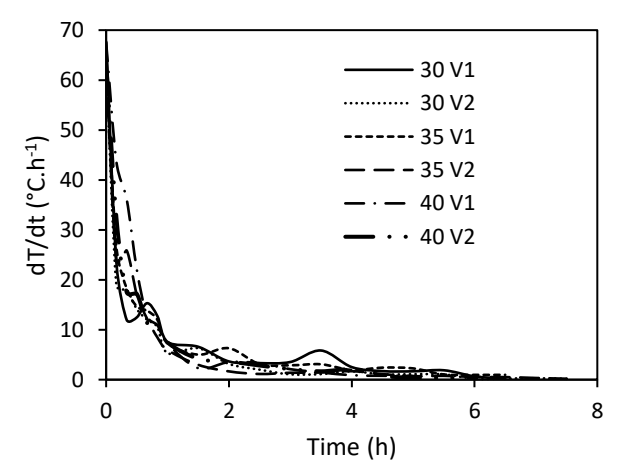
(c) Drying rate at 1000 W



(d) Rate of change in temperature at 500 W



(e) Rate of change in temperature at 750 W



(f) Rate of change in temperature at 1000 W

Figure 4.4 Variation in the drying rate and the rate of change in the core temperature of the beef sample during drying

4.3.5 Effective moisture diffusivity

The effective moisture diffusivity (D_{eff}) of marinated beef subjected to infrared assisted hot air drying ranged between $4.560 \times 10^{-10} \text{ m}^2.\text{s}^{-1}$ and $13.7 \times 10^{-10} \text{ m}^2.\text{s}^{-1}$ (Table 4.5). These values are within the range of values obtained by Li *et al.* (2018) for beef jerky dried under mid and far IR radiation. The D_{eff} values obtained in this study are greater than those reported in previous research on hot air drying of meat product such kaddid (Chabbouh *et al.*, 2013), eland jerky (Kucerova *et al.*, 2015), chicken breast meat (Ismail, 2017), and beef (Mewa *et al.*, 2018) and biltong (Muga *et al.*, 2020). According to Li *et al.* (2018), the selective heating of water molecules by the IR radiation causes the immobilized water in the myofibrillar network to migrate out of the network. The migration of the immobilised water out of the myofibrillar network increases the internal free water content, consequently expediting the transport of the free water to the surface by diffusion.

Table 4.5 Effective moisture diffusivity of marinated beef during IRHAD

Drying air temperature (°C)	Drying air velocity (m.s ⁻¹)	D_{eff} (m ² .s ⁻¹)		
		1000 W	750 W	500 W
30	1.5	11.4E-10 ^d	6.85E-10 ^b	4.56E-10 ^a
35	1.5	11.4E-10 ^d	9.13E-10 ^c	6.85E-10 ^b
40	1.5	13.7E-10 ^e	9.13E-10 ^c	6.85E-10 ^b
30	2.5	9.13E-10 ^c	4.56E-10 ^a	4.56E-10 ^a
35	2.5	9.13E-10 ^c	6.85E-10 ^b	6.85E-10 ^b
40	2.5	11.4E-10 ^d	9.13E-10 ^c	6.85E-10 ^b

Means within a column followed by the same letter are not significantly different according to Fisher's unprotected least significant difference test ($p < 0.05$).

The IR power level caused significant ($p \leq 0.05$) variations in D_{eff} under all drying conditions. The temperature of the drying air only caused significant variations between 30 and 40 °C, whereas, the drying air velocity had a significant effect on the D_{eff} at IR emitter power levels of 1000 and 750 W but not at 500 W. Khir *et al.* (2011) reported that D_{eff} increases with increase in sample temperature during IR drying. The effect of the IR power, the temperature and velocity

of the drying air on the D_{eff} in this study is attributed to their influence on the core temperature of the beef sample.

4.3.6 Activation energy

The activation energy (E_a) ranged between 40.97 – 59.16 $\text{kJ}\cdot\text{mol}^{-1}$ (Figure 4.5). The E_a obtained in this study is comparable to the E_a of 32.8 $\text{kJ}\cdot\text{mol}^{-1}$ obtained by Li *et al.* (2018) during mid- and far-IR drying of beef. The difference between the E_a obtained in this study and that reported by Li *et al.* (2018) may be due to the difference in the range of IR wavelength used in both studies. The wavelength of the IR radiation used by Li *et al.* (2018) ranged between 2.9 – 3.1 and 5.8 – 6.2 μm , whereas, the wavelength of the IR radiation used in study ranged between $5.38 \pm 0.17 - 12.73 \pm 0.43 \mu\text{m}$. The IR radiation wavelengths used by Li *et al.* (2018) can effectively heat up the water molecules due to their proximity to the maximum absorption wavelengths of water of 3 μm and 6 μm (Aboud *et al.*, 2019). Consequently, the availability of free water in the food sample increases. Increased availability of free water in the food matrix is associated with reduced E_a (Hwang *et al.*, 2009).

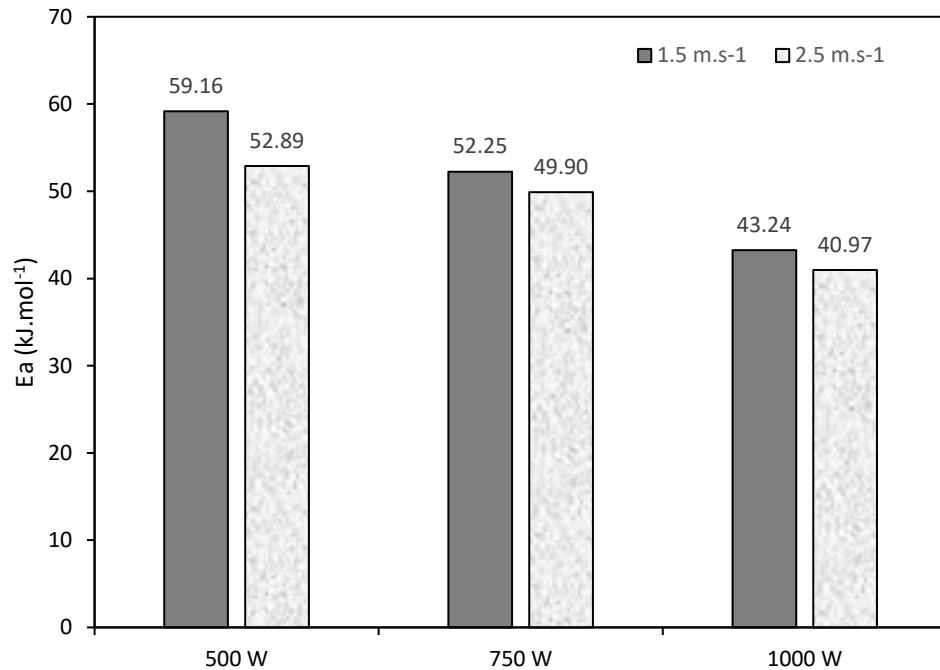


Figure 4.5 Activation Energy of marinated beef under different IRHAD experimental conditions

The inverse relationship between the E_a and the power level of the IR emitter observed in this study is attributed to the change in the wavelength of the IR radiation. Increasing the power of the IR emitter shortens the wavelength of the IR radiation from $12.73 \pm 0.43 - 5.38 \pm 0.17 \mu\text{m}$. The absorption of the IR radiation by the water molecules in the beef sample increases as the radiation wavelength decreases towards the maximum absorption wavelength of water of $6 \mu\text{m}$, thus lowering the activation energy.

4.3.7 Selection of the best thin layer drying model

The average coefficient of determination and the average root mean square error for the five thin layer drying models considered in this study is shown in Table 4.6. All the five models had an $R^2 > 0.9977$ and a $\text{RMSE} < 0.0177$. The high R^2 and the low RMSE indicate that all the five models can predict the changes in MR of marinated beef subjected to IRHAD with acceptable accuracy (Nguyen *et al.*, 2019). Overall, the Two-Term model had the highest R^2 (0.9982-0.9993) and the lowest RMSE (0.0062-0.0099) across all the IRHAD conditions. Therefore, the Two-Term model, is the most suitable model in predicting the drying behaviour of marinated beef subjected to IRHAD.

Table 4.6 The average R^2 and RMSE for the thin layer models at different IR power levels

S/No	Model	R^2			RMSE		
		500 W	750 W	1000 W	500 W	750 W	1000 W
1	Two-Term	0.9993	0.9982	0.9993	0.0062	0.0099	0.0065
2	Approximation of Diffusion	0.9989	0.9981	0.9992	0.0080	0.0099	0.0057
3	Midilli	0.9978	0.9980	0.9988	0.0177	0.0104	0.0085
4	Page	0.9977	0.9960	0.9975	0.0109	0.0143	0.0118
5	Logarithmic	0.9977	0.9964	0.9961	0.0107	0.0139	0.0141

A summary of the Two-Term model coefficients and the statistical parameters for all the experimental drying conditions is presented in Table 4.7.

Table 4.7 Model coefficient and statistical parameters for the Two-Term thin-layer drying model

IR Power	T (°C)	Air vel (m.s ⁻¹)	Model Coefficient				R ²	RMSE
			K	K2	a	b		
500 W	30	1.5	0.7236	0.0686	0.1444	0.8566	0.9992	0.0063
	30	2.5	0.2642	0.0459	0.3569	0.6446	0.9987	0.0084
	35	1.5	0.3293	0.0755	0.2384	0.7719	0.9988	0.0086
	35	2.5	0.1039	-0.155	0.9913	0.0070	0.9997	0.0042
	40	1.5	0.4083	0.0671	0.3456	0.6629	0.9998	0.0038
	40	2.5	0.7276	0.0808	0.2245	0.7813	0.9994	0.0057
	Mean						0.9993	0.0062
750 W	30	1.5	0.0560	0.4278	0.6141	0.3766	0.9991	0.0069
	30	2.5	0.5176	0.0532	0.3654	0.6472	0.9992	0.0067
	35	1.5	1.094	0.124	0.2192	0.77	0.9978	0.0116
	35	2.5	0.0568	0.3687	0.5287	0.4783	0.9992	0.0071
	40	1.5	0.2071	-0.2568	0.9406	0.0135	0.9948	0.0188
	40	2.5	0.7417	0.1078	0.3	0.6899	0.9990	0.0080
	Mean						0.9982	0.0099
1000 W	30	1.5	0.0368	0.4232	0.3359	0.6652	0.9996	0.0053
	30	2.5	0.114	1.129	0.7512	0.2458	0.9994	0.0061
	35	1.5	1.428	0.1494	0.2012	0.8051	0.9994	0.0063
	35	2.5	0.4459	0.0746	0.4666	0.5225	0.9995	0.0057
	40	1.5	0.1733	1.32	0.774	0.235	0.9987	0.0093
	40	2.5	1.434	0.1364	0.2524	0.7504	0.9993	0.0064
	Mean						0.9993	0.0065

The plot of the experimental MR and the MR predicted using the Two-Term model is shown in Figure 4.6. The data points lie along the 45 ° line which confirms the high degree of agreement between the experimental and predicted MR values.

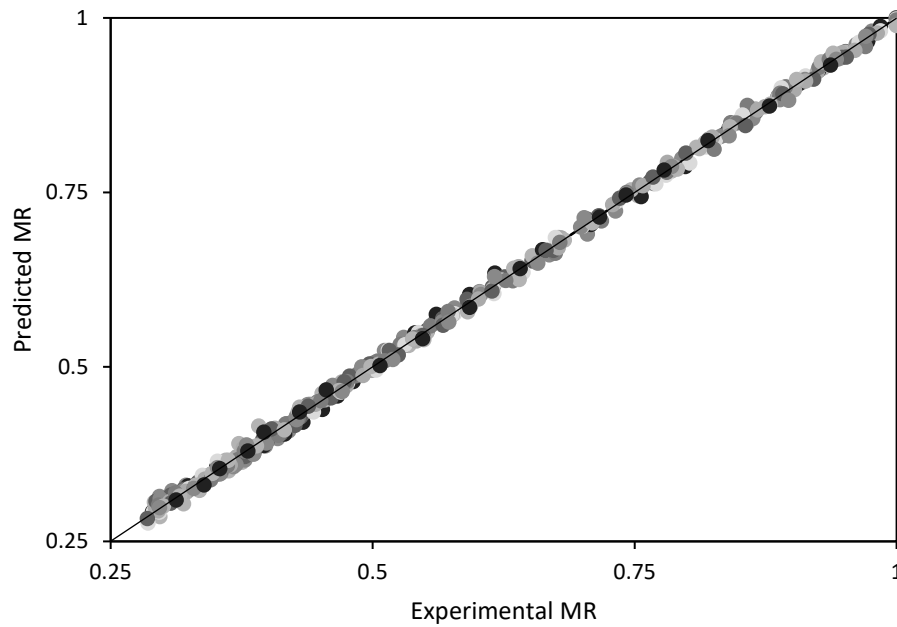


Figure 4.6 Comparison between the MR predicted by the Two-Term model and the experimental MR for all the drying conditions

4.4 Conclusion

The IRHAD of marinated beef is significantly affected by the power level of the IR emitter, the temperature and velocity of the drying air. The power level of the IR emitter is the predominant factor that influences the drying process of marinated beef subjected to IRHAD. The power level of the IR emitter determines the temperature of the emitter, thus influencing the core temperature of the marinated beef sample. The drying air temperature and drying air velocity have a direct and inverse relationship, respectively, with IR emitter temperature and the core temperature of the beef samples. The core temperature of the beef sample is the most critical parameter that influences the drying kinetics of marinated beef subjected to IRHAD. The combined effect of the power level of the IR emitter, temperature and velocity of the drying air on the; drying time, drying rate, effective moisture diffusivity, and the activation energy; is directly related to how these factors influence the core temperature of the beef sample. The drying of marinated beef at IR power levels of 500 W and 750 W, have a short rising rate drying period followed by the falling rate drying period. The drying process at 1000 W has a short constant rate period sandwiched between the rising rate and the first falling rate period. The rising and falling rate

drying periods imply that the moisture transport during IRHAD of marinated occurs partly by surface evaporation and predominantly by diffusion. The Two-Term thin-layer drying model best describes the drying of marinated beef under IRHAD. The effective moisture diffusivity ranges from $4.560 \times 10^{-10} \text{ m}^2.\text{s}^{-1}$ and $13.7 \times 10^{-10} \text{ m}^2.\text{s}^{-1}$ while, the activation energy ranges between $40.97 - 59.16 \text{ kJ.mol}^{-1}$. The results from this study can inform the application of IRHAD in biltong processing. A power level of 1000 W with an IR radiation wavelength of $5.39 \pm 0.17 \mu\text{m}$ resulted in the shortest drying time, the highest effective moisture diffusivity and the lowest activation energy. The power level of the IR emitter of 1000 W combined with a temperature and velocity of the drying air of $40 \text{ }^\circ\text{C}$ and 1.5 m.s^{-1} , respectively, highly improved the drying kinetics of biltong, hence, is recommended as a possible drying alternative for biltong processing.

4.5 References

- Abe, T and Afzal, T. 1997. Thin-layer infrared radiation drying of rough rice. *Journal of Agricultural Engineering Research* 67 (4): 289-297.
- Aboud, SA, Altemimi, AB, RS Al-Hilphy, A, Yi-Chen, L and Cacciola, F. 2019. A Comprehensive Review on Infrared Heating Applications in Food Processing. *Molecules* 24 (22): 4125.
- Afzal, T, Abe, T and Hikida, Y. 1999. Energy and quality aspects during combined FIR-convection drying of barley. *Journal of food engineering* 42 (4): 177-182.
- Ali, SZ, De Luca, A, Hopper, R, Boual, S, Gardner, J and Udrea, F. 2015. A low-power, low-cost infra-red emitter in CMOS technology. *IEEE Sensors Journal* 15 (12): 6775-6782.
- AOAC. 2012. *Official Methods of Analysis of AOAC International*. Association of Official Analysis Chemists International, Gaithersburg, USA.
- Attwell, E. 2003. Biltong wakes up. *Food Reviews* 30 (2): 11-13.
- Bellagha, S, Sahli, A, Farhat, A, Kechaou, N and Glenza, A. 2007. Studies on salting and drying of sardine (*Sardinella aurita*): Experimental kinetics and modeling. *Journal of Food Engineering* 78 (3): 947-952.
- Chabbouh, M, Sahli, A and Bellagha, S. 2013. Does the spicing step affect the quality and drying behaviour of traditional kaddid, a Tunisian cured meat? *Journal of the Science of Food and Agriculture* 93 (14): 3634-3641.

- Cherono, K. 2014. Infrared Drying of Biltong. Unpublished MSc thesis, Bioresources Engineering, University of KwaZulu-Natal, Pietermaritzburg, South Africa.
- Cherono, K, Mwithiga, G and Schmidt, S. 2016. Infrared drying as a potential alternative to convective drying for biltong production. *Italian journal of food safety* 5 (3): 140-145.
- Das, I, Das, S and Bal, S. 2004. Drying performance of a batch type vibration aided infrared dryer. *Journal of Food Engineering* 64 (1): 129-133.
- Doymaz, İ. 2012. Infrared drying of sweet potato (*Ipomoea batatas* L.) slices. *Journal of food science and technology* 49 (6): 760-766.
- Duan, Z-h, Jiang, L-n, Wang, J-l, Yu, X-y and Wang, T. 2011. Drying and quality characteristics of tilapia fish fillets dried with hot air-microwave heating. *Food and Bioproducts processing* 89 (4): 472-476.
- Dzimba, FEJ, Faria, J and Walter, EHM. 2007. Testing the sensory acceptability of biltong formulated with different spices. *African Journal of Agricultural Research* 2 (11): 547-577.
- Elstein. 2014. Ceramic infrared emitters. [Internet]. Elstein-Werk M. Steinmetz GmbH & Co. Available from: http://www.elstein.com/fileadmin/user_upload/PDFs/INT/Katalog/Catalogue_EN.pdf. [Accessed: 18 March 2020].
- Erbay, Z and Icier, F. 2010. A review of thin layer drying of foods: theory, modeling, and experimental results. *Critical reviews in food science and nutrition* 50 (5): 441-464.
- Ertekin, C and Firat, MZ. 2017. A comprehensive review of thin-layer drying models used in agricultural products. *Critical reviews in food science and nutrition* 57 (4): 701-717.
- Feyissa, AH, Adler-Nissen, J and Gernaey, K. 2009. Model of Heat and Mass Transfer with Moving Boundary during Roasting of Meat in Convection-Oven. *Excerpt from the Proceedings of the COMSOL Conference, Milan, Italy,*
- Feyissa, AH, Gernaey, KV and Adler-Nissen, J. 2013. 3D modelling of coupled mass and heat transfer of a convection-oven roasting process. *Meat science* 93 (4): 810-820.
- Hebbar, HU, Vishwanathan, K and Ramesh, M. 2004. Development of combined infrared and hot air dryer for vegetables. *Journal of food engineering* 65 (4): 557-563.
- Henning, M, Hagedorn-Hansen, D and Von Leipzig, KH. 2018. A conceptual framework to increase competitiveness in a biltong factory. *South African Journal of Industrial Engineering* 29 (3): 108-120.

- Hwang, S-S, Cheng, Y-C, Chang, C, Lur, H-S and Lin, T-T. 2009. Magnetic resonance imaging and analyses of tempering processes in rice kernels. *Journal of Cereal Science* 50 (1): 36-42.
- Ismail, O. 2017. An experimental and modeling investigation on drying of chicken meat in convective dryer. *Studia Universitatis Babes-Bolyai Chemia* 62 (4): 459-469.
- Jaturonglumlert, S and Kiatsiriroat, T. 2010. Heat and mass transfer in combined convective and far-infrared drying of fruit leather. *Journal of Food Engineering* 100 (2): 254-260.
- Jones, M. 2017. Profiling of traditional South African biltong in terms of processing, physicochemical properties and microbial stability during storage. Unpublished PhD thesis, Food Science, Stellenbosch University, Stellenbosch, South Africa.
- Jones, M, Arnaud, E, Gouws, P and Hoffman, LC. 2017. Processing of South African biltong—A review. *South African Journal of Animal Science* 47 (6): 743-757.
- Karel, M and Lund, DB. 2003. *Physical principles of food preservation*. Marcel Dekker, Inc, New York, United States.
- Khair, R, Pan, Z, Salim, A, Hartsough, BR and Mohamed, S. 2011. Moisture diffusivity of rough rice under infrared radiation drying. *LWT-Food Science and Technology* 44 (4): 1126-1132.
- Kocabiyik, H. 2010. Combined Infrared and Hot Air Drying. In: eds. Pan, Z and Atungulu, GG, *Infrared heating for food and agricultural processing*. CRC Press.
- Kocabiyik, H and Tezer, D. 2009. Drying of carrot slices using infrared radiation. *International journal of food science & technology* 44 (5): 953-959.
- Kowalski, SJ and Mierzwa, D. 2009. Convective drying in combination with microwave and IR drying for biological materials. *Drying Technology* 27 (12): 1292-1301.
- Kucerova, I, Hubackova, A, Rohlik, B-A and Banout, J. 2015. Mathematical modeling of thin-layer solar drying of Eland (*Taurotragus oryx*) Jerky. *International journal of food engineering* 11 (2): 229-242.
- Kumar, DP, Hebbar, HU and Ramesh, M. 2006. Suitability of thin layer models for infrared-hot air-drying of onion slices. *LWT-Food Science and Technology* 39 (6): 700-705.
- Li, X, Xie, X, Zhang, C-h, Zhen, S and Jia, W. 2018. Role of mid-and far-infrared for improving dehydration efficiency in beef jerky drying. *Drying Technology* 36 (3): 283-293.

- Mewa, EA, Okoth, MW, Kunyanga, CN and Rugiri, MN. 2018. Drying modelling, moisture diffusivity and sensory quality of thin layer dried beef. *Current Research in Nutrition and Food Science Journal* 6 (2): 552-565.
- Midilli, A, Kucuk, H and Yapar, Z. 2002. A new model for single-layer drying. *Drying technology* 20 (7): 1503-1513.
- Mongpraneet, S, Abe, T and Tsurusaki, T. 2002. Accelerated drying of welsh onion by far infrared radiation under vacuum conditions. *Journal of Food Engineering* 55 (2): 147-156.
- Muga, F, Workneh, T and Marenya, M. 2020. Modelling the Thin-Layer Drying of Beef Biltong Processed Using Hot Air Drying. *Journal of Biosystems Engineering* 45 (1): 1-12.
- Naidoo, K and Lindsay, D. 2010. Survival of *Listeria monocytogenes*, and enterotoxin-producing *Staphylococcus aureus* and *Staphylococcus pasteurii*, during two types of biltong-manufacturing processes. *Food Control* 21 (7): 1042-1050.
- Nasiroglu, S and Kocabiyik, H. 2009. Thin-layer infrared radiation drying of red pepper slices. *Journal of Food Process Engineering* 32 (1): 1-16.
- Nguyen, TVL, Nguyen, MD, Nguyen, DC, Bach, LG and Lam, TD. 2019. Model for Thin Layer Drying of Lemongrass (*Cymbopogon citratus*) by Hot Air. *Processes* 7 (1): 21-30.
- Nortjé, K, Buys, E and Minnaar, A. 2005. Effect of γ -irradiation on the sensory quality of moist beef biltong. *Meat science* 71 (4): 603-611.
- Onwude, DI, Hashim, N, Abdan, K, Janius, R and Chen, G. 2019. The effectiveness of combined infrared and hot-air drying strategies for sweet potato. *Journal of Food Engineering* 241 (2019): 75-87.
- Ott, T, Schossig, M, Norkus, V and Gerlach, G. 2015. Efficient thermal infrared emitter with high radiant power. *Journal of Sensors and Sensor Systems* 4 (2): 313.
- Pan, Z, Atungulu, G and Li, X. 2014. Infrared heating. In: ed. Sun, D-W, *Emerging technologies for food processing*. Elsevier.
- Pan, Z and Atungulu, GG. 2010. *Infrared heating for food and agricultural processing*. CRC Press,
- Puente-Díaz, L, Ah-Hen, K, Vega-Gálvez, A, Lemus-Mondaca, R and Scala, KD. 2013. Combined infrared-convective drying of murta (*Ugni molinae* Turcz) berries: kinetic modeling and quality assessment. *Drying Technology* 31 (3): 329-338.

- Rastogi, NK. 2012. Recent trends and developments in infrared heating in food processing. *Critical reviews in food science and nutrition* 52 (9): 737-760.
- Ratti, C and Mujumdar, AS. 2007. Infrared Drying. In: ed. Mujumdar, AS, *Handbook of Industrial Drying*. Taylor & Francis, Boca Raton, FL.
- Riadh, MH, Ahmad, SAB, Marhaban, MH and Soh, AC. 2015. Infrared heating in food drying: An overview. *Drying Technology* 33 (3): 322-335.
- Saayman, M. 2015. Biltong of great value to South African economy. [Internet]. Available from: <https://www.food24.com/biltong-of-great-value-to-sa-economy/#:~:text=It%20was%20found%20that%20venison,popularity%20of%20the%20meat%20used>. [Accessed: 31 August 2020].
- Sadin, R, Chegini, G and Khodadadi, M. 2017. Drying characteristics and modeling of tomato thin layer drying in combined infrared-hot air dryer. *Agricultural Engineering International: CIGR Journal* 19 (1): 150-157.
- Sharma, G, Verma, R and Pathare, P. 2005. Thin-layer infrared radiation drying of onion slices. *Journal of Food Engineering* 67 (3): 361-366.
- Soydan Karabacak, M, Esin, A and Cekmecelioglu, D. 2014. Drying behavior of meat samples at various fiber directions and air conditions. *Drying technology* 32 (6): 695-707.
- Srikiatden, J and Roberts, JS. 2007. Moisture transfer in solid food materials: A review of mechanisms, models, and measurements. *International Journal of Food Properties* 10 (4): 739-777.
- Strydom, P and Zondagh, B. 2014. Biltong: A major South African ethnic meat product. In: eds. Dikeman, M and Devine, C, *Encyclopaedia of meat sciences*. Academic Press, London, UK.
- Sui, Y, Yang, J, Ye, Q, Li, H and Wang, H. 2014. Infrared, convective, and sequential infrared and convective drying of wine grape pomace. *Drying Technology* 32 (6): 686-694.
- Toğrul, H. 2005. Simple modeling of infrared drying of fresh apple slices. *Journal of Food Engineering* 71 (3): 311-323.
- Trujillo, FJ, Wiangkaew, C and Pham, QT. 2007. Drying modeling and water diffusivity in beef meat. *Journal of Food Engineering* 78 (1): 74-85.
- von Gersdorff, GJ, Porley, VE, Retz, SK, Hensel, O, Crichton, S and Sturm, B. 2018. Drying behavior and quality parameters of dried beef (biltong) subjected to different pre-treatments and maturation stages. *Drying Technology* 36 (1): 21-32.

- Wang, Z, Sun, J, Liao, X, Chen, F, Zhao, G, Wu, J and Hu, X. 2007. Mathematical modeling on hot air drying of thin layer apple pomace. *Food Research International* 40 (1): 39-46.
- Xie, X, Li, X, Zhang, C, Jia, W, Li, Y, Sun, H, Wang, Z and Mu, G. 2013. Combined mid-infrared and hot air drying reduces energy-consumption and improves quality of jerky. *Transactions of the Chinese Society of Agricultural Engineering* 29 (23): 217-226.
- Zhu, A and Shen, X. 2014. The model and mass transfer characteristics of convection drying of peach slices. *International Journal of Heat and Mass Transfer* 72 (2): 345-351.

5. A HEAT AND MASS TRANSFER MODEL FOR PREDICTING THE DRYING OF BEEF DURING BILTONG PROCESSING USING INFRARED ASSISTED HOT AIR DRYING

This chapter is based on the following manuscript.

Muga, F. C., Marenya, M. O., and Workneh, T. S. A heat and mass transfer model for predicting the drying of beef during biltong processing using infrared assisted hot air drying. *Journal of Biosystems Engineering*, Manuscript ID JBIS-D-21-00029.

Abstract

The infrared assisted hot air drying (IRHAD) is a possible alternative to the conventional hot air drying (HAD) of biltong. The application of IRHAD in biltong processing would require a better understanding of the mechanisms of heat and mass transfer during the drying process. Therefore, the aim of this study was to develop a coupled heat and mass transfer model to predict the temperature and moisture content of beef during biltong processing using IRHAD. The developed model was implemented and solve using Ansys Fluent CFD software. Drying experiments conducted using an infrared assisted hot air dryer was used to determine the moisture diffusivity, and the heat and mass transfer coefficients used in the model. The experiments were done at an infrared emitter power level of 750 W, drying air temperature of 30, 35 and 40 °C and velocity of 1.5 and 2.5 m.s⁻¹. The simulation slightly overpredicted the temperature in the first hour of drying and underpredicted the temperature towards end of the drying period. Consequently, the predicted moisture ratio (MR) was underpredicted at the onset of drying and agreed with the experimental values towards the end of the drying period. The simulation results were validated using a new set of experimental results and the suitability of the model assessed using the R² (0.9790 for temperature and 0.9579 for MR) and RMSE (1.99 for temperature and 0.0698 for MR). The model can guide the application of IRHAD in the processing of biltong and forms a theoretical basis for analysing the application of IRHAD to other food and biobased products.

Keywords: Ansys Fluent, Biltong, CFD, Heat transfer, Mass transfer, Modelling

Nomenclature

A	Surface area, m^2
c_p	Specific heat, $J.kg^{-1}.K^{-1}$
C	Moisture concentration, $mol.m^{-3}$
D	Moisture diffusivity of beef, $m^2.s^{-1}$
D_a	Mass diffusivity of air-vapour, $m^2.s^{-1}$
F	Shape view factor
h	Heat transfer coefficient, $W.m^{-2}.K^{-1}$
h_m	Mass transfer coefficient, $m.s^{-1}$
h_{lv}	Latent heat of evaporation, $J.kg^{-1}$
HAD	Hot air drying
IR	Infrared
IRHAD	Infrared assisted hot air drying
K	Thermal conductivity of beef, $W.m^{-1}.K^{-1}$
L	Length of IR emitter, m
Le	Lewis number
m	Molecular mass, $kg.mol^{-1}$
M	Moisture content wet basis, $kg.kg^{-1}$
P	Pressure, Pa
P_0	Rate of radiation heat transfer, W
QIR	volumetric IR heat source, $W.m^{-3}$
R_t	Total thermal resistivity, m^{-2}
t	Time, s
T	Temperature, K
u	Velocity, $m.s^{-1}$
V	Volume, m^3
W	Width of IR emitter, m
y	Mass fraction
Z	Distance between the emitter and the surface of the sample, m

Subscripts

<i>a</i>	air
<i>abs</i>	Absorbed energy
<i>b</i>	Beef
<i>c</i>	Carbohydrates
<i>eff</i>	effective
<i>eq</i>	Equilibrium
<i>f</i>	Fats
<i>IR</i>	Infrared emitter
<i>p</i>	Protein
<i>t</i>	Instantaneous
<i>w</i>	Water
0	Initial

Greek letters

α	IR absorption coefficient
α_a	thermal diffusivity of air, $W.m^{-1}.K^{-1}$
β	Quality factor
ρ	Density, $kg.m^{-3}$
δ	IR penetration depth, m
ε	emissivity
μ	viscosity of air, $Pa.s^{-1}$
η	Efficiency
σ	Stefan-Boltzmann constant, $W.m^{-2}.K^{-4}$

5.1 Introduction

Biltong is predominantly dried using hot air dryers (Jones *et al.*, 2017). However, recent research (Cherono, 2014; Muga *et al.*, 2021) have shown that infrared (IR) heating is promising in producing biltong of quality while using less energy to dry the meat to the required levels of moisture. Understanding the heat and mass transfer mechanism during the drying is critical in applying new drying technologies or optimizing the existing drying processes. Previous research (Jones, 2017; Muga *et al.*, 2020) on biltong have characterised the drying kinetics and established empirical models for the hot air drying (HAD), infrared drying (IRD) (Cherono, 2014), and infrared assisted hot air drying (IRHAD) (Muga *et al.*, 2021) of meat during biltong processing. The empirical models are less demanding computationally, hence suitable for automatic control of the drying processes (Ertekin and Firat, 2017). However, empirical models in the mentioned studies, are specific to the experimental conditions and cannot be used to predict the moisture ratio of meat outside the conditions for which they were developed (Kucuk *et al.*, 2014; Ertekin and Firat, 2017). Moreover, the empirical models cannot predict the temporal and spatial change in temperature and moisture distribution. Consequently, it is necessary to develop a mechanistic model for the drying of meat during biltong processing.

The transfer of heat and mass play an important role in the drying of food products (Srikiatden and Roberts, 2007). The temperature and water content of solid food products vary in space and time during heat treatment (Feyissa *et al.*, 2009). The entire history and spatial distribution of temperature and moisture influence the quality and the safety of the processed foods. A solid food undergoes many changes during drying. A food product being dried undergoes phase changes through evaporation of water (Adler-Nissen, 2007; Datta, 2007), shrinkage, pore formation (Yang *et al.*, 2001; Talla *et al.*, 2004; Tornberg, 2005), crust formation (Jefferson *et al.*, 2006), and colour change (Purlis, 2010). These changes may influence the heat and mass transfer mechanisms directly (e.g., phase change, formation of porous media) or influence the heat and mass transfer properties such as thermal conductivity, diffusivity and permeability (Feyissa *et al.*, 2009).

The heating of solid foods involve external and internal heat transfer processes (Therdthai and Zhou, 2003). A solid food and a heating medium exchange heat at their boundaries by

conduction, convection, or a combination of these mechanisms (Gupta, 2001; Therdthai and Zhou, 2003). The governing equations for the heat transfer inside a solid food are based on the principle of conservation of energy (Bird *et al.*, 2001). In the case of electromagnetic heating such as IR and microwave heating, a volumetric heat generation term is often included in the governing equation for heat transfer (Pan *et al.*, 2014).

Incorporating the IR heating in the governing equation for heat transfer is taxing due to the complexity of the optical characteristics, radiative energy extinction, and combined conductive and/or convective heat transfer phenomena (Krishnamurthy *et al.*, 2008a; Pan and Atungulu, 2011). The absorption or penetration, and extinction of IR energy in food materials is critical in modeling IR heating processes (Prakash, 2011; Tanaka and Uchino, 2011). The IR power absorption by food can be considered as an exponential decay function penetrating from the surface to the interior of food materials (Datta and Ni, 2002; Tanaka and Uchino, 2011). Consequently, the IR power absorption appears as a volumetric heat source term in the energy balance equation (Onwude *et al.*, 2018). Alternatively, the heat flux of the IR radiation can be incorporated in the boundary condition at the modelled food surface (Li, 2012). At shallow IR penetration depths of <1 mm, no significant difference has been found in the accuracy of temperature prediction when the IR energy is modelled as a volumetric heat source or as a boundary layer condition (Prakash, 2011; Tanaka and Uchino, 2011).

Drying of foods is also characterised by loss of mass mainly in the form of water (Mondal and Datta, 2008; Sumnu and Sahin, 2008). The transport of water within and outside the food is driven by the water concentration gradients. Water migrates through different mechanisms such as: molecular diffusion, pressure driven flow, capillary diffusion, and thermo-diffusions (Srikiatden and Roberts, 2007). The governing equation for the loss of water in solid foods is based on the principle of conservation of mass (Bird *et al.*, 2001; Celma *et al.*, 2008; Ponkham *et al.*, 2012).

According to Feyissa *et al.* (2009), most mass transfer models are based entirely on the Fick's diffusion. The ensuing transient diffusion equation for water transport is solved using experimentally determined effective diffusivity (Shilton *et al.*, 2002; Wang and Singh, 2004; Kondjoyan *et al.*, 2006; Onwude *et al.*, 2018). Other mass transfer phenomena such as pressure-

driven flow and the evaporation-condensation processes are critical during intensive heating at temperatures >100 °C such as roasting of meat (Feyissa *et al.*, 2013). The mass transfer processes during drying occur simultaneously with the heat transfer and involve interrelated physical phenomena (Datta, 2007; Huang *et al.*, 2007). The solution of the coupled partial differential equations that describe the heat and mass transfer during drying is a complex process that requires computerised numerical techniques.

One such technique that uses suitable computer software programs to solve complex heat and mass transfer problems is the computational fluid dynamics (CFD) (Solomon *et al.*, 2021). COMSOL Multiphysics and Ansys Fluent are the most popular CFD softwares. COMSOL Multiphysics employs advanced numerical methods to model and simulate physics based problems (Khan *et al.*, 2018). Several studies (Feyissa *et al.*, 2009; Feyissa *et al.*, 2013; Onwude *et al.*, 2018; Khan *et al.*, 2020; Pham *et al.*, 2020) have used COMSOL Multiphysics to implement and simulate different drying models. Ansys Fluent is a multipurpose CFD software that has several physics models for a variety of applications such as heat transfer, multiphase flows, turbulent flows and chemical mixing. Ansys Fluent has been used to predict the heat and moisture transfer during drying of food products (Erriguible *et al.*, 2007; Wang *et al.*, 2008; Darabi *et al.*, 2015).

The objectives of the current study was to; (1) formulate the governing equations and boundary conditions for the coupled heat and mass transfer process during the IRHAD of beef biltong, (2) solve the coupled equations using Ansys Fluent CFD software, and (3) validate the model by comparing the predicted and experimental results.

5.2 Development of The Coupled Heat and Mass Transfer Model for IRHAD of Beef Biltong

The slab shaped product is heated through radiation and convection. The product surface is heated through the convective heat transfer, whereas the radiative heat flux is absorbed by the product and generates volumetric heating within the top layer of the product. The heat is transferred to the centre of the product via conduction. Meanwhile, moisture is transport within the product to the surface by diffusion and convection process. Synchronously, the liquid water

evaporates from the product surface into the hot drying air. The mechanisms of the heat and mass transport during the IRHAD process is illustrated in Figure 5.1.

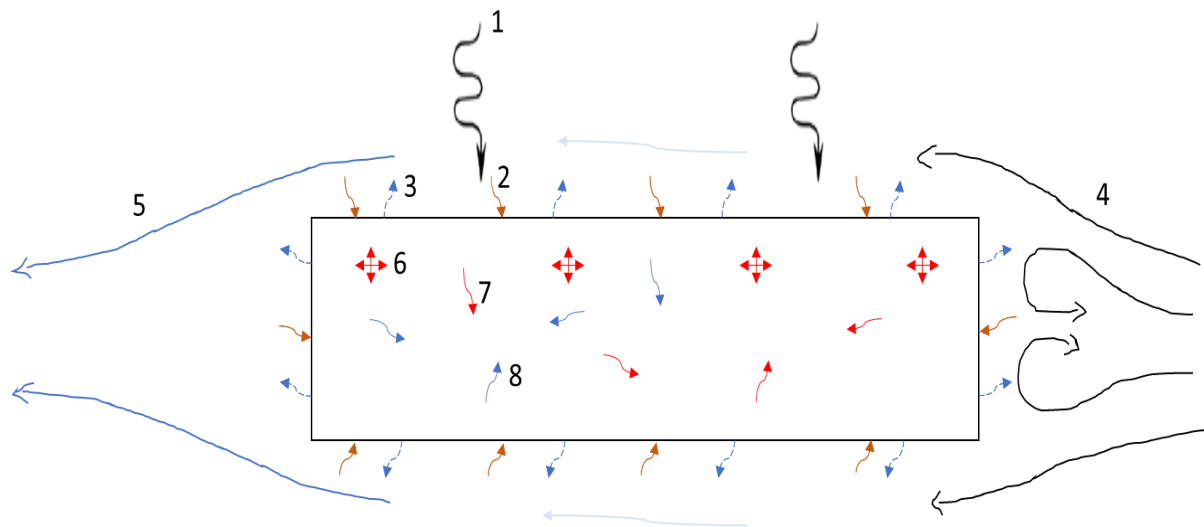


Figure 5.1 A schematic representation of the coupled heat and mass transfer during IRHAD process; 1 - IR radiation, 2 - convective heat transfer, 3 - evaporation, 4 - incoming drying air, 5 - outgoing moist drying air, 6 - volumetric heating due to absorbed IR radiation, 7 - internal heat transfer, 8 - internal moisture transfer

The assumptions made to formulate the governing equations for the coupled heat and mass transfer during the IRHAD process include;

- i. The material properties are homogenous,
- ii. The initial temperature and moisture content is uniform throughout the product,
- iii. There is no resistance to moisture movement and evaporation only takes place at the surface,
- iv. Fat transport is negligible since biltong is made from lean meat,
- v. Dissolved matter lost with water can be neglected in the material and energy balance.

The governing equations for the heat and mass transfer model for the IRHAD are based on the principle of conservation of momentum, energy and mass (Bird *et al.*, 2001).

5.2.1 Momentum equation

The governing equation for the flow of air around the product is based on the conservation of momentum and continuity as shown in Equations 5.1 and 5.2 (Solomon *et al.*, 2021).

$$\rho_a(u_a \cdot \nabla u_a) = -\nabla P + \nabla \cdot (\mu(\nabla u_a + (\nabla u_a)^T)) \quad (5.1)$$

$$\nabla \cdot u_a = 0 \quad (5.2)$$

Where:

ρ_a = density of air (kg.m^{-3}),

u_a = velocity of air (m.s^{-1}),

P = pressure (Pa),

μ = dynamic viscosity of air (Pa.s^{-1}), and

T_a = Temperature of air (K).

5.2.2 Heat transfer

The heat transfer inside a solid food matrix is mainly due to thermal conduction and partly due to convection (Bird *et al.*, 2001). A heat source term is added to the governing equation for heat transfer during IRHAD to cater for the volumetric heating caused by the IR radiation (Pan and Atungulu, 2011). The general equation for heat transfer including conduction, convection and radiation is given by Equation 5.3.

$$\rho_b c_{p,b} \frac{\delta T_b}{\delta t} = \nabla(k_b \nabla T_b) - \rho_w c_{p,w} u_w \nabla T_b + QIR \quad (5.3)$$

Where:

T_b = temperature of beef (K),

ρ_b = density of beef (kg.m^{-3}),

ρ_w = density of water (kg.m^{-3}),

$c_{p,b}$ = specific heat of beef ($\text{J.kg}^{-1}.\text{K}^{-1}$),

$c_{p,w}$ = specific heat of water ($\text{J.kg}^{-1}.\text{K}^{-1}$),
 k_b = thermal conductivity of beef ($\text{W.m}^{-1}.\text{K}^{-1}$),
 u_w = velocity of water (m.s^{-1}),
 t = time (s), and
 QIR = volumetric IR heat source (W.m^{-3}).

The volumetric IR heat source (QIR) can be expressed in terms of the heat absorbed by the material being dried (Onwude *et al.*, 2018). According to Lambert's Law, IR power absorption by food materials follows an exponential decay function penetrating from the surface to the interior of the food materials may be expressed as shown in Equation 5.4 (Datta and Ni, 2002; Pan and Atungulu, 2011; Tanaka and Uchino, 2011).

$$\dot{E}_{IR,abs} = P_0 \exp^{-\alpha\delta} \quad (5.4)$$

Where:

$\dot{E}_{IR,abs}$ = Rate of IR heat absorption by the product (W),
 P_0 = Rate of radiation heat transfer to the product (W),
 α = overall IR absorption coefficient, and
 δ = IR penetration depth of meat (m).

The overall IR absorption coefficient (α) is calculated using Equation 5.5 (Jaturonglumlert and Kiatsiriroat, 2010; Onwude *et al.*, 2018).

$$\alpha = \varepsilon_{IR}\varepsilon_b F_{b,IR} F_{IR,b} \quad (5.5)$$

Where:

ε_{IR} = emissivity of the IR emitter,
 ε_b = emissivity of beef,
 $F_{IR,b}$ = shape view factor between beef sample and IR emitter, and
 $F_{b,IR}$ = shape view factor between IR emitter and the beef sample.

The rate of radiation heat transfer from the IR emitter to the beef sample is calculated using Equation 5.6 (Pan and Atungulu, 2011).

$$P_0 = \frac{\sigma(T_{IR}^4 - T_b^4)}{R_t} \quad (5.6)$$

Where:

σ = Stefan-Boltzmann radiation constant ($\text{W.m}^{-2}.\text{K}^{-4}$),

T_{IR} = Temperature of the IR emitter (K), and

R_t = Total thermal resistivity.

The total thermal resistivity is obtained from Equation 5.7 (Onwude *et al.*, 2018).

$$R_t = \frac{1-\varepsilon_{IR}}{A_{IR}\varepsilon_{IR}} + (A_{IR}F_{b,IR})^{-1} + \frac{1-\varepsilon_b}{A_b\varepsilon_b} \quad (5.7)$$

Where:

A_b = surface area of the beef sample (m^2), and

A_{IR} = surface area of the IR emitter (m^2).

The surface area of the IR emitter is larger than the surface area of the beef sample. Therefore, the shape view factor between the IR emitter surface and the beef sample surface is determined using Equation 5.8, 5.9, and 5.10 (Swasdisevi *et al.*, 2009).

$$F_{b,IR} = \frac{1}{2\pi} \left(\frac{X}{\sqrt{1+X^2}} \tan^{-1} \frac{Y}{\sqrt{1+X^2}} + \frac{Y}{\sqrt{1+Y^2}} \tan^{-1} \frac{X}{\sqrt{1+Y^2}} \right) \quad (5.8)$$

$$X = \frac{L}{Z} \quad (5.9)$$

$$Y = \frac{W}{Z} \quad (5.10)$$

Where:

L = length of IR emitter (m),

W = width of IR emitter (m), and

Z = distance between the emitter and the surface of the beef sample (m).

The shape view factor between the surface of the beef sample and the surface of the IR emitter is calculated from the $F_{b,IF}$ using Equation 5.11 (Cengel *et al.*, 1998).

$$A_b F_{b,IR} = A_{IR} F_{IR,b} \quad (5.11)$$

The volumetric IR heat source can then be calculated using Equation 5.12.

$$QIR = \frac{\dot{E}_{IR,abs}}{V_b} \quad (5.12)$$

Where V_b is the volume of the beef sample (m^3).

5.2.3 Mass transfer

The mass transfer during IRHAD is based on diffusion and convective mass transfer processes. The general equation of mass transfer is formulated in terms of the material flux as expressed in Equation 5.13 (Bird *et al.*, 2001).

$$\frac{\delta C}{\delta t} = \nabla(D\nabla C) - u_w \nabla C \quad (5.13)$$

Where:

C = moisture concentration in the beef sample ($mol.m^{-3}$),

D = moisture diffusivity ($m^2.s^{-1}$), and

u_w = velocity of water ($m.s^{-1}$).

The moisture concentration, C, is related to the moisture content of the sample being dried and is as expressed in Equation 5.14 (Law *et al.*, 2016; Solomon *et al.*, 2021).

$$C = \frac{M\rho_b}{m_w} \quad (5.14)$$

Where:

M = moisture content of beef, wet basis (kg.kg^{-1})

m_w = molecular mass of water (kg.mol^{-1})

The moisture diffusivity, D , can be estimated based on shrinkage of the beef during drying. The shrinkage dependent moisture diffusivity is calculated from the sample area as shown in Equation 5.15 and 5.16 (Onwude *et al.*, 2018).

$$\frac{D_{eff}}{D} = \left(\frac{A_{b,0}}{A_{b,t}} \right)^2 \quad (5.15)$$

$$A_{b,t} = A_{b,0} \left(\frac{\rho_w + M\rho_b}{\rho_w + M_0\rho_b} \right) \quad (5.16)$$

Where:

D_{eff} = effective moisture diffusivity calculated from the slope method ($\text{m}^2.\text{s}^{-1}$),

$A_{b,0}$ = initial surface area of beef (m^2), and

$A_{b,t}$ = instantaneous surface area of beef (m^2).

5.2.4 Boundary and initial conditions

The convective heat transfer and evaporation occur at the open boundaries. The heat and mass transfer boundary conditions at the open boundaries is defined by Equation 5.17 and 5.18, respectively (Onwude *et al.*, 2018).

$$k_b \nabla T_b + \rho_w c_{p,w} u_w \nabla T_b = h(T_a - T_b) - h_{lv} h_m \rho_w (C - C_{eq}) \quad (5.17)$$

$$D \nabla M + u_w M = h_m (C - C_{eq}) \quad (5.18)$$

Where:

h = heat transfer coefficient ($\text{W.m}^{-2}.\text{K}^{-1}$),

h_m = mass transfer coefficient (m.s^{-1}),

h_{lv} = latent heat of evaporation ($J.kg^{-1}$), and

C_{eq} = equilibrium moisture concentration in beef ($mol.m^{-3}$).

The equilibrium moisture concentration, C_{eq} , is calculated from the equilibrium moisture content using Equation 14. The equilibrium moisture content of beef can be determined from the empirical relationship (Equation 5.19) developed from a logistic regression curve of water holding capacity versus temperature (Van der Sman, 2007; Feyissa *et al.*, 2013).

$$M_{eq} = 0.745 - \frac{0.345}{(1+30 \exp(-0.25 (T_b - T_\sigma)))} \quad (5.19)$$

Where T_σ (52 °C) is the centre of a logistic regression curve of water holding capacity versus temperature (Van der Sman, 2007).

The initial conditions for both heat and mass transfer are shown in Equations 5.20 and 5.21 (Feyissa *et al.*, 2013).

$$T_b = T_o \quad \text{at} \quad t = 0 \quad (5.20)$$

$$M = M_o \quad \text{at} \quad t = 0 \quad (5.21)$$

5.2.5 Heat and mass transfer coefficients

The convective heat transfer coefficient is obtained from experimental data using the lumped analytical method as expressed in Equation 5.22 (Feyissa *et al.*, 2013; Onwude *et al.*, 2018).

$$\frac{T_b - T_a}{T_{b,0} - T_a} = \exp\left(-\left(\frac{hA_b}{\rho_b c_{p,b} V_b}\right) t\right) \quad (5.22)$$

The convective heat transfer coefficient (h) is estimated from the slope of the graph of $\ln\left(\frac{T_b - T_a}{T_{b,0} - T_a}\right)$ against drying time (Equation 5.23).

$$\text{slope} = \frac{hA_b}{\rho_b c_{p,b} V_b} \quad (5.23)$$

The mass transfer coefficient (h_m) is analogous to the heat transfer coefficient and is evaluated using Equation 5.24 and 5.25 (Pasban *et al.*, 2017; Onwude *et al.*, 2018).

$$h_m = \frac{h}{\rho_a c_{p,a} (Le)^{2/3}} \quad (5.24)$$

$$Le = \frac{\alpha_a}{D_a} \quad (5.25)$$

Where:

Le = Lewis number

α_a = thermal diffusivity of air, ($\text{W}\cdot\text{m}^{-1}\cdot\text{K}^{-1}$) and

D_a = mass diffusivity of air-vapour ($\text{m}^2\cdot\text{s}^{-1}$).

5.2.6 Thermophysical properties of beef

The thermal conductivity of beef is estimated as $0.47 \text{ W}\cdot\text{m}^{-1}\cdot\text{C}^{-1}$, whereas the density and heat capacity of beef are determined using Equations 5.26 and 5.27, respectively (Rao *et al.*, 2014).

$$\rho_b = \frac{1}{\sum_i \frac{y_i}{\rho_i}} \quad (5.26)$$

$$c_{p,b} = (1.6y_c + 2y_p + 2y_f + 4.2y_w) \times 10^3 \quad (5.27)$$

Where:

i = water, protein, carbohydrate, and fats.

ρ_i = densities of water, protein, carbohydrate, fat ($\text{kg}\cdot\text{m}^{-3}$), and

y_i = mass fraction of water (y_w), protein (y_p), carbohydrate (y_c), and fats (y_f).

5.2.7 Model Inputs

The initial model input values, constants, thermophysical properties and relevant parameters used in the simulation of the coupled heat and mass transfer are provided in Table 5.1.

Table 5.1 Model input parameters

Quantity	Symbol	Value	Reference
Density of meat	ρ_m	1056.386 kg.m ⁻³	Current study
Specific heat capacity of meat	$c_{p,m}$	3642 J.kg ⁻¹ .K ⁻¹	Current study
Thermal conductivity of meat	k_m	0.47 W.m ⁻¹ .C ⁻¹	(Rao <i>et al.</i> , 2014)
Density of water	ρ_w	1000 kg.m ⁻³	(Rao <i>et al.</i> , 2014)
Density of air	ρ_a	1.073 kg.m ⁻³	(Kumar <i>et al.</i> , 2015)
Specific heat of water	$c_{p,w}$	4170 J.kg ⁻¹ .K ⁻¹	(Rao <i>et al.</i> , 2014)
Specific heat of air	$c_{p,a}$	1005.04 J.kg ⁻¹ .K ⁻¹	(Kumar <i>et al.</i> , 2015)
IR penetration depth of meat	δ	0.001 m	Current study
Emissivity of meat	ϵ_m	0.9	Current study
Emissivity of the IR emitter	ϵ_{IF}	0.9	(Elstein, 2014)
Stefan-Boltzmann constant	σ	5.67 × 10 ⁻⁸ W.m ⁻² .K ⁻⁴	(Pan and Atungulu, 2010b)
Initial Temperature	T_0	20	Current study
Drying air Temperature	T_a	30	Current study
Initial moisture content of meat	M_0	0.75	Current study
Temperature of the IR emitter	T_{IF}	400	Current study
Average Effective moisture diffusivity	D_{eff}	7.61 × 10 ⁻¹⁰ m ² .s ⁻¹	Current study
Permeability of beef	K	10 ⁻¹⁷ m ²	(Feyissa <i>et al.</i> , 2013)
Heat transfer coefficient	h	0.4617T _a - 8.4642	Current study
Mass transfer coefficient	h_m	0.0005T _a - 0.0086	Current study
Latent heat of evaporation	h_{lv}	2.3 × 10 ⁶ J.kg ⁻¹	(Yunus, 2019)
Thermal diffusivity of air	α_a	2.18 × 10 ⁻⁵ m ² .s ⁻¹	(Yunus, 2019)
Mass diffusivity of air-vapour	D_a	2.5 × 10 ⁻⁵ m ² .s ⁻¹	(Yunus, 2019)
Mass fraction of water	y_w	0.75	(Tornberg, 2005)
Mass fraction of protein	y_p	0.2	(Tornberg, 2005)
Mass fraction of carbohydrate	y_c	0.02	(Tornberg, 2005)
Mass fraction of fat	y_f	0.03	(Tornberg, 2005)
Density of protein	ρ_p	1320	(Rao <i>et al.</i> , 2014)
Density of carbohydrate	ρ_c	1600	(Rao <i>et al.</i> , 2014)
Density of fat	ρ_f	920	(Rao <i>et al.</i> , 2014)

5.3 Implementation and Solution of The Heat and Mass Transfer Model

The implementation of the heat and mass transfer model and the numerical solution of the coupled partial differential equations was done using the Ansys Fluent software (Ansys 2020R2, Ansys Inc., Canonsburg, USA). A flowchart detailing the procedure for the implementation of the model and simulation in Ansys Fluent CFD software is shown in Figure 5.2.

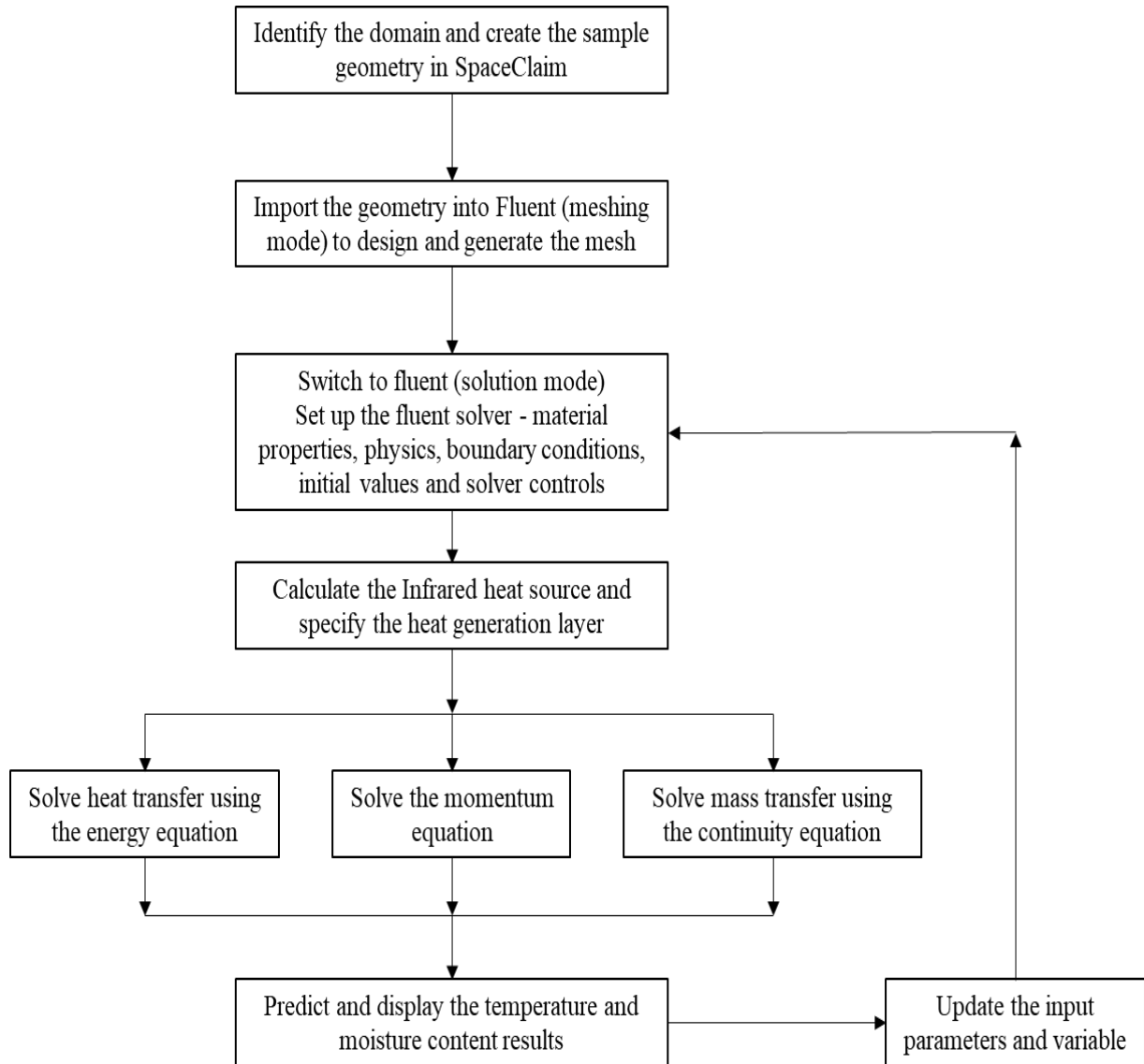


Figure 5.2 Flowchart of the procedure for the implementation of the heat and mass transfer model and simulation of temperature and moisture content during IRHAD

The Ansys Fluent software achieves the mass, momentum, and energy balance by solving the continuity equation, Navier–Stokes equation, and the energy equation, respectively, within a specified domain (Norton and Sun, 2006). Using Ansys, the computational domain (geometry definition), mesh generation, specification of the physics models, definition of the boundary layer conditions, solution, post-processing and visualisation of the results are all done in the Fluent toolbox.

5.3.1 Geometry and mesh generation

The beef sample and the drying chamber was represented as 2D rectangular geometries measuring 150 mm by 15 mm and 300 mm by 200 mm, respectively (Figure 5.3). The drying air inlet was specified as a velocity inlet, whereas the outlet was a pressure outlet. The geometry was created in SpaceClaim.

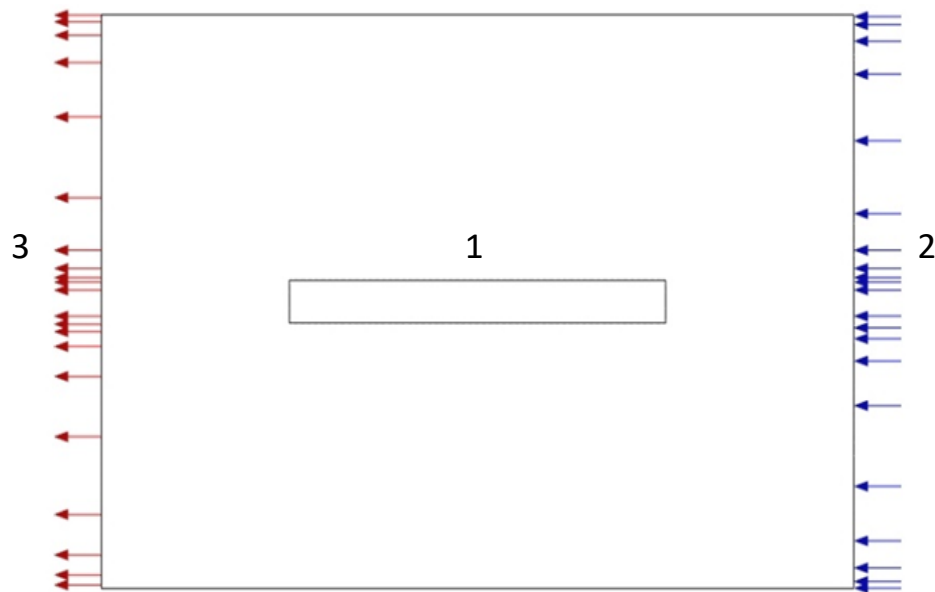


Figure 5.3 The 2D geometry of the beef sample and the surrounding drying air; 1 – beef sample, 2 – incoming drying air, 3 – outgoing moist drying air

The geometry was imported into Fluent (meshing mode) to generate the mesh. The generated mesh was refined at the boundaries. Thereafter, a mesh sensitivity analysis was used to check and improve the quality of the mesh as described by Kumar and Dilber (2007). A series of

simulations were done with increasing finer meshes until there was no impact on the solution with a change in mesh density. The final mesh had a maximum and minimum element size of 0.003 m and 0.001 m, respectively, and a maximum element growth rate of 1.2. The mesh had a total of 58800 elements, a minimum orthogonal quality of 1.0, and a maximum aspect ratio of 1.9. The final mesh is shown in Figure 5.4.

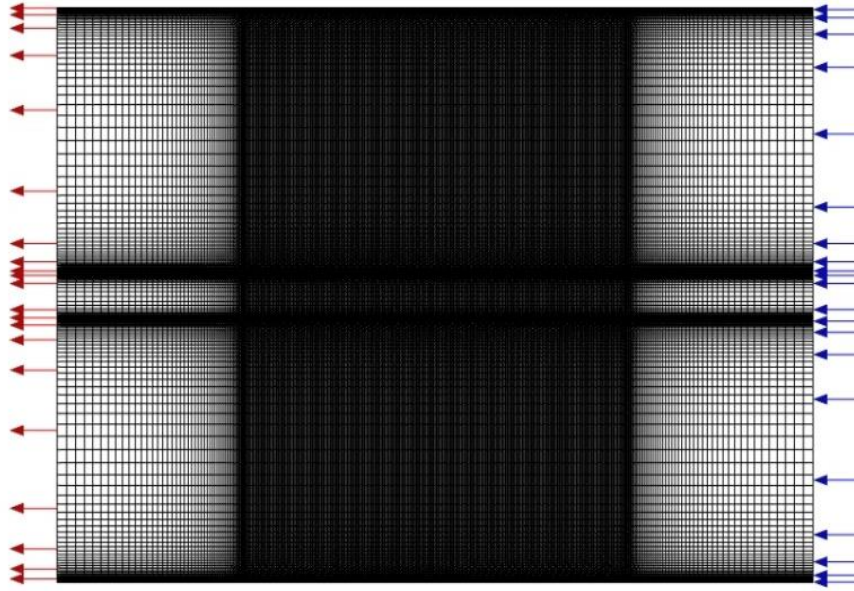


Figure 5.4 The final mesh generated from Ansys Fluent for use in the simulation of the heat and mass transfer

5.3.2 Implementation of the CFD model

The mesh information was transferred to the Fluent solver by switching from meshing mode to solution mode. The Reynolds-averaged Navier-Stokes (RANS) approach was used due to its effective performance for wall bounded boundary layer flows (Wang *et al.*, 2018). The turbulent flow of the drying air around the beef sample was modelled using the Standard k-epsilon ($k-\epsilon$) model using the model parameters shown in Appendix C (Figure 8.5).

The volumetric heating due to the Infrared radiation was incorporated in the model as a heat generation layer, 1 mm below the top surface of the beef sample. The energy equation was selected to solve for the temperature. The mass transfer from liquid water to water vapour at the

surface of the beef sample was solved using a user defined function (UDF), written in C programming language (Appendix D). The UDF was added to the Fluent solver as a compiled executable code.

The solution was based on a pressure-velocity coupling with a simple scheme (Wang *et al.*, 2018). The gradient for the spatial discretisation was based on the least square cell and the pressure set to presto. The momentum and energy were solved using the second order upwind method, whereas the turbulent kinetic energy, turbulence dissipation rate, and the transient formulation were all solved using the first order upwind method (Appendix C, Figure 8.6). The residuals for the continuity equation, energy, area weighted temperature, area weighted volume fraction of water and vapour, and the k- ϵ were monitored for convergence during the iterations (Appendix C, Figure 8.7).

The solution was initialized using a standard initialization with the reference frame set relative to the cell zone. The initial values set for the key solution monitors is shown in Appendix C, Figure 8.8. The calculation was set to run for 3600000 time steps with a time step size of 0.005 s and a maximum of 20 iterations per time step (Appendix C, Figure 8.9). The simulations were carried out on a local computer Intel(R) Core(TM) i7-6500U CPU @ 2.50GHz (4 CPUs) with an installed RAM of 16GB, running under Windows 10 (64 bit) (HP ProBook 450 G3, Hewlett-Packard, Palo Alto, California, USA).

5.4 Materials and Methods

5.4.1 Sample preparation

The samples were prepared as outlined in Muga *et al.* (2020).

5.4.2 The drying unit

An existing hot air cabinet dryer (Muga *et al.*, 2020) was retrofitted with an IR emitter as outlined in Muga *et al.* (2021).

5.4.3 Drying experiments

The IRHAD experiments followed the procedure described by Muga *et al.* (2021). The IRHAD experiments were done at an IR power level of 750 W, drying air temperatures of 30, 35, and 40 °C, and drying air velocity of 1.5 and 2.5 m.s⁻¹. The results from the experiments were used to determine the effective moisture diffusivity, and the heat and mass transfer coefficients. The effective moisture diffusivity was determined using the slope method as outlined in Muga *et al.* (2021), whereas the heat and mass transfer coefficients were determined using the lumped parameter method using Equations 5.22 – 5.25 (Feyissa *et al.*, 2013; Onwude *et al.*, 2018).

5.4.4 Validation of the heat and mass transfer model

A new set of experimental data was collected at an IR power level of 1000 W, drying air temperature of 40 °C and a drying air velocity of 1.5 m.s⁻¹. The new dataset was compared with the model predictions. The suitability of the model was judged based on the R² and the RMSE (Muga *et al.*, 2020; Muga *et al.*, 2021; Solomon *et al.*, 2021).

5.5 Results and Discussion

5.5.1 Air flow characteristics

The simulated velocity distribution pattern of air at an IR power level of 750 W, drying air temperature of 30 °C and a drying air velocity of 2.5 m.s⁻¹, is shown in Figure 5.5. The velocity of the drying air decreased around the chamber wall due to the resistance between the wall and the stream of the drying air. The air stream around the centre of the drying chamber, between the beef sample and the chamber wall, exhibited velocity values above the inlet drying air velocity. These findings concur with the results reported by Solomon *et al.* (2021) on the air flow around a layer of injera (a sour fermented flat bread made from teff flour) during hot air drying.

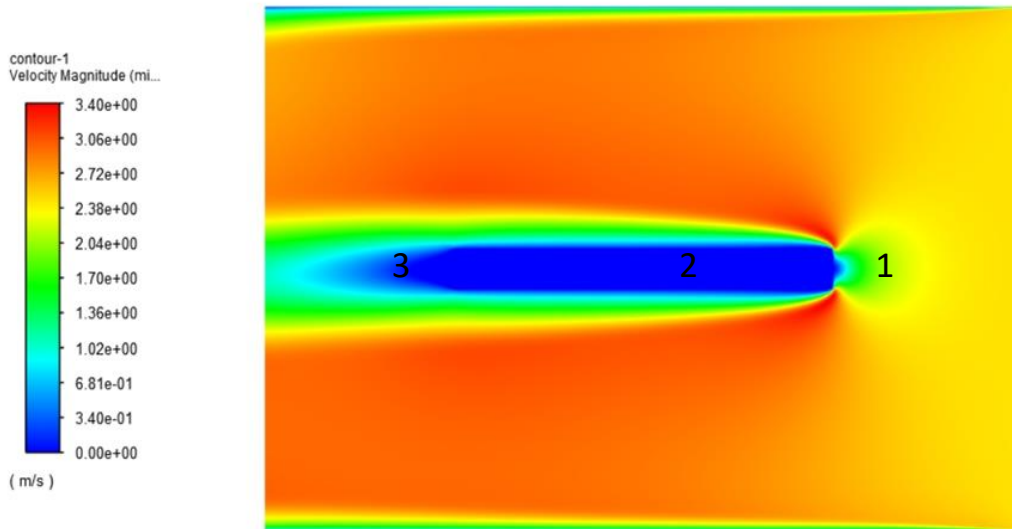


Figure 5.5 Velocity contour around the beef sample; 1 – recirculation zone, 2 – beef sample, 3 – dead zone

The simulated velocity of the drying air also decreased around the beef sample. The slab of beef acts as an obstruction to the air flow, thus creating a recirculation zone at the leading edge and a dead zone at the extreme end of the beef sample. The air flow around the sample is turbulent, with a higher turbulence intensity observed at the leading edge of the beef sample as shown in Figure 5.6. These findings agree with the observations made by Defraeye *et al.* (2012) and Khan *et al.* (2020) from their simulation of the air movements around food materials during drying.

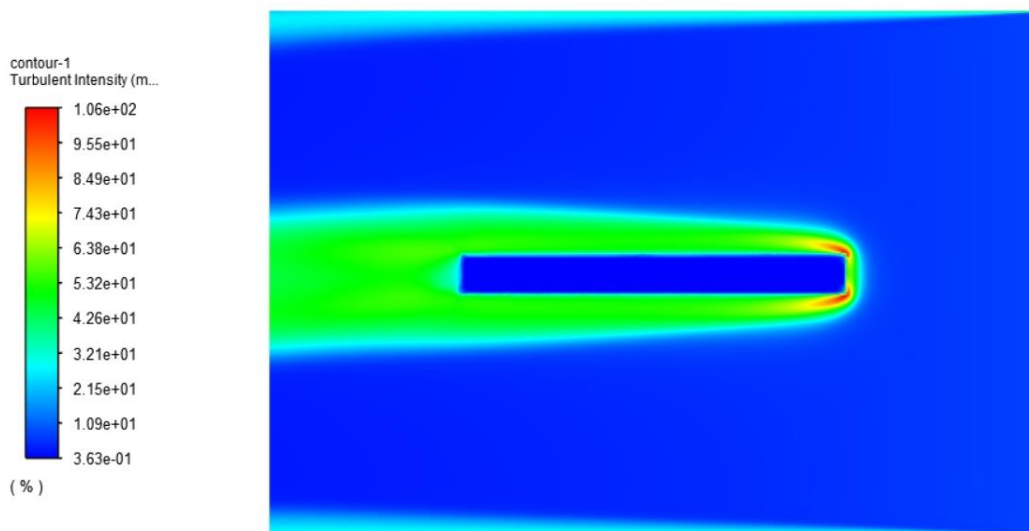


Figure 5.6 Turbulence intensity of the drying air around the beef sample

5.5.2 Temperature distribution

The distribution of the simulated temperature in the beef sample at an IR emitter power level of 750 W, drying air temperature of 30 °C, and drying air velocity of 2.5 m.s⁻¹ is shown in Figure 5.8. The temperature profile of the beef sample at the onset of drying is uniform and lower than the drying air temperature (Figure 5.7 (a)). The temperature profile in Figure 5.7 (b) and (c) indicate that at the onset of drying, the highest temperature is observed around the top surface of the beef sample. This is due to the volumetric heating provided by the absorption of the IR radiation at the top surface. It is notable that the temperature of the beef sample is raised from the initial temperature of 20 °C to within the temperature of the drying air in approximately 10 minutes. This is significantly quicker than the product heat up time during hot air drying (HAD) of marinated beef (Muga *et al.*, 2020). According to Muga *et al.* (2020), HAD took approximately 10 hours to heat up the beef sample to the equilibrium temperature which was approximately 0.5 - 1.8 °C below the drying air temperature. The quick product heat up time during IRHAD is due to the synergistic interaction between the hot air and the IR radiation in heating up the beef sample as reported in previous studies (Kumar *et al.*, 2005; Krishnamurthy *et al.*, 2008b; Onwude *et al.*, 2018).

These results indicate that the surface of the beef sample is at a lower temperature than the core of the beef sample. This is due to the evaporation driven mass transfer that occurs at the surface of the beef sample. This observation is consistent with the simulation results reported by Solomon *et al.* (2021).

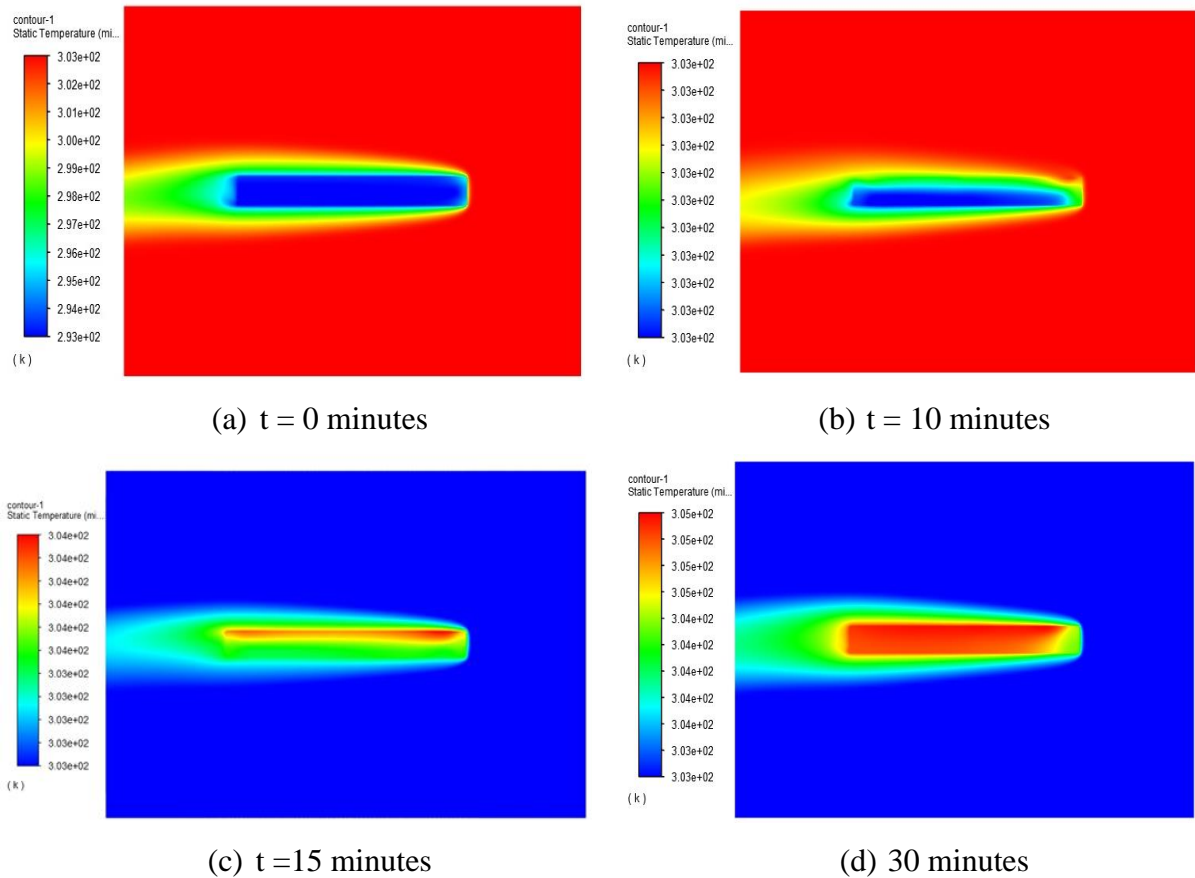


Figure 5.7 Temperature distribution in meat at different times during drying. The temperature scale is in Kelvin (K)

The results presented in Figure 5.7 indicate that the beef sample is heated from the top surface towards the bottom surface. This is due to the application of the IR heat source from the top surface. Symmetrical heating of the beef sample can be improved by providing an IR heat source from both the top and bottom surface. The beef sample reaches an equilibrium temperature of 33 °C during IRHD at IR emitter power level of 750 W, drying air temperature of 30 °C, and drying air velocity of 2.5 m.s⁻¹. The equilibrium temperature of 33 °C is within the sample temperatures attained during HAD of beef biltong at hot air temperature of 40 °C (Muga *et al.*, 2020). Hence, will likely result in biltong quality that is similar the quality of biltong processed using conventional HAD. However, increasing the IR emitter power level beyond 750 W may lead to beef sample temperatures beyond 50 °C as reported by Muga *et al.* (2021). Higher temperatures beyond 50 °C may be a concern for biltong producers since protein denaturation begins at temperatures between 40 and 50 °C (Li *et al.*, 2018). Nonetheless, Cherono *et al.* (2016) reported

no significant difference in the crude protein content of biltong produced using IR heating and HAD, despite recording core sample temperatures of up to 90 °C during IR heating.

5.5.3 Mean moisture content and temperature curves

The predicted moisture ratio (MR) of meat and the corresponding experimental results is shown in Figure 5.8. The simulation took 16 hours to lose 50 % of the original weight of the beef sample as compared to 14 hours recorded during the actual experiment. The simulated results show a predominantly falling rate drying period as reported in Muga *et al.* (2021). The simulated results indicate a higher drying rate at the onset of drying than the experimental results. The higher drying rate at the beginning of the drying process is attributed to the quicker increase in sample temperature from the simulations compared to the experimental data (Figure 5.9).

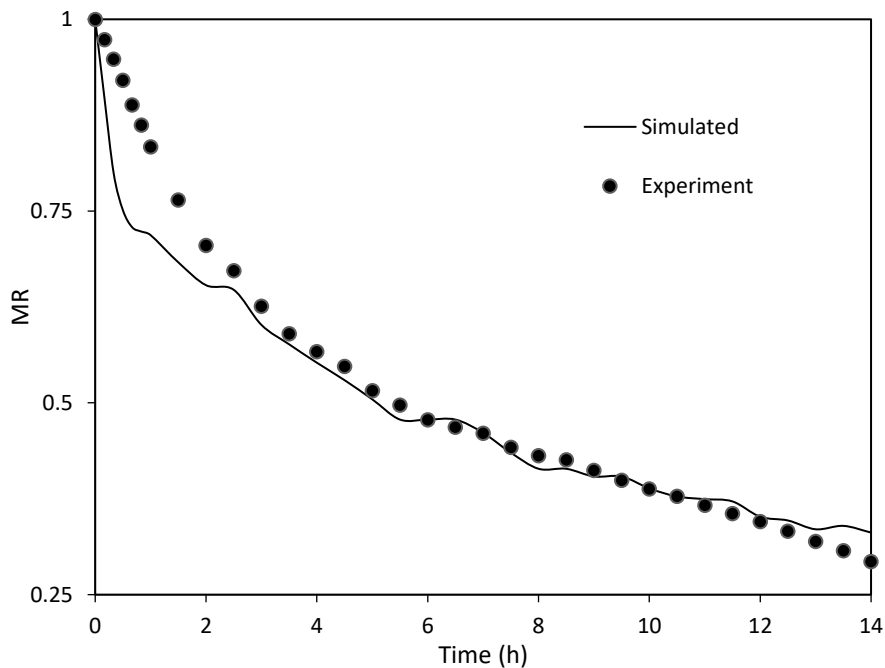


Figure 5.8 Experimental and predicted moisture content at an IR power level of 750 W, drying air temperature of 30 °C and drying air velocity of 2.5 m.s⁻¹

The simulated temperature of the beef sample was underpredicted towards the end of drying. However, the difference between the simulated and experimental temperature data was generally between 1 – 2 °C which is within the acceptable margin of error in temperature measurements.

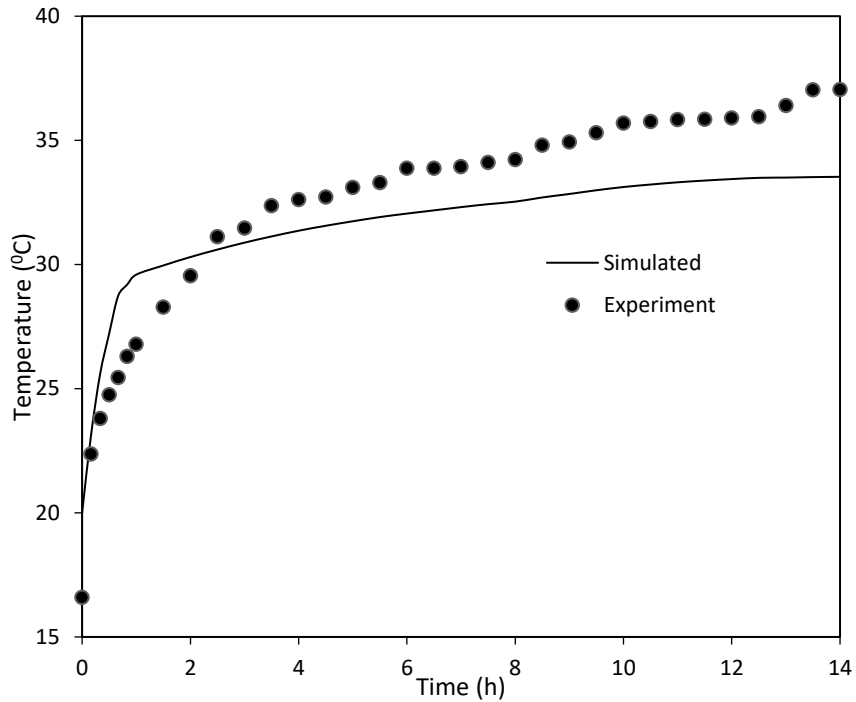


Figure 5.9 Experimental and simulated core temperature of the beef sample at an IR power level of 750 W, drying air temperature of 30 °C and drying air velocity of 2.5 m.s⁻¹

5.5.4 Model validation

The model was validated using a new set of experimental data collected at an IR power level of 1000 W, drying air temperature of 40 °C and drying air velocity of 1.5 m.s⁻¹. The coefficient of determination (R^2) and the root mean square error (RMSE) were 0.9579 and 0.0698, respectively, for the MR curve (Figure 5.10). The sample core temperature curve had an R^2 and an RMSE of 0.9790 and 1.99, respectively (Figure 5.11). The model predicts the temperature better ($R^2 = 0.9790$) than the MR ($R^2 = 0.9579$). The model accounts for all modes of heat transfer (conduction, convection, and radiation) in beef during IRHAD, while considering diffusion and convection as the only modes of mass transfer. Ignoring other modes of moisture transport such as pressure driven flow, although minimal, may cause the underprediction of the MR (Figure 5.10) compared to the temperature. Additionally, a moving boundary may be better at capturing the effects of shrinkage during drying compared to the shrinkage dependent moisture diffusivity (Feyissa *et al.*, 2009). Nevertheless, the model is reasonably acceptable given the high values of the R^2 (0.9579 and 0.9790) and low values of RMSE (0.0698 and 1.99) for both MR and

temperature. Previous studies by Swasdisevi *et al.* (2009) and Solomon *et al.* (2021) reported values of the R^2 within the same range as those reported in this study for models for the combined far-infrared and vacuum drying of bananas and the hot air drying of injera, respectively.

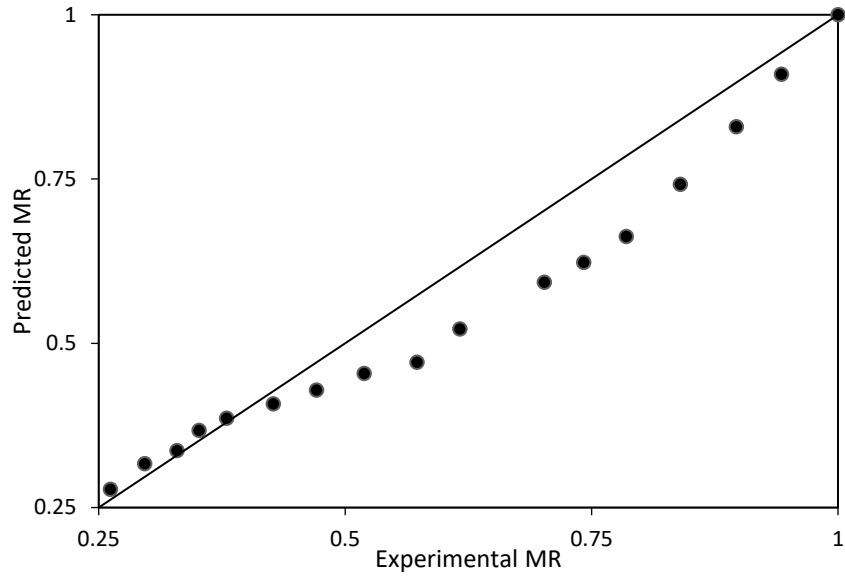


Figure 5.10 Comparison between the predicted and actual MR at an IR power level of 1000 W, drying air temperature of 40 °C and velocity of 1.5 m.s⁻¹

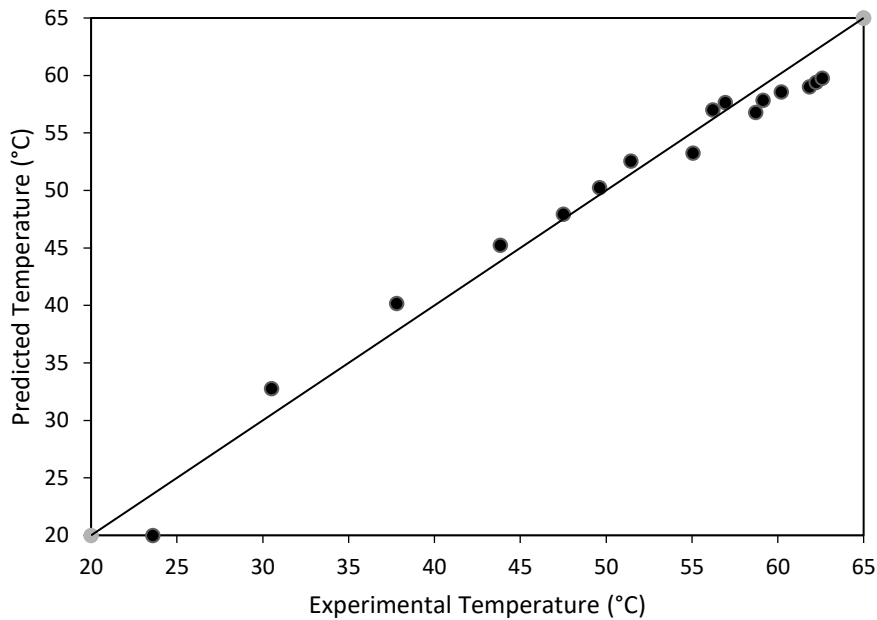


Figure 5.11 Comparison between the predicted and experimental core sample temperature at IR power level of 1000 W, drying air temperature of 40 °C and velocity of 1.5 m.s⁻¹

The simulation results indicated a sharp increase in temperature at the onset of drying, hence the sparse distribution of data points between 20 and 45 °C. The data points were cluster between 55 and 65 °C due to the minimal change in temperature towards the final stages of drying.

5.6 Conclusion

This chapter outlined the model for predicting the heat and mass transfer during IRHAD of a slab of beef being processed into biltong. The strategies for implementing and solving the developed model using Ansys Fluent have been outlined and the necessary model input parameters provided. The model suitably characterized the flow of the drying air around the slab of beef sample, the temperature distribution in the sample, and the moisture content during drying. The simulated results from the model are reasonably acceptable given the high values of the R^2 (0.9579 and 0.9790) and low values of RMSE (0.0698 and 1.99) for both MR and temperature. The model predicts the temperature better ($R^2 = 0.9790$) than the MR ($R^2 = 0.9579$). The accuracy of the model in predicting the MR may be improved by incorporating pressure driven flows and a moving boundary which may be necessary due to shrinkage especially at high sample temperatures caused by high IR emitter power levels. The proposed model provides a good understanding of the heat and mass transfer dynamics during IRHAD of a slab of beef being dried into biltong. The model can safely be used to guide the application of IRHAD in the processing of biltong. The model can also serve as a theoretical basis for the analysis of the IRHAD of other food and biobased products.

5.7 References

- Adler-Nissen, J. 2007. Continuous wok-frying of vegetables: Process parameters influencing scale up and product quality. *Journal of food engineering* 83 (1): 54-60.
- Bird, R, Sterwart, W and Lightfoot, E. 2001. *Transport phenomena*. John Wiley and Sons Inc., New York.
- Celma, AR, Rojas, S and Lopez-Rodriguez, F. 2008. Mathematical modelling of thin-layer infrared drying of wet olive husk. *Chemical Engineering and Processing: Process Intensification* 47 (9-10): 1810-1818.

- Cengel, YA, Klein, S and Beckman, W. 1998. *Radiation heat transfer*. In: ed. Cengel, YA, Heat transfer: a practical approach. WBC McGraw-Hill, Boston, USA.
- Cherono, K. 2014. Infrared Drying of Biltong. Unpublished MSc thesis, Bioresources Engineering, University of KwaZulu-Natal, Pietermaritzburg, South Africa.
- Cherono, K, Mwithiga, G and Schmidt, S. 2016. Infrared drying as a potential alternative to convective drying for biltong production. *Italian journal of food safety* 5 (3): 140-145.
- Darabi, H, Zomorodian, A, Akbari, M and Lorestani, A. 2015. Design a cabinet dryer with two geometric configurations using CFD. *Journal of Food Science and Technology* 52 (1): 359-366.
- Datta, A. 2007. Porous media approaches to studying simultaneous heat and mass transfer in food processes. II: Property data and representative results. *Journal of food engineering* 80 (1): 96-110.
- Datta, A and Ni, H. 2002. Infrared and hot-air-assisted microwave heating of foods for control of surface moisture. *Journal of Food Engineering* 51 (4): 355-364.
- Defraeye, T, Herremans, E, Verboven, P, Carmeliet, J and Nicolai, B. 2012. Convective heat and mass exchange at surfaces of horticultural products: A microscale CFD modelling approach. *Agricultural and Forest Meteorology* 162 (3): 71-84.
- Dzimba, FEJ, Faria, J and Walter, EHM. 2007. Testing the sensory acceptability of biltong formulated with different spices. *African Journal of Agricultural Research* 2 (11): 547-577.
- Erriguible, A, Bernada, P, Couture, F and Roques, M-A. 2007. Simulation of vacuum drying by coupling models. *Chemical Engineering and Processing: Process Intensification* 46 (12): 1274-1285.
- Ertekin, C and Firat, MZ. 2017. A comprehensive review of thin-layer drying models used in agricultural products. *Critical reviews in food science and nutrition* 57 (4): 701-717.
- Feyissa, AH, Adler-Nissen, J and Gernaey, K. 2009. Model of Heat and Mass Transfer with Moving Boundary during Roasting of Meat in Convection-Oven. *Excerpt from the Proceedings of the COMSOL Conference, Milan, Italy*.
- Feyissa, AH, Gernaey, KV and Adler-Nissen, J. 2013. 3D modelling of coupled mass and heat transfer of a convection-oven roasting process. *Meat science* 93 (4): 810-820.
- Gupta, T. 2001. Individual heat transfer modes during contact baking of Indian unleavened flat bread (chapati) in a continuous oven. *Journal of Food Engineering* 47 (4): 313-319.

- Huang, H, Lin, P and Zhou, W. 2007. Moisture transport and diffusive instability during bread baking. *SIAM Journal on Applied Mathematics* 68 (1): 222-238.
- Jaturonglumlert, S and Kiatsiriroat, T. 2010. Heat and mass transfer in combined convective and far-infrared drying of fruit leather. *Journal of Food Engineering* 100 (2): 254-260.
- Jefferson, D, Lacey, A and Sadd, P. 2006. Understanding crust formation during baking. *Journal of Food Engineering* 75 (4): 515-521.
- Jones, M. 2017. Profiling of traditional South African biltong in terms of processing, physicochemical properties and microbial stability during storage. Unpublished PhD thesis, Food Science, Stellenbosch University, Stellenbosch, South Africa.
- Jones, M, Arnaud, E, Gouws, P and Hoffman, LC. 2017. Processing of South African biltong—A review. *South African Journal of Animal Science* 47 (6): 743-757.
- Khan, MIH, Joardder, M, Kumar, C and Karim, M. 2018. Multiphase porous media modelling: A novel approach to predicting food processing performance. *Critical reviews in food science and nutrition* 58 (4): 528-546.
- Khan, MIH, Welsh, Z, Gu, Y, Karim, M and Bhandari, B. 2020. Modelling of simultaneous heat and mass transfer considering the spatial distribution of air velocity during intermittent microwave convective drying. *International Journal of Heat and Mass Transfer* 153 (4): 119-128.
- Kondjoyan, A, Rouaud, O, McCann, M, Havet, M, Foster, A, Swain, M and Daudin, J. 2006. Modelling coupled heat–water transfers during a decontamination treatment of the surface of solid food products by a jet of hot air. I. Sensitivity analysis of the model and first validations of product surface temperature under constant air temperature conditions. *Journal of Food Engineering* 76 (1): 53-62.
- Krishnamurthy, K, Jun, S, Irudayaraj, J and Demirci, A. 2008a. Efficacy of infrared heat treatment for inactivation of staphylococcus aureus in milk. *Journal of food process engineering* 31 (6): 798-816.
- Krishnamurthy, K, Khurana, HK, Soojin, J, Irudayaraj, J and Demirci, A. 2008b. Infrared heating in food processing: an overview. *Comprehensive reviews in food science and food safety* 7 (1): 2-13.
- Kucuk, H, Midilli, A, Kilic, A and Dincer, I. 2014. A review on thin-layer drying-curve equations. *Drying Technology* 32 (7): 757-773.

- Kumar, A and Dilber, I. 2007. *Fluid flow and its modeling using computational fluid dynamics*. CRC Press, Boca Raton,
- Kumar, C, Millar, GJ and Karim, M. 2015. Effective diffusivity and evaporative cooling in convective drying of food material. *Drying Technology* 33 (2): 227-237.
- Kumar, PD, Umesh Hebbar, H, Sukumar, D and Ramesh, M. 2005. Infrared and hot-air drying of onions. *Journal of Food Processing and Preservation* 29 (2): 132-150.
- Law, M, Liew, E, Chang, S, Chan, Y and Leo, C. 2016. Modelling microwave heating of discrete samples of oil palm kernels. *Applied Thermal Engineering* 98 702-726.
- Li, X. 2012. A study of infrared heating technology for tomato peeling: Process characterization and modeling. Unpublished thesis, University of California, Davis, California.
- Li, X, Xie, X, Zhang, C-h, Zhen, S and Jia, W. 2018. Role of mid-and far-infrared for improving dehydration efficiency in beef jerky drying. *Drying Technology* 36 (3): 283-293.
- Mondal, A and Datta, A. 2008. Bread baking—a review. *Journal of Food Engineering* 86 (4): 465-474.
- Muga, F, Workneh, T and Marennya, M. 2020. Modelling the Thin-Layer Drying of Beef Biltong Processed Using Hot Air Drying. *Journal of Biosystems Engineering* 45 (1): 1-12.
- Muga, FC, Marennya, MO and Workneh, TS. 2021. Modelling the Thin-Layer Drying Kinetics of Marinated Beef during Infrared-Assisted Hot Air Processing of Biltong. *International Journal of Food Science* 2021 (2021): 1 - 15.
- Norton, T and Sun, D-W. 2006. Computational fluid dynamics (CFD)—an effective and efficient design and analysis tool for the food industry: a review. *Trends in Food Science & Technology* 17 (11): 600-620.
- Onwude, DI, Hashim, N, Abdan, K, Janius, R, Chen, G and Kumar, C. 2018. Modelling of coupled heat and mass transfer for combined infrared and hot-air drying of sweet potato. *Journal of Food Engineering* 228 (2019): 12-24.
- Pan, Z, Atungulu, G and Li, X. 2014. *Infrared heating*. In: ed. Sun, D-W, Emerging technologies for food processing. Elsevier.
- Pan, Z and Atungulu, GG. 2010. *Infrared heating for food and agricultural processing*. CRC Press,
- Pan, Z and Atungulu, GG. 2011. *Combined infrared heating and freeze-drying*. In: eds. Pan, Z and Atungulu, GG, Infrared heating for food and agricultural processing. CRC Press, Nwey York.

- Pasban, A, Sadrnia, H, Mohebbi, M and Shahidi, SA. 2017. Spectral method for simulating 3D heat and mass transfer during drying of apple slices. *Journal of Food Engineering* 212 (3): 201-212.
- Pham, ND, Khan, M and Karim, M. 2020. A mathematical model for predicting the transport process and quality changes during intermittent microwave convective drying. *Food chemistry* 325 (1): 126-132.
- Ponkham, K, Meeso, N, Soponronnarit, S and Siriamornpun, S. 2012. Modeling of combined far-infrared radiation and air drying of a ring shaped-pineapple with/without shrinkage. *Food and Bioproducts Processing* 90 (2): 155-164.
- Prakash, B. 2011. Mathematical modeling of moisture movement within a rice kernel during convective and infrared drying. Unpublished thesis, University of California, Davis,
- Purlis, E. 2010. Browning development in bakery products—A review. *Journal of Food Engineering* 99 (3): 239-249.
- Rao, MA, Rizvi, SS, Datta, AK and Ahmed, J. 2014. *Engineering properties of foods*. CRC press,
- Shilton, N, Mallikarjunan, P and Sheridan, P. 2002. Modeling of heat transfer and evaporative mass losses during the cooking of beef patties using far-infrared radiation. *Journal of Food Engineering* 55 (3): 217-222.
- Solomon, AB, Fanta, SW, Delele, MA and Vanierschot, M. 2021. Modeling and simulation of heat and mass transfer in an Ethiopian fresh injera drying process. *Heliyon* 7 (2): e06201.
- Srikiatden, J and Roberts, JS. 2007. Moisture transfer in solid food materials: A review of mechanisms, models, and measurements. *International Journal of Food Properties* 10 (4): 739-777.
- Sumnu, SG and Sahin, S. 2008. *Food engineering aspects of baking sweet goods*. CRC Press,
- Swasdisevi, T, Devahastin, S, Sa-Adchom, P and Soponronnarit, S. 2009. Mathematical modeling of combined far-infrared and vacuum drying banana slice. *Journal of Food Engineering* 92 (1): 100-106.
- Talla, A, Puiggali, J-R, Jomaa, W and Jannot, Y. 2004. Shrinkage and density evolution during drying of tropical fruits: application to banana. *Journal of Food Engineering* 64 (1): 103-109.
- Tanaka, F and Uchino, T. 2011. *Heat and Mass Transfer Modeling of Infrared Radiation for Heating*. In: eds. Pan, Z and Atungulu, G, *Infrared Heating for Food and Agricultural Processing*. CRC Press, New York.

- Therdthai, N and Zhou, W. 2003. Recent advances in the studies of bread baking process and their impacts on the bread baking technology. *Food Science and Technology Research* 9 (3): 219-226.
- Tornberg, E. 2005. Effects of heat on meat proteins—Implications on structure and quality of meat products. *Meat science* 70 (3): 493-508.
- Van der Sman, R. 2007. Soft condensed matter perspective on moisture transport in cooking meat. *AIChE Journal* 53 (11): 2986-2995.
- von Gersdorff, GJ, Porley, VE, Retz, SK, Hensel, O, Crichton, S and Sturm, B. 2018. Drying behavior and quality parameters of dried beef (biltong) subjected to different pre-treatments and maturation stages. *Drying Technology* 36 (1): 21-32.
- Wang, H, Yang, W, Senior, P, Raghavan, R and Duncan, S. 2008. Investigation of batch fluidized-bed drying by mathematical modeling, CFD simulation and ECT measurement. *AIChE Journal* 54 (2): 427-444.
- Wang, L and Singh, R. 2004. Finite element modeling and sensitivity analysis of double-sided contact-heating of initially frozen hamburger patty. *Transactions of the ASAE* 47 (1): 147.
- Wang, X, Zhang, G and Choi, CY. 2018. Effect of airflow speed and direction on convective heat transfer of standing and reclining cows. *Biosystems Engineering* 167 (3): 87-98.
- Yang, H, Sakai, N and Watanabe, M. 2001. Drying model with non-isotropic shrinkage deformation undergoing simultaneous heat and mass transfer. *Drying Technology* 19 (7): 1441-1460.
- Yunus, AC. 2019. *Heat and mass transfer: fundamentals and applications*. McGraw-Hill Education,

6. THERMODYNAMIC MODELLING OF THE HOT AIR DRYING AND INFRARED ASSISTED HOT AIR DRYING OF BEEF BILTONG

This chapter is based on the following manuscript.

Muga, F. C., Workneh, T. S., and Marenya, M. O. Thermodynamic modelling of the hot air drying and infrared assisted hot air drying of beef biltong. *Journal of Food and Bioprocess Technology*. Manuscript ID FABT-D-21-00404.

Abstract

The aim of this chapter was to formulate a thermodynamic model for evaluating and comparing the energy and exergy efficiency, drying efficiency, energy utilisation, and specific energy consumption during HAD and IRHAD of beef being processed into biltong. The mathematical model presented in this study uses the heat and mass transfer parameters to evaluate the indices of energy and exergy utilisation. Data collected from HAD and IRHAD experiments were used to verify the developed model and illustrate its applicability in modelling actual drying processes. The HAD experiments were conducted at drying air temperature of 30, 35, and 40 °C; and velocity of 1.5 and 2.5 m.s⁻¹. The IRHAD were conducted at infrared (IR) power level of 500, 750, and 1000 W; drying air temperature of 30, 35, and 40 °C; and velocity of 1.5 and 2.5 m.s⁻¹. The results indicated that increasing the drying air temperature increased the energy and exergy efficiency while decreasing the specific energy consumption during HAD. Contrarily, increasing the air velocity decreased the energy and exergy efficiency and increased the SEC. The power level of the IR emitter significantly affected the efficiencies of the IRHAD. Increasing the level of power of the IR emitter increased both the energy and exergy efficiency, whereas increase in the drying air temperature and velocity had a negative impact on the energy and exergy efficiency during IRHAD. The IRHAD had significantly higher energy and exergy efficiency compared to HAD. The mathematical model presented in this study is useful in identifying the optimal drying conditions for both HAD and IRHAD of beef during biltong processing. Moreover, the model can be applied in assessing the and exergy efficiency, drying efficiency, energy utilisation and specific energy consumption of existing drying processes.

Keywords: Biltong, energy, exergy, mathematical modelling, and specific energy consumption

Nomenclature

A	Surface area, m^2	Subscripts
c_p	Specific heat, $J.kg^{-1}.K^{-1}$	a Air
ex	Specific exergy, $J.kg^{-1}$	abs Absorbed energy
\dot{E}	Energy flow rate, W	b Beef
$\dot{E}x$	Exergy rate, W	c Carbohydrates
EU	Energy utilisation rate, W	des Destruction
F	Shape view factor	D Drying
h_{lv}	Latent heat of evaporation, $J.kg^{-1}$	ex Exergy
HAD	Hot air drying	ev Evaporation
IRHAD	Infrared assisted hot air drying	E Energy
L	Length of IR emitter, m	f Fats
\dot{m}	Mass flow rate, $kg.s^{-1}$	HAD Hot air drying
P_0	Rate of radiation heat transfer to the product, W	in Inlet
R_t	Total thermal resistivity, m^{-2}	IR Infrared
SEC	Specific energy consumption, $J.kg^{-1}$	$IRHAD$ Infrared assisted hot air drying
T	Temperature, K	out Outlet
W	Width of IR emitter, m	p Protein
y	Mass fraction	w Water
Z	Distance between the emitter and the surface of the sample, m	0 Reference

Greek letters

α	Overall IR absorption coefficient
β	Quality factor
ρ	Density, $kg.m^{-3}$
δ	IR penetration depth of beef, m
ε	Emissivity
σ	Stefan-Boltzmann constant ($W.m^{-2}.K^{-4}$),
η	Efficiency

6.1 Introduction

Hot air drying (HAD) is one of the most energy intensive drying methods and is associated with low quality of the dried agricultural products due to loss of colour, loss of heat sensitive nutrients, textural damage, and deformation (Ratti, 2001; Sharma and Prasad, 2001; Kowalski and Mierzwa, 2009). Contrarily, infrared (IR) and microwave heating when used singly or in combination with convective drying techniques, improves the energy efficiency and results in finished products with acceptable quality (Krishnamurthy *et al.*, 2008b; Aghbashlo, 2016). Muga *et al.* (2021) reported that the incorporation of IR radiation in the infrared assisted hot air drying (IRHAD) of biltong resulted in shorter drying time compared to the independent use of HAD. Thus, implying an improvement in the energy use efficiency during IRHAD compared to HAD.

Improving the energy use efficiency is critical in reducing the costs associated with the energy sources, thus boosting the economic sustainability of drying processes (Aghbashlo, 2016). A thermodynamic analysis is essential in evaluating the efficiency of energy utilisation (Golpour *et al.*, 2020). Analysis of the energy and exergy during drying processes is necessary in the design, analysis, and optimisation of drying systems (Liu *et al.*, 2019; Golpour *et al.*, 2020). According to Aghbashlo *et al.* (2008), evaluating the energy and exergy available at different points in the system informs the selection of optimal operating conditions and parameters that aid in the design of the drying systems.

A number of studies have analysed the energy and exergy during the drying of plant-based food products including; pistachio (Midilli and Kucuk, 2003), red pepper slices (Akpınar, 2004), banana slices (Mousa and Farid, 2002; Swasdisevi *et al.*, 2009), mulberry (Akbulut and Durmuş, 2010) carrots cubes (Nazghelichi *et al.*, 2010), mushroom slices (Reyes *et al.*, 2013; Şevik *et al.*, 2013; Liu *et al.*, 2019), and potatoes (Golpour *et al.*, 2020). Recent studies (Jones, 2017; Muga *et al.*, 2020) on the drying of beef into biltong are limited to the thin layer drying kinetics during HAD, IR drying (Cherono, 2014), IRHAD (Muga *et al.*, 2021), and the microbial quality of biltong (Naidoo and Lindsay, 2010c; Naidoo and Lindsay, 2010b; Petit *et al.*, 2014; Cherono *et al.*, 2016). However, there is no literature on the analysis of the energy and exergy usage during the drying of beef to produce biltong at different drying conditions. Evaluating the energy and exergy usage during the drying of beef for biltong production using HAD and IRHAD would

highlight the suitability of IRHAD as an alternative to HAD in biltong production. Therefore, the objective of this study was to formulate a thermodynamic model for evaluating and comparing the energy and exergy efficiency, drying efficiency, energy utilisation, and specific energy consumption during HAD and IRHAD of beef being processed into biltong.

6.2 Development of The Thermodynamic Model for The HAD and IRHAD of Beef Biltong

The drying chamber can be modelled as a control volume in which the wet product, the drying air, and the IR radiation are introduced. The energy and mass that exit the control volume are a stream of humidified air and the dried material (Dinçer and Zamfirescu, 2016). To facilitate the formulation of the model, the energy lost through the chamber walls is assumed to be minimal due to sufficient insulation of the drying chamber. Consequently, the energy and exergy losses in the drying system is attributed to the outgoing drying air. The exchange of energy and mass between the drying air, IR radiation and the product being dried is shown in Figure 6.1.

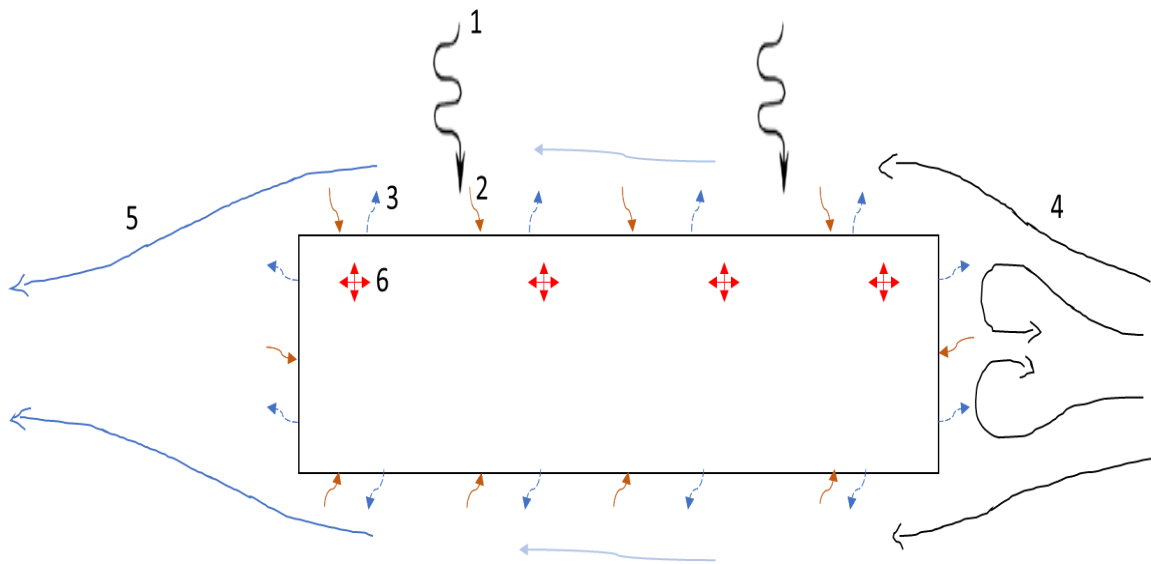


Figure 6.1 The exchange of energy and mass during IRHAD process; 1 – IR radiation, 2 – convective heat transfer from hot air to product, 3 - evaporation, 4 - incoming drying air, 5 - outgoing moist drying air, 6 – IR energy absorbed by the product

6.2.1 Energy analysis

From Figure 6.1, the sum of mass of the drying air and wet product at the inlet should be equal to the sum of the moist drying air and dried product at the outlet. Similarly, the sum of the IR energy and the energy of the drying air at inlet should be equal to the sum of energy of the drying air at the outlet and the energy gained by the dried product. Following the First Law of Thermodynamics, the general equation for the conservation of mass and energy is represented by Equation 6.1 and 6.2, respectively.

$$\sum \dot{m}_{in} = \sum \dot{m}_{out} \quad (6.1)$$

$$\sum \dot{E}_{in} = \sum \dot{E}_{out} \quad (6.2)$$

Where:

$$\dot{m}_{in} = \text{mass inflow rate (kg.s}^{-1}\text{),}$$

$$\dot{m}_{out} = \text{mass outflow rate (kg.s}^{-1}\text{),}$$

$$\dot{E}_{in} = \text{energy inflow rate (W), and}$$

$$\dot{E}_{out} = \text{energy outflow rate (W).}$$

The inflow and outflow velocity of the drying air are constant, hence, the mass balance equation for the drying air can be written as shown in Equation 6.3.

$$\dot{m}_{a,in} = \dot{m}_{a,out} = \dot{m}_a \quad (6.3)$$

Where:

$$\dot{m}_{a,in} = \text{mass flow rate of air at the inlet (kg.s}^{-1}\text{),}$$

$$\dot{m}_{a,out} = \text{mass flow rate of air at the outlet (kg.s}^{-1}\text{), and}$$

$$\dot{m}_a = \text{mass flow rate of air (kg.s}^{-1}\text{).}$$

The energy balance equation for the HAD process is represented by Equation 6.4, whereas the energy balance equation for the IRHAD processes is represented by Equation 6.5.

$$\dot{m}_{a,in}c_{p,a} \Delta T_{a,in} = \dot{m}_{a,out}c_{p,a} \Delta T_{a,out} + \dot{m}_b c_{p,b} \Delta T_b + \dot{m}_w h_{lv} \quad (6.4)$$

$$\dot{m}_{a,in}c_{p,a} \Delta T_{a,in} + \dot{E}_{IR,abs} = \dot{m}_{a,out}c_{p,a} \Delta T_{a,out} + \dot{m}_b c_{p,b} \Delta T_b + \dot{m}_w h_{lv} \quad (6.5)$$

Where:

$\Delta T_{a,in}$ = difference between ambient and dryer inlet air temperature (K),

$\Delta T_{a,out}$ = difference between the dryer inlet and outlet air temperature (K),

ΔT_b = change in the temperature of beef (K),

\dot{m}_b = mass of beef (kg),

\dot{m}_w = mass of water (kg),

$c_{p,b}$ = specific heat of beef ($J.kg^{-1}.K^{-1}$),

$c_{p,a}$ = specific heat of air ($J.kg^{-1}.K^{-1}$),

h_{lv} = latent heat of evaporation ($J.kg^{-1}$), and

$\dot{E}_{IR,abs}$ = rate of IR energy absorption (W).

The IR energy absorbed by the meat sample, $\dot{E}_{IR,abs}$, was calculated according to Lambert's Law, as shown in Equation 5.4 – 5.11 (§ 5.2.2).

The energy influx from the hot air, in the case of HAD, and both the hot air and IR radiation, in the case of IRHAD, is used to calculate the specific energy consumption (SEC) of the dryer. The SEC is calculated as the ratio of the total energy inflow to the mass of water removed as shown in Equations 6.6 and 6.7 for the HAD (SEC_{HAD}) and the IRHAD (SEC_{IRHAD}), respectively.

$$SEC_{HAD} = \frac{\dot{m}_{a,in}c_{p,a}T_{a,in}}{m_w} \quad (6.6)$$

$$SEC_{IRHAD} = \frac{\dot{m}_{a,in}c_{p,a}T_{a,in} + \dot{E}_{IR,abs}}{m_w} \quad (6.7)$$

The energy utilisation (EU) for both the HAD and the IRHAD is the sum of the energy needed to heat up the solid food matrix and the energy needed to evaporate the moisture from the beef (Equation 6.8).

$$EU = m_b c_{p,b} \Delta T_b + m_w h_{lv} \quad (6.8)$$

The energy efficiency (η_E) and the drying efficiency (η_D) for the HAD and IRHAD is determined using Equations 6.97, 6.10, 6.11, and 6.12 (Dinçer and Zamfirescu, 2016; Mondal *et al.*, 2020).

$$\eta_{E,HAD} = \frac{m_w h_{lv}}{\dot{m}_{a,in} c_{p,a} T_{a,in}} \quad (6.9)$$

$$\eta_{E,IRHAD} = \frac{m_w h_{lv}}{\dot{m}_{a,in} c_{p,a} T_{a,in} + Q_{IR}} \quad (6.10)$$

$$\eta_{D,HAD} = \frac{m_b c_{p,b} \Delta T_b + m_w h_{lv}}{\dot{m}_{a,in} c_{p,a} T_{a,in}} \quad (6.11)$$

$$\eta_{D,IRHAD} = \frac{m_b c_{p,b} \Delta T_b + m_w h_{lv}}{\dot{m}_{a,in} c_{p,a} T_{a,in} + Q_{IR}} \quad (6.12)$$

Where:

$\eta_{E,HAD}$ = energy efficiency for the HAD,

$\eta_{E,IRHAD}$ = energy efficiency for the IRHAD,

$\eta_{D,HAD}$ = drying efficiency for the HAD, and

$\eta_{D,IRHAD}$ = drying efficiency for the IRHAD.

6.2.2 Exergy analysis

The total exergy inflow, outflow and losses are determined according to the Second Law of Thermodynamics. The exergy balance equation for the HAD process and the IRHAD process is shown in Equation 6.13 and 6.14, respectively (Aghbashlo, 2016; Motevali *et al.*, 2018; Golpour *et al.*, 2020).

$$\frac{m_m(ex_{b,out} - ex_{b,in})}{\Delta t} = \dot{E}x_{a,in} - \dot{E}x_{a,out} + \dot{E}x_{ev} - \dot{E}x_{des} \quad (6.13)$$

$$\frac{m_m(ex_{b,out}-ex_{b,in})}{\Delta t} = \dot{E}x_{a,in} - \dot{E}x_{a,out} + \dot{E}x_{IR,abs} + \dot{E}x_{ev} - \dot{E}x_{des} \quad (6.14)$$

Where:

- $ex_{b,in}$ = specific exergy of beef at the inlet (J.kg⁻¹),
- $ex_{b,out}$ = specific exergy of beef at the outlet (J.kg⁻¹),
- $\dot{E}x_{a,in}$ = exergy rate of air at the inlet (W),
- $\dot{E}x_{a,out}$ = exergy rate of air at the outlet (W),
- $\dot{E}x_{IR,abs}$ = absorption rate of exergy from IR radiation (W),
- $\dot{E}x_{ev}$ = rate exergy due to evaporated water (W),
- $\dot{E}x_{loss}$ = rate of exergy lost (W), and
- $\dot{E}x_{des}$ = rate of exergy destruction (W).

The specific exergy of the beef sample and the drying air is determined from Equation 6.15 (Darvishi *et al.*, 2014), whereas, the exergy rate of air is determined from Equation 6.16 (Motevali *et al.*, 2018).

$$ex_b = c_{p,b} \left((T_m - T_0) - T_0 \ln \left(\frac{T_0}{T_b} \right) \right) \quad (6.15)$$

$$\dot{E}x_a = \dot{m}_a c_{p,a} \left((T_a - T_0) - T_0 \ln \left(\frac{T_0}{T_a} \right) \right) \quad (6.16)$$

Where:

T_0 = the reference temperature (K).

The absorption rate of exergy from IR radiation is calculated from the exergy flux of the IR emitter. The exergy flux of the IR emitter is determined using Equation 6.17 (Aghbashlo, 2016).

$$E x_{IR} = \sigma T_{IR}^4 \left(\varepsilon_{IR} + \frac{1}{3} \left(\frac{T_0}{T_{IR}} \right)^4 - \frac{4}{3} \varepsilon_{IR}^{0.75} \left(\frac{T_0}{T_{IR}} \right) \right) \quad (6.17)$$

Where:

$E_{x_{IR}}$ = IR exergy flux (W.m⁻²).

The exergy value of a system is related to its energy value by a quality factor obtained as a ratio of the exergy to the energy (Aghbashlo, 2016; Motevali *et al.*, 2018). The energy flux from the IR emitter (E_{IR}) is calculated using Equation 6.18.

$$E_{IR} = \varepsilon_{IR} \sigma T_{IR}^4 \quad (6.18)$$

From Equation 6.17 and 6.18, the quality factor, β , is expressed as shown in Equation 6.19. Subsequently, the rate of IR exergy absorbed by the meat sample can be calculated from the rate of IR energy absorbed by the meat sample (Equation 6.20).

$$\beta = 1 + \frac{1}{3 \varepsilon_{IR}} \left(\frac{T_0}{T_{IR}} \right)^4 - \frac{4 T_0}{3 \varepsilon_{IR}^{0.25} T_{IR}} \quad (6.19)$$

$$\dot{E}_{x_{IR,abs}} = \beta \dot{E}_{IR,abs} \quad (6.20)$$

The rate of exergy transfer due to evaporation is determine using Equation 6.21 (Icier *et al.*, 2010; Darvishi *et al.*, 2014).

$$\dot{E}_{x_{ev}} = \dot{m}_w h_{lv} \left(1 - \frac{T_0}{T_b} \right) \quad (6.21)$$

The exergy efficiency of HAD and IRHAD is then determined as shown in Equation 6.22 and 6.23, respectively (Dincer and Sahin, 2004; Icier *et al.*, 2010; Aghbashlo, 2016; Motevali *et al.*, 2018).

$$\eta_{Ex,HAD} = \frac{\dot{m}_w h_{lv} \left(1 - \frac{T_0}{T_b} \right)}{\dot{m}_a c_{p,a} \left((T_a - T_{0,a}) - T_{0,a} \ln \left(\frac{T_0}{T_a} \right) \right)} \quad (6.22)$$

$$\eta_{Ex,IRHAD} = \frac{\dot{m}_w h_{lv} \left(1 - \frac{T_0}{T_b}\right)}{\dot{m}_a c_{p,a} \left((T_a - T_{0,a}) - T_{0,a} \ln \left(\frac{T_0}{T_a} \right) \right) + \beta \dot{E}_{IR,abs}} \quad (6.23)$$

Where:

$\eta_{Ex,HAD}$ = exergy efficiency of HAD, and

$\eta_{Ex,IRHAD}$ = exergy efficiency of IRHAD.

6.2.3 Determination of the thermophysical properties of air and meat

The specific heat capacity air is dependent on the air temperature, whereas the specific heat capacity and density of meat is derived from its proximate composition. Therefore, the specific heat capacity of the drying air is calculated as a function of the drying air temperature (°C) as shown in Equation 6.24 (Mondal *et al.*, 2020).

$$C_{p,a} = 1.0029 + 5.4 \times 10^{-2} T_a \quad (6.24)$$

The density and heat capacity of meat is determined using Equations 5.26 and 5.27, respectively (§5.2.6).

6.2.4 Model Inputs

A summary of the input parameters required for the complete thermodynamic analysis of the energy and exergy performance of the HAD and the IRHAD processing of marinated beef into biltong is shown in Table 6.1.

Table 6.1 Model input parameters

Quantity	Symbol	Value	Reference
Density of water	ρ_w	1000 kg.m ⁻³	(Rao <i>et al.</i> , 2014)
Density of air	ρ_a	1.073 kg.m ⁻³	(Kumar <i>et al.</i> , 2015)
Specific heat of water	$c_{p,w}$	4170 J.kg ⁻¹ .K ⁻¹	(Rao <i>et al.</i> , 2014)
IR penetration depth of meat	δ	0.001 m	Current study
Emissivity of meat	ϵ_m	0.9	Current study
Emissivity of the IR emitter	ϵ_{IF}	0.9	(Elstein, 2014)
Stefan-Boltzmann constant	radiation σ	5.67 × 10 ⁻⁸ W.m ⁻² .K ⁻⁴	(Pan and Atungulu, 2010b)
Reference Temperature	T_0	22 °C	Current study
Latent heat of evaporation	h_{lv}	2.3 × 10 ⁶ J.kg ⁻¹	(Yunus, 2019)
Mass fraction of water	γ_w	0.75	(Tornberg, 2005)
Mass fraction of protein	γ_p	0.2	(Tornberg, 2005)
Mass fraction of carbohydrate	γ_c	0.02	(Tornberg, 2005)
Mass fraction of fat	γ_f	0.03	(Tornberg, 2005)
Density of protein	ρ_p	1320 kg.m ⁻³	(Rao <i>et al.</i> , 2014)
Density of carbohydrate	ρ_c	1600 kg.m ⁻³	(Rao <i>et al.</i> , 2014)
Density of fat	ρ_f	920 kg.m ⁻³	(Rao <i>et al.</i> , 2014)

6.3 Materials and Methods

6.3.1 Sample preparation

The samples were prepared as outlined in Muga *et al.* (2020).

6.3.2 The drying unit

A detailed description of the drying unit is given in Muga *et al.* (2021).

6.3.3 Drying experiments

The procedure for the HAD experiments is described in Muga *et al.* (2020), whereas the procedure for the IRHAD is described in Muga *et al.* (2021).

6.3.4 Thermodynamic model verification and data analysis

The mathematical expressions (Equations 6.1 – 6.24) that constitute the thermodynamic model were implemented in Microsoft Excel 2019 (Microsoft Corporation, Washington, USA). The thermodynamic model was used to calculate the SEC, EU, energy efficiency, exergy efficiency, and the drying efficiency from the data obtained from the HAD and the IRHAD experiments. The results obtained from the thermodynamic model were subjected to the analysis of variance (ANOVA) at 5 % level of significance. Where a significant ANOVA result was found, the mean separation was done using Fisher's Unprotected LSD method. All data analysis was done using GenStat® 18th Edition (VSN International Ltd, Hemel Hempstead, United Kingdom).

6.4 Results and Discussion

6.4.1 Energy Analysis

The values for the energy efficiency and the specific energy consumption, obtained during the HAD of marinated beef being processed into biltong, is presented in Figure 6.2. HAD of marinated beef showed energy efficiency of less than 10%. The low efficiency level is typical of the HAD of agricultural products (Motevali *et al.*, 2014; Golpour *et al.*, 2020). The highest HAD energy efficiency of 8.41 % was obtained at a drying air temperature of 40 °C and a drying air velocity of 1.5 m.s⁻¹, whereas the minimum of 4.79 % was obtained at drying air temperature of 30 °C and a drying air velocity of 2.5 m.s⁻¹. The HAD results (Figure 6.2) indicate that increasing the temperature of the drying air increased the energy efficiency. In contrast, increasing the velocity of the drying air decreased the energy efficiency of the HAD of marinated beef.

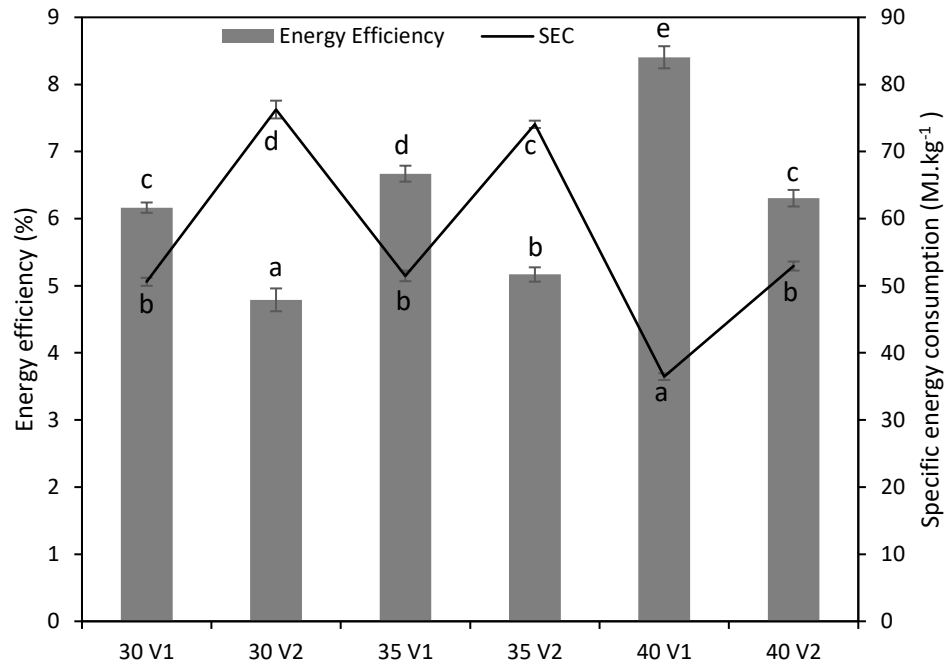


Figure 6.2 Energy efficiency and specific energy consumption at the selected HAD conditions (V1 = 1.5 m.s⁻¹ and V2 = 2.5 m.s⁻¹). Means with the same letter are not significantly different according to Fisher's unprotected least significant difference test ($p < 0.05$)

The specific energy consumption decreased with increasing temperature of the drying air. Contrarily, increasing the velocity of the drying air increased the specific energy consumption. The highest specific energy consumption of 76.26 MJ.kg⁻¹ was obtained at 30 °C and a drying air velocity of 2.5 m.s⁻¹, while, the lowest specific energy consumption of 36.46 MJ.kg⁻¹ was obtain at 40 °C and a drying air velocity of 1.5 m.s⁻¹. The range of values obtained for the energy efficiency and specific energy consumption in this study agree with those report by Motevali *et al.* (2014) during the HAD of chamomile plant.

The temperature and velocity of the drying air significantly ($p \leq 0.05$) affected the energy efficiency and the specific energy consumption during the HAD of marinated beef. Increasing the temperature of the drying air increases the heat and mass transfer coefficient (Feyissa *et al.*, 2013). Consequently, shorter drying times are obtained at these drying conditions which translates into lower specific energy consumption, thus higher energy efficiency.

The values of the heat and mass transfer coefficients calculated from a lumped parameter analysis is summarised in Table 6.2. The heat and mass transfer coefficients increase with increasing velocity of the drying air. However, lower energy efficiencies and higher specific energy consumption were obtained with increasing velocity of the drying air. This phenomenon is attributed to the sharp increase in the energy content of the drying air with increasing drying air velocity (Table 6.2). Increasing the velocity of the drying air increased the mass flow rate of air that resulted in a higher heat content. The increase in the heat and mass transfer coefficient at higher velocities of the drying air is insufficient to produce a commensurate drying rate to reduce the specific energy consumption. Previous studies by Catton *et al.* (2011), Sami *et al.* (2011), and Golpour *et al.* (2020) reported a similar trend where increasing the velocity of the drying air decreased the energy efficiency while increasing the specific energy consumption during HAD of agricultural products.

Table 6.2 Heat and mass transfer coefficient and energy content of drying air at selected drying conditions during HAD

Drying air temperature (°C)	Drying air velocity (m.s ⁻¹)	Heat transfer coefficient (W.m ⁻² .K ⁻¹)	Mass transfer coefficient (m.s ⁻¹)	Energy content of air at inlet (W)
30	1.5	5.19±0.10 ^a	0.0053±0.0001 ^a	14.56±1.08 ^a
35	1.5	8.08±0.25 ^c	0.0082±0.0002 ^c	26.69±0.79 ^c
40	1.5	9.81±0.28 ^d	0.0100±0.0009 ^d	38.82±1.13 ^d
30	2.5	6.93±0.21 ^b	0.0070±0.0001 ^b	24.26±0.64 ^b
35	2.5	10.97±0.37 ^e	0.0111±0.0003 ^d	44.48±1.48 ^e
40	2.5	13.85±0.57 ^f	0.0141±0.0002 ^e	64.70±1.29 ^f

Means within a column followed by the same letter are not significantly different according to Fisher's unprotected least significant difference test ($p < 0.05$).

A summary of the IR emitter temperature, IR intensity and the IR energy absorbed by the marinated beef sample is given in Table 6.3. The IR energy absorbed by the meat varied significantly ($p \leq 0.05$) with the power level of the IR emitter. The maximum amount of IR energy absorption of 24.00 ± 0.08 W, occurred at an IR emitter power level of 1000 W, 30 °C,

and a drying air velocity of 1.5 m.s^{-1} , whereas the minimum IR energy absorption of 3.20 ± 0.04 W occurred at an IR emitter power level of 500 W, 40°C , and a drying air velocity of 2.5 m.s^{-1} . The velocity of the drying air also had a significant ($p \leq 0.05$) influence on the IR energy absorbed by the marinated beef sample, whereas the temperature of the drying air had no significant ($p \geq 0.05$) influence on the IR energy absorption.

Table 6.3 Temperature of the IR emitter, IR intensity and the IR energy absorbed by the marinated meat sample during IRHAD at selected drying conditions

Emitter Power level (W)	Drying air temperature ($^\circ\text{C}$)	Drying air velocity (m.s^{-1})	IR emitter temperature	IR Intensity (W.m^{-2})	IR Energy (W) Absorbed
500	30	1.5	233.10 ± 2.61^c	509.15 ± 2.91^b	3.82 ± 0.02^b
500	35	1.5	232.19 ± 3.10^{bc}	507.27 ± 4.33^b	3.80 ± 0.02^b
500	40	1.5	237.59 ± 2.05^c	504.85 ± 4.80^b	3.79 ± 0.04^b
500	30	2.5	220.63 ± 1.46^a	431.26 ± 2.50^a	3.23 ± 0.02^a
500	35	2.5	219.03 ± 2.62^a	429.63 ± 3.67^a	3.22 ± 0.03^a
500	40	2.5	222.80 ± 2.62^{ab}	426.81 ± 4.75^a	3.20 ± 0.04^a
750	30	1.5	396.16 ± 5.39^g	1470.07 ± 5.17^d	11.03 ± 0.04^d
750	35	1.5	407.60 ± 5.23^h	1463.23 ± 6.95^d	10.97 ± 0.05^d
750	40	1.5	426.42 ± 6.09^i	1461.71 ± 7.98^d	10.96 ± 0.06^d
750	30	2.5	346.65 ± 9.85^d	1076.28 ± 3.77^c	8.07 ± 0.03^c
750	35	2.5	361.69 ± 9.12^e	1070.15 ± 6.10^c	8.03 ± 0.05^c
750	40	2.5	374.10 ± 12.17^f	1066.65 ± 6.01^c	8.00 ± 0.05^c
1000	30	1.5	543.30 ± 8.73^k	3200.54 ± 11.10^f	24.00 ± 0.08^f
1000	35	1.5	548.21 ± 7.36^k	3199.89 ± 10.92^f	24.00 ± 0.08^f
1000	40	1.5	566.51 ± 3.60^l	3196.97 ± 10.36^f	23.98 ± 0.08^f
1000	30	2.5	523.98 ± 4.47^j	2791.57 ± 7.42^e	20.94 ± 0.06^e
1000	35	2.5	524.49 ± 5.32^j	2791.27 ± 7.39^e	20.93 ± 0.06^e
1000	40	2.5	527.21 ± 6.17^j	2786.42 ± 8.94^e	20.90 ± 0.07^e

Means within a column followed by the same letter are not significantly different according to Fisher's unprotected least significant difference test ($p < 0.05$).

The increasing in the power level of the IR emitter increased the IR emitter temperature which increased the IR intensity on the surface of the marinated beef sample. The increased IR intensity increased the amount of IR energy absorbed by the meat sample (Pan *et al.*, 2014). Conversely, increasing the velocity of the drying air induced a cooling effect on the IR emitter. The cooling effect on the IR emitter lowered its temperature resulting in reduced IR intensity on the surface of the meat sample, hence the reduced IR energy absorption by the meat sample (Table 6.3).

The levels of energy efficiency during IRHAD is shown in Figure 6.3. The highest efficiency (25.21 %) was obtained at an IR emitter power level of 1000 W, 30 °C, and a drying air velocity of 1.5 m.s⁻¹. The lowest efficiency (7.14 %) was obtained at an IR emitter power level of 500 W, 40 °C, and a drying air velocity of 2.5 m.s⁻¹. The energy efficiency increased with increasing levels of IR emitter power and decrease with increasing velocity of the drying air. However, increasing the drying air temperature decreased the energy efficiency during IRHAD which contrasts the HAD findings.

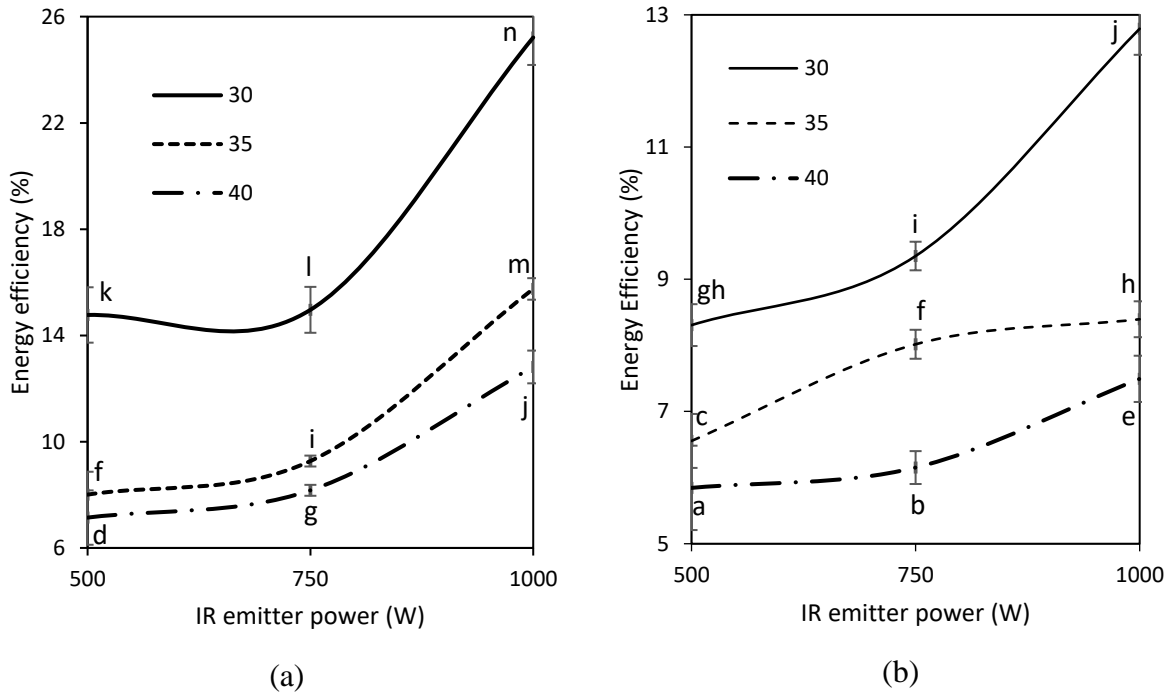


Figure 6.3 Variations in the energy efficiency of IRHAD with IR emitter power level and drying air temperature at (a) 1.5 m.s⁻¹ and (b) 2.5 m.s⁻¹. Means with the same letter are not significantly different according to Fisher's unprotected LSD test ($p < 0.05$)

A summary of the specific energy consumption values at different IRHAD conditions is presented in Table 6.4. The maximum (66.29 MJ.kg⁻¹) and minimum (11.94 MJ.kg⁻¹) specific energy consumption, corresponded to the lowest and highest energy efficiency, respectively. The specific energy consumption decreased with increasing power levels of the IR emitter and increased with increasing temperature and velocity of the drying air. Studies by Darvishi *et al.* (2014), Motevali *et al.* (2014), Surendhar *et al.* (2019), and Golpour *et al.* (2020) reported similar findings.

Table 6.4 Specific energy consumption at the selected IRHAD conditions

Drying temperature (°C)	air velocity (m.s ⁻¹)	Specific Energy Consumption (MJ.kg ⁻¹)		
		1000 W	750 W	500 W
30	1.5	11.94±0.57 ^b	20.03±0.67 ^c	21.74±0.54 ^d
35	1.5	10.08±0.50 ^a	24.29±0.58 ^e	39.81±0.50 ^h
40	1.5	24.29±0.31 ^e	38.32±0.49 ^h	43.49±0.79 ^j
30	2.5	33.73±0.38 ^f	34.30±0.39 ^f	36.92±0.38 ^g
35	2.5	42.47±0.55 ⁱ	42.47±0.64 ⁱ	47.32±0.49 ^l
40	2.5	45.90±0.72 ^k	49.68±0.76 ^m	66.28±0.77 ⁿ

Means within a column followed by the same letter are not significantly different according to Fisher's unprotected LSD test ($p < 0.05$). ANOVA results contained in Appendix B.

The power level of the IR emitter significantly ($p \leq 0.05$) affected the energy efficiency and the specific energy consumption due to its influence on the IR intensity and the energy absorbed by the meat sample. Increasing the power level of the IR emitter increased the IR energy absorbed by the marinated beef sample, thus increasing the magnitude of energy expended in moisture evaporation. Consequently, the water vapour pressure and moisture diffusion inside the meat and on the surface increased (Aghbashlo, 2016). Hence, the observed increase in energy efficiency during IRHAD.

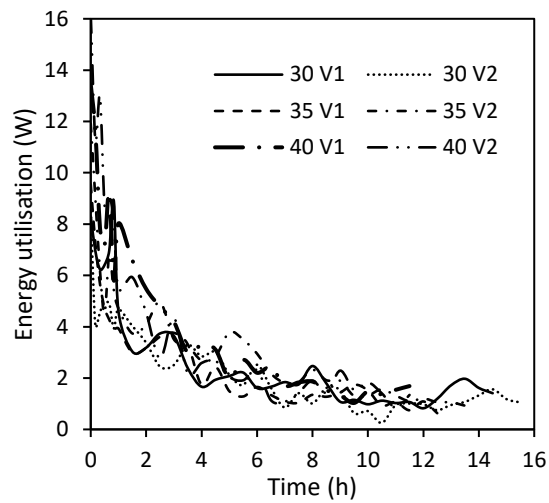
Both the drying air temperature and the drying air velocity significantly ($p \leq 0.05$) influenced the energy efficiency and the specific energy consumption during IRHAD. Increasing the temperature of the drying air inversely affected the energy efficiency and increased the specific energy consumption during IRHAD. This observation contradicts the observation made during

HAD. Contrary observations were also made by Golpour *et al.* (2020) and Motevali *et al.* (2018) who reported an increase in energy efficiency and a decrease in specific energy consumption with increasing drying air temperature during HAD and hybrid infrared hot air drying, respectively. Nonetheless, since the energy and exergy variations for a particular dryer exhibit a similar trend, the results from this study can be correlated to those reported by Aghbashlo (2016) which showed that the exergy efficiency decreased with increasing drying air temperature during a combined infrared-convective drying process. The decrease in the energy efficiency with increasing drying air temperature may be attributed to the predominant influence of the IR radiation on the drying process of marinated beef during IRHAD as reported by Muga *et al.* (2021). According to Cheronno (2014), the effective interaction between the IR radiation and meat during IR drying generates sufficient volumetric heat to promote rapid water transport out of the meat. It can be inferred that, at a given power level of the IR emitter and drying air velocity, increasing the drying air temperature does not appreciably increase the temperature of the meat sample. Therefore, a major portion of the increased heat energy of the drying air is lost in the exhaust air without useful application in moisture removal. Hence, the low energy efficiency at higher temperatures of the drying air.

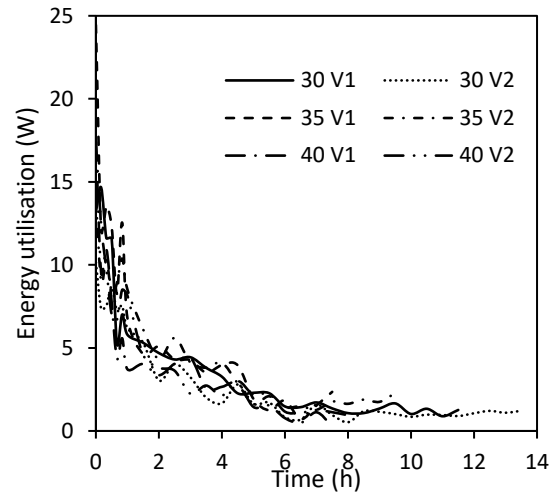
Increasing the velocity of the drying air negatively affected the energy efficiency and increased the specific energy consumption during IRHAD, just like in HAD. Similar to the drying air temperature, increasing the velocity increases the heat energy of the of the drying air, most of which is lost to in the exhaust air, thus lowering the energy efficiency of the drying process. Furthermore, according to Muga *et al.* (2021), increasing the velocity of the drying air induces a cooling effect on the IR emitter, besides increasing the evaporative cooling on the surface of the meat. The cooling effect on the IR emitter combined with the evaporative cooling on the surface of the meat, lowers the heat influx into the meat, subsequently diminishing the energy efficiency.

The energy utilisation varies during the drying process as shown in Figure 6.4 (a, b, and c). The energy utilisation is highest during the onset of drying which coincides with the periods of maximum drying rate. The energy utilisation falls sharply after the initial period, as the drying front recedes into the meat sample. A significant portion of the energy supplied during drying is used to evaporate the moisture from the product with a small portion used to heat up the solid food matrix (Golpour *et al.*, 2020). Consequently, the energy utilisation curve follows an

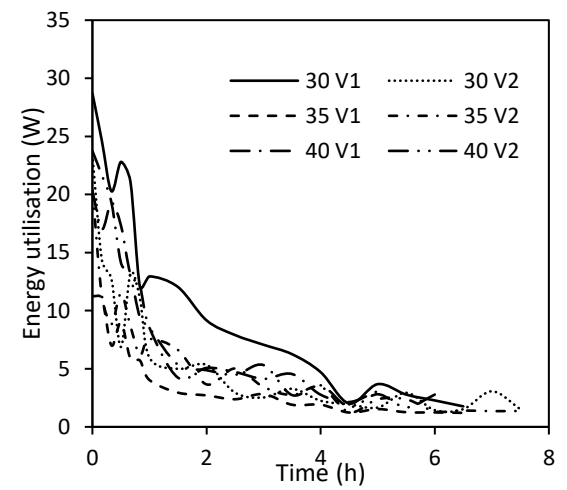
exponential decay that is typical of a diffusion controlled drying process of biltong (Muga *et al.*, 2020). However, the energy supplied by the hot air and the IR emitter is constant. This results in the sharp decrease in the energy efficiency as the moisture content of the meat decreases over time (Figure 6.4 (d), (e), and (f)). Thus, there is need for a modulated supply of energy for drying that would reduce the energy input for both the drying air and the IR emitter with time to improve the efficiency of the drying process.



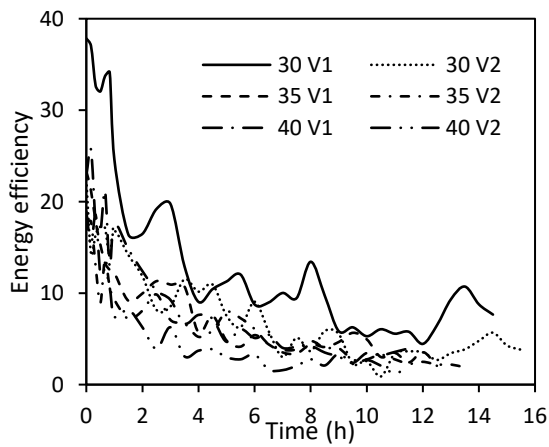
(a)



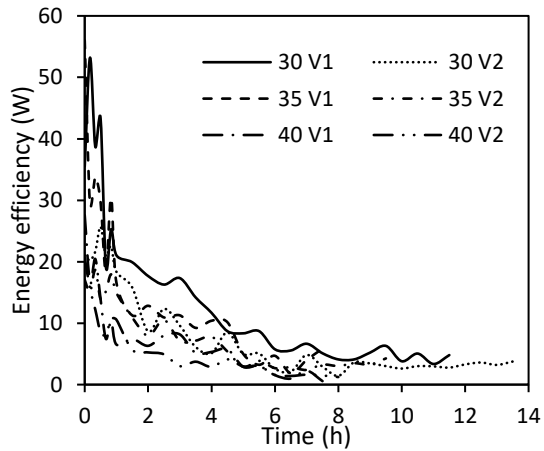
(b)



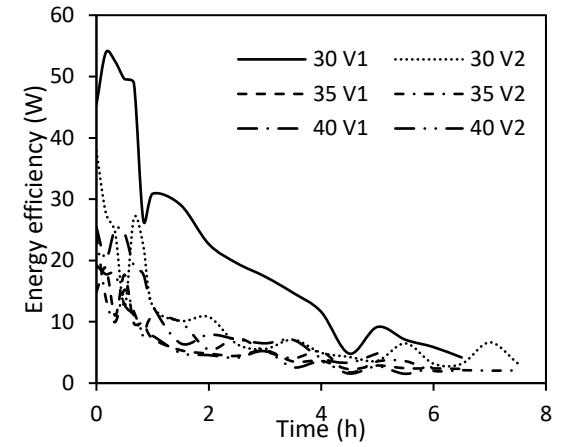
(c)



(d)



(e)



(f)

Figure 6.4 Variations in energy utilisation and energy efficiency over time during IRHAD at 500 W (a, d), 750 W (b, e), and 1000 W (c, f)

The addition of the IR significantly increased the energy efficiency over that reported during HAD. The highest improvement in energy efficiency was observed at the IR emitter power level of 1000 W, with a maximum of 309.06 % recorded at 30 °C and 1.5 m.s⁻¹. The lowest increase in energy efficiency was 5.26 % for IR power level of 500 W, drying air temperature of 40 °C and velocity of 2.5 m.s⁻¹ (Table 6.5).

Table 6.5 Improvement in energy efficiency during IRHAD over energy efficiency during HAD

Drying temperature (°C)	air velocity (m.s ⁻¹)	Improvement in energy efficiency (%)		
		500 W	750 W	1000 W
30	1.5	139.61	142.74	309.06
35	1.5	20.05	38.98	136.13
40	1.5	14.37	17.68	52.44
30	2.5	73.42	95.24	167.02
35	2.5	26.83	55.12	62.45
40	2.5	5.26	7.87	18.87

The values obtained for the drying efficiency (η_D) were in proximity with those of the energy efficiency (η_E) as shown in Table 6.6. As previously mentioned, most of the energy supplied during drying is used to evaporate the moisture from the product with a small portion used to heat up the solid food matrix. Therefore, the drying efficiency is higher than the energy efficiency because of the additional energy that is used to heat up the solid food matrix. These observations are similar to the results reported by Vieira *et al.* (2007), Charoenvai *et al.* (2013), and Motevali *et al.* (2014).

Table 6.6 Comparison between the energy and drying efficiency at selected IRHAD conditions

Drying temperature (°C)	air velocity (m.s ⁻¹)	Efficiency (%)							
		1000 W		750 W		500 W		HA	
		η_E	η_D	η_E	η_D	η_E	η_D	η_E	η_D
30	1.5	25.21	29.07	14.96	16.37	14.77	15.76	6.16	6.52
35	1.5	15.75	17.16	9.27	9.91	8.01	8.92	6.67	7.12
40	1.5	12.81	14.67	8.17	8.74	7.14	8.21	8.41	8.80
30	2.5	12.79	13.60	9.35	9.35	8.31	8.47	4.79	5.10
35	2.5	8.40	9.20	8.02	8.47	6.55	6.99	5.17	5.49
40	2.5	7.49	9.20	6.15	6.68	5.84	6.28	6.30	6.58

6.4.2 Exergy Analysis

The exergy efficiency followed a similar trend as the energy efficiency. The exergy efficiency of the HAD was significantly ($p \leq 0.05$) affected by the temperature and velocity of the drying air (Figure 6.5). The highest exergy efficiency of 3.78 % was observed at a drying air temperature and velocity of 40 °C and 1.5 m.s⁻¹. The lowest exergy efficiency of 1.70 % was observed at a drying air temperature and velocity of 30 °C and 2.5 m.s⁻¹. The exergy efficiency increased with increasing drying air temperature and decreased with increasing velocity of the drying air. This observation is attributed to the effect of the drying air temperature and velocity on available energy as discussed previously under the energy efficiency of HAD. These results are similar to the findings of Devani and Yelamarthi (2019) and Lingayat *et al.* (2020).

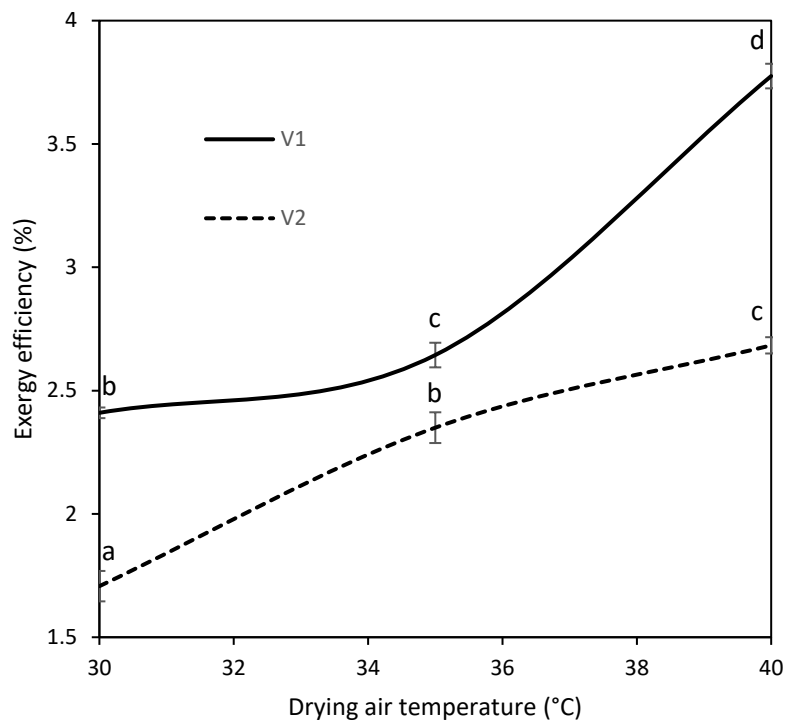


Figure 6.5 Variation in exergy efficiency with the drying air temperature and velocity during HAD ($V1 = 1.5 \text{ m.s}^{-1}$ and $V2 = 2.5 \text{ m.s}^{-1}$). Means with the same letter are not significantly different according to Fisher's unprotected LSD test ($p < 0.05$)

The exergy efficiency during IRHAD was significantly ($p \leq 0.05$) influenced by the power level of the IR emitter, the temperature and velocity of the drying air (Figure 6.6). The highest exergy efficiency (79.94 %) and lowest (4.59 %) were observed at 1000 W, 30 °C and 15 m.s⁻¹; and 500 W, 35 °C, and 2.5 m.s⁻¹, respectively. The exergy efficiency increased with increasing power level of the IR emitter owing to the increased IR energy absorbed by the meat sample. Increasing the temperature and velocity of the drying air decreased the energy efficiency because a significant portion of the energy supplied by the drying air at the higher levels of temperature and velocity is lost in the exhaust air. These findings are consistent with those reported by Aghbashlo (2016) and Motevali *et al.* (2018)

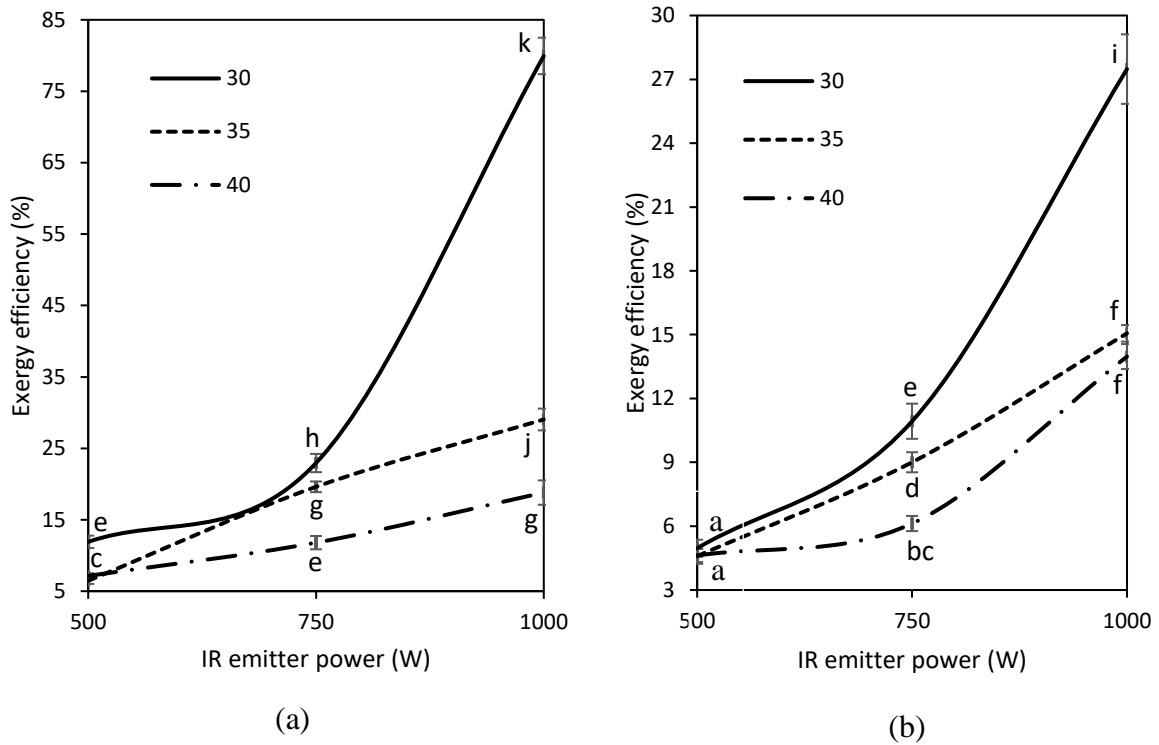


Figure 6.6 Variations in the exergy efficiency of IRHAD with IR emitter power level and drying air temperature at (a) 1.5 m.s⁻¹ and (b) 2.5 m.s⁻¹. Means with the same letter are not significantly different according to Fisher's unprotected LSD test ($p < 0.05$)

6.5 Conclusion

The developed thermodynamic model indicates that the energy and exergy efficiency of HAD increases with increasing drying air temperature but decreases with increasing drying air velocity. The HAD energy efficiency at the drying air velocity of 1.5 m.s⁻¹ increased from 6.16 % at 30 °C to 8.4 % at 40 °C which is a 36.6 % improvement in energy efficiency. The specific energy consumption dropped from 50.588 MJ.kg⁻¹ at 30 °C to 36.46 MJ.kg⁻¹ at 40 °C which is a 28 % decrease in energy consumption. The thermodynamic analysis indicate that a drying air temperature of 40 °C and a drying air velocity of 1.5 m.s⁻¹ offer the optimal energy utilisation for the tested HAD conditions. The results from the IRHAD treatments indicate that the IR radiation dominates the energy and exergy efficiency during IRHAD. Increasing the power level of the IR emitter increases the energy and exergy efficiency, whereas increasing the drying air temperature and velocity inversely affects the energy and exergy efficiency. The energy efficiency at a drying temperature of 30 °C increased from 14.77 % recorded at IR emitter power of 500 W to 25.21 %

at 1000 W which is a 71 % increase in energy efficiency. Increasing the drying air temperature from 30 to 40 °C at an IR emitter power of 1000 W reduced the energy efficiency from 25.21 to 12.81 % which is a 49 % decrease in energy efficiency. The thermodynamic analysis of the IRHAD of beef for biltong processing indicate that optimal energy utilisation is achieved at IR emitter power of 1000 W combined with a drying air temperature and velocity of 30 °C and 1.5 m.s⁻¹, respectively. The energy and exergy efficiency is greater in IRHAD than HAD. Consequently, IRHAD requires less specific energy consumption than HAD. Whereas the increase in temperature of the drying air increases the energy and exergy efficiency and reduces the specific energy consumption during HAD, the opposite is true for IRHAD. In both HAD and IRHAD, increasing the drying air velocity inversely affects the energy and exergy efficiency and directly influences the specific energy consumption. The mathematical model presented in this study can be applied to identify the optimum drying conditions for both HAD and IRHAD of marinated beef during biltong processing. Furthermore, the model can be used to assess the energy and exergy efficiency, drying efficiency, energy utilisation, and specific energy consumption of existing drying processes.

6.6 References

- Aghbashlo, M. 2016. Exergetic simulation of a combined infrared-convective drying process. *Heat and Mass Transfer* 52 (4): 829-844.
- Aghbashlo, M, Kianmehr, MH and Arabhosseini, A. 2008. Energy and exergy analyses of thin-layer drying of potato slices in a semi-industrial continuous band dryer. *Drying Technology* 26 (12): 1501-1508.
- Akbulut, A and Durmuş, A. 2010. Energy and exergy analyses of thin layer drying of mulberry in a forced solar dryer. *Energy* 35 (4): 1754-1763.
- Akpınar, EK. 2004. Energy and exergy analyses of drying of red pepper slices in a convective type dryer. *International Communications in Heat and Mass Transfer* 31 (8): 1165-1176.
- AOAC. 2012. *Official Methods of Analysis of AOAC International*. Association of Official Analysis Chemists International, Gaithersburg, USA.
- Catton, W, Carrington, G and Sun, Z. 2011. Exergy analysis of an isothermal heat pump dryer. *Energy* 36 (8): 4616-4624.

- Cengel, YA, Klein, S and Beckman, W. 1998. *Radiation heat transfer*. In: ed. Cengel, YA, Heat transfer: a practical approach. WBC McGraw-Hill, Boston, USA.
- Charoenvai, SC, Yingyuen, W, Jewyee, A, Rattanadecho, P and Vongpradubchai, S. 2013. Analysis of Energy Consumption in a Drying Process of Particleboard Using a Combined Multi-Feed Microwave-Convective Air and Continuous Belt System (CMCB). *Science & Technology Asia* 25 (3): 1-15.
- Cherono, K. 2014. Infrared Drying of Biltong. Unpublished MSc thesis, Bioresources Engineering, University of KwaZulu-Natal, Pietermaritzburg, South Africa.
- Cherono, K, Mwithiga, G and Schmidt, S. 2016. Infrared drying as a potential alternative to convective drying for biltong production. *Italian journal of food safety* 5 (3): 140-145.
- Darvishi, H, Zarein, M, Minaei, S and Khafajeh, H. 2014. Exergy and energy analysis, drying kinetics and mathematical modeling of white mulberry drying process. *International Journal of Food Engineering* 10 (2): 269-280.
- Devani, Y and Yelamarthi, PS. 2019. Energetic and exergetic analyses of Barnyard millet drying using continuous multistage fluidized bed dryer. *Journal of Food Process Engineering* 42 (7): e13247.
- Dincer, I and Sahin, A. 2004. A new model for thermodynamic analysis of a drying process. *International Journal of Heat and Mass Transfer* 47 (4): 645-652.
- Dinçer, İ and Zamfirescu, C. 2016. *Drying phenomena: theory and applications*. John Wiley & Sons,
- Dzimba, FEJ, Faria, J and Walter, EHM. 2007. Testing the sensory acceptability of biltong formulated with different spices. *African Journal of Agricultural Research* 2 (11): 547-577.
- Elstein. 2014. Ceramic infrared emitters. [Internet]. Elstein-Werk M. Steinmetz GmbH & Co. Available from: http://www.elstein.com/fileadmin/user_upload/PDFs/INT/Katalog/Catalogue_EN.pdf. [Accessed: 18 March 2020].
- Feyissa, AH, Gernaey, KV and Adler-Nissen, J. 2013. 3D modelling of coupled mass and heat transfer of a convection-oven roasting process. *Meat science* 93 (4): 810-820.
- Golpour, I, Kaveh, M, Chayjan, RA and Guiné, RP. 2020. Energetic and exergetic analysis of a convective drier: A case study of potato drying process. *Open Agriculture* 5 (1): 563-572.

- Icier, F, Colak, N, Erbay, Z, Kuzgunkaya, EH and Hepbasli, A. 2010. A comparative study on exergetic performance assessment for drying of broccoli florets in three different drying systems. *Drying Technology* 28 (2): 193-204.
- Jaturonglumert, S and Kiatsiriroat, T. 2010. Heat and mass transfer in combined convective and far-infrared drying of fruit leather. *Journal of Food Engineering* 100 (2): 254-260.
- Jones, M. 2017. Profiling of traditional South African biltong in terms of processing, physicochemical properties and microbial stability during storage. Unpublished PhD thesis, Food Science, Stellenbosch University, Stellenbosch, South Africa.
- Jones, M, Arnaud, E, Gouws, P and Hoffman, LC. 2017. Processing of South African biltong—A review. *South African Journal of Animal Science* 47 (6): 743-757.
- Kowalski, SJ and Mierzwa, D. 2009. Convective drying in combination with microwave and IR drying for biological materials. *Drying Technology* 27 (12): 1292-1301.
- Krishnamurthy, K, Khurana, HK, Soojin, J, Irudayaraj, J and Demirci, A. 2008. Infrared heating in food processing: an overview. *Comprehensive reviews in food science and food safety* 7 (1): 2-13.
- Kumar, C, Millar, GJ and Karim, M. 2015. Effective diffusivity and evaporative cooling in convective drying of food material. *Drying Technology* 33 (2): 227-237.
- Lingayat, A, Chandramohan, V and Raju, V. 2020. Energy and exergy analysis on drying of banana using indirect type natural convection solar dryer. *Heat Transfer Engineering* 41 (6-7): 551-561.
- Liu, Z-L, Bai, J-W, Wang, S-X, Meng, J-S, Wang, H, Yu, X-L, Gao, Z-J and Xiao, H-W. 2019. Prediction of energy and exergy of mushroom slices drying in hot air impingement dryer by artificial neural network. *Drying Technology* 72 (2): 1-12.
- Midilli, A and Kucuk, H. 2003. Energy and exergy analyses of solar drying process of pistachio. *Energy* 28 (6): 539-556.
- Mondal, MHT, Hossain, MA, Sheikh, MAM, Akhtaruzzaman, M and Sarker, MSH. 2020. Energetic and exergetic investigation of a mixed flow dryer: A case study of maize grain drying. *Drying Technology* 74 (1): 1-15.
- Motevali, A, Jafari, H and Hashemi, JS. 2018. Effect of IR intensity and air temperature on exergy and energy at hybrid infrared-hot air dryer. *Chemical Industry and Chemical Engineering Quarterly* 24 (1): 31-42.

- Motevali, A, Minaei, S, Banakar, A, Ghobadian, B and Khoshtaghaza, MH. 2014. Comparison of energy parameters in various dryers. *Energy Conversion and Management* 87 711-725.
- Mousa, N and Farid, M. 2002. Microwave vacuum drying of banana slices. *Drying Technology* 20 (10): 2055-2066.
- Muga, F, Workneh, T and Marennya, M. 2020. Modelling the Thin-Layer Drying of Beef Biltong Processed Using Hot Air Drying. *Journal of Biosystems Engineering* 45 (1): 1-12.
- Muga, FC, Marennya, MO and Workneh, TS. 2021. Modelling the Thin-Layer Drying Kinetics of Marinated Beef during Infrared-Assisted Hot Air Processing of Biltong. *International Journal of Food Science* 2021 (2021): 1-15.
- Naidoo, K and Lindsay, D. 2010a. Potential cross-contamination of the ready-to-eat dried meat product, biltong. *British Food Journal* 112 (4): 350-363.
- Naidoo, K and Lindsay, D. 2010b. Survival of *Listeria monocytogenes*, and enterotoxin-producing *Staphylococcus aureus* and *Staphylococcus pasteurii*, during two types of biltong-manufacturing processes. *Food Control* 21 (7): 1042-1050.
- Nazghelichi, T, Kianmehr, MH and Aghbashlo, M. 2010. Thermodynamic analysis of fluidized bed drying of carrot cubes. *Energy* 35 (12): 4679-4684.
- Onwude, DI, Hashim, N, Abdan, K, Janius, R, Chen, G and Kumar, C. 2018. Modelling of coupled heat and mass transfer for combined infrared and hot-air drying of sweet potato. *Journal of Food Engineering* 228 (2019) 12-24.
- Pan, Z, Atungulu, G and Li, X. 2014. *Infrared heating*. In: ed. Sun, D-W, Emerging technologies for food processing. Elsevier.
- Pan, Z and Atungulu, GG. 2010. *Infrared heating for food and agricultural processing*. CRC Press,
- Pan, Z and Atungulu, GG. 2011. *Combined infrared heating and freeze-drying*. In: eds. Pan, Z and Atungulu, GG, Infrared heating for food and agricultural processing. CRC Press, Nwey York.
- Petit, T, Caro, Y, Petit, A-S, Santchurn, SJ and Collignan, A. 2014. Physicochemical and microbiological characteristics of biltong, a traditional salted dried meat of South Africa. *Meat science* 96 (3): 1313-1317.
- Rao, MA, Rizvi, SS, Datta, AK and Ahmed, J. 2014. *Engineering properties of foods*. CRC press,
- Ratti, C. 2001. Hot air and freeze-drying of high-value foods: a review. *Journal of food engineering* 49 (4): 311-319.

- Reyes, A, Mahn, A, Cubillos, F and Huenulaf, P. 2013. Mushroom dehydration in a hybrid-solar dryer. *Energy conversion and management* 70 31-39.
- Sami, S, Etesami, N and Rahimi, A. 2011. Energy and exergy analysis of an indirect solar cabinet dryer based on mathematical modeling results. *Energy* 36 (5): 2847-2855.
- Şevik, S, Aktaş, M, Doğan, H and Koçak, S. 2013. Mushroom drying with solar assisted heat pump system. *Energy Conversion and Management* 72 171-178.
- Sharma, G and Prasad, S. 2001. Drying of garlic (*Allium sativum*) cloves by microwave–hot air combination. *Journal of Food Engineering* 50 (2): 99-105.
- Strydom, P and Zondag, B. 2014. Biltong: A major South African ethnic meat product. In: eds. Dikeman, M and Devine, C, *Encyclopaedia of meat sciences*. Academic Press, London, UK.
- Surendhar, A, Sivasubramanian, V, Vidhyeswari, D and Deepanraj, B. 2019. Energy and exergy analysis, drying kinetics, modeling and quality parameters of microwave-dried turmeric slices. *Journal of Thermal Analysis and Calorimetry* 136 (1): 185-197.
- Swasdisevi, T, Devahastin, S, Sa-Adchom, P and Soponronnarit, S. 2009. Mathematical modeling of combined far-infrared and vacuum drying banana slice. *Journal of Food Engineering* 92 (1): 100-106.
- Tanaka, F and Uchino, T. 2011. *Heat and Mass Transfer Modeling of Infrared Radiation for Heating*. In: eds. Pan, Z and Atungulu, G, *Infrared Heating for Food and Agricultural Processing*. CRC Press, New York.
- Tornberg, E. 2005. Effects of heat on meat proteins–Implications on structure and quality of meat products. *Meat science* 70 (3): 493-508.
- Vieira, M, Estrella, L and Rocha, S. 2007. Energy efficiency and drying kinetics of recycled paper pulp. *Drying Technology* 25 (10): 1639-1648.
- von Gersdorff, GJ, Porley, VE, Retz, SK, Hensel, O, Crichton, S and Sturm, B. 2018. Drying behavior and quality parameters of dried beef (biltong) subjected to different pre-treatments and maturation stages. *Drying Technology* 36 (1): 21-32.
- Yunus, AC. 2019. *Heat and mass transfer: fundamentals and applications*. McGraw-Hill Education,

7. CONCLUSION AND RECOMMENDATION

7.1 Conclusion

Biltong has become an economically important product in the South African meat industry due to its increased demand locally and internationally. Literature reviewed in this study showed limited control in the production of biltong. Drying is a critical part of the biltong making process, yet the drying kinetics of biltong are not sufficiently characterised. The HAD kinetics data available in literature do not cover the wide range of temperature used in the processing of biltong. Moreover, the HAD procedures are not enough to inhibit the growth of spoilage and potentially toxic microorganisms in biltong. Consequently, there is need for alternative drying methods. In this regard, IR has shown potential in decontamination of food products without compromising their quality. An IRHAD is a possible drying method for biltong. The synergistic effect between the IR and the hot air improves the energy efficiency, shortens, the drying time, and results in dried products of better quality. There is need for sufficient characterisation of the IRHAD mechanism of beef being processed into biltong. Modelling the coupled heat and mass transfer in beef, as well as the energy use during IRHAD will ascertain the suitability of the application of IRHAD in the processing of beef to produce biltong.

The objectives of this study were to; 1. evaluate the drying kinetics during HAD and IRHAD of beef being processed into biltong, 2. evaluate the suitability of selected thin layer drying models for simulating the HAD and IRHAD of beef being processed into biltong, 3. formulate the governing equations and boundary conditions for the coupled heat and mass transfer process during the IRHAD of beef biltong, 4. identify the numerical solution for the coupled heat and mass transfer model using CFD and validate the model using experimental data, and finally 5. formulate and verify a thermodynamic model for evaluating the energy and exergy use during HAD and IRHAD of beef being processed into biltong.

The HAD kinetics of marinated beef being processed into biltong is significantly affected by the drying air temperature, whereas the velocity of the drying air only influences the drying rate in the first falling rate period. The results indicate that processing biltong at HAD temperature of

40 °C increases the core sample temperatures and drying rate by 28 % and 100 %, respectively, and reduces the drying time by 40 % compared to HAD at 30 °C. Diffusion is the predominant mode of moisture transport during the drying of marinated beef being processed into biltong. The D_{eff} of marinated beef being processed into biltong ranges from $1.60 \times 10^{-10} \text{ m}^2 \cdot \text{s}^{-1}$ to $2.28 \times 10^{-10} \text{ m}^2 \cdot \text{s}^{-1}$, while the activation energy is 28.2126 and 17.7068 $\text{kJ} \cdot \text{mol}^{-1}$ at a drying air velocity of 1.5 and 2.5 $\text{m} \cdot \text{s}^{-1}$, respectively. The D_{eff} is highly sensitive to changes in drying air temperature at lower air velocity as indicated by the higher E_a observed at 1.5 $\text{m} \cdot \text{s}^{-1}$. The results indicate that the drying kinetics during HAD is more sensitive to temperature changes than the drying air velocity. Consequently, more emphasis should be put in selecting the optimal temperature that would give the desired biltong quality characteristics. The results from this study cover the range of temperatures (30 – 40 °C) predominantly used by biltong processors and offer new information on the influence of two levels of air velocity on the HAD kinetics of marinated beef, thus, can be used to optimise the HAD processing of biltong.

The IRHAD experiments shows that the drying of marinated beef is significantly affected by the power level of the IR emitter, the temperature and velocity of the drying air. The power level of the IR emitter is the predominant factor that influences the drying process of marinated beef subjected to IRHAD. The power level of the IR emitter determines the temperature of the emitter, thus influencing the core temperature of the marinated beef sample. The core temperature of the marinated beef sample is the most critical parameter that influences the drying kinetics under IRHAD. The combined effect of the power level of the IR emitter, temperature and velocity of the drying air on the; drying time, drying rate, effective moisture diffusivity, and the activation energy; is proportional to the influence of these factors on the core temperature of the beef sample. The IR emitter power level of 1000 W combined with a drying air temperature and velocity of 40 °C and 1.5 $\text{m} \cdot \text{s}^{-1}$, respectively, resulted in the shortest drying time of 5.61 hours. This is 292 % lower than the shortest drying time (22 hours) obtained during HAD at drying air temperature and velocity of 40 °C and 2.5 $\text{m} \cdot \text{s}^{-1}$, respectively. This indicating the superiority of IRHAD over HAD in shortening the drying time and subsequently lowering the specific energy consumption due to the increased energy efficiency. The moisture transport during IRHAD of marinated beef is partly due to surface evaporation and predominantly due to diffusion. The effective moisture diffusivity values ranged between $4.560 \times 10^{-10} \text{ m}^2 \cdot \text{s}^{-1}$ and $13.7 \times 10^{-10} \text{ m}^2 \cdot \text{s}^{-1}$.

¹, whereas the activation energy values ranged from 40.97 to 59.16 kJ.mol⁻¹. These findings imply that there is greater utilisation of energy during IRHAD than HAD of marinated beef when making biltong.

The Two-Term thin-layer drying model is the most suitable thin layer model for predicting the moisture ratio during the HAD and IRHAD of marinated beef into biltong. The simplicity and ease of computation makes the thin layer drying model easily applicable in automated control of biltong processing. Nonetheless, a mechanistic model is necessary to decode the mechanisms of heat and mass transfer during IRHAD of marinated beef being processed into biltong.

This study developed a mechanistic model for predicting the heat and mass transfer during IRHAD of a slab of beef being processed into biltong. The heat and mass model incorporates both convective and radiative heat transfer. The IR heat is modelled as a heat generation layer following Lambert's law of electromagnetic extinction. Diffusion is the main mode of water transport. The shrinkage of meat during drying is incorporated into the model by using a shrinkage dependent moisture diffusivity. The model is implemented in Ansys Fluent CFD software. The strategies for implementing and solving the developed model using Ansys Fluent are outlined and the necessary model input parameters provided. The model suitably characterises the flow of the drying air around the slab of beef sample, the temperature distribution in the sample, and the moisture content during drying. The simulated results from the model are reasonably acceptable given the high values of the R² (0.9579 and 0.9790) and low values of RMSE (0.0698 and 1.99) for both MR and temperature. The model predicts the temperature better (R² = 0.9790) than the MR (R² = 0.9579). The accuracy of the model in predicting the MR may be improved by incorporating pressure driven flows and a moving boundary which may better account for shrinkage, especially at high sample temperatures caused by high IR emitter power levels.

The developed heat and mass transfer model is supplemented by the thermodynamic model for evaluating the energy and exergy utilisation. The developed thermodynamic model indicates that the energy and exergy efficiency of HAD increases with increasing drying air temperature but decreases with increasing drying air velocity. The energy efficiency increases by 36.6 % whereas the specific energy consumption drops by 28 % when drying air temperature increases from 30

°C to 40 °C at drying air velocity of 1.5 m.s⁻¹. The IR radiation dominates the energy and exergy efficiency during IRHAD. Increasing the power level of the IR emitter increases the energy and exergy efficiency, whereas increasing the drying air temperature and velocity inversely affects the energy and exergy efficiency. The energy efficiency at a drying temperature of 30 °C increased by 71 % when the IR emitter power increased from 500 W to 1000 W. Increasing the drying air temperature from 30 to 40 °C at an IR emitter power of 1000 W reduced the energy efficiency by 49 %. The thermodynamic analysis indicates that the optimal drying conditions in terms of energy utilisation are; HAD drying air temperature and velocity of 40 °C and 1.5 m.s⁻¹, respectively, and IRHAD conditions of 1000 W combined with a drying air temperature and velocity of 30 °C and 1.5 m.s⁻¹. At these optimal conditions, the drying time and specific energy consumption values for IRHAD are less than the values for HAD by 70 % and 67 % respectively, whereas the energy efficiency for IRHAD is 200 % higher than that for HAD. This further highlights the superiority of IRHAD over HAD in the processing of beef biltong.

The drying kinetics provided in this study give an in-depth synthesis of the influence of varying temperature and drying velocity that is missing from previous studies on HAD of biltong. Moreover, the study assesses the application of IRHAD as a new way of processing biltong. The study is the first attempt at the mechanistic modelling of the heat and mass transfer during the drying of beef to produce biltong. The proposed heat and mass transfer model provide a virtual basis for analysing the temperature and moisture content variations during IRHAD treatment combinations before physical implementation. No previous study has evaluated the energy utilisation during the processing of biltong. Therefore, the thermodynamic model provides valuable insight into the energy and exergy dynamics during the processing of biltong. The energy and exergy analysis may be critical in assessing the financial suitability of conventional and alternative biltong drying methods with regards to energy utilisation. The analysis of the drying kinetics in combination with the two mathematical models presented in this study, can safely be used to guide the application of IRHAD in the processing of biltong.

7.2 Recommendations

The following recommendations for further research were made from this study;

- i. coupling of the heat and mass transfer model and the thermodynamic model to enable the performance of comprehensive optimisation experiments at different process parameters,
- ii. it is necessary to conduct quality analysis of the dried biltong to further guide the selection of the appropriate drying methods. The models for the quality and safety attributes can be integrated with the heat and mass transfer model to aid in further optimisation of the biltong processing procedures.

8. APPENDIX

8.1 Appendix A

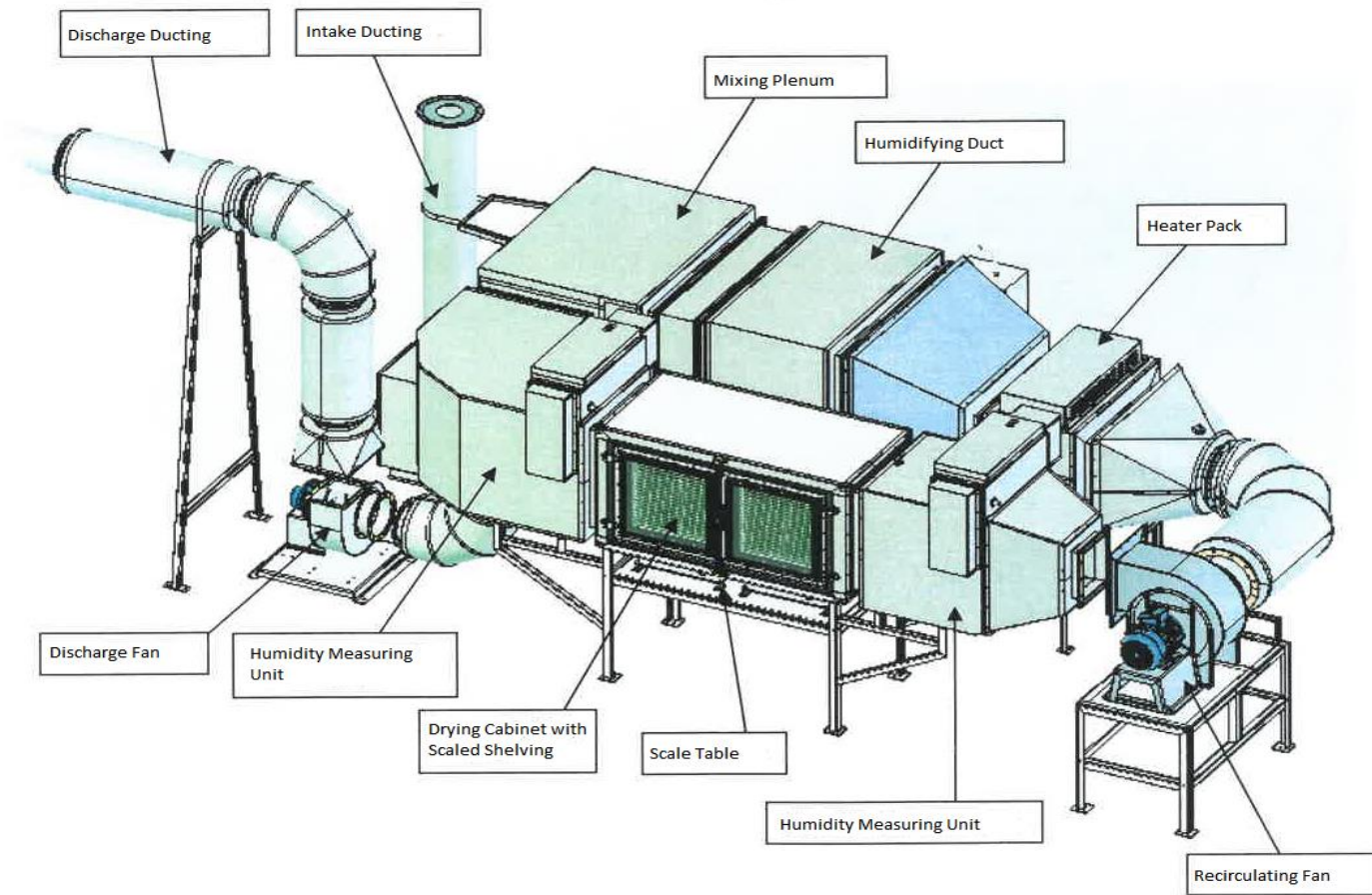


Figure 8.1 Layout of the laboratory drying unit

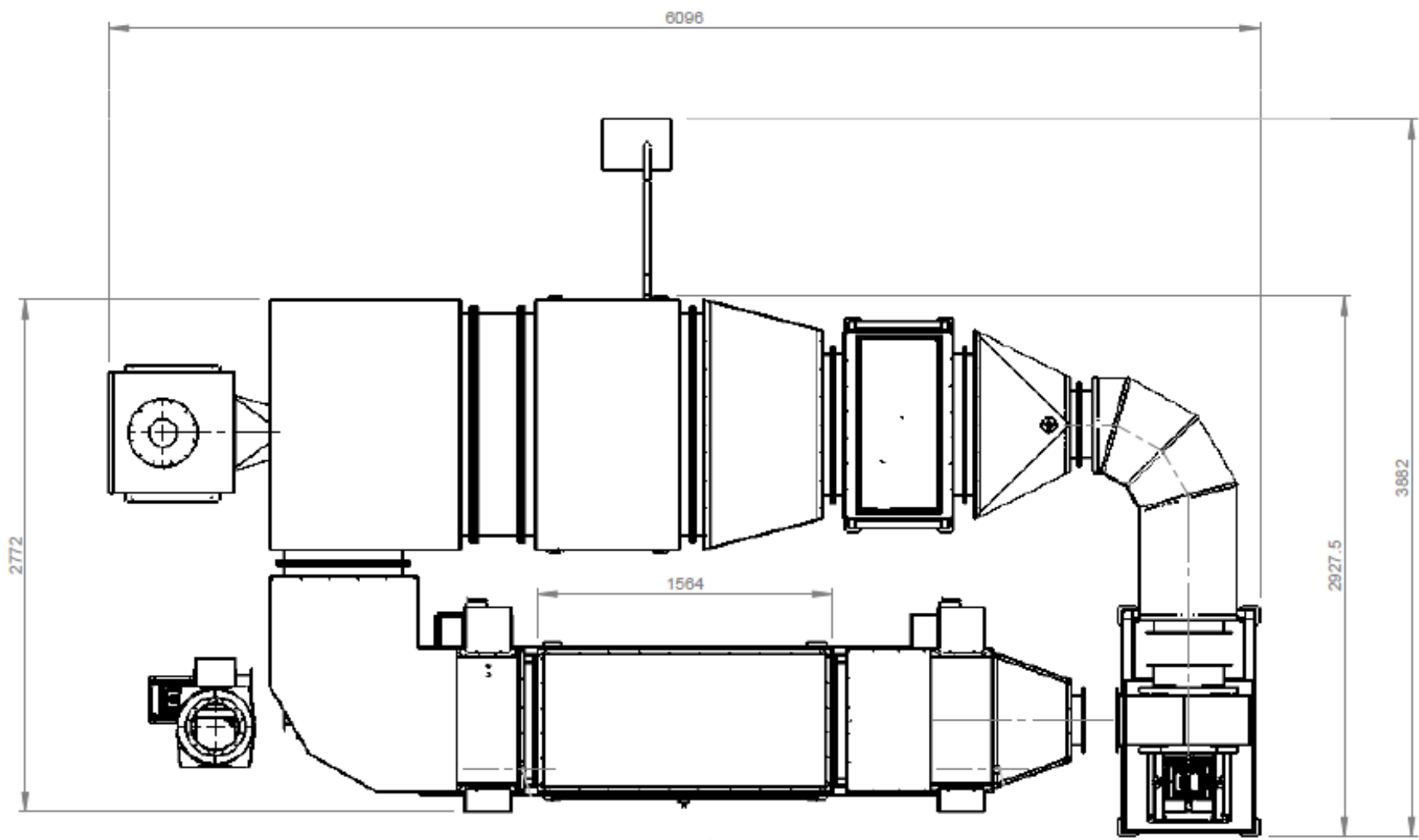


Figure 8.2 Top view of the laboratory drying unit

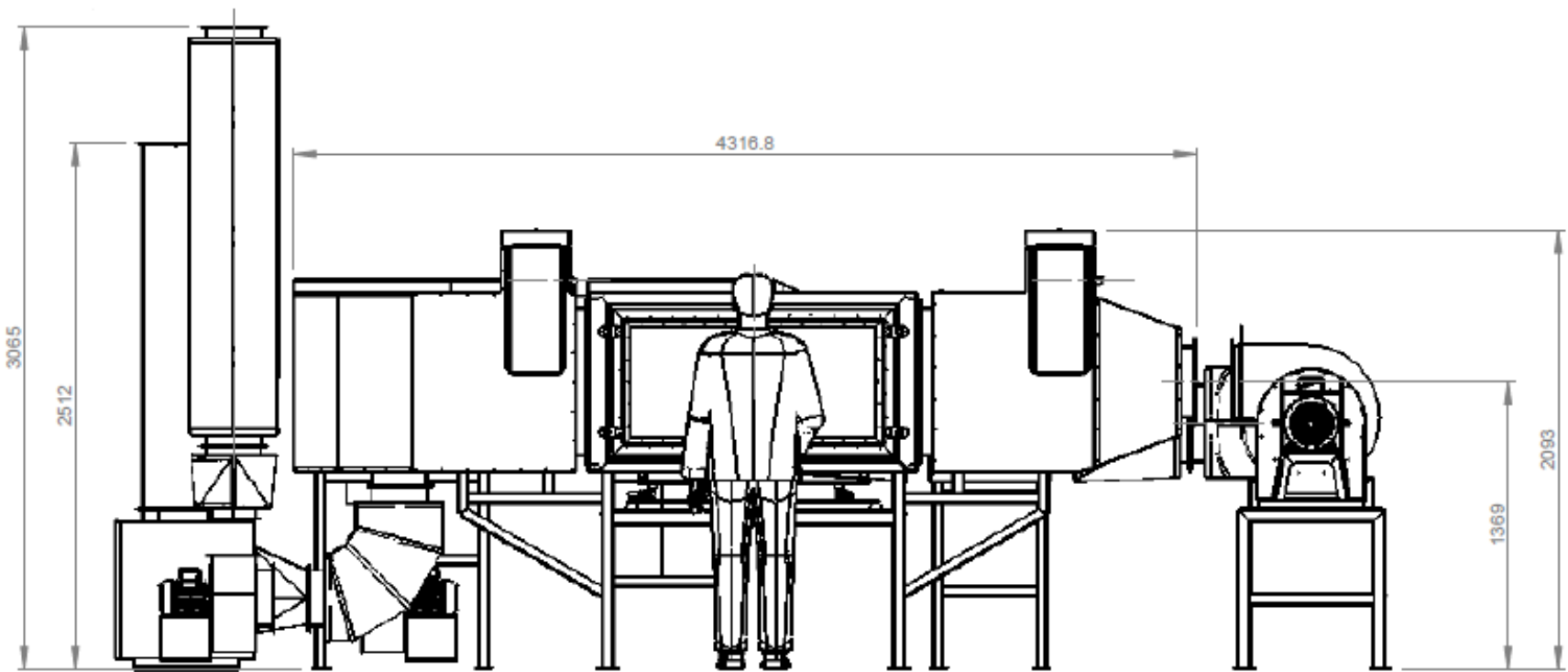


Figure 8.3 Front view of the laboratory drying unit

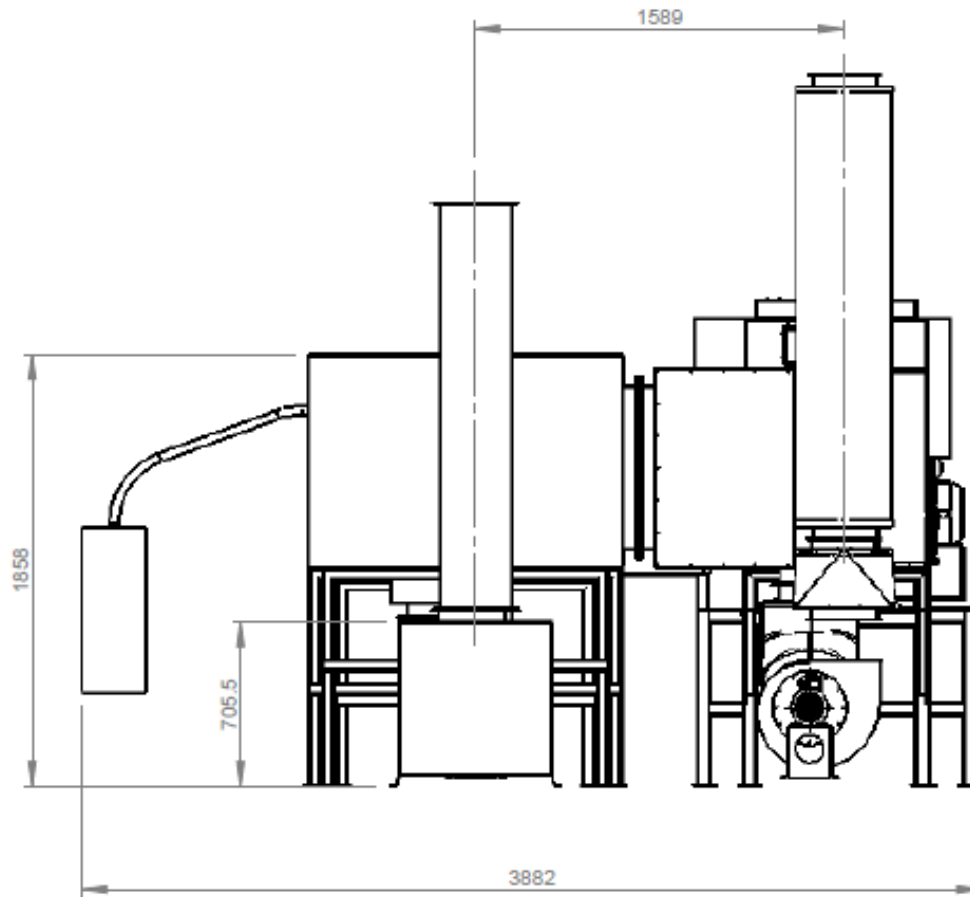


Figure 8.4 Left view of the laboratory drying unit

8.2 Appendix B

Table 8.1 ANOVA results for the IR emitter temperature

Source of variation	d.f.	s.s.	m.s.	v.r.	F pr.
IR_Power	2	872765.06	436382.53	11427.44	<.001
Temp	2	2146.43	1073.22	28.1	<.001
Velocity	1	12196.54	12196.54	319.39	<.001
IR_Power.Temp	4	1008.43	252.11	6.6	<.001
IR_Power.Velocity	2	2925.22	1462.61	38.3	<.001
Temp.Velocity	2	198.23	99.12	2.6	0.089
IR_Power.Temp.Velocity	4	167.31	41.83	1.1	0.374
Residual	36	1374.74	38.19		
Total	53	892781.98			

Table 8.2 ANOVA results for the core temperature of the beef sample

Source of variation	d.f.	s.s.	m.s.	v.r.	F pr.
IR_Power	2	1507.85641	753.92821	10145.31	<.001
Temp	2	403.57624	201.78812	2715.38	<.001
Velocity	1	114.29025	114.29025	1537.96	<.001
IR_Power.Temp	4	97.39153	24.34788	327.64	<.001
IR_Power.Velocity	2	25.33353	12.66676	170.45	<.001
Temp.Velocity	2	4.91308	2.45654	33.06	<.201
IR_Power.Temp.Velocity	4	0.66877	0.16719	2.25	0.083
Residual	36	2.67527	0.07431		
Total	53	2156.70508			

Table 8.3 ANOVA results for the drying time

Source of variation	d.f.	s.s.	m.s.	v.r.	F pr.
IR_Power	2	381.97991	190.98996	3112.93	<.001
Temp	2	106.56384	53.28192	868.44	<.001
Velocity	1	16.87845	16.87845	275.1	<.001
IR_Power.Temp	4	28.57221	7.14305	116.42	<.001
IR_Power.Velocity	2	2.23616	1.11808	18.22	<.001
Temp.Velocity	2	3.95744	1.97872	32.25	<.091
IR_Power.Temp.Velocity	4	2.24767	0.56192	9.16	<.101
Residual	36	2.20873	0.06135		
Total	53	544.64441			

Table 8.4 ANOVA results for the SEC

Source of variation	d.f.	s.s.	m.s.	v.r.	F pr.
IR_Power	2	0.1513659	0.07568296	4691.34	<.001
Temp	2	0.008597	0.00429847	266.45	<.001
Velocity	1	0.0063947	0.00639472	396.39	<.001
IR_Power.Temp	4	0.0026967	0.00067417	41.79	<.001
IR_Power.Velocity	2	0.0042686	0.00213427	132.3	<.001
Temp.Velocity	2	0.0001012	0.00005057	3.13	0.056
IR_Power.Temp.Velocity	4	0.0011508	0.00028769	17.83	<.068
Residual	36	0.0005808	0.00001613		
Total	53	0.1751555			

8.3 Appendix C

Viscous Model ×

Model

- Laminar
- Spalart-Allmaras (1 eqn)
- k-epsilon (2 eqn)
- k-omega (2 eqn)
- Transition k-kl-omega (3 eqn)
- Transition SST (4 eqn)
- Reynolds Stress (5 eqn)
- Scale-Adaptive Simulation (SAS)
- Detached Eddy Simulation (DES)

k-epsilon Model

- Standard
- RNG
- Realizable

Near-Wall Treatment

- Standard Wall Functions
- Scalable Wall Functions
- Non-Equilibrium Wall Functions
- Enhanced Wall Treatment
- Menter-Lechner
- User-Defined Wall Functions

Options

- Viscous Heating
- Curvature Correction
- Production Kato-Launder
- Production Limiter

Model Constants

Cmu:

C1-Epsilon:

C2-Epsilon:

TKE Prandtl Number:

TDR Prandtl Number:

Energy Prandtl Number:

Wall Prandtl Number:

User-Defined Functions

Turbulent Viscosity:

Turbulence Damping Options

- Turbulence Damping

Figure 8.5 Standard k-ε model parameters

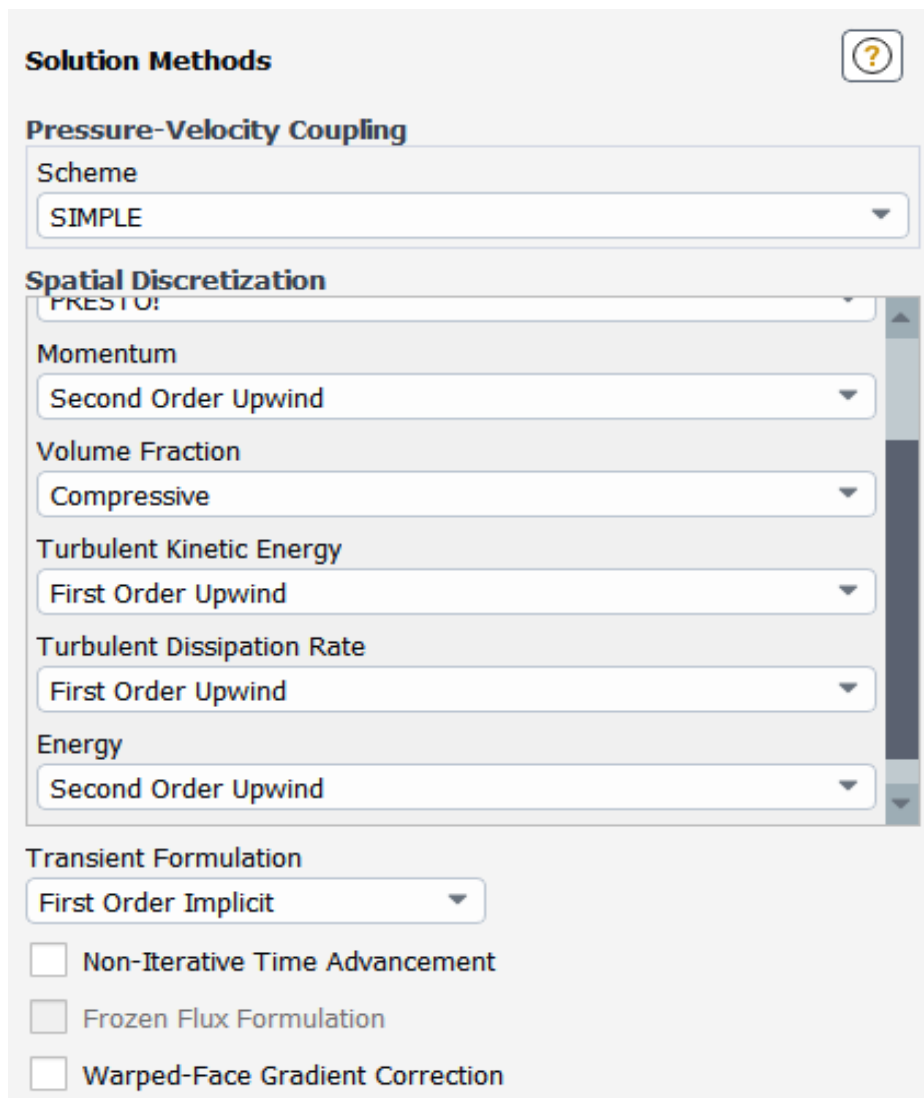


Figure 8.6 Solution setup in Ansys Fluent

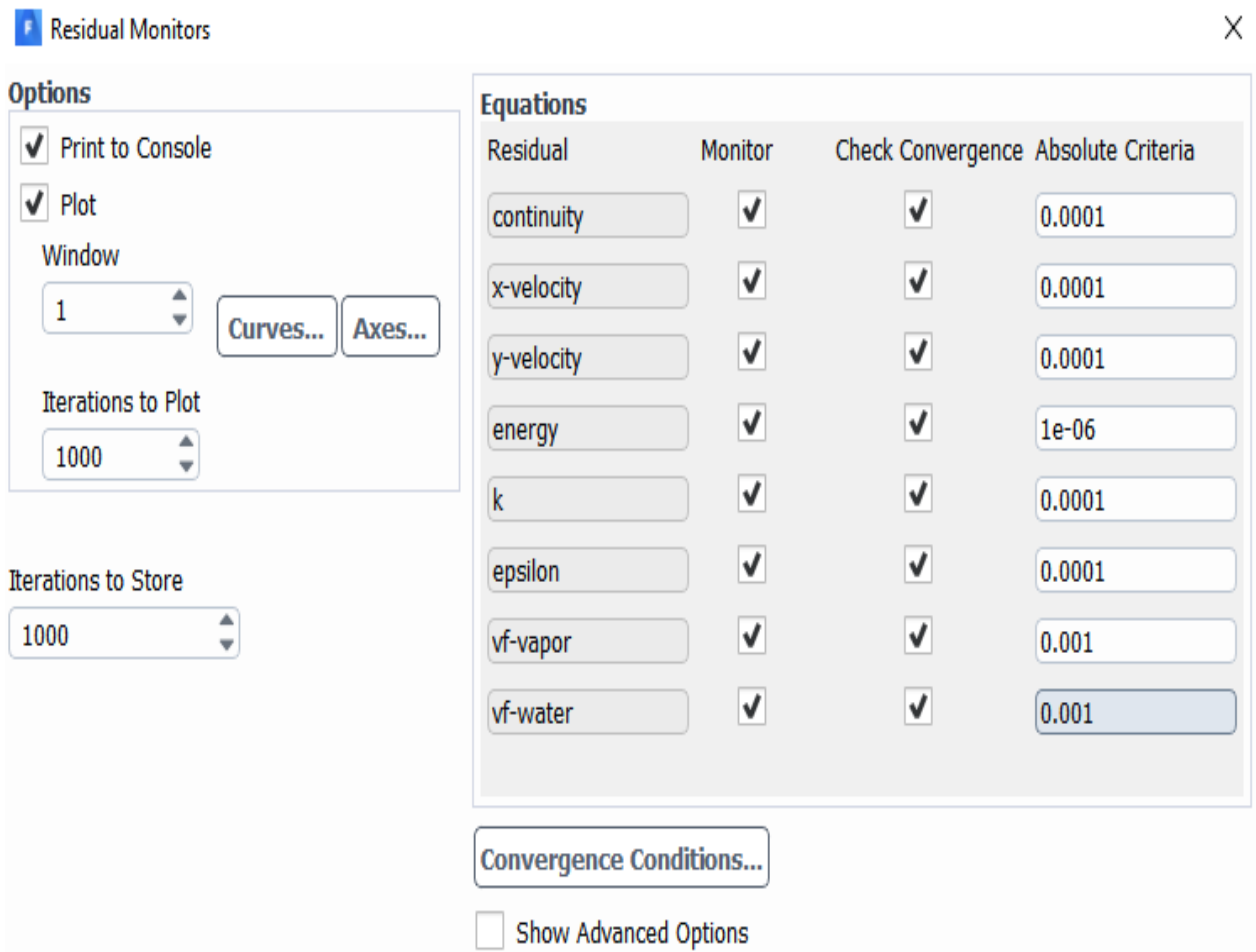


Figure 8.7 Residual monitors for convergence

Initialization Methods

Hybrid Initialization
 Standard Initialization

Compute from

Reference Frame

Relative to Cell Zone
 Absolute

Initial Values

Y Velocity (m/s)

Turbulent Kinetic Energy (m2/s2)

Turbulent Dissipation Rate (m2/s3)

Temperature (k)

vapor Volume Fraction

water Volume Fraction

Figure 8.8 Solution initialization methods

Run Calculation 

Time Advancement

Type: Method:

Parameters

Number of Time Steps: Time Step Size (s):

Max Iterations/Time Step: Reporting Interval:

Profile Update Interval:

Options

Extrapolate Variables
 Report Simulation Status

Solution Processing

Statistics

Data Sampling for Time Statistics

Figure 8.9 Run calculation setup

8.4 Appendix D

```
/******  
UDF to apply mass transfer rate from liquid to gas phase at the interface  
*****  
#include "udf.h"  
#include "materials.h"  
#include "sg.h"  
#include "sg_mphase.h"  
#include "flow.h"  
#include "mem.h"  
#include "metric.h"  
  
#define MW_W 18.0 /*Water molecular weight*/  
#define MW_A 29.0 /*air molecular weight*/  
#define R 8.314 /*Universal gas constant*/  
#define pi 3.14159 /* PI number*/  
#define Rho_air 1.22 /*Air density [kg/m3]*/  
#define Pwa 7384.94 /*(Pw-Pa) [Pa]*/  
#define Va 0 /* Air Velocity [m/s]*/  
  
DEFINE_MASS_TRANSFER(liq_gas_source, c, thread, from_index, from_species_index,  
to_index, to_species_index)  
{  
/****** Declare variables *****/  
real b, m_lg, T_cell, P_cell, P_sat;  
/*real NV_VEC(G);*/  
real X_W, Y_W, Y_A;  
real x[ND_ND];  
real cur_ts;  
face_t f;  
real D[ND_ND], DX, DY;  
int i, pdomain_index, kk;  
real ad;  
Thread *liq = THREAD_SUB_THREAD(thread, from_index);  
Thread *gas = THREAD_SUB_THREAD(thread, to_index);  
  
/****** Define variables *****/  
T_cell = C_T(c,thread); /*cell mixture temperature*/  
P_cell = C_P(c,thread); /*cell mixture pressure*/  
C_CENTROID(x,c,thread);  
cur_ts = CURRENT_TIMESTEP; /* real time step size (in seconds)*/  
  
m_lg = 0.0;  
if (C_VOF(c,liq)!=0 && C_VOF(c,liq)!=1)  
{  
/* compute saturation pressure for water vapor using polynomial fit */  
P_sat = 0.638780966e-8*pow(T_cell-273.15,6)+0.203886313e-5*pow(T_cell-273.15,5) +  
0.30224699e-3*pow(T_cell-273.15,4) + \  
0.265027242e-1*pow(T_cell-273.15,3) +1.43053301*pow(T_cell-273.15,2)+  
44.3986062*(T_cell-273.15) + 611.176750;  
  
/* calculate molar fraction X_W from mass fraction Y_W */  
Y_W = C_VOF(c,gas)*C_R(c,gas)/ (C_VOF(c,liq)*C_R(c,liq) + C_VOF(c,gas)*C_R(c,gas) +  
(1-C_VOF(c,liq)-C_VOF(c,gas))*Rho_air);
```

```

    Y_A = (1-C_VOF(c,liq)-C_VOF(c,gas)*Rho_air)/ (C_VOF(c,liq)*C_R(c,liq) +
C_VOF(c,gas)*C_R(c,gas) + (1-C_VOF(c,liq)-C_VOF(c,gas))*Rho_air);
    X_W = (Y_W/MW_W)/((Y_W/MW_W) + (Y_A/MW_A));

    /**** Compute the interfacial area density ****/

    DX=0.0;
    DY=0.0;
    for (kk=0; kk<4; kk++)
    {
        F_AREA(D,C_FACE(c,thread,kk), C_FACE_THREAD(c,thread,kk));
        if (ABS(D[0])>DX)
            DX = ABS(D[0]);
        if (ABS(D[1])>DY)
            DY = ABS(D[1]);
    }
    /* Message("mesh dimensions are [%g,%g]!\n",DX,DY);*/
    ad = DX/(DY*DX); /* calculate interfacial area density*/
    /*Message("AD = %f\n",ad);*/
    /**** Computed the area density ad = length of interface / area of cell ****/
    /* Compute m_lg*/
    if (P_sat - (P_cell*X_W) > 0.0)
    {
        b = 1.22 - 0.19*Va + 0.038*Va*Va;
        m_lg = cur_ts * ad * (1e-6)*(20.56+27.21*Va+6.92*Va*Va)*pow(0.001*Pwa,b);
    }

}

if (-0.0075<x[1] && x[1]<0.0075 && 0.074<x[0] && x[0]<0.075)
{

}
else if (-0.0075<x[1] && x[1]<0.0075 && -0.075<x[0] && x[0]<-0.074)
{

}
else if (0.0065<x[1] && x[1]<0.0075 && -0.074<x[0] && x[0]<0.074)
{

}
else if (-0.0075<x[1] && x[1]<-0.0065 && -0.074<x[0] && x[0]<0.074)
{

}
else
{
    m_lg=0.0;
}

return (m_lg); /* return value of mass transfer rate */

}

```